PETROLOGY AND GEOCHEMISTRY OF PRECIOUS AND BASE METAL MINERALIZATION, NORTH AMETHYST VEIN SYSTEM MINERAL COUNTY, COLORADO

by

Nora Katherine Foley

Dissertation submitted to the Faculty of the

Virginia Polytechnic Institute and State University

in partial fulfillment of the requirements for the degree of

DOCTOR OF PHILOSOPHY

in

Geological Sciences

APPROVED:

James R Craig

J. R. Craig, Chairman

R J Bod

R. J. Bodnar

P. B. Barton, Jr.

Donald Rimstidt

J. D. Rimstidt

A. K. Sinha

A. K. Sinha

July, 1990

Blacksburg, Virginia

PETROLOGY AND GEOCHEMISTRY OF PRECIOUS AND BASE METAL MINERALIZATION, NORTH AMETHYST VEIN SYSTEM MINERAL COUNTY, COLORADO

by

Nora Katherine Foley

(ABSTRACT)

Gold, silver and base metal-rich minerals of the North Amethyst vein occupy fractures in 26 Ma volcanic rocks near the southern margin of the San Luis caldera, at the northern edge of the Creede district, San Juan Mountains, Colorado. The veins contain two associations of mineral assemblages that are separated locally by breccias and sediments. The earlier, fine-grained association consists of quartz, rhodonite, Mn-carbonates, hematite, magnetite, electrum, Au-Ag-sulfides, Ag-sulfosalts, and base metal sulfides. The second association consists of coarser-grained quartz, calcite, sericite, chlorite, hematite, adularia, fluorite, base metal sulfides, and Ag-tetrahedrite. The first association (fluid boiling at >350^{o}C to 270^{o}C, <2 wt% NaCl equiv.) has a calculated depth of >1000m; the second association (nonboiling, base-metal assemblages: 280^{o}C to 220^{o}C, 5-11 wt%; boiling, quartz + fluorite + calcite: 270-220^{o}C, 0-4.5 wt%) may have formed at ~500 meters. Deeper estimates from geologic reconstruction (~1500m) support mineralogial evidence that CO_2 played a role in mineral deposition. The second association also may have formed much later in time than the Au-rich stages, perhaps after extensive erosion. Adularia of the second association has an age of 25.13 Ma (M. Lanphere, pers. commun., 1987).

Paragenetically early Au-rich North Amethyst galenas have lead isotopic compositions that are less radiogenic than galenas that formed later, as part of the second association. Galenas from central and southern Creede veins overlap compositions of galenas from the later North Amethyst association. Alpha-Corsair vein galenas are isotopically similar to North Amethyst Au-stage galenas. All galenas are isotopically more radiogenic than host volcanics and probably derived their lead compositions from both Precambrian basement and Tertiary volcanics or their equivalents.

The first association (Mn-Au) is absent in the southern and central Creede district, whereas, the second association correlates with assemblages of the southern and central district. The local and early occurrence of the Mn-Au assemblages may indicate that they formed in a localized hydrothermal system that predated the extensive hydrothermal system from which ores of the central and southern Creede district are proposed to have been deposited. Least radiogenic and paragenetically early mineral assemblages hold the most promise for gold exploration in the central San Juan area.

ACKNOWLEDGEMENTS

I would like to thank Drs. Paul B. Barton, Jr. and Philip M. Bethke of the U. S. Geological Survey for suggesting this project, and providing an initial set of samples. Their continued interest in all scientific endeavors related to the Creede mining district has resulted in a substantial and coherent database of characteristics of this classic epithermal deposit, with which newly discovered mineralization like the North Amethyst vein system can be compared. I also would like to thank my committee members, Drs. Robert J. Bodnar, A. Krishna Sinha, and J. Donald Rimstidt for their helpful suggestions, comments, and discussions which substantially improved the content of this dissertation.

I would like especially to thank Dr. James R. Craig, chairman of both my M.S. and Ph.D committees, without whose support it might have been logistically impossible for me to balance family, work, studies, and degree. His suggestions, comments, discussions, and enthusiasm for the project, both above and below ground, were invaluable. His willingness to undertake a long-distance dissertation demonstrates his unerring confidence that where there is a will, there should be a way!

I would like to thank Homestake Mining Company for access to exploratory workings of the North Amethyst vein and, more importantly, for providing me the opportunity to study the gold mineralization. Dr. Stan Caddey, Mr. Craig Byington, and Mr. Dave Vardiman, all of Homestake Mining Company, contributed generously of both their time and knowledge of the mineralization. By providing access to samples they collected

thoughout the development of the underground workings, they substantially improved my ability to interpret hand sample textures and vein relationships in the larger context of the vein system.

My association with colleagues at the U.S. Geological Survey has continued to be scientifically rewarding and interesting. Dr. Robert A. Ayuso, Mr. Harvey Belkin, Ms. Jane Hammarstrom, Mr. Daniel Hayba, Ms. Marta K. Flohr, Dr. Geoffrey Plumlee, Dr. John Slack, and Mr. Donald Sweetkind were extremely helpful during the last stages of this project and for that I am grateful. Mr. James McGee and Mr. James Emory provided assistance in the electron microprobe laboratory, and access to computer facilities for drafting at the USGS were arranged through Ms. Jane Timmons. Lead isotopic studies at the USGS were possible due to the technical expertise and access to faciliites provided by Drs. Joseph Arth and Robert A. Ayuso.

TABLE OF CONTENTS

INTRODUCTION.....1

PART I. Mineralogy, paragenesis and mineral chemistry of gold, silver and base-metal ores of the North Amethyst vein system, San Juan Mountains, Mineral County, Colorado.....4

PART II. Fluid inclusion thermometry and geochemistry of gold, silver, and base-metal ores of the North Amethyst vein system, San Juan Mountains, Mineral County, Colorado.....104

PART III. Lead isotopic geochemistry of the North Amethyst vein system, the Creede mining district, and vicinity, San Juan Mountains, Mineral County, Colorado.....179

APPENDICES.....260

VITA.....325

LIST OF TABLES

Table		*Page*
Part I.		
1	Ages of lavas, ash-flow sheets and mineralization	12
2	Stages of mineralization and brecciation events	18
3	Minerals of the North Amethyst vein system	26
4	Samples analysed by electron microprobe	27
5	Analyses of carbonate	30
6	Analyses of electrum	31
7	Analyses of manganese silicates	32
8	Analyses of sphalerite	33
9	District-wide correlation of vein-related events	90
Part II.		
1	Stages of mineralization and brecciation event	117
2	Samples used in fluid inclusion study	132
3	Fluid inclusion data	134
Part III.		
1	Ages of lavas, ash-flow sheets and mineralization	188
2	Stages of mineralization and brecciation events	193
3	District-wide correlation of vein-related events	194
4	Lead isotope data on Precambrian rocks	203
5	Samples used in lead isotope study	210
6	Lead isotope data	216

LIST OF FIGURES

Figure		*Page*
Part I.		
1	Map of the San Juan volcanic field, Colorado	10
2	Geologic map of Creede mining district and vicinity	14
3	Plan map of North Amethyst vein system	17
4	Photographs of North Amethyst vein assemblages	21
5	Photographs of North Amethyst vein assemblages	24
6	Cross-section vein of mine workings	34
7	Compositions of carbonates on ternary diagram	39
8	Compositions of carbonates compared to binary solvii	40
9	Histogram of electrum compositions	46
10	Compositions of manganese silicates on ternary diagram	51
11	Progression of events in the development of vein system	62
12	Composite paragenesis diagram	63
13	Schematic diagrams of early vein assemblages	64
14	Schematic diagrams of alpha and beta stages	65
15	Schematic diagram showing breccia with alpha-1 fragments	72
16	Relationship between beta-1 and beta-2 stages	74
17	Insets showing breccia-2	78
18	Schematic diagram showing stage 1	81
19	Schematic diagram showing breccia-3	83
20	Schematic diagram showing stage 2 minerals	84
21	Development of breccia 4	86
22	Schematic diagam showing development of stage 3	87

Part II.

1	Geologic map of Creede mining district and vicinity	109
2	Crossection view of North Amethyst mineralization	114
3	Compositions of coexisting electrum and sphalerite	121
4	Stability fields of minerals of Mn-Au association	122
5	Stability field of base metal - silica association	124
6	Reported CO_2 concentrations of hydrothermal fluids	129
7	Cross-section view of mine workings	131
8	Photographs of fluid inclusions	141
9	Histograms of Th data for North Amethyst system	144
10	Temperature - salinity relations for North Amethyst ores	145
11	Relationship between temperature, salinity, and depth	155
12	Comparison of fluid inclusion data for Creede veins	161

Part III.

1	Map of the San Juan volcanic field, Colorado	185
2	Geologic map of the Creede mining district and vicinity	186
3	Lead isotope provinces of the western United States	202
4	Lead isotope compositions of volcanics, San Juan, Colorado	205
5	Cross-section view showing mine workings	214
6	Lead isotope compositions for North Amethyst vein system	218
7	Lead isotope compositions for Alpha - Corsair system	220

Part III. continued

8	Lead isotope compositions for southern Amethyst system	222
9	Lead isotope compositions for Bulldog Mountain vein system	223
10	Lead isotope compositions for OH and P veins	225
11	Lead isotope compositions of galenas from other veins	227
12	Galena data relative to San Juan volcanics	229
13	Lead isotopic ratios across the Creede district	232
14	Summary diagram showing possible lead sources	241

INTRODUCTION

The North Amethyst vein system, located at the northern edge of the historic Creede mining district in Mineral County, Colorado, was discovered in 1983 by Homestake Mining Company as a result of extensive drilling in the vicinity of the intersection of the northern Amethyst and Equity faults. Homestake explored the property, which is currently dormant, by developing drifts on the Amethyst structure.

The discovery was of major scientific importance for two primary reasons: 1) the mineralization was gold-rich, and 2) it significantly enlarged the area of known high-grade epithermal mineralization related to structures of the Creede district. The Creede mining district is a classic silver-, and base-metal-rich epithermal deposit (Steven and Eaton, 1976) of the adularia-sericite type (Heald et al., 1987). The central and southern parts of the Creede mining district have provided an ideal laboratory for study of the genesis of volcanic-hosted, silver- and base-metal-bearing epithermal ore deposits. Only minor amounts of electrum have been reported to occur in the veins of the main mining area (Appendix A). The discovery of the gold-rich epithermal mineralization provides an opportunity to significantly advance our understanding of the metallogeny of deposits of this type. Extensive geological, mineralogical, fluid inclusion, and stable isotope studies have been used to identify and document many processes involved in the development of the geologic, hydrologic, and geochemical setting of the central and southern Creede mineralization.

The principal goal of this study is to present an integrated analysis of the mineral chemistry, paragenesis, fluid inclusion thermometry, and lead isotope geochemistry of the recently discovered gold, silver, and base metal mineralization. Part 1 of this study is a systematic investigation of the mineralogy, mineral chemistry and paragenesis of the Au-, Ag-, and base-metal ores. The paragenetic relationships of the ores were derived from study of selected samples collected from over 1250 meters of exploratory workings distributed over four levels. Comparison of the mineralogy and paragenesis is made with the central and southern parts of the Creede district. District-wide mineralogical stages are distinguished from mineralization having a more local distribution. Part 2 integrates the mineralogy and paragenesis with a detailed study of the fluid inclusion thermometry of the mineralization, and gives an analysis of the geochemical setting of ore mineralization. The thermal and chemical evolution path of the mineralizing fluids, documented by fluid inclusion thermometry, forms a critical basis for evaluating possible mechanisms leading to ore deposition. Part 3 applies data from Parts 1 and 2 to a detailed study of the lead systematics of ore minerals of the North Amethyst vein system. The ores are also examined as part a regional study of the lead isotope geochemistry of the more important mineral deposits of the central San Juan Mountains, including the Cascade mine of the Bondholder district, the Alpha - Corsair, Bulldog Mountain, OH, P, Amethyst, and Solomon - Holy Moses veins of the central and southern Creede district, and the Emma mine of the Spar City district.

A brief discussion of the geology of ore deposits of the central and southern parts of the Creede mining district, as set forth in previous studies, is included in Appendix A. Results of previous studies of mineralization occurring in structures related to the northern Amethyst and Equity faults are also summarized in Appendix A. A description of access to workings, sampling methods, and analytical techniques is included in Appendix B. Appendix C is a compilation of electron microprobe data collected during the course of this study.

PART 1:

Mineralogy, paragenesis and mineral chemistry of gold, silver and base-metal ores of the North Amethyst vein system, San Juan Mountains, Mineral County, Colorado

LISTING OF CONTENTS

ABSTRACT

INTRODUCTION

GEOLOGIC SETTING

PREVIOUS STUDIES

STYLE OF MINERALIZATION

VEIN MINERALOGY AND COMPOSITIONAL RANGES

Ag-, and Ag-Cu sulfide minerals
Barite $BaSO_4$
Bournonite $PbCuSbS_3$
Carbonate group (rhombic)
Chalcopyrite $CuFeS_2$
Chlorite group
Electrum Au,Ag
Fluorite CaF_2
Galena PbS
Gypsum $CaSO_4 \cdot 2H_2O$
Hematite Fe_2O_3
Manganese-silicate minerals
Magnetite Fe_3O_4
Marcasite FeS_2
Polybasite $(Ag,Cu)_{16}Sb_2S_{11}$
Potassium feldspar $KAlSi_3O_8$
Proustite Ag_3AsS_3-Pyrargyrite Ag_3SbS_3
Pyrite FeS_2
Quartz SiO_2
Silver Ag^o
Sphalerite (Zn,Fe,Mn,Cd)S
Stephanite Ag_5SbS_4
Tetrahedrite $(Cu,Ag,Fe,Zn)_{12}(Sb,As)_4S_{13}$
Uytenbogaardtite Ag_3AuS_2

MINERAL ASSOCIATIONS AND ASSEMBLAGES

Alteration and Pre-ore Vein Assemblages
Manganese - Gold Association
Alpha stage
Beta stage
Breccia-1
Transitional Breccias and Sediments
Breccia-2
"Black" quartz breccia

Base Metal-Silica Association
Stage 1
Breccia-3
Stage 2
Breccia-4
Stage 3

CORRELATION OF MINERAL ASSEMBLAGES WITH OTHER VEIN SYSTEMS

CONCLUSIONS

REFERENCES

ABSTRACT

Gold-rich adularia-sericite-type mineralization occurs near the southern margin of the San Luis caldera, at the intersection of the Equity fault and the northern extension of the Amethyst fault system. Mineralization is confined primarily to steeply dipping structures in silicified rhyolite and dacite. Intense sericitic alteration occurs at higher levels in the system, and wallrock adjacent to some veins is bleached. The ores are multiply brecciated, and vein filling locally shows sedimentary textures.

Textural, mineralogical, and chemical criteria indicate that there are at least two partially coextensive associations of mineral assemblages separated locally by a period of major brecciation and sedimentation. An older Au-bearing association consists of two fine-grained ore stages, both of which contain electrum, uytenbogaardtite, tetrahedrite, Ag-sulfosalts, and Ag- and base-metal-sulfides, and the assemblages: 1) manganese-silicates + manganese-carbonates + quartz, and 2) magnetite + hematite + pyrite + quartz. A younger crosscutting association contains calcite, adularia, fluorite, and quartz, plus the assemblages: 1) coarse-grained base-metal-sulfides and 2) hematite + chlorite + quartz. Quartz, Mn-rich calcite, and trace pyrite line late vugs.

Mineralogic, lead-isotopic and fluid inclusion characteristics of the younger association are similar to those of ores of the southern and central parts of the Creede mining district. In contrast, the Au and Mn-silicate assemblages of the older association are rare to absent in the southern and central parts of the district. The local and early

occurrence of the manganese and gold assemblages may indicate that they formed in a small localized hydrothermal cell that predated the extensive hydrothermal system from which ores of the central and southern parts of the Creede district are proposed to have been deposited (e.g., Bethke, 1988). If similar early cells were present in the southern and central parts of the district, they may have been replaced or incorporated into later assemblages, or they may remain to be discovered. In the latter case, paragenetically early mineral assemblages hold the most promise for gold exploration.

INTRODUCTION

The North Amethyst vein system is located just south of the Continental Divide along the southern margin of the San Luis caldera in Mineral County, Colorado. The precious- and base-metal-bearing veins fill steeply dipping structures related to an extension of the Amethyst fault, a north-northwest-trending normal fault system that cuts rhyolitic and rhyodacitic volcanics of the central portion of the San Juan volcanic complex, and adjacent structures of the east-west-trending reverse Equity fault. The veins lie just inside the northern boundary of the historic Creede mining district.

Homestake Mining Company discovered the gold-bearing ores and delineated an extensive high-grade zone adjacent to old workings of the near-surface Equity mine. Available published geologic descriptions of the mineralization prior to this study are limited mainly to historical reports on the Equity mine and some preliminary studies of the newly discovered ore (Appendix A).

This paper is the first part of a detailed investigation of the petrology of the complex ores of the North Amethyst area, and concentrates on mineralization in higher grade areas delineated by underground workings. The mineralogy, mineral chemistry, and paragenesis of the ore of the North Amethyst veins are presented here. A comparison is made with adularia-sericite-type (Heald et al., 1987), Ag-, and base-metal-rich mineralization of the southern Amethyst, Bulldog Mountain, P, and OH veins of the main Creede mining district. Only a limited amount of petrologic interpretation is included in this paper, instead the paper focusses on the mineralogy and stage assemblages. The petrology, fluid inclusion thermometry, and lead isotopic geochemistry of the vein system are covered in Foley (1990b, 1990c).

GEOLOGIC SETTING

The San Juan volcanic field is an erosional remnant of a much larger volcanic field that covered part of the southern Rocky Mountains in the middle Tertiary (Steven, 1975, Lipman et al., 1978). The present extent of the major ash-flow tuffs and their associated calderas are shown in Figure 1. The volcanic field rests upon an eroded base consisting of Proterozoic crystalline metavolcanics, metasediments, and granitiod rocks, and, possibly remnants of Paleozoic, Mesozoic and Tertiary sedimentary rock (summarized by Steven and Lipman, 1976, Lipman et al., 1978, Bickford, 1988, Baars and Stevenson, 1984, and Gries, 1985). The composite volcanic field consisted dominantly of andesite-dacite lavas and associated volcaniclastic rocks erupted from precaldera

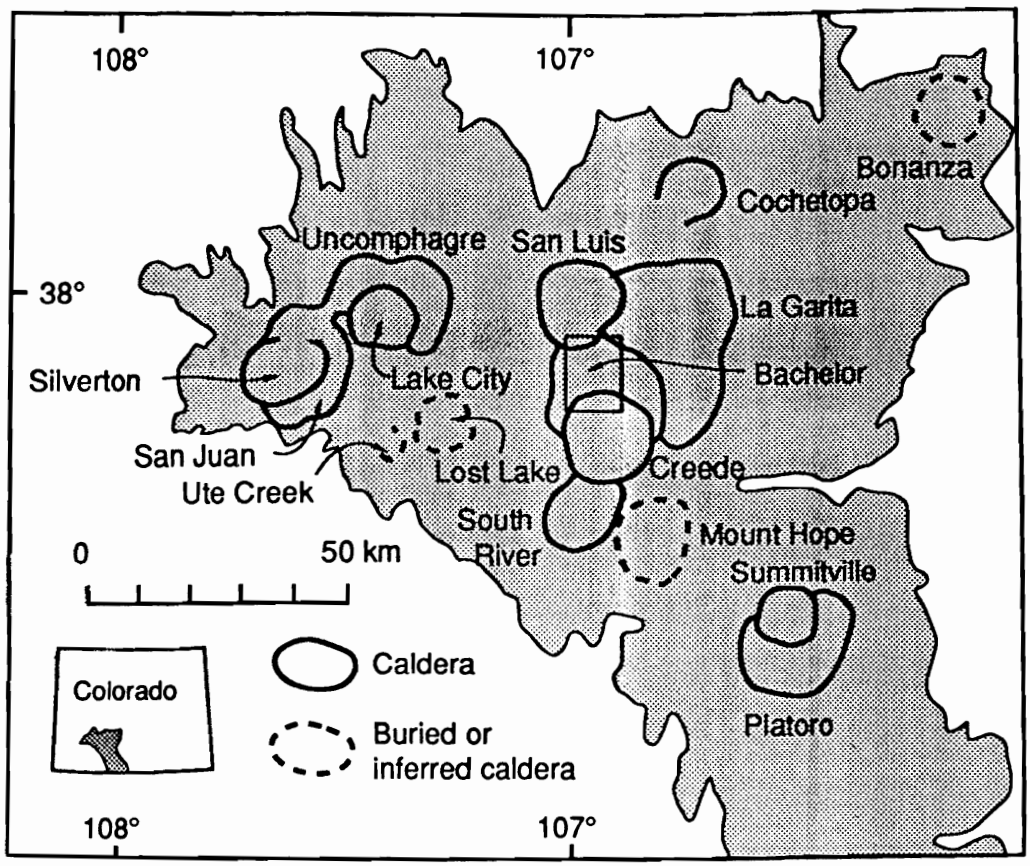

Figure 1. Map of the San Juan volcanic field in southwestern Colorado showing the extent of major ash flow tuffs and associated calderas. From Plumlee (1989), after Steven and Lipman (1976), and incorporating changes suggested by Lipman and Sawyer (1988). Box in center outlines area of Figure 2, a map of the Creede mining district and vicinity.

volcanoes in early Oligocene time, mainly between 35 and 30 million years ago. A large negative Bouguer gravity anomoly underlies much of the San Juan volcanic field and is believed to reflect a large composite batholith emplaced beneath the field (Plouff and Pakister, 1972). From about 28 to 26 million years (Table 1), the central San Juan volcanic field experienced widespread silicic ash-flow eruptions and related caldera subsidence (Lipman et al., 1970, Lipman et al., 1978; Lipman and Sawyer, 1988; Lanphere, 1988). The mineralization of the Creede district is located in a complex set of nested calderas formed by the pyroclastic eruptions.

Mid-Tertiary sediments accumulated locally within the San Juan field. The most voluminous sediments are those of the Creede Formation, which were deposited in the moat of the Creede caldera and in channels incised in the caldera wall. They consist of stream channel gravels, landslide breccias, travertines, bedded lacustrine sediments and water-lain tuffs (Steven and Ratte, 1965). Thin, local sediments interbedded with volcanic units have also been found in the north-central part of the district by mining companies. Bachelor caldera moat sediments consisting mainly of lacustrine sediments including bedded ash and fine siltstones and local lenses of sand and pebble conglomerates, some of which have been reworked and locally argillized, have been identified by Chevron Resources, Inc, (O'Brient, pers. commun., 1982) and Homestake Mining Company (S. Caddey and C. Byington, pers. commun., 1983). Near the caldera walls, the sediments include megabreccias, laharic breccias, and rare organic-rich lacustrine carbonates (S. Caddey, C. Byington, pers. commun., 1983; D. Sawyer, pers. commun., 1987). Within the San

Table 1. Radiometric ages of lavas, ash-flow sheets, and mineralization of the central San Juan Mountains.

Caldera	Ashflow	Age (Ma)	Ref.
San Luis	Quartz latite of Baldy Cinco (Stewart Peak)	25.72 +/- 0.13	2
San Luis	Nelson Mountain	26.13 +/- 0.08	1
San Luis	Rat Creek Tuff	26.45 +/- 0.07	1
Creede	Snowshoe Mountain Tuff	26.80 +/- 0.10	1
South River	Wason Park Tuff	27.15 +/- 0.12	1
Bachelor	Campbell Mountain Tuff	27.2 +/- 0.2	4
Bachelor	Carpenter Ridge Tuff	27.61 +/- 0.21	1
La Garita	Fish Canyon Tuff	27.80 +/- 0.2	1
Mount Hope	Masonic Park Tuff	28.25 +/- 0.2	1
Regional K-metasomatic event		26.4 +/- 1.3	4

Caldera	Mineralization	Age (Ma)	
San Luis	Northern Amethyst vein		
	adularia	25.13 +/- 0.13	1
Bachelor	OH vein		
	adularia	25.1 +/- 0.6	3
	sericite,	25.7 +/- 1.2	3
	sericite,	25.5 +/- 0.8	3
	sericite	25.3 +/- 1.4	3
	illite-smectite	24.8 +/- 1.3	4

References: 1, Lanphere (1987, 1988); 2, M. Lanphere, written commun. (1989); 3, Bethke et al., (1976), revised by Hon and Mehnert (1983) using new IUGS constants; 4, Vergo (1987).

Luis caldera, fluvial and lake-bed sediments (few tens of meters thick) that accumulated in local depositional basins overlie the main Equity dacite facies of the Nelson Mountain Tuff (Nelson Mountain Tuff) which hosts the North Amethyst ores (Lipman and Sawyer, 1988).[1]

The complex history of movement and reactivation along faults of the Creede graben has been described in detail by Steven and Ratte (1965). Normal faults are the dominant structural element controlling the location of mineralization in the central San Juan area and most are related to evolution of the Oligocene calderas (Figure 2). The reverse Equity Fault, which formed by fault-bounded uplift of a triangular block presumably related to a shallow underlying intrusion (Lipman and Sawyer, 1988), is also mineralized. The dominant structural features are the well-formed caldera expressions and the north-northwest trending Creede graben which initially formed as a keystone graben in the Bachelor caldera (Figure 2). The major faults from west to east include the Alpha-Corsair, Bulldog Mountain, Amethyst, and Solomon-Holy Moses faults. The OH, P and other minor faults cut the central block of the graben, are nearly vertical, and had primarily strike-slip motion (S. Caddey, pers. commun., 1985).

A single radiometric age determination (Table 1) on adularia ($^{40}Ar/^{39}Ar$ incremental heating ages) from drillcore from the North

---

1 Volcanic units named in this text follow the terminology of Lipman and Sawyer (1988), however, Lipman notes (P. Lipman, written commun., May, 1990) that it is unclear whether volcanic rocks in the vicinity of the Equity mine are part of the Nelson Mountain Tuff or Carpenter Ridge Tuff.

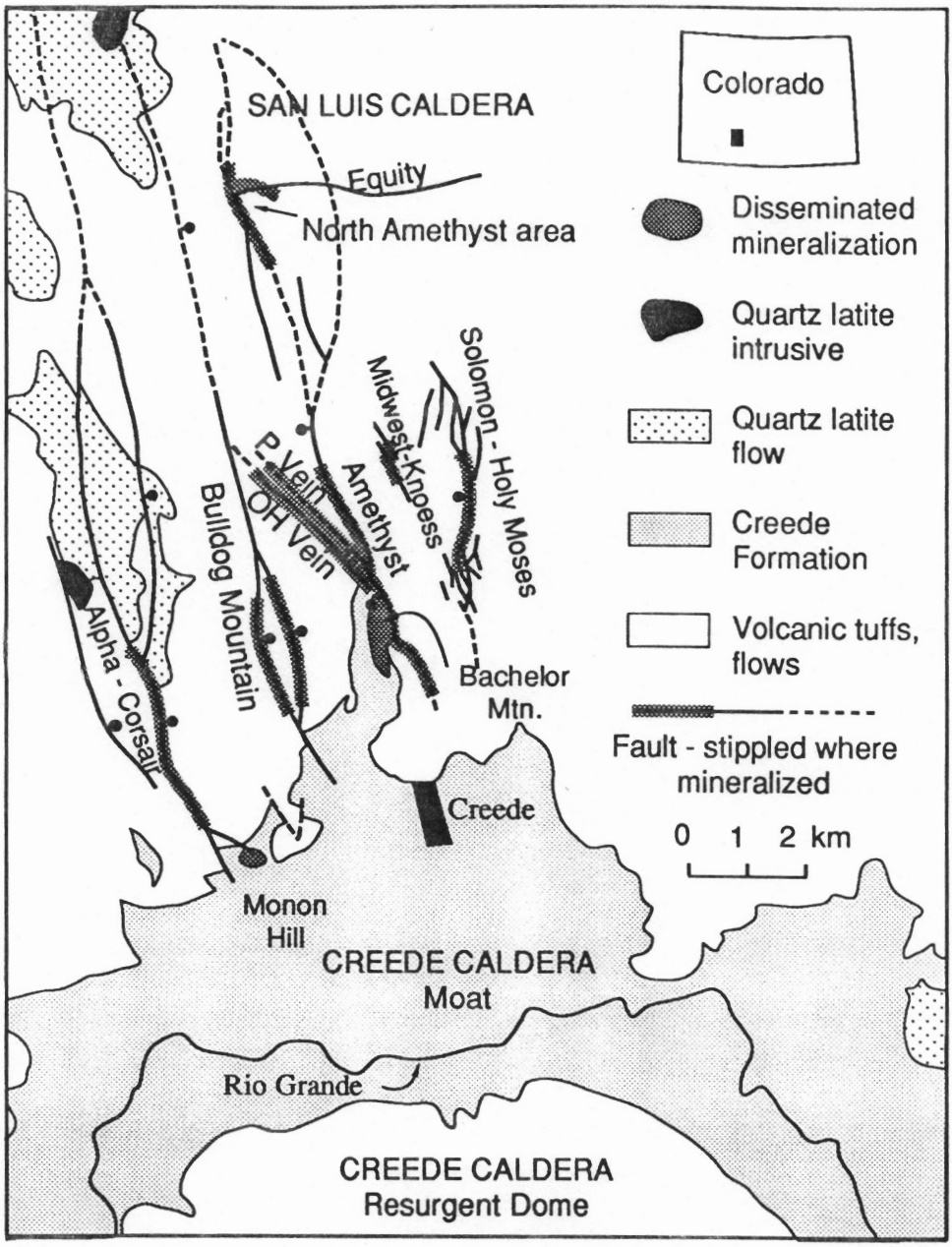

Figure 2. Generalized geologic map of the Creede mining district and vicinity. The graben structure formed by named faults is within the Bachelor caldera and links the San Luis and Creede calderas. North Amethyst vein system is at intersection of the Equity fault and the Amethyst fault. From Plumlee (1989), geology after Bethke and Lipman (1987) and Lipman and Sawyer (1988).

Amethyst vein system indicates an age of 25.13 +/- .13 Ma (Lanphere, pers. commun., 1987). The adularia is associated with base-metal mineralization of the later hydrothermal event occurring along the North Amethyst vein system. The gold-bearing ores predate the base-metal mineralization and the vein adularia (Foley and Vardiman, 1988), and, thus, their age falls in the interval between the host rock, the Nelson Mountain Tuff, and the adularia, i.e., 26.13 to 25.13 Ma. At least three volcanic units were deposited, however, as part of the San Luis caldera complex after the Nelson Mountain Tuff; these include the tuff of Cathedral peak, rhyolite of Mineral Mountain, and volcanics of Stewart Peak which include the rocks of Baldy Cinco (Lipman and Sawyer, 1988). Radiometric age-dates on gangue associated with ore mineralization from the main Creede mining district indicate that the minerals were deposited at about 25 Ma (Table 1).

PREVIOUS STUDIES

Mineralization in the central San Juan area has been the subject of numerous reports and papers since the area was first mined in the early 1880's. The relationship of the mineralization to regional geologic setting was first described in detail by Steven and Ratte (1960, 1965) and Steven (1968). The area around the Creede mining district has been the subject of continuing research since the late 1950's by P.M. Bethke, P.B. Barton, Jr., R.O. Rye, P.W. Lipman, E. Roedder and others of the U. S. Geological Survey and by several universities (see Appendix A). Their work has been published in a series of papers on the Creede district (Steven and Eaton, 1975; Bethke et al., 1976; Roedder, 1977;

Barton et al., 1977; Bethke and Rye, 1979; Hayba et al., 1985; Plumlee, 1989; Foley et al., 1990; and others to follow). Historic accounts of ores of the Equity mine and preliminary reports of the more recently discovered North Amethyst ores are described in Appendix A.

STYLE OF MINERALIZATION

The vertical and lateral extent, and overall shape, of ore occurrences of the North Amethyst vein system (Figure 3) are not well-delineated due to the complex nature of the mineralization and the complex structural character of the veins. A detailed structural analysis of the North Amethyst vein system is currently underway by S. Caddey and C. Byington of Homestake Mining Company (written commun., 1988) to resolve composite vein - structure relationships. Some general observations, however, can be made relative to ore zones of the Bulldog and Amethyst vein systems of the main mining district at Creede as described by Plumlee (1989).

Mineralization of the North Amethyst vein system fills structures related to the northern Amethyst and Equity faults. The North Amethyst veins are mineralogically complex, and the assemblages can be divided into two contrasting associations: a Mn-Au association and a base metal - silica association. The minerals found in each association are grouped in Table 2 according to the stages in which they are typically found, and discussed in greater detail below. Both mineral associations occur along almost the entire extent of the underground workings, a distance of roughly 600 meters along strike of the vein. The base-metal association is displayed over a vertical extent of about 150 meters, and

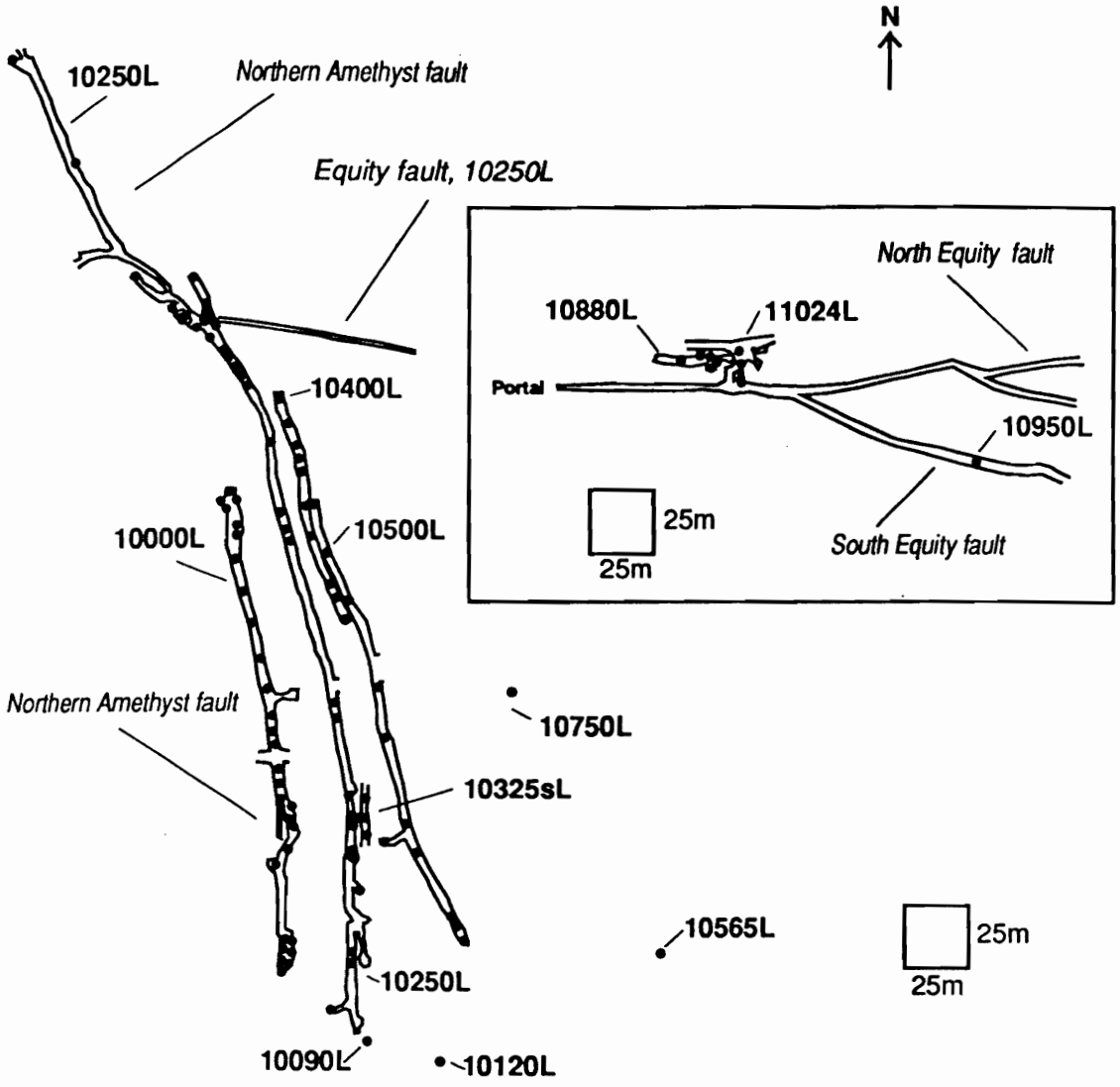

Figure 3. Plan map showing levels of the North Amethyst vein system along the northern Amethyst and Equity faults. Sample localities are shown by solid dots; localities off the vein are on the decline. Inset box of the Equity structure is at the same scale, but offset to the west by approximately 75 m.

Table 2. Stages of mineralization and brecciation events of the North amethyst vein system.

STAGE	NORTH AMETHYST VEIN MINERAL ASSEMBLAGE
Base metal - silica association:	
3	Mn-calcite >> Quartz > Pyrite
Breccia-4	Mn-calcite cement, fragments of earlier assemblages, breccias and minerals, [wallrock]
2b	Quartz > Calcite > Rhodocrosite > Adularia > Fluorite > Chlorite = Pyrite
Breccia-3	Quartz + chlorite cement, fragments of wallrock, and coarse stage 1 sulfides
1b	Quartz > Sphalerite > Galena > Pyrite > Chalcopyrite > Tetrahedrite
1a	Quartz > Pyrite = Hematite > Chlorite
Breccia-2	Quartz cement, fragments of α-,and β-stages, wallrock, sedimented structures black quartz breccia
Mn - Au association:	
β-2	Sphalerite > Galena > Chalcopyrite > Pyrite > Tetrahedrite > Ag- and Au-minerals > Electrum {Magnetite, Hematite}
Breccia-1	Quartz cement, fragments of α- and β-1 stages
β-1	Sphalerite > Galena > Chalcopyrite > Pyrite > Tetrahedrite > Ag- and Au-minerals > Electrum {Magnetite, Hematite}
α	Rhodocrosite = Quartz > Mn-calcite = Rhodonite > K-feldspar > Sphalerite > Pyrite > Galena > [Barite]

Abbreviations: >>, much greater than; >, greater than; =, approximately equal; {} distribution unknown, local occurrence; [], molds.

minerals of the Mn-Au association occur over an apparently larger vertical interval of 600 meters.

Ore zones of the main mining district typically are of much greater horizontal than vertical extent. For example, the ore zone comprising the Bulldog Mountain vein system was mined for approximately three kilometers laterally and 200 to 300 meters vertically (Plumlee, 1989). The combined productive ore zones of the central and southern Amethyst veins were of similar vertical extent, and of even greater lateral extents.

Only the dominantly base-metal-rich assemblages are found in core drilled just south of the North Amethyst underground workings. Further to the south, the base-metal assemblages occur, at least discontinuously, along much of the Amethyst fault (D. Sweetkind, pers. commun., 1990). If these assemblages are truly coeval, the base metal mineralization of the northern Amethyst may have lateral and vertical extents more like those of the main mining district.

In contrast to the base-metal-rich assemblages, the complete gold-bearing assemblages of the North Amethyst system are not found in drillcore to the south of the North Amethyst workings, nor are they reported to occur in underground workings. (As discussed in greater extent below, isolated occurrences of electrum have been reported in ore of main mining district). This suggests that the gold-bearing assemblages may have a more restricted lateral extent compared to ore zones of the main mining district.

The veins of the North Amethyst system vary in width and mineral content due to their complex structural character and to the high degree

of structural activity contemporaneous with and occurring after mineralization. Veins can vary from a few centimeters to greater than two meters in width and they record multiple assemblages.

Most assemblages are brecciated, and vein fillings locally show sedimentary textures. The fracturing events are recorded in crosscutting vein relationships, and in breccias which developed at sites of intense structural activity. Multiple periods of movement resulted in different breccias characterized by certain fragment types and cements; these are used to elucidate timing relations.

Minerals were deposited in a number of stages that are characterized by distinctive textural styles. Extensive brecciation and recrystallization overprints the earlier stages, but a striking textural contrast between stages of the earlier Mn-Au association and those of the later base-metal association is retained in many veins.

The minerals of the Mn-Au association were deposited in two stages that show a variety of textures (Figure 4a-h). The earliest stage of sulfide-bearing mineralization, the alpha—stage, was deposited primarily in open fractures, in some cases around preexisting barite and quartz crystals. The crypto-crystalline material shows a faint mineralogic banding that is clearly visible on aged surfaces due to manganese oxidation. The alpha—stage also shows some evidence for replacement of volcanic wallrock. Embayed remnant feldspar grains are caught up in a fine-grained "frozen mush" consisting dominantly of rhodocrosite, manganese-pyroxenoids and other carbonates, and quartz. The second stage of the Mn-Au association, the beta—stage, consists of fine-grained

Figure 4. Photographs of North Amethyst vein assemblages. a) Vein of alpha-stage manganese-carbonates and -silicates and quartz cutting volcanic wallrock. Field of view: 1 meter. b) Close-up view of bleached wallrock (w), sphalerite grains (s), and alpha-stage material. Penny for scale. c) View of gold-rich beta-stage sulfide vein cutting finegrained Mn-carbonates and -silicates of alpha stage. Pickhammer for scale. d) Close-up view of gold-bearing beta-stage sulfide vein cutting finegrained banded Mn-carbonates, and -silicates and quartz. Scale bar equals 1 cm. e) Equigranular sulfide assemblage of beta-stage. Scale ba equals 25 micrometers. f) Close-up of gold (A), sphalerite (s), and chalcopyrite (c) of beta-stage. g) View of sedimented vein. h) Graded bedding in silicious sediment. Note small offsets in bedding, fine-to-coarse texture, clasts of altered volcanics, rounded quartz crystals, and small sulfide aggregates.

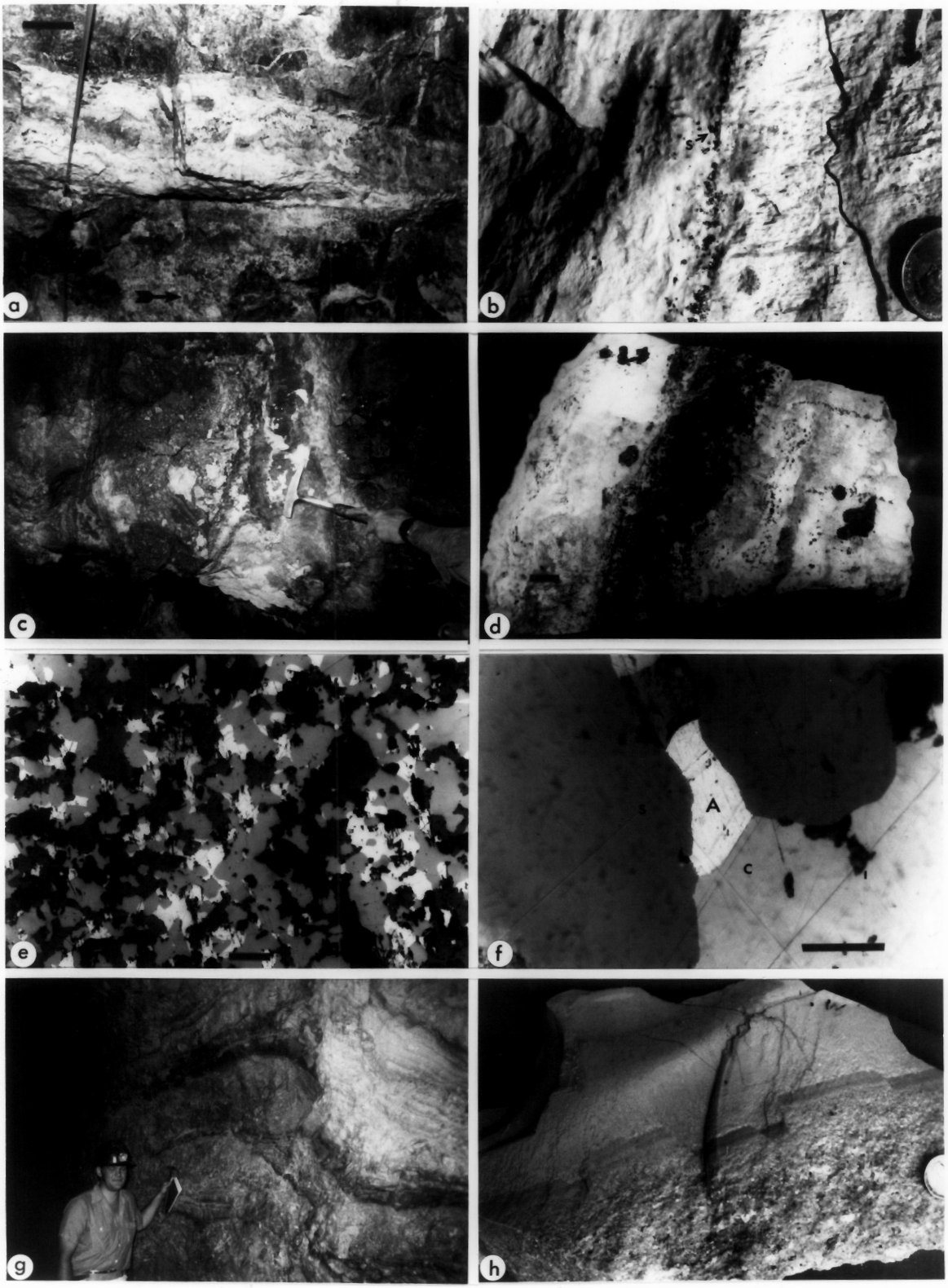
a
b
S
c
d
e
f
S
A
C
I
g
h

precious and base-metal-sulfide rich seams that cut and recrystallized the alpha-stage.

Vein mineralization of the later base metal - silica association filled open spaces in existing fractures and in breccias developed by continued movement (Figure 5a-h). Although many veins filled completely, some large vugs lined with crystals of the latest stages remained open. Minerals of this association are generally coarser-grained and show crustification sequences. Dissolution and replacement textures are also common.

VEIN MINERALOGY AND COMPOSITIONAL RANGES

Detailed descriptions of ore and gangue minerals are given below for common minerals and for those used to constrain conditions of ore formation. The minerals are listed in alphabetical order and grouped by type for convenience. Table 3 describes the relative abundance and distribution of minerals in each assemblage, and include all minerals reported for the deposit. Compositional ranges for carbonates, electrums, manganese silicates, and sphalerites described in Table 4, are listed in Tables 5 through 8. Sample distribution for the microprobe study is shown in Figure 6. Sample selection method and analytical details are described in Appendix B; all analyses are listed in Appendix C. Ore minerals were identified based on descriptions presented by Ramdohr (1969) and Craig and Vaughan (1981).

Figure 5. Photographs of North Amethyst vein assemblages. a) Meter-wide vein of coarse base-metal sulfides of Stage 1, base metal-silicate assocaition. Pickhammer for scale. b) Close-up of base-metal sulfide of stage 1 and quartz, calcite, and chlorite of stage 2. Penny for scale. c) Reflected light photograph of sphalerite (S), galena (G), and quartz (Q) of the stage 1 assemblage. Scale bar equals 5 millimeters. d) Transmitted light photograph of sphalerite, note colorbanding paralleling growth zones defined by fluid inclusions. Scale bar equals 1 cm. e) 2-3 centimeter long quartz crystals of stage 2 coated with calcite of stage 3, calcite is dusted with tiny pyrite cubes. Penny for scale. f) Brecciated stage 1 sulfides coated with fluorite (F) of stage 2. Note pockets of quartz sediment (s) between fluorite and calcite of stage 3. Penny for scale. h) Pink calcite and pyrite of stage 3. Penny for scale.

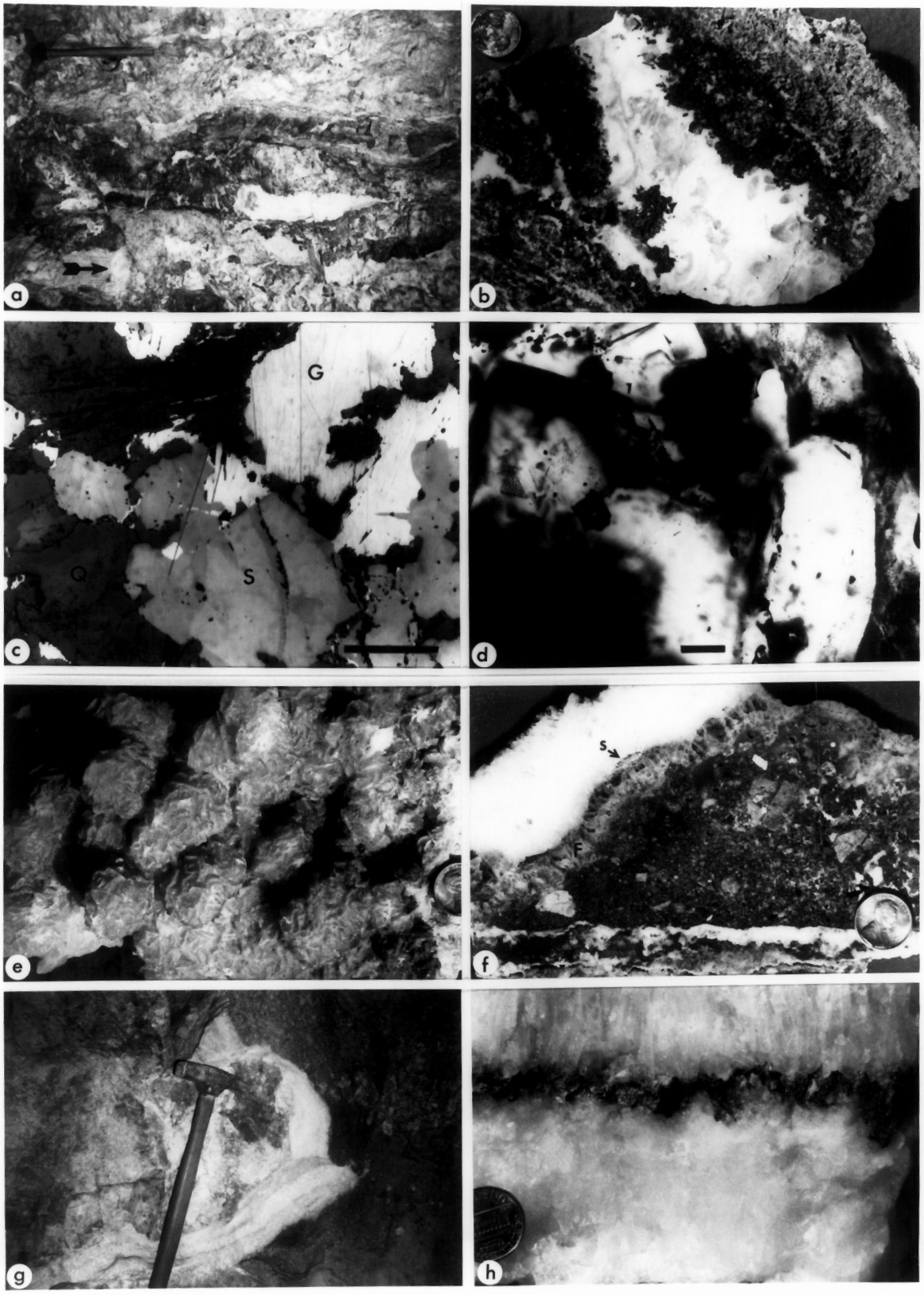
a
b
G
Q
S
c
d
e
S
F
f
g
h

Table 3. Assemblages and minerals of the North Amethyst vein system.

Stage	Pre-ore	α-1	β-1	β-2	1-a	1-b	2-a	2-b	3	Post-Ore
Sericite	X	X	-	-	X	X	X	-	-	-
K-feldspar	A	X	-	-	-	-	X	X	-	-
Quartz	X	X	X	X	X	X	X	X	X	-
Barite	?	?	-	-	-	-	-	-	-	-
Pyrite	X	X	X	X	X	X	-	X	X	-
Hematite	-	-	-	X	X	X	-	-	-	-
Magnetite	-	X	X	X	-	-	-	-	-	-
Chlorite	-	-	-	-	X	X	X	-	-	-
Rhodocrosite	-	X	-	-	-	-	-	X	-	-
Rhodonite	-	X	-	-	X	-	-	-	-	-
Mn-calcite	-	X	-	-	-	-	X	-	X	-
Kutnahorite	-	X	-	-	-	-	-	-	-	-
Alleganyite	-	?	-	-	-	-	-	-	-	-
Bustamite	-	?	-	-	-	-	-	-	-	-
Pyroxmangite	-	X	-	-	-	-	-	-	-	-
Inesite	-	-	-	-	-	-	-	-	-	-
Sphalerite	-	X	X	X	-	X	-	-	-	-
Galena	-	X	X	X	-	X	-	-	-	-
Chalcopyrite	-	-	X	X	-	X	-	-	-	-
Marcasite	-	-	-	X	-	-	-	-	X	-
Acanthite	-	-	X	X	-	-	-	-	-	-
Pyrargyrite	-	-	X	X	-	-	-	-	-	-
Electrum	-	-	X	X	-	-	-	-	-	-
Uytenbogaardtite	-	-	X	X	-	-	-	-	-	-
Polybasite	-	-	?	X	-	-	-	-	-	-
Tetrahedrite	-	-	X	X	-	X	-	-	-	-
Jalpaite	-	-	X	X	-	-	-	-	-	-
Stephanite	-	-	-	X	-	-	-	-	-	-
Bournonite	-	-	-	X	-	-	-	-	-	-
Siderite	-	-	-	-	-	-	-	X	-	-
Fluorite	-	-	-	-	-	-	X	-	X	-
Stromeyerite	-	-	-	-	-	-	-	-	-	X
Native Ag	-	-	-	-	-	-	-	-	-	X
Gypsum	-	-	-	-	-	-	-	-	-	X

Abbreviations: X, present; -, not present; A, wallrock alteration; ?, previously reported by Homestake Mining Company (C. Byington, S. Caddey, D. Vardiman, Pers. commun., 1987), not found in this study.

Table 4. Locations and descriptions of samples from the North Amethyst vein system analysed by electron microprobe.

Sample No.	Location	Description
DMV-1	10250 level, E-126+75'N	Coarse-grained (up to 1cm wide) Stage-1 lemon-yellow crystals of sphalerite intergrown with galena and chalcopyrite in 2 mm to 1 cm wide veinlets cutting bleached volcanic rock.
DMV-3A	10315 level 2' south	Seam of fine-grained electrum-bearing sulfide at contact of volcanic wallrock with breccia (beta stage).
GSP-MM-10-86	10000 level, E-125	20 cm-wide seam of gold-bearing fine-grained sulfides of β-stage in fracture cutting vein of Mn-carbonate, and Mn-silicate and quartz. Rounded grains of sphalerite, with chalcopyritized rims, intergrown with chalopyrite, galena, electrum and other precious- and base-metal minerals of beta stage.
GSP-MN-87	10000 level E-125+35'N	Large (up to 1 cm wide) color-banded crystals of sphalerite of stage 1 intergrown with quartz and chlorite, coated by stage 3 pink calcite.
GSP-MO-2-86	10000 level, E-126+ 50' N, in scram off vein structure.	Coarse veins of honey-brown sphalerite, galena, chalcopyrite, pyrite, and quartz of stage-1 cutting meter-wide brecciated vein of Mn-carbonate and -silicate, and quartz.

NKF-A-1-87	10250 level, E-127+ 140' N	Coarse- to medium-grained sulfides of zinc, lead, and copper of stage I, later quartz and calcite of stage 2.
NKF-K-11-87	10250 level, E-85	Fluorite at base overlain by thick crust of calcite color-banded from pink to white-flesh.
NKF-M-13-87	10090 level, E-120	Small (1-2 mm wide) rounded sphalerite grains of Alpha stage rimmed with chalcopyrite disease, contained in fine grained admixture of rhodonite, rhodocrosite, and quartz.
NKF-Q-17-87	10000 level, 25' from north face	Meter-wide vein of Mn-carbonates and silicates containing disseminated galena (alpha-stage), sulfides, quartz and rhodocrosite.
NKF-R-18-87	10000 level, E-126+25'S	Banded hematite, magnetite, sulfides, quartz, and electrum (alpha stage). Cut by later fractures containing coarse-grained sulfides of stage 1.
NKF-X-24-87	10000 level, below 1S ore body, 30' N of borehole cross-cut.	Coarse-grained sulfides, quartz and late carbonate on chlorite + pyrite alteration (stage-1). Yellow to red-brown sphalerite intergrown with other stage 1 minerals, overgrown by quartz, fluorite, calcite of stage 2.
NKF-AA-24-87	10000 level, E-125	15 cm-wide seam of high-grade ore in vein of Mn-carbonates and silicates. Galena taken from gold-bearing zone (beta stage).

NKF-BB-54-87	10250 level	Finegrained Mn-carbonate, Mn-silicate, and quartz material of α-stage.
NKF-BK-63f-87	10250 level, No. 2 dogleg.	Disseminated sulfides in recrystallized Mn-carbonates and silicates. Finegrained minerals of alpha stage cut by late veins containing red- brown to yellow sphalerite of stage 1, pyrite, chalcopyrite, and quartz and calcite gangue.
NKF-BM-65-87	10250 level, S2	Rounded cobble of fine-grained sulfide containing gold and sphalerite (β stage) in breccia.

Collected by: DMV, David M. Vardiman; GSP, Geoffrey S. Plumlee; NKF, Nora K. Foley.

Table 5. Representative electron microprobe analyses of carbonate from the North Amethyst vein system.

	1	2	3	4	5	6	7
CaO	46.90	24.08	11.75	6.10	48.31	5.83	39.13
MgO	0.25	0.00	0.01	0.00	0.01	0.86	0.11
FeO	0.65	0.59	0.77	0.83	0.23	34.36	0.50
MnO	8.64	34.63	47.20	53.16	8.25	19.93	17.21
SrO	0.14	0.01	0.01	0.03	0.08	0.04	0.09
BaO	0.08	0.00	0.09	0.08	0.09	0.12	0.01
CO2	42.91	39.53	38.49	38.31	43.24	38.98	41.41
TOTAL	99.56	98.85	98.32	98.51	100.21	100.12	98.47
	Number of ions on the basis of 6(O)						
Ca	1.72	0.94	0.47	0.25	1.75	0.23	1.46
Mg	0.01	0.00	0.00	0.00	0.00	0.05	0.01
Fe	0.02	0.02	0.02	0.03	0.01	1.08	0.01
Mn	0.25	1.05	1.51	1.72	0.24	0.63	0.52
Sr	0.00	0.00	0.00	0.00	0.00	0.00	0.00
Ba	0.00	0.00	0.00	0.00	0.00	0.00	0.00
CO3	2.00	2.00	2.00	2.00	2.00	2.00	2.00
m%Ca	85.77	46.81	23.31	12.50	87.68	11.73	73.14
m%Mg	0.63	0.00	0.03	0.00	0.02	2.40	0.30
m%Fe	0.93	0.91	1.23	1.33	0.33	54.00	0.62
m%Mn	12.49	52.26	75.35	86.09	11.84	31.73	25.85

1. NKF-M-13-87, finegrained pale pink calcite from α-1 stage.

2. NKF-BB-54-87, finegrained "kutnahorite" from α-2 stage.

3. NKF-BB-54-87, mediumgrained "poodle-hair" rhodocrosite from α-2 stage.

4. NKF-BB-54-87, mediumgrained pink rhodocrosite of α-1 stage.

5. GSP-MN-24-87, Colorless to pale cream calcite of Stage 2 (intergrown with #7).

6. GSP-MN-1-87, yellowish manganoan siderite of Stage 2 (intergrown with #6).

7. NKF-K-11-87, true pink manganoan calcite of Stage 3.

Table 6. Representative electron microprobe analyses of electrum from the North Amethyst vein system.

	1	2	3	4	5	6	7
Ag	57.52	49.33	42.77	36.76	38.80	33.40	32.90
Au	40.74	49.31	56.02	61.31	59.65	64.34	65.73
TOTAL	98.26	98.64	98.79	98.07	98.45	97.74	98.63
				Atomic proportion			
Ag+1	0.72	0.65	0.58	0.52	0.54	0.49	0.48
Au+1	0.28	0.35	0.42	0.48	0.46	0.51	0.52

1. NKF-AA-27-87, silver-rich electrum grain contained in matrix of siliceous quartz.

2. NKF-AA-27-87, electrum contained in chalcopyrite.

3. NKF-AA-27-87, electrum rimmed by acanthite and uytenbogaardtite.

4. NKF-BM-65-87, electrum grain intergrown with sphalerite, galena and chalcopyrite.

5. NKF-BM-65-87, electrum rimmed by silver minerals including acanthite and uytenbogaardtite.

6. GSP-MM-10a, gold-rich electrum grain entirely rimmed by pyrite.

7. DMV-3a, gold-rich electrum grain contained in pyrite.

Table 7. Representative analyses of manganese silicates from the North Amethyst vein system.

	1	2	3	4	5	6	7
SiO2	45.41	45.64	45.35	47.10	47.06	46.49	45.00
Al2O3	0.13	0.27	0.13	0.55	0.20	0.25	0.32
Fe2O3	0.00	0.00	0.00	0.00	0.00	0.00	-
FeO	1.91	5.87	2.70	2.21	2.98	1.03	1.73
MnO	47.95	47.01	47.79	45.22	43.23	41.79	37.48
MgO	0.42	0.31	0.56	0.39	0.71	0.03	0.47
CaO	3.65	1.51	1.73	6.02	6.32	10.59	6.78
Total	99.47	100.61	98.26	101.49	100.50	100.18	91.78
	Number of ions on the basis of 6(O),						36(O)
Si IV	1.98	1.98	2.00	1.99	2.00	1.98	9.88
Al IV	0.01	0.01	0.00	0.01	0.00	0.01	0.08
T site	1.98	1.99	2.00	2.00	2.00	1.99	10.00
Al VI	-	-	0.00	0.01	0.01	-	-
Fe +3	-	-	-	0.00	-	-	-
Fe +2	0.07	0.21	0.10	0.08	0.11	0.04	0.32
Mn +2	1.77	1.72	1.78	1.61	1.55	1.51	6.97
Mg	0.03	0.02	0.04	0.02	0.04	0.00	0.15
Ca	0.17	0.07	0.08	0.27	0.29	0.48	1.60
M1,M2	2.04	2.03	2.00	2.00	2.00	2.03	9.00

1. NKF-AA-27-2-87, colorless to pale pink crystals of rhodonite having relatively low calcium contents.

2. NKF-AA-27-2-87-3M, pyroxmangite crystal adjacent to (1).

3. NKF-AA-27-2-87-3M, pyroxmangite crystal adjacent to (1).

4. EQ-16-1, fine crystals of rhodonite intermixed with rhodocrosite, calcite and quartz.

5. NKF-Q-17-87, colorless to pink crystals of rhodonite adjacent to vuggy quartz.

6. NKF-M-13-87, calcian rhodonite.

7. Inesite from the Equity vein, FeO determined colorimetrically, MnO by XRF, all other elements by gravimetrics (Van Loenen, 1980).

Table 8. Representative electron microprobe analyses of sphalerite from the North Amethyst vein system.

	1	2	3	4	5	6	7	8	9
Fe+2	0.22	0.80	0.60	1.58	0.67	0.59	4.78	2.12	0.78
Cd+2	0.32	0.34	0.31	0.28	0.53	0.34	0.43	0.34	0.33
Mn+2	0.19	0.80	0.63	0.69	0.24	0.06	0.57	0.56	0.16
S-2	32.69	33.11	32.88	33.03	32.77	33.10	32.96	32.73	32.59
Zn+	66.86	64.99	65.98	64.08	66.56	66.90	61.27	63.48	66.67
Total	100.28	100.04	100.40	99.66	100.77	100.99	100.01	99.23	100.53
Fe +2	0.00	0.01	0.01	0.03	0.01	0.01	0.08	0.04	0.01
Cd +2	0.00	0.00	0.00	0.00	0.00	0.00	0.00	0.00	0.00
Mn +2	0.00	0.01	0.01	0.01	0.00	0.00	0.01	0.01	0.00
S	0.99	1.01	0.99	1.01	0.98	0.99	0.99	1.00	0.98
Zn +2	0.99	0.97	0.98	0.96	0.98	0.99	0.90	0.95	0.98
Total	1.99	2.01	1.99	2.01	1.98	1.99	1.99	2.00	1.98

1. NKF-M-13-87, core of sphalerite crystal occurring in sulfide stringer in finegrained admixture of rhodocrosite, rhodonite, and quartz.

2. NKF-AA-27-87, core of sphalerite crystal occurring in sulfide stringers in finegrained admixture of rhodocrosite, rhodonite, and quartz.

3. NKF-BM-65-87, sphalerite crystal occurring in finegrained gold-bearing sulfide seam containing pyrite.

4. NKF-BM-67-87, sphalerite crystal occurring in finegrained gold-bearing sulfide seam containing pyrite + magnetite + hematite.

5. NKF-X-24-87, coarsegrained lemon-yellow sphalerite crystal of late base-metal mineralization.

6. NKF-R-18-87, colorless sphalerite in coarse-grained banded crystal occurring in veinlet cutting earlier gold-bearing sulfide seam.

7. NKF-R-18-87, red-brown sphalerite in coarse-grained banded crystal occurring in veinlet cutting earlier gold-bearing sulfide seam.

8. NKF-R-18-87, sphalerite from earlier gold-bearing seam containing magnetite + hematite + pyrite, cut by veinlet containing coarser sphalerite (No. 6 and 7).

9. GSP-MN-87, coarse crystals of late-stage yellow sphalerite rimmed with minor chalcopyrite disease.

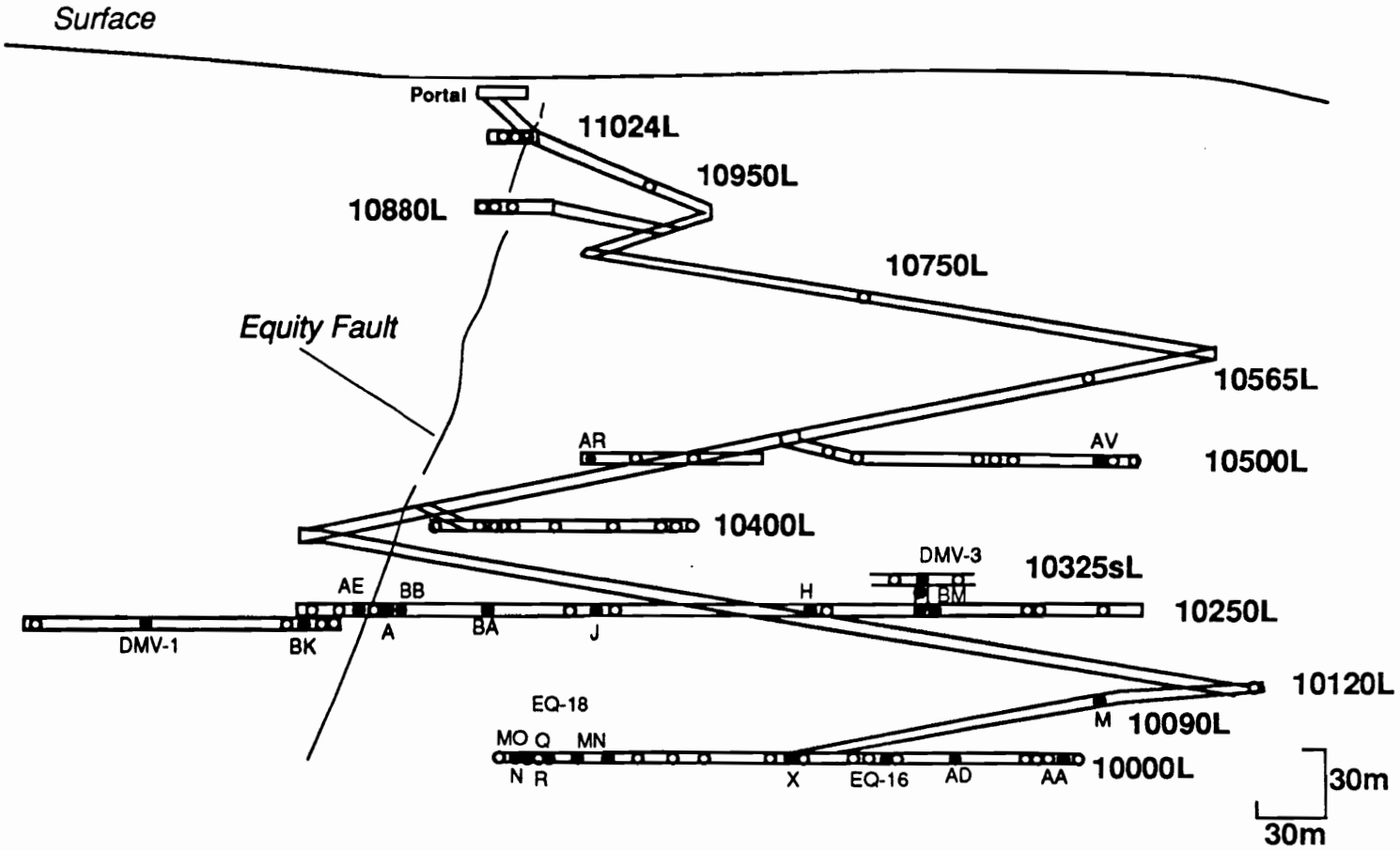

Figure 6. Cross-section view of mine workings, locations of samples used in electron microprobe study are named. See Table 4 for sample descriptions.

Ag-, and Ag-Cu-sulfide minerals

Four silver and copper-bearing sulfide minerals occur in the early gold-rich stage of mineralization - acanthite, jalpaite, mckinstryite, and stromeyerite. These phases were identified based on optical properties and analysis by EDS, but were not examined by XRD. Where possible the compositions were estimated by EDA and electron microprobe analysis. The Cu-Ag-S minerals do not yield reliable temperatures of specific conditions of ore deposition due to their exceedingly fast reaction rates (Skinner, 1966), but are included in this discussion because of their economic importance.

Acanthite (Ag_2S) - Argentite (Ag_2S)

Small (<0.03 mm) and irregularly shaped grains of acanthite occur alone in quartz gangue and at the margins of galena, pyrargyrite, and chalcopyrite grains and as inclusions in pyrite and galena. The silver sulfide is contemporaneous with chalcopyrite and pyrargyrite. It is also found alone, and with polybasite, in association with galena, with chalcopyrite and electrum, and rimming and enveloping rounded grains of galena. Some small (<0.01 mm) and rounded grains are contained within galena, however, no clearcut exsolution textures were observed.

Jalpaite (Ag_3CuS_2)

A soft, light-gray, silver and copper-bearing sulfide mineral with grains 10-25 μm in width found intergrown with or enclosed by acanthite that is in turn bordered by chalcopyrite and galena, is tentatively identified as jalpaite based on an absence of Sb or As, high Ag relative to Cu, good polish, and distinct anisotropism without the striking blue-

violet tints of stromeyerite. The mineral also occurs in aggregates with acanthite and silver-bearing tetrahedrite that are enclosed by gangue.

Mckinstryite ($Ag_{1.3}Cu_{0.7}S$)

Locally, anhedral crystals of mckinstryite (15 μm-wide) are found intergrown with uytenbogaardtite and stromeyerite. The mineral also occurs in late veinlets with silver. While optical properties of this phase closely resemble those of stromeyerite, the two Cu-Ag sulfides can be distinguished optically when intergrown. Identification was confirmed by electron microprobe where possible.

Stromeyerite (AgCuS)

A strong anisotropy compared to acanthite and very slow light etch and composition compared to jalpaite distinguish stromeyerite from those minerals, however, the similarity in appearance, composition, and X-ray pattern between stromeyerite and mckinstryite (Djule, 1958; Skinner, 1966; Skinner et al., 1966) hinder their identification.

A mineral resembling stromeyerite occurs as small <20 μm-wide anhedral grains in aggregates intergrown with chalcopyrite and acanthite, and is associated with wire silver filling cavities and microfractures that cut sulfide-rich zones. It has also been found with jalpaite. Ternary phase relations described by Skinner (1966) for the Cu-Ag-sulfides indicate that while the association stromeyerite + native silver is stable at temperatures reasonable for this deposit, occurrences of stromeyerite with jalpaite or acanthite do not coexist stably. These associations would rapidly react to form mckinstryite, or mckinstryite + jalpaite. In absence of adequate amounts of material for

separation and detailed identification, it is assumed that "stromeyerite" intergrown with jalpaite or acanthite is in fact mckinstryite.

Barite ($BaSO_4$)

This mineral was not found in samples collected from underground workings, however, tabular molds up to 3 cm in length resembling barite do occur in samples from lower elevations in the workings, especially to the south. The mineral is found in drillcore samples from the southern end of the underground workings and in core drilled to the south of the exploratory workings. Tabular and bladed crystals of colorless to pale-cream barite ranging in length from 1-10 mm occur in veinlets with quartz, calcite, and minor pyrite.

Bournonite ($PbCuSbS_3$)

A gray-white phase occurs with galena rimming corroded sphalerite, and as small aggregates of equant to slightly platy grains (<<100 μm) associated with acanthite, electrum, tetrahedrite, chalcopyrite, and galena. Twinning, color adjacent to galena, very slight anisotropy and lack of internal reflections are indicative of bournonite.

Carbonate Group minerals

Carbonate minerals are abundant in all stages of the North Amethyst paragenesis and each stage is characterized by carbonates of different composition, color, and texture. The early Mn-Au association is characterized by three fine-grained carbonates: a manganoan calcite, kutnahorite[2], and a calcian rhodocrosite. The later Base Metal - Silica

2 Capobianco and Navrotsky (1987) recommend that the name kutnahorite be applied to the 50:50 phase having dolomite-type ordering and that naturally occurring phases without any dolomite-type ordering be termed

association contains coarser-grained manganoan calcite, mangano-siderite (oligonite), and a calcian rhodocrosite. Each mineral has a range of compositions; representative analyses are given in Table 5; all analyses are plotted in Figure 7 and listed in Appendix C.

Calcite ($Ca_{.73-.91}Mn_{.26-.09}CO_3$)

Three calcites are distinguished based on paragenetic position, color, and grainsize, however, they overlap in composition. Calcite associated with the early Mn-Au stages is very finegrained (crystals less that 50 lm in width) and occurs intergrown with microcrystalline manganese silicates, rhodocrosite and quartz. Calcite of this stage shows a range in manganese contents from about 10 to about 30 mole percent $MnCO_3$. They are intergrown with rhodocrosite and kutnahorite. Peacor et al. (1978) has suggested a possible solvus between calcite and kutnahorite to account for the compositions of some natural carbonates, comparison with the North Amethyst data suggests temperatures of formation above 350°C (Figure 8).

Calcite that occurs in the early stages of the Base Metal - Silica association is colorless to pale yellow, and generally has lower manganese contents than other analysed carbonates (9-15 mole percent $MnCO_3$). The crystals range in size from a few millimeters to 2-3 centimeters and are intergrown with 0.1 to 1.0 mm-wide grains of oligonite, the manganoan siderite.

---

pseudokutnahorite. The fine-grained nature of these samples hindered their characterization, hence, ordering (or the lack of ordering) is not implied by the use of "kutnahorite".

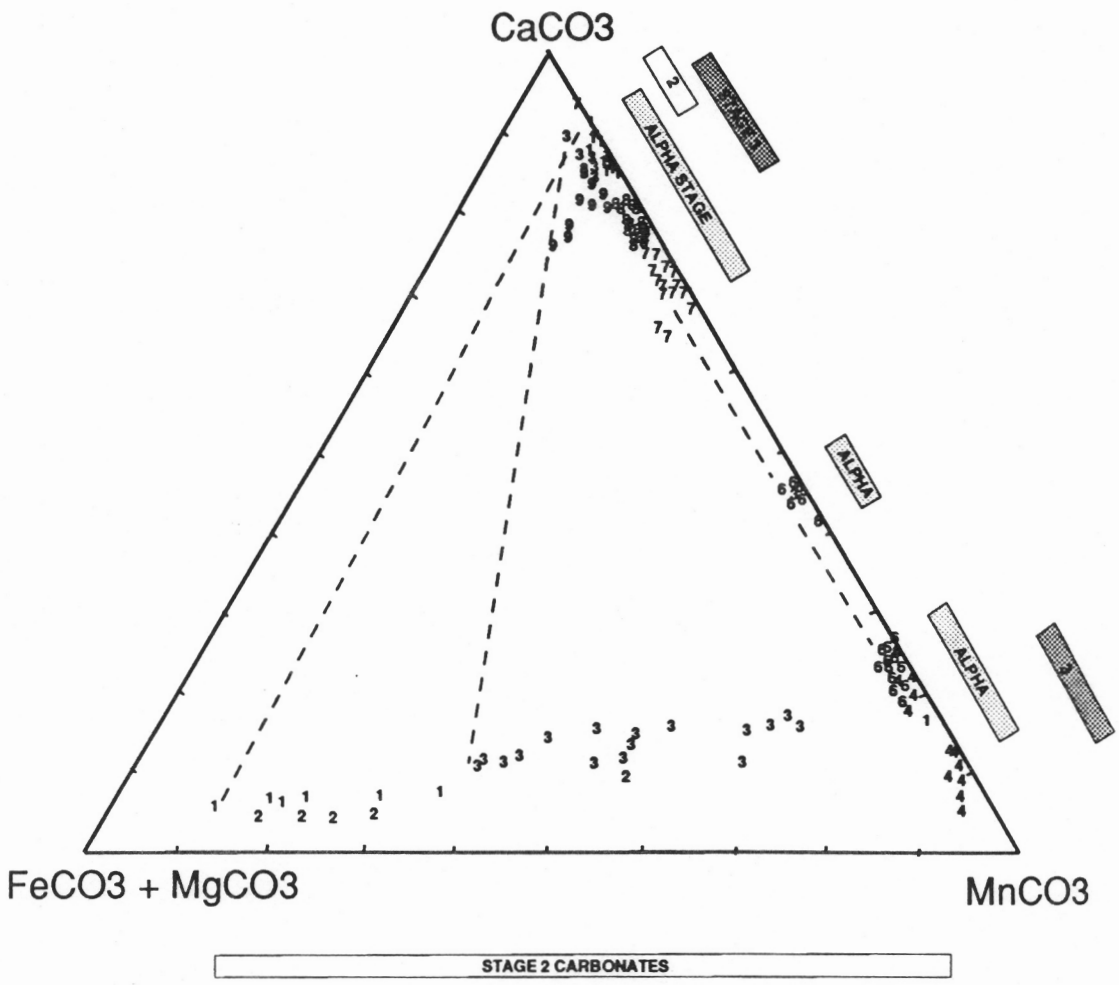

Figure 7. Ternary diagram showing compositions of carbonates for three stages of the North Amethyst vein mineralization. Numbers refer to sample localities listed in Table 4. Bars show range of compositions for carbonates present in more than one stage. Possible tie-lines are dashed.

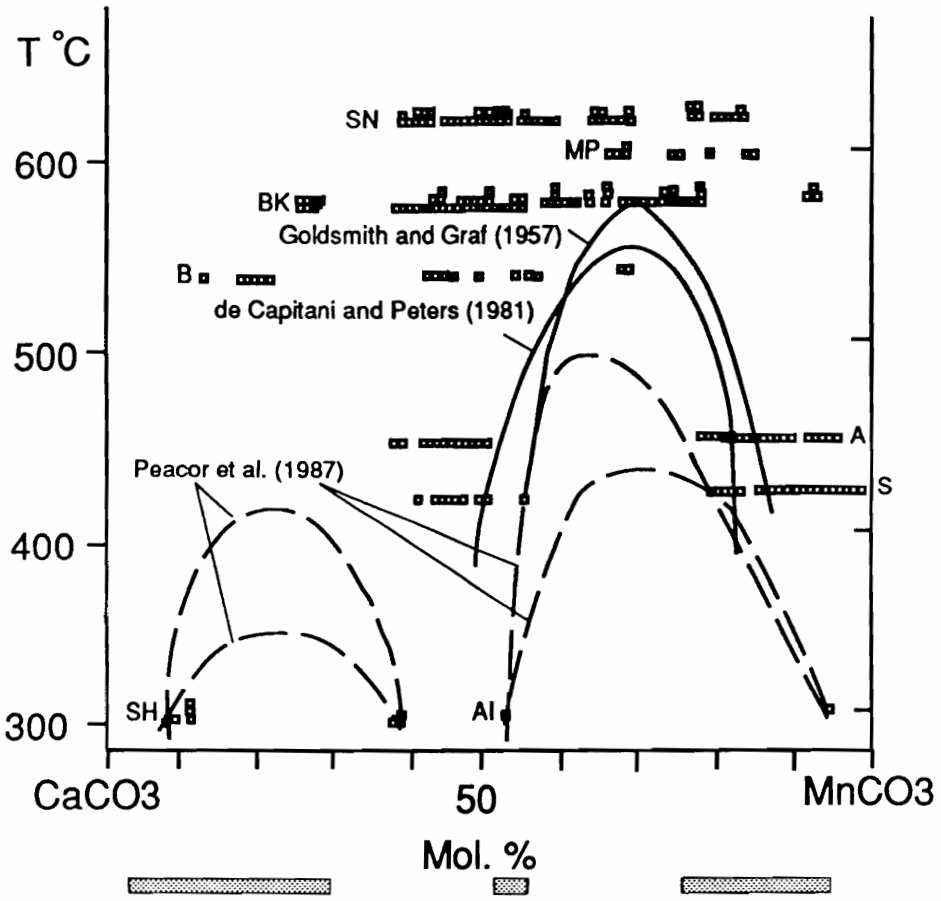

Figure 8. Compositions of carbonates from Alpha stage mineralization plotted as bars below CaCO3-MnCO3 binary showing proposed solvii from experimental studies (solid lines) and studies of naturally occurring carbonates (dashed lines). Carbonate studies include: SN, Serro do Navio (Scarpelli, 1970); S, Scerscen (Bernina), A, Alagna, N. Italy, MP, Muretta Pass (Peters et al., 1978); B, Buritirama (Parana) (Peters et al., 1977); BK, Bald Knob (Winters et al., 1981); AL, Andros Island; SH, Sterling Hill, (Peacor et al., 1987). After deCapitani and Peters (1981).

The last stage of the Base metal - Silica association is composed dominantly of a pink to pale cream manganoan calcite, especially in the northern part of the ore zone. Thick crusts up to 15 cm in thickness of crystalline carbonate are found mainly lining late vugs and open-spaces in the vein. The compositional range for this calcite is similar to calcite of the Mn-Au stages.

Kutnahorite, ($Ca_{.47}Mn_{.52}CO_3$).

A manganese and calcium-bearing carbonate having a composition equivalent to kutnahorite, the manganese analog of dolomite, has been identified intergrown with finegrained rhodrocrosite, Mn-calcite, and Mn-silicates of the early association (Table 5). X-ray diffraction analyses of the mixture suggested primarily quartz, rhodonite, pyroxmangite, and carbonate having a wide range of Ca-Mn solid solution. Microprobe analyses of the carbonates yield some compositions in the range $Cc_{46}Rc_{54}$ to $Cc_{53}Rc_{47}$ with less than 1% $(Fe,Mg)CO_3$. The material is too finegrained to permit single crystal X-ray study to determine if the kutnahorite is ordered; long-range cation ordering kutnahorite is not detectable using conventional powder X-ray diffraction techniques (Peacor et al., 1987).

Rhodocrosite ($\sim Mn_{.86-.76}Ca_{.13-.24}CO_3$)

In the early Mn-Au association, rhodocrosite is the most abundant carbonate and occurs in an microcrystalline (<50 μm) admixture composed mainly of rhodonite, quartz, and Mn-calcite. The admixture is zoned mineralogically on the scale of 100's of micrometers, and coarser rhodocrosite (up to 0.5 mm in width) occurs in some of the zones and in patches that cut across zones. The patches consist of mats of

intergrown curls that resemble poodle-hair and are thus termed poodle-hair rhodocrosites. Compositions of the poodle-hair rhodocrosites are similar to, and as calcic as, those of the finer-grained material (up to $Cc_{24}Rc_{76}$).

In the Base Metal - Silica association rhodocrosite is associated with amethystine quartz and fluorite. Rhodocrosite also occurs in most later stages of the North Amethyst paragenesis in small (<5 mm wide) veinlets, and as 1-5 mm-wide, near-gem-quality crystals that line small vugs and perch on earlier mineralization.

Rhodocrosites intergrown with kutnahorite in the earliest assemblage suggest temperatures in excess of 425°C and possibly in excess of 500°C. The most Ca-rich rhodocrosite has a composition of $Cc_{23}Rc_{75}$ and contains less than 2 mole percent combined $FeCO_3$ + $MgCO_3$. This composition is somewhat less calcic than the critical point of the $CaCO_3$-$MnCO_3$ solvus as reported by deCapitani and Peters (1981) at 540°C and a composition of $Cc_{32}Rc_{68}$ (Experiments were run at 2 and 10 kb, no significant differences due to pressure were detected; deCapitani and Peters, 1981) . When compared to possible solvii consistent with natural and experimental systems proposed by Peacor et al. (1987), rhodocrosites and kutnahorites from the North Amethyst indicate temperatures above 425°C (kutnahorite-rhodocrosite; Figure 8). Temperatures above 300°C are unusual for mineralization occurring in the typically shallow epithermal environment (Heald et. al., 1987), however, a probable minimum of 1500 meters of rock overlay the base of North Amethyst mineralization (Foley, 1990b; Lipman and Sawyer, 1988). A simple analysis based on temperature-depth calculations of Haas (1971)

indicates that the boiling point of a nonsaline fluid at 1500 meters is about 320°C, more saline fluids would boil at higher temperatures; thus, temperatures in the range of 350°C for the North Amethyst ores, though unusual, are not unreasonable (Foley, 1990b).

Rhodocrosites from all later stages of mineralization have a more restricted compositional range and lie outside experimental solvii (Goldsmith and Graf, 1957; diCapitani and Peters, 1981) at temperatures of less than 400°C.

Siderite, manganoan ($Fe_{.57}Mn_{.32}Ca_{.11}CO3$)

Iron- and manganese-bearing carbonate oligonite is found in one assemblage of the later base-metal silica association. The mineral occurs as discrete crystals 0.1 to 1.0 mm-wide within a coarser calcite (see above). The carbonates are intergrown primarily with chlorite, quartz, hematite, and minor adularia and sphalerite, and were deposited just after a major period of base metal mineralization.

Wetlaufer (1977), in a study of carbonate minerals occurring in the central and southern parts of the Creede district documented significant compositional variations in rhodocrosite and siderite. She found that Bulldog Mountain rhodocrosite compositions from the early pre-ore stage lie along the $FeCO_3$-$MnCO_3$ join and typically contain 68-93 mole percent $MnCO_3$. $CaCO_3$ contents vary from 2 to 15 mole percent and $MgCO_3$ contents are generally less than 4 mole percent. A later intra-ore siderite-manganosiderite stage was found to contain 33 to 94 mole percent $FeCO_3$, 6 to 67 mole percent $MnCO_3$, 1 to 13 mole percent $CaCO_3$ and 1 to 10 mole percent $MgCO_3$.

Chalcopyrite ($CuFeS_2$)

Chalcopyrite is abundant in three sulfide-bearing stages of mineralization and is not found in stages composed dominantly of gangue. Size is highly variable; diameters of the irregular grains range from a few micrometers to a few millimeters. Earlier occurrences are generally finer-grained, than later occurrences.

Chalcopyrite is generally later than, and replaces, sphalerite and extensive chalcopyrite disease textures are present in all sphalerite-bearing stages. Micrometer-sized grains are rounded to rod-shaped and are generally concentrated at the rims of sphalerite crystals.

In earlier stages, chalcopyrite is found in sphalerite and as somewhat larger separate grains bordering and corroding sphalerite. Allotriomorphic grains of chalcopyrite are found intergrown with galena, tetrahedrite, silver minerals, and electrum filling spaces around crystals of sphalerite and pyrite.

In the later stages, chalcopyrite occurs as anhedral grains bordering sphalerite and is commonly intergrown with galena. It also occurs as isolated grains that are entirely surrounded by quartz and carbonate gangue.

Oxidation of the chalcopyrite to bornite, chalcocite and covellite has been reported for the North Amethyst ores (S. Caddey, D. Vardiman, pers. commun., 1988), but this was not observed in any of the samples studied.

Chlorite ($A_{5-6}Z_4O_{10}(OH)_8$, A=Al,Fe^{2+},Fe^{3+},Mg,Mn;Z=Al,Fe^{3+},Si)

In the North Amethyst veins, chlorite primarily occurs in the later association where it is intergrown with hematite, quartz, pyrite.

Assemblages containing the finegrained (<100 μm-wide flakes) green layer silicate formed just prior to, and concurrently with, the period of major base metal sulfide mineralization in the later association. Some chlorite is also found intergrown with quartz and calcite deposited after the base metal sulfides.

No quantitative compositional data are available for North Amethyst chlorites. They are iron-rich like other Creede chlorites (Barton, et al., 1977), and contain substantial manganese (by EDA).

Electrum ($\sim Au_{0.3-0.5}Ag_{0.7-0.5}$)

Electrum is characteristic of one early stage of the North amethyst paragenesis. The mineral is intimately intergrown with a variety of base-, and precious-metal sulfides and generally formed late with respect to the base-metal sulfides. The whitish-yellow silver-rich grains (Figure 9) occur most frequently as small rounded inclusions (3 to 25 micrometers) in chalcopyrite and uytenbogaardite, although they are also found in acanthite, pyrargyrite, and galena. More rarely electrum occurs as small (3-30 micrometers) separate grains in quartz gangue, and adjacent to sphalerite aggregates rimmed with galena and chalcopyrite. Larger grains, up to 75 micrometers in diameter and visible in hand speciman, occur with pyrargyrite, chalcopyrite, and galena. They fill interstices between, and in part replace, sphalerite grains at lower elevations in the mine. Representative electrum compositions are given in Table 6 and plotted in Figure 9. Analysed electrum contained entirely within pyrite (No. 6, 7, Table 6) has slightly higher Au contents than electrum rimmed by chalcopyrite or Au-Ag sulfides.

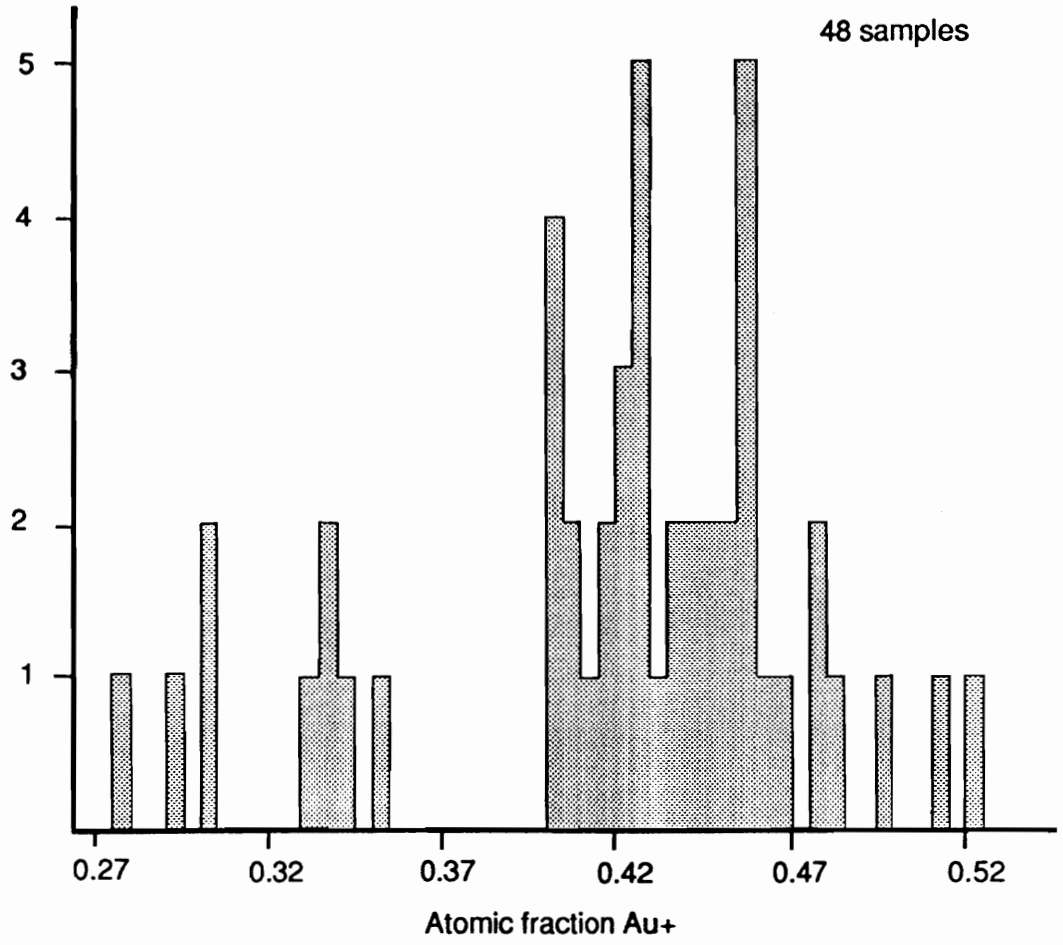

Figure 9. Histogram of gold content of electrum occurring in Beta-stage assemblages.

Fluorite (CaF_2)

Large cubes of fluorite up to 13 millimeters on a side are found lining vugs, veins, and cavities in the North Amethyst vein system. The crystals are most frequently green; purple and colorless varieties are less common. No clearcut relationship between color and paragenetic position was discerned. Fluorite is generally late in the paragenesis and usually grows on quartz, however, many late quartz crystals contain numerous small octahedra of colorless to palest green fluorite indicating near contemporaneous deposition. Fluorite crystals are sometimes dusted with fine gray quartz sediment that is overgrown by coarse cream-to-pink, manganese-rich calcite and/or pyrite. In small vugs, fluorite may follow quartz and adularia.

Galena (PbS)

Galena occurs in both principal sulfide stages of the North Amethyst paragenesis. It generally occurs intergrown with chalcopyrite and is similar to chalcopyrite in size range and texture where they are found together.

In the earlier association, galena is found as isolated anhedral grains and in aggregates bordering and corroding sphalerite and pyrite in a gangue of fine-grained manganese carbonates, manganese silicates and quartz. In sulfide-rich assemblages, galena is usually in mutual contact with chalcopyrite, pyrargyrite, acanthite, uytenbogaardtite, acanthite, and polybasite. Occasionally bournonite rims some galena. Micrometer-wide rounded grains of galena also occur along fractures in

the outer zones of sphalerite crystals and larger grains (10-100 μm-wide) in an almost equigranular mix of sphalerite and chalcopyrite.

In the later mineral association, anhedral grains and aggregates of 2-3 mm-wide galena are found bordering sphalerite or enclosed by gangue. The galena is often intergrown with chalcopyrite or tetrahedrite. The generally allotriomorphic texture of galena and the occurrence along cracks in sphalerite crystals suggests that it may have formed slightly later than sphalerite and pyrite. Skeletal crystals of galena also grow on sphalerite and project into quartz and calcite filled vugs.

Gypsum ($CaSO_4 \cdot 2H_2O$)

Large curls of gypsum ranging in size from a few centimeters to tens of centimeters are found in open vugs and cavities along the vein structures. Gypsum having a fine-grained foam-like texture also occurs in vugs and cavities. These crystals certainly formed later than all of the ore stage minerals, and probably are of recent (modern) age.

Hematite (Fe_2O_3)

Hematite, the most abundant iron oxide mineral, occurs in both mineral associations of the North Amethyst paragenesis. It is found intergrown with precious- and base-metal sulfides, and other iron oxides in the earlier association, and intergrown with quartz, chlorite and base-metal sulfides in the later association.

Blades of hematite, 0.1 to 1.0 mm long, in electrum-bearing samples of the earlier association are intergrown with rounded anhedral magnetite grains (<50 μm in diameter) and cubes of pyrite. In some sections, the hematite is replaced by magnetite, in other areas the

hematite has altered to a finegrained limonite. Abundant hematite colors some ore samples a deep red hue.

Thin, transparent-red, hematite flakes having well-developed hexagonal outlines occur in the later association as fine to medium grained crystals (<60 μm wide) intergrown with quartz, chlorite, pyrite, sphalerite, galena, and chalcopyrite. The flakes are also included in sphalerite and quartz crystal where they frequently are clustered along colored growth zones.

Manganese-silicate minerals

At least four Mn-silicate minerals occur in the earliest assemblage of the North Amethsyt ores. Rhodonite is the most abundant by far, pyromangite, caryopilite (?), and inesite occur in much smaller quantities. The complete assemblage includes rhodocrosite, quartz. Kutnohorite and Mn-calcite are also present in small amounts.

Caryopilite ($Mn_6Si_4O_{10}(OH)_8$)

Radiating sheaths of a red-brown hydrated layer silicate (~<0.01x0.05 mm) are found in small matted 2 mm-wide clumps in the early Mn-Au association. The mineral has been tentatively identified as caryopilite based on petrography and EDA.

Inesite ($Ca_2Mn_7Si_{10}O_{28}(OH)_2 \cdot 5H_2O$)

Acicular crystals of inesite (Table 7) up to 2 cm in length form radiating sheaths that fill fractures cutting silicified wallrock and early manganese-carbonate and -silicate-bearing assemblages in higher levels of the North Amethyst workings. Minerals intergrown with the coarse pale pink to flesh-colored crystals include quartz, rhodocrosite, manganese calcite, galena, sphalerite, pyrite, and pyrargyrite.

Pyroxmangite ($Ca_{.04}Mn_{.89-.86}Fe_{.05-.1}Mg_{.02.01}SiO_3$)

Pyroxmangite (Table 7, Figure 10) is present in the earliest stage of mineralization. The mineral ranges in size from a few micrometers to, at most, 100 micrometers in length and is tentatively identified by X-ray diffraction analysis, petrographic study, and electron microprobe analysis, but, has not been confirmed by single crystal techniques. It is found intergrown primarily with rhodocrosite, rhodonite, and quartz. Microprobe analyses of the mineral (Table 7) show a small variation in calcium, iron, and manganese.

Rhodonite ($Ca_{.08-.24}Mn_{.88-.76}SiO3$)

Rhodonite is the most abundant manganese silicate present in the early stages of the paragenesis (Table 7, Figure 10). The mineral occurs primarily in a cryptocrystalline admixture of quartz, carbonates, and other manganese silicates and as coarser crystal edging small quartz-filled vugs. The coarser-grained crystals range up to 50 micrometers in width and 200 μm in length.

Pyroxmangite and rhodonite are polymorphs of $MnSiO_3$. Rhodonite is the high temperature form and is stable above about 350^{o}C at pressures of 1-2 kb (Maresch and Mottana, 1976). The presence of both rhodonite and pyroxmangite can be used to constrain temperature if the compositions do not depart markedly from $MnSiO_3$, and pressure is known. In this case because up to 11 weight percent CaO and 2 weight percent FeO + MgO replaces MnO, and pressures are not well constrained (Foley, 1990b), the assemblage can only be used qualitatively. To a first approximation based on ionic radii, the substitution of Mg+ and Fe+

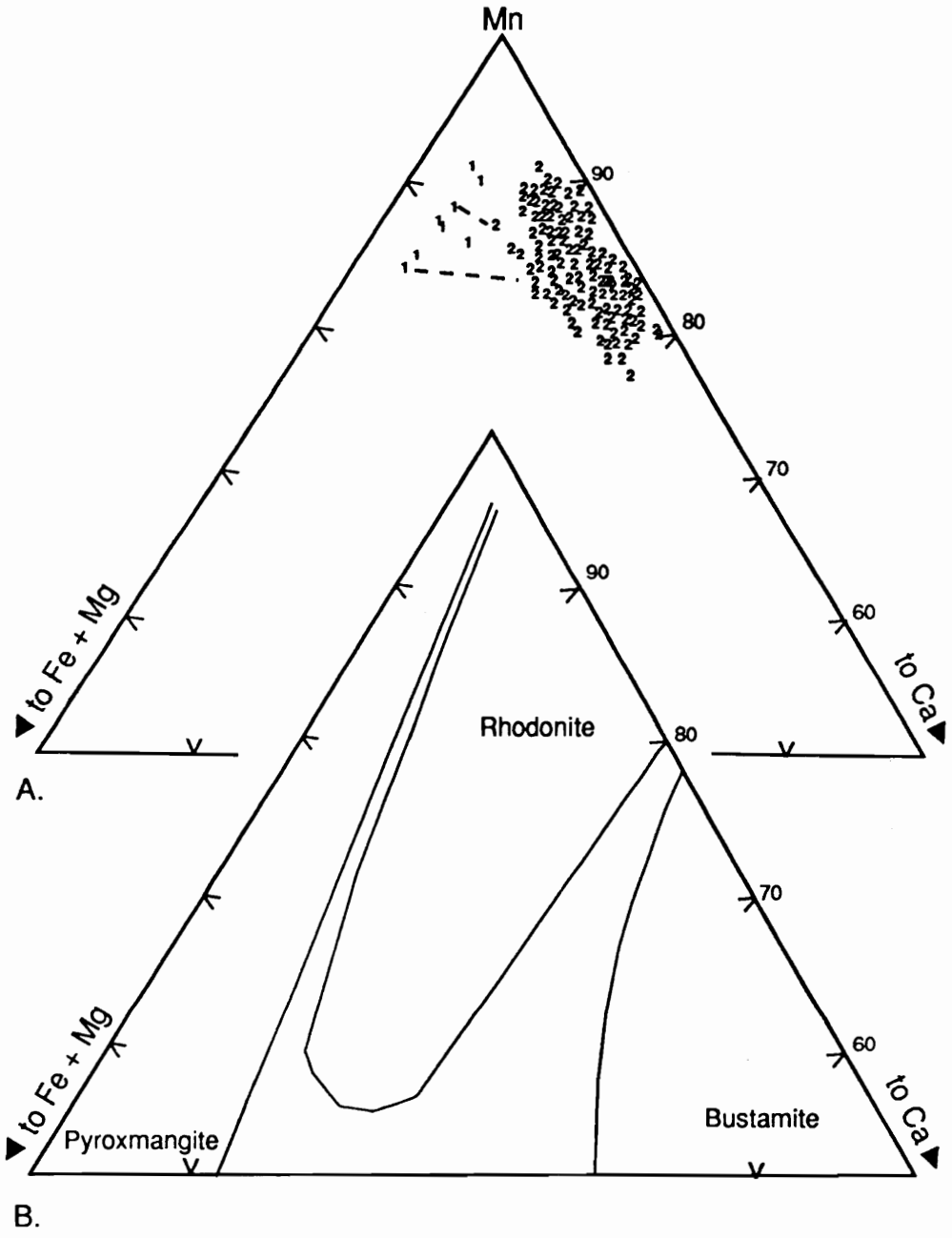

Figure 10. a) Compositions of all pyroxmangite and rhodonite analysed for Alpha stage mineralization. See Table 4 for sample descriptions and text for discussion. Possible tie-lines are dashed. b) Plot of stability fields consistent with well characterized naturally occurring pyroxenoids in metamorphic environments (estimated at 650 +/- 100 °C for all occurrences; from Peacor et al., 1978, after Ohashi et al., 1975).

would stabilize pyroxmangite at higher temperatures, whereas the substitution of Ca+ should stabilize rhodonite to lower temperatures (Maresch and Mottana, 1976). Pyroxmangite of $MnSiO_3$ composition is the stable phase at atmospheric pressure below 350-405°C (Maresch and Mottana, 1976).

Magnetite ($FeFe_2O_4$)

Magnetite is found in the earlier mineral association of the North Amethyst paragenetic sequence, and is primarily associated with hematite and pyrite in a quartz-rich gangue. It occurs as equant grains (<0.5 mm-wide) intergrown with euhedral pyrite and laths of hematite, and as replacement of hematite. Some magnetite contains minute micrometers-sized blebs of electrum.

Marcasite (FeS_2)

Characteristic reflection pleachroism and strong anisotropy distinguish marcasite from other iron sulfides. The mineral occurs primarily as 50-100 micrometer-wide tabular or carrot-shaped crystals growing on pyrite and, at times, is coated with chalcopyrite. Anhedral marcasite is found coating and filling cracks in pitted crystals of pyrite.

Polybasite ($(Ag,Cu)_{16}Sb_2S_{11}$)

Polybasite occurs with galena, marginal to and replacing sphalerite, and at times, intergrown with chalcopyrite. It is most commonly associated with acanthite and generally is late. The softness of the mineral, light etching, and darker color adjacent to galena help to distinguish it from pyrargyrite.

Potassium feldspar ($K_{.98-.92}Na_{.01-.07}AlSi_3O_8$)

Feldspar occurs as anhedral to subhedral grains extensively replaced by fine-grained manganese-carbonate, rhodonite and other manganese silicates, and quartz in the earliest vein stage. The feldspars vary in composition from Or_{93} to Or_{96} and have barium contents that vary from ~0.1 to 2.4 weight percent BaO (Appendix C). These feldspars are compositionally similar to wallrock phenocrysts adjacent to the veins except for local high barium contents, and may have been incorporated into the vein during formation of the earliest stages of mineralization.

Potassium feldspar also occurs as 0.1 to 1.0 mm-long euhedral barium-rich crystals of adularia intergrown with amethystine quartz and filling small vugs, cavities, and fractures in most vein material. Adularia ranges in Or contents from 92 to 98 and contains 0.4 to 1.6 weight percent BaO (Appendix C).

Pyrargyrite (Ag_3SbS_3) - Proustite (Ag_3AsS_3)

Pyrargyrite primarily occurs alone in small (>10 micrometer) anhedral grains scattered through a silicious gangue, and in aggregates with acanthite that border galena and sphalerite. It also occurs intergrown with acanthite and native silver in aggregates that border or are enclosed by chalcopyrite. Other grains are intergrown with acanthite and uytenbogaardite, and rim chalcopyrite, tetrahedrite, and galena. Subhedral prismatic to anhedral crystal aggregates are enclosed by rhodochrosite and quartz, and occur along cracks in broken pyrite cubes.

Pyrite (FeS_2)

Pyrite is one of the most abundant and ubiquitious sulfide minerals, occurring in almost all stages of both mineral associations. It is primarily associated with either quartz-chlorite-hematite or other base-metal sulfides. Pyrite shows idiomorphic crystal development and appears to be early in all occurrences. Cubes are the most common shape, although some overgrowths and aggregates are anhedral. Thin botryoidal crusts of pyrite occur locally late in the paragenesis.

In the early association, subhedral equant pyrite crystals are bordered by sphalerite, rimmed by chalcopyrite, galena, and contain inclusions of all three. The crystals range in size up to a millimeter on edge, however, most are in the range 0.1 to 0.3 mm. Some of these crystals also contain rounded blebs of electrum. Grain margins of the pyrite crystals are often corroded and replaced by sphalerite and galena.

Some crystals are isotopic to faintly anisotropic and twinned. There is often a zonal arrangement with sphalerite, acanthite, and pyrargyrite crystals suggesting that while pyrite began to crystallize early, deposition continued as other sulfides and sulfosalts began to form. Later pyrite overgrowths on these crystals do not show inclusions. Rarely, marcasite crystals sit on pyrite. Pyrite also occurs as isolated equant cubes in quartz and carbonate gangue.

In the later association, euhedral pyrite is found in a mix of quartz, hematite and chlorite, and intergrown with euhedral sphalerite and anhedral galena and chalcopyrite. The crystals are much larger in size, and pyrite cubes of up to a centimeter on edge occur, although

rarely. Most pyrite crystals in this association are a millimeter or less on a side. Pyrite crystals in the size range 0.1 to 0.5 mm dust singly terminated quartz crystals and coarse crystalline calcite (Figure 5e) in the latest stage. They also occur as millimeter-thick layers within generations of carbonate. At times, 50-100 micrometer-sized carrot-shaped marcasite crystals overly this latest pyrite.

Quartz SiO_2

Quartz occur in all mineralogical stages and shows a variety of textures ranging from cryptocrystalline interlocking grains to large terminated euhedral crystals. Quartz also occurs as a chalcedonic cementing medium in many breccias.

In the early stages of mineralization, <50 μm-sized quartz is intergrown in a microcrystalline mix of manganese-silicates and -carbonates. It fills barite molds and small vugs that occur within the mix.

In later stages, quartz occurs most often as larger (0.2 cm - 5 cm) crystals intergrown with base-metal-sulfides, fluorite, and calcite. Where they project into vugs, the crystals are euhedral and terminated. Much of the quartz is amethystine, especially the outer parts of crystals. The larger crystals contain solid inclusions, including fluorite octahedra, laths of rhodonite (?), and carbonate crystals. Fluid and solid inclusions often are found decorating acicular structures that radiate from the bases of the quartz crystals.

Quartz also forms the cement for many of the breccias and sediments found within the ore zones. Quartz cement is generally gray in color and chalcedonic, coarser areas show a granular textures with

quartz overgrowths. In some samples, the quartz has sutured grain boundaries. One of the breccias has a distinctive black quartz cement; the color apparently results from fine sulfides and electrum admixed with the quartz. Some sedimented areas consist of fine parallel laminations, distinguished by subtle variations in color and grain size. The chalcedonic laminations have a mosaic texture, with sutured grain boundaries between fine crystalline quartz, that may reflect recrystallized amorphous silica sediment.

Silver (Ag^{o})

Native silver occurs primarily alone as scarce 10-100 μm-sized grains in fractures, and as millimeter-long wire aggregates in cavities or resting on broken surfaces. It is also found as scarce grains enclosed by gangue that border galena, and are rarely bordered by acanthite. In some samples it borders sphalerite in aggregates that include chalcopyrite and jalpaite and possibly stromeyerite. Textural relationships indicate that native silver occurs much later in the paragenetic sequence than most other silver minerals.

Sphalerite (Zn,Fe,Mn,Cd)S

Sphalerite is one of the most abundant sulfide minerals in the deposit. The mineral is found in two stages of the early Mn - Au assocation and in one stage of the later Base Metal - Silica association. Sphalerites in different stages vary in grain size, color, and composition.

Small (<2 mm) rounded grains of intensely chalcopyritized sphalerite occur in small stringers in some of the cryptocrystalline admixture of manganese silicates and carbonates and quartz that comprise

the earliest stage. The mineral is intergrown with cubes of pyrite and anhedral galena and contains generally low and subequal amounts of iron, cadmium, and manganese (Table 8, No. 1, 2).

Abundant sphalerite also is present in the precious and base-metal seams of the Mn-Au association. The zinc sulfide is often rimmed and replaced by electrum, pyrargyrite, acanthite, chalcopyrite, uytenbogaardite, and galena. Sphalerite corrodes and sometimes replaces pyrite. Small equant grains also occur in siliceous gangue, with sparse micron-sized exsolution blebs of chalcopyrite. Sphalerite is bordered and corroded by all of the other sulfides, especially galena and chalcopyrite, and tetrahedrite. All sphalerite of this stage is extensively chalcopyritized, and most crystals have a composition similar to that of the stage described above (Table 8, No. 3). An important exception to this is that sphalerite intergrown with magnetite and hematite has a more iron-rich composition (Table 8, No. 4, 8), generally containing around 2 percent iron by weight.

Sphalerite crystals of the later base-metal stage range in width from about a millimeter to a maximum of about 2 centimeters, and in hue from colorless to greenish to pale-yellow to dark red-brown. The subhedral, equant crystals form aggregates that are intergrown with galena, euhedral pyrite, chalcopyrite, and minor tetrahedrite. All sphalerite of this association is chalcopyritized, the crystals contain numerous microscopic inclusions of chalcopyrite that are especially abundant at the rims. Some grains are tetrahedritized; abundant minute blebs of tetrahedrite are concentrated at grain boundaries.

While most grains are uniform in color, many larger crystals of sphalerite are colorbanded on a simple scale. The colors falling into three groups - red-brown, yellow and colorless - that show only minor color variation. On the scale of individual crystals, the contact between colors is sharp rather than gradational.

The majority of the banded samples studied have colorless or yellow cores and red-brown rims (thin section thicknesses ranging from 60 micrometers to 1 millimeter). Rims are more finely banded than cores, in shades ranging from moderate red-brown to deep red-brown, however, they still do not show the beautifully well-developed banding of samples typical of the OH vein in the main Creede district as described by Barton et al., (1977) and Roedder, (1977). Other samples show an alternating set of color bands, from red-brown to yellow to red-brown; these are less common. No attempt was made to correlate color-banding in the sphalerite because of the lack of continuity of possible marker horizons.

Analysed sphalerite from the later stages displays higher and more variable iron contents (up to 8 mole percent FeS) than earlier sphalerites (Table 8, No. 5, 6, 7, 8). Some of the darkest sphalerites were not analysed, so the true range may be higher. Measured iron contents are not as high as those of sphalerite from the OH vein of the main mining district (Barton et al., 1977), which contain up to 16 mole percent FeS, but the most typical contents of North Amethyst sphalerite (~1 mole percent FeS) are similar to the most typical contents of OH sphalerite (~1-2 mole percent FeS).

Stephanite (Ag_5SbS_4)

A silver sulfosalt resembling stephanite occurs intergrown with pyrargyrite and polybasite in aggregates in a siliceous matrix. It is also found alone filling cavities and fractures in the siliceous matrix.

Tetrahedrite-tennantite, argentian $(Cu,Fe,Ag,Zn)_{12}(Sb,As)_4S_{13}$)

Tetrahedrite occurs in all sulfide-bearing stages, usually in association with sphalerite, galena, pyrite, and chalcopyrite. Reported to be silver-rich (S. Caddey, C. Byington, D. Vardiman, pers. commun., 1987), energy dispersive analysis confirms that much of the tetrahedrite contains appreciable amounts of silver and arsenic.

In the early association, tetrahedrite is found most often adjacent to sphalerite and galena, and in aggregates with chalcopyrite and acanthite. Scarce anhedral grains of tetrahedrite occur marginal to and intergrown with chalcopyrite and acanthite. The mineral also occurs with polybasite, intergrown with pyrargyrite and acanthite, alone, and intergrown with galena and chalcopyrite in cavity fillings.

In the later association, 50-70 μm-sized tetrahedrite is found most often with contemporaneous chalcopyrite and galena in aggregates that border sphalerite. Rounded micrometer-sized grains of tetrahedrite are found in sphalerite in a texture similar to that of chalcopyrite disease.

Growth banding was not observed in any of the samples, possibly due to their small grain size. Growth banding is described in tetrahedrite from the Bulldog vein of the Creede district (Plumlee, 1989). Plumlee found that the growth bands reflected compositional variations in Ag, As, and Sb.

Uytenbogaardtite (Ag_3AuS_2)

Uytenbogaardtite most often occurs intergrown with acanthite containing micrometer-sized electrum (~$Au_{.3-.4}Ag_{.7-.6}$) grains. When intergrown with acanthite, uytenbogaardtite can be readily distinguished from the acanthite, and from many other silver minerals, by its extremely rapid light etching. Small and irregularly-shaped anhedral grains of uytenbogaardtite also occur alone, or in contact with other minerals such as pyrargyrite, and especially, chalcopyrite.

Experimental work by Barton (1978) demonstrated that uytenbogaardtite is stable at relatively low temperatures (<200°C) with gold-bearing argentite, but that only below 113°C can uytenbogaardtite coexist with acanthite. Barton also showed that uytenbogaardtite is stable with relatively Au-rich electrum compositions (0.8-0.9 atomic fraction Au). The textures described above are similar to those described by Barton et al. (1978) for uytenbogaardtite from the Comstock lode; they suggested that the textures may reflect exsolution during cooling of a higher temperature gold-bearing argentite + silver-rich electrum assemblage. Upon cooling the argentite would exsolve uytenbogaardtite leaving the original silver-rich electrum with acanthite and uytenbogardtite.

MINERAL ASSOCIATIONS AND ASSEMBLAGES

The ore and gangue mineralization of the North Amethyst vein system is paragenetically complex; the two associations are mineralogically, texturally, and chemically distinct. The associations overlap spatially, but were separated in time by a period of extensive

brecciation and sedimentation. The earlier association is characterized by two mineralogic stages, whereas the second, later association is subdivided into three stages on the basis of mineralogy and textural relationships. Successive stages in each association are generally marked by relatively sharp rather than gradational changes in mineralogy, and by periods of movement, brecciation, sedimentation, or replacement. In only a few instances are the transitions characterized by intergrowths or interbanding between mineral assemblages of adjacent stages.

A flowchart (Figure 11) describes the sequence of events relating to formation of the North Amethyst mineralization. The general sequence of mineral deposition is shown in Figure 12. Temporal and spatial relationships between mineralization, brecciation, and sedimentation are shown in a series of diagrams beginning with Figure 13.

Alteration and Pre-ore Vein Assemblages

Several types of wallrock alteration have been observed in the North Amethyst vein system. These include intense sericitic alteration at higher levels in the system, two stages of potassium metasomatism of the wallrock at depth, and a bleaching of the wallrock adjacent to some vein structures at all levels (Figure 11, 13). A detailed examination of the alteration assemblages was beyond the scope of this study, and is unwarranted because of existing regional studies of alteration relationships in the Creede area underway by P. Bethke, D. Sawyer and others. However, certain observations can be made on the basis of field relations, hand sample study, geochemical variations, and some X-ray diffraction analysis.

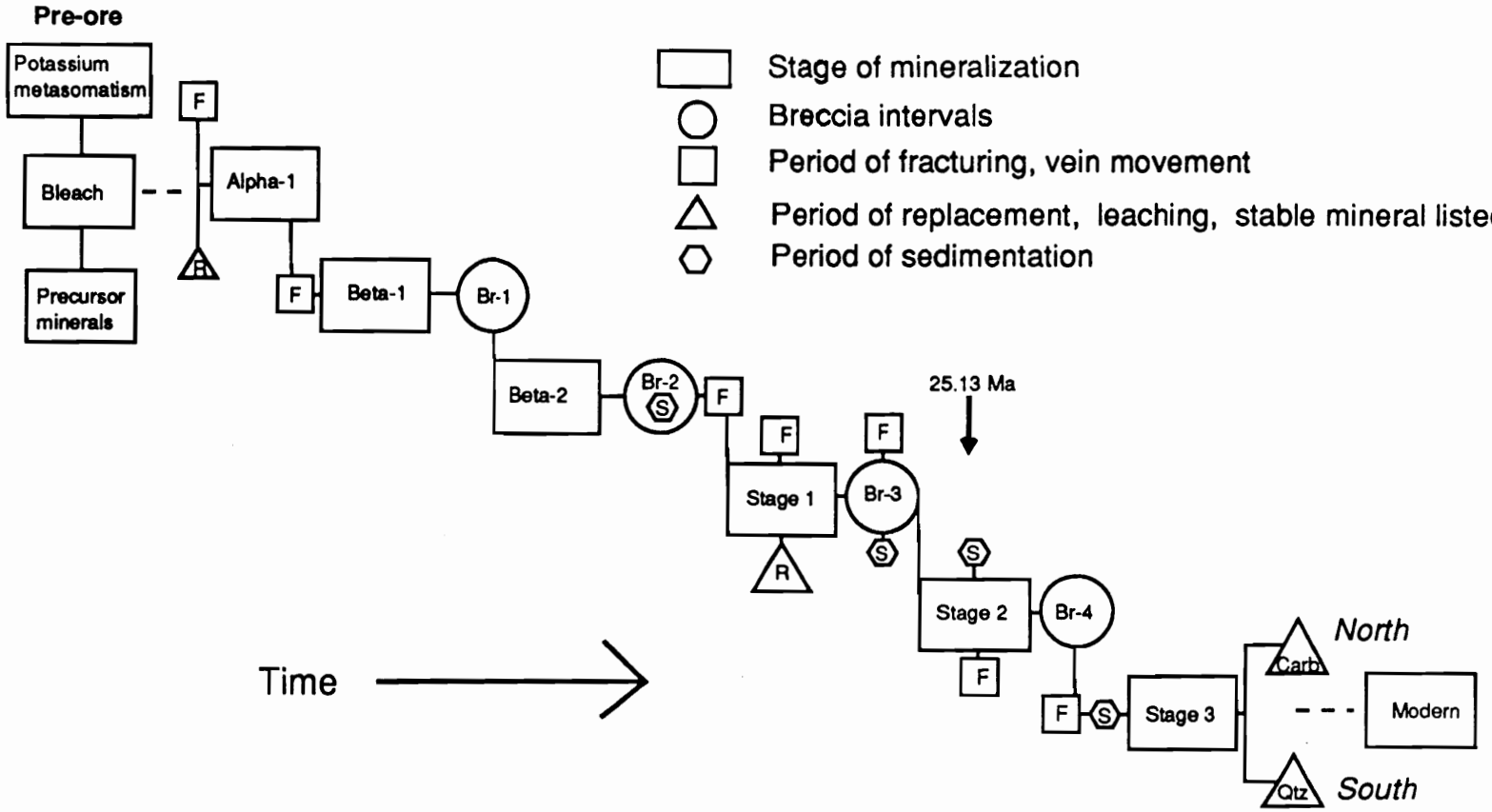

Figure 11. Progression of events in the development of the North Amethyst ores. See text for description of stages and named breccias (Br-#). Heavy arrow locates dated adularia relative to other minerals. F, fracture; R, replacement; S, sedimentation; Carb, carbonate; Qtz, quartz.

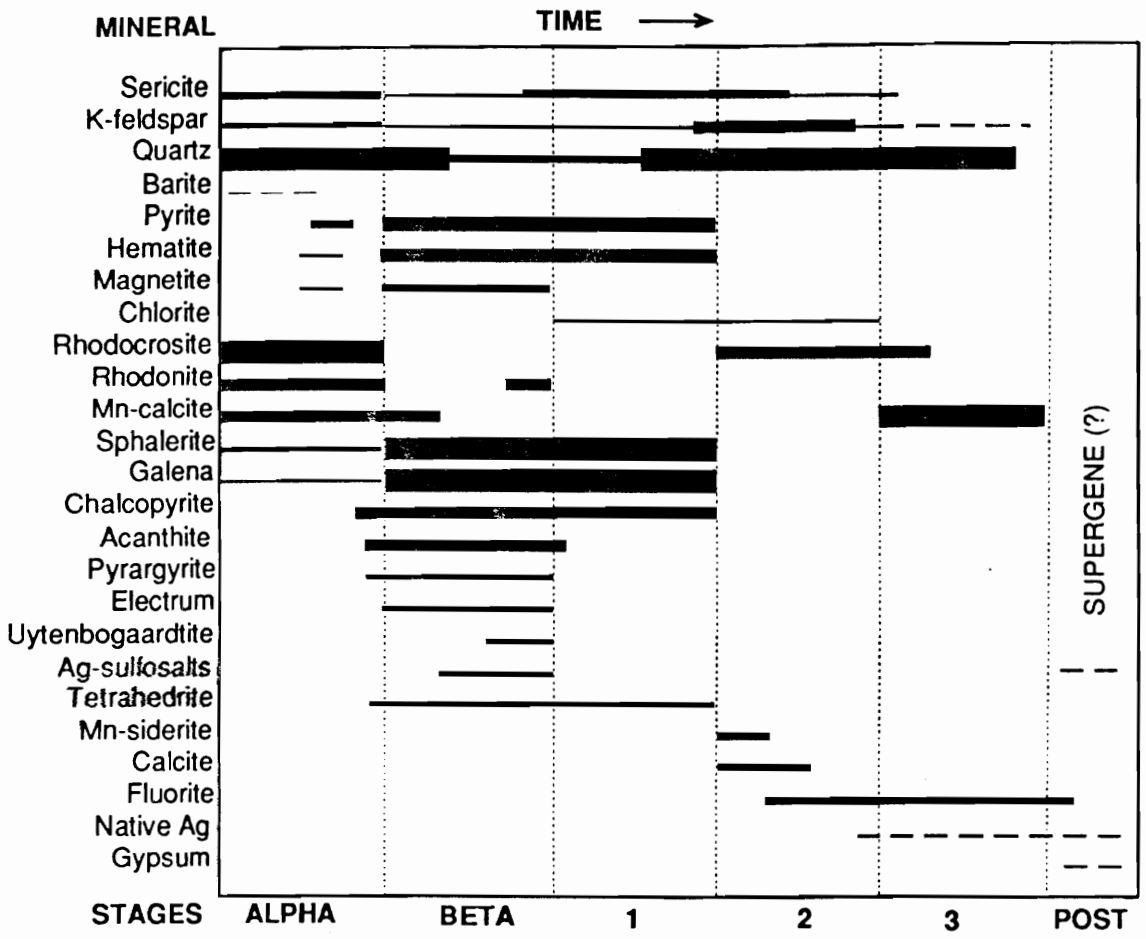

Figure 12. Composite paragenesis diagram for the North Amethyst mineralization. Mineral deposition shown in black, leaching is not shown because of its local character (see Figure 11); thickness of bar for a given mineral is proportional to its abundance. Dashed vertical lines show temporal boundaries for stages. Most transitions are defined by brecciation (see Figure 10).

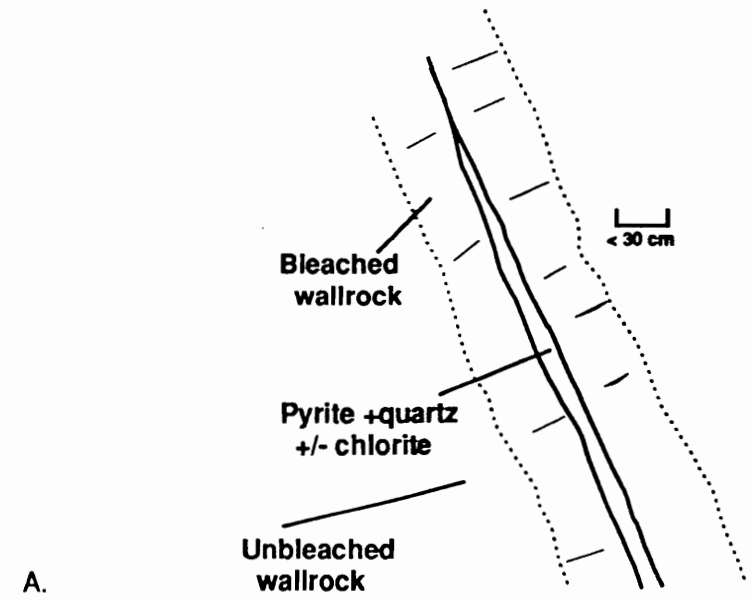

A.

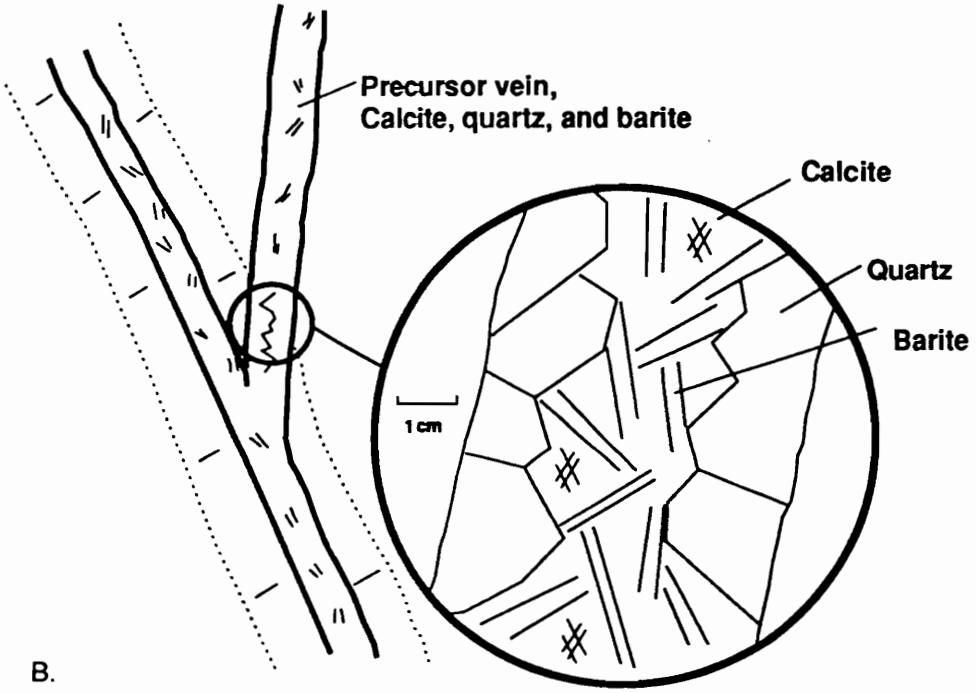

B.

Figure 13. a) Schematic diagram showing bleached and unbleached wallrock adjacent to early pyrite + chlorite + quartz vein. b) Schematic diagram showing relationship between precursor veins and bleached and unbleached wallrock.

Intense "sericitic" alteration characterized by illite-smectite clay minerals is generally restricted to above the 10400 level of the North Amethyst vein workings (see Figure 6). Geochemical analysis of selected material (Foley, unpub. data) shows that the altered rock consists of about 90% SiO_2 + Al_2O_3, 4% K_2O, and 2.5% combined Fe_2O_3 + FeO + MgO; measured precious metal values (~5 ppm Au) are higher than those of unaltered rock, but lower than those of substantially less-altered wallrock adjacent to veins lower in the workings (20-40 ppm Au).[3] The light-colored sericitic alteration is cut by seams of fine-grained dark-colored clay (mixed illite-smectite by XRD). Quartz veins also cut the sericitic material; sharp contacts suggest that the veins formed when the rock was more competent, prior to the peak alteration event. Clearcut paragenetic relationships between ore mineralization and this intense alteration were not found; however, the alteration zone appears to overlie the zone of base-metal mineralization and cuts across the zone of gold-bearing mineralization. Gold and manganese-silicate bearing assemblages occur at elevations above and below the intense alteration zone, but the base-metal-rich later stages are only below, as is true for veins in the main Creede district. No information is available on the presence or absence of alteration assemblages above the highest elevations of gold mineralization, although rocks cropping out on the hillside above the North Amethyst portal are stained by iron oxides all along the trace of the Equity fault.

---

3 Average Au values are notoriously difficult to determine because of the effect of a single nugget of electrum on a bulk analysis, so these values are given only for completeness of the data set, in absence of true averages.

Well-developed clay alteration zones cap vein structures throughout much of the central and southern Creede district (Steven and Eaton, 1975; Barton et al., 1977; Horton, 1983). Barton et al. (1977) and Bethke and Rye (1979) proposed that the caps formed primarily due to reaction of the wallrock with acidic fluid that resulted from condensation of ore fluid that boiled at depth. An age-date on illite-smectite from the cap material in the southern part of the district is in agreement with dates measured on vein adularia and sericite (Table 1). This interpretation could explain the relationship between overlying alteration zone and base-metal mineralization in the North Amethyst area, however, any relationship to gold mineralization is left unexplained.

Wallrocks of the North Amethyst vein are potassium metasomatized at depth. A general increase in potassium content of the wallrock with depth is reported by Sawyer et al. (1989), who suggest that the intensity of potassium metasomatism may increase with depth in the vein system. This pattern may be influenced by type and distribution of veins within the wallrock because bleached wallrock has elevated potassium contents over adjacent unbleached wallrock at all depths (Foley, unpublished data, 1990). Moreover, the barium contents of potassium feldspar in the bleached wallrock are higher than barium contents of unbleached wallrock suggesting that the bleaching event was chemically distinct from the regional pre-ore potassium metasomatic event (Foley, unpublished data, 1990). Sharp contacts between bleached and unbleached wallrock, coupled with the chemical distinctions cited above suggest that the bleaching event postdated the potassium

metasomatism, however, this needs to be substantiated by studies that delineate the extent of the metasomatism within the Nelson Mountain Tuff, and that determine mass transfer between the zones. Within the central and southern Creede district, a bleaching event confined to wallrock adjacent to vein does postdate the regional potassium metasomatism of the Carpenter Ridge Tuff (P. Barton and P. Bethke, pers. comm., 1989).

The bleaching event (Figure 13a) resulted in a color change from gray and gray-tan to off-white of widths ranging from a few centimeters to tens of centimeters in wallrock adjacent to some veins. The event apparently predates all mineralization because vein minerals of both associations fill structures that cut both bleached and unbleached wallrock. In drillcore away from the underground workings similar bleached fractures are filled with a fine-grained mixture of pyrite, quartz and, at times, hematite and/or chlorite.

Unbleached Nelson Mountain Tuff forms the wall for many of the mineralized veins. In general, the rock is hard and brittle, medium to dark grey, and retains volcanic textures consisting of phenocrysts (<2 mm) and flattened pumice in a very fine groundmass. The brittle nature indicates that the Nelson Mountain Tuff is silicified adjacent to veins, although chemical analyses of the rock show that SiO_2 contents are not elevated over those typical for volcanics of dacitic-rhyolitic composition based on the IUGS classification scheme (LeMaitre, 1984; Foley, unpub. data). In the northern part of the workings, the veins cut slightly coarsergrained volcanics, possibly intrusive dacitic Nelson

Mountain Tuff (Equity facies; Lipman and Sawyer, 1988), that are propyllitized; they contain epidote, calcite and abundant chlorite.

Most of the wallrock visible underground is cut by small (less than 3 centimeter) fractures that are crosscut in turn by minerals of the two main associations (Figure 13b). These fractures are filled primarily with quartz and calcite, and cut both bleached and unbleached wallrock. In drillcore away from the intensely mineralized area, bleached fractures contain mainly quartz, calcite, and pyrite, and occasionally barite and minor amounts of base-metal sulfides. In drillcore south of the exploratory workings barite has also been identified in similar fractures (D. Sweetkind, pers. commun., 1990). Barite was not found in samples collected underground and examined in this study although it has been reported (S. Caddey, C. Byington, D. Verdiman, pers. commun., 1987). As described earlier, possible barite molds have been identified in samples of early assemblages collected form the underground workings.

Manganese - Gold Association

The manganese-gold association is so named because of the presence of electrum and gold-silver sulfide in one stage and because of the abundance of manganese-bearing minerals in the other stage. The occurrence and proportion of these two elements distinguish this association from the later base-metal-rich association of the North Amethyst and from other mineralization thoughout the Creede district.

The first stage, alpha, is characterized by manganese-carbonates and -silicates, and minor base-metal sulfides; the second stage, beta, has abundant precious and base-metal minerals, and minor quartz and carbonate gangue. Each stage has two mineralogically similar substages

identified by crosscutting relationships. The sulfide-rich substages were separated by a period of fracturing and the development of a breccia having characteristic fragments.

Alpha-stage

The first vein filling event directly related to ore mineralization in the North Amethyst area appears to have been movement and fracturing of the volcanic wallrock, accompanied by introduction of manganese-rich fluids that deposited a fine-grained, almost cryptocrystalline, banded mixture predominantly consisting of rhodocrosite, manganoan calcite, rhodonite, pyroxmangite, and quartz (Figure 11, 14a). Locally, platy, tabular molds of barite (?) surrounded by this finegrained material and infilled with coarser adularia and quartz (probably stage-2 mineralization; see below) are found within the alpha-stage. Minor sulfides, primarily pyrite, sphalerite and galena, occur in stringers in the manganese-carbonate, -silicate and quartz matrix.

Vein widths of alpha-stage vary from a few centimeters to a meters or more. Features that characterize the stage are best preserved in the narrower veins; wider veins show multiple fracturing events and recrystallization of minerals.

Alpha-1 substage veins cut bleached and unbleached wallrock and precursor veins indicating that both the bleaching event and the development of precursor veins predated this stage. In general, contacts of vein and wallrock are sharp, however, the occurrence of embayed and partially replaced grains of potassium feldspar in the Mn-rich matrix suggests that some metasomatic replacement of wallrock may have occurred.

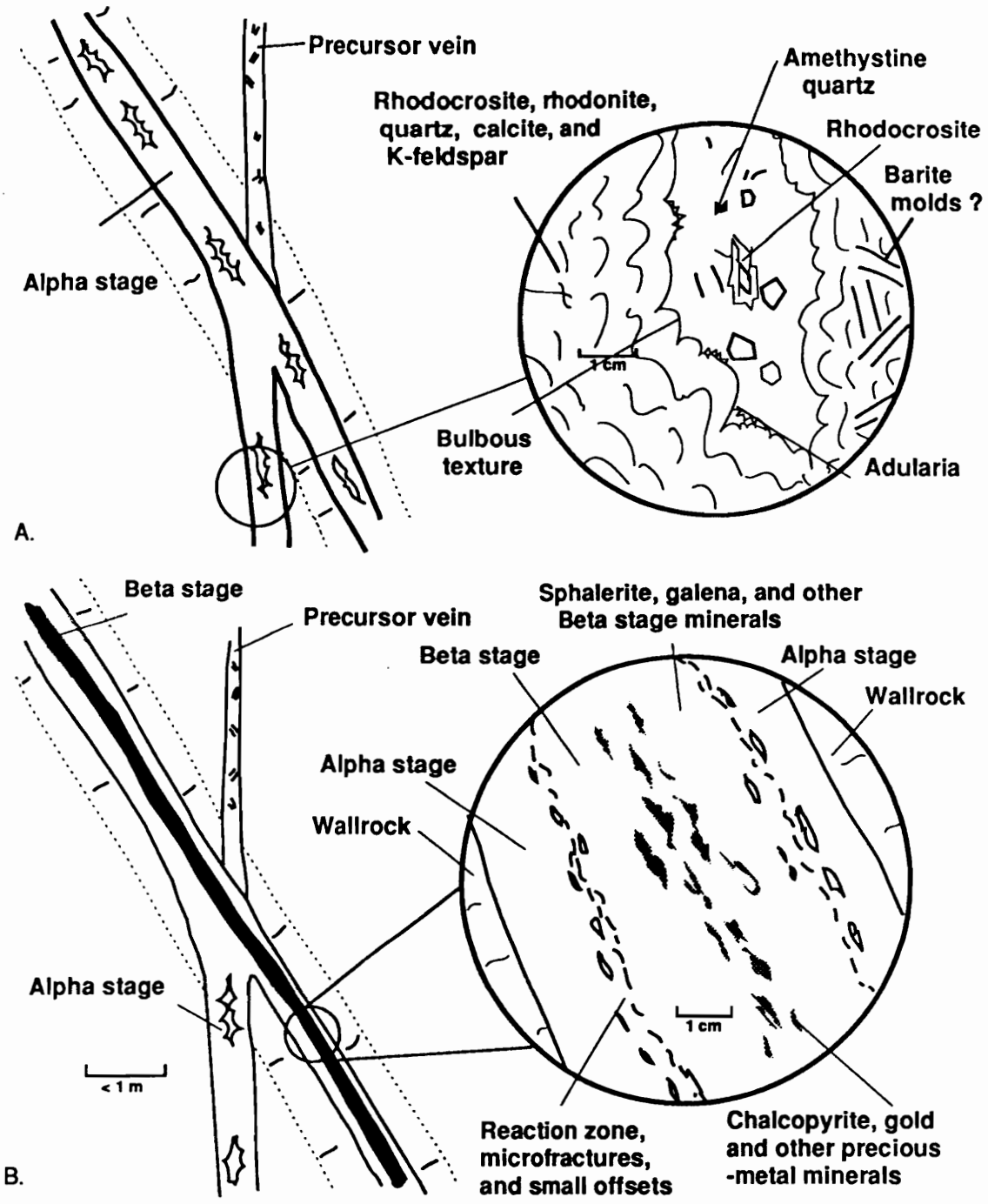

Figure 14. a) Schematic diagram showing relationships among alpha stage, precursor vein, and bleached and unbleached wallrock. Inset shows banded nature of finegrained Mn-rich carbonates, silicates, quartz, and sulfides. b) Beta-stage sulfide seam, location was probably controlled by structurally weak, vuggy zone at core of alpha stage.

Deposition appears to have progressed from the walls in toward the center of the veins leaving open spaces. The walls of the spaces have a rounded, bulbous texture and were filled later with 1-2 mm adularia rhombs, coarse (~2-3 cm) amethystine quartz, rhodocrosite (1-5 mm), and, locally, fluorite (1-2 mm) and sphalerite (1-2 mm; probably stage-2 mineralization; see below).

The alpha-2 substage consisted of a second influx of manganese-rich fluids that deposited a fine-grained mixture of quartz, rhodocrosite, and Mn-silicate minerals around fragments of alpha-1 substage and wallrock (Figure 15). This substage is more quartz-rich than the earlier alpha-stage and has a greater proportion of base-metal sulfides. Definition of this stage and it's exact position in the paragenesis is complicated by evidence that most later fluids reacted with or recrystallized the alpha-stage to some extent. Alpha-2 stage is probably a product of the local reaction of later fluids with minerals of the alpha-1 stage.

Beta-stage

Continued movement of the North Amethyst vein and fracturing of the alpha-stage assemblage caused the vein system to open up again. Precious and base-metal-rich fluids invaded the fractures and precipitated a complex suite of gold-, silver-, copper-, zinc-, lead-, and iron-bearing sulfides and sulfosalts (Figure 12, 14b). The location of the sulfide-rich seams may have been controlled in part by the structurally weak vuggy zones in the core of the alpha-stage vein material. Seam widths vary from a few millimeters to tens of

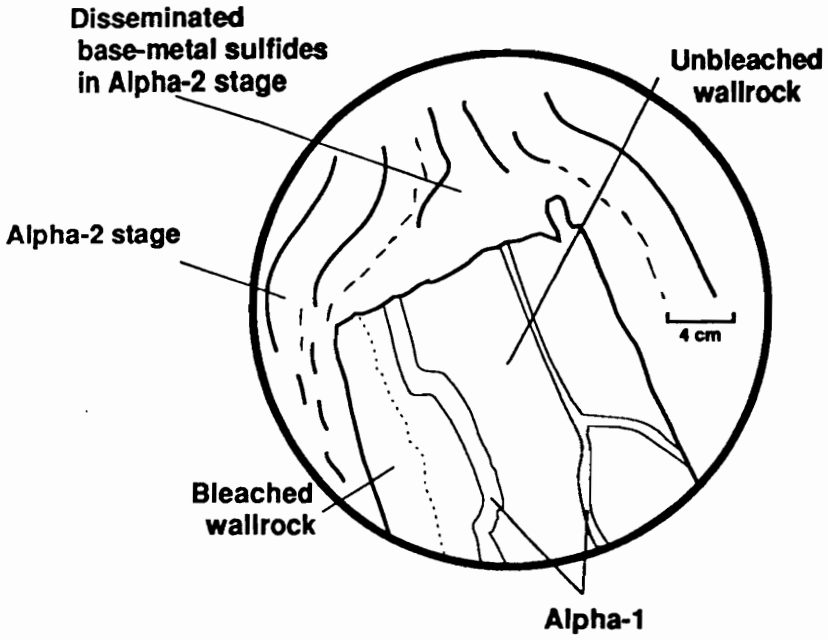

Figure 15. Two periods of Mn-carbonate and -silicate mineralization of Alpha stage are shown by the occurrence of clasts of one in the other.

centimeters, although most samples studied had widths of 2 to 3 centimeters.

The occurrence of rounded cobbles of beta-stage in breccias and sedimented zones cut by later competent seams of beta-stage sulfides was the basis for defining two substages (beta-1 and beta-2). The two have essentially identical mineralogies and differ only in their occurrence (Figure 15). Lead isotopic compositon of galenas from the two substages are identical within analytical error (Foley, 1990c). Electrum compositions and sphalerite compositions are also virtually identical for the two substages (Tables 6 and 8).

Precious metal minerals were deposited in two pulses separated by a period of brecciation and sedimentation along parts of the vein. The breccia that developed between the two beta substages (Breccia-1) is characterized by an unsorted mix of subangular to rounded pieces of fine-grained gold-bearing ore, angular fragments of bleached and unbleached wallrock, and fragments of alpha stage held together with a microcrystalline dominantly quartz cement (Figure 16).

Beta-stage fluids appear to have irregularly altered the alpha-stage minerals from a dominantly Mn-carbonate, Mn-silicate, quartz assemblage to a Mn-carbonate and quartz assemblage. Hanging wall sides of the sulfide-rich seams are often recrystallized to a coarse Mn-calcite, whereas footwalls are altered to a dusty fine-grained mixture of rhodocrosite and quartz (Figure 4d).

The complex suite of precious- and base-metal-sulfides precipitated by beta-stage fluids is listed in Table 3, and the paragenetic sequence for important beta-stage minerals is shown in

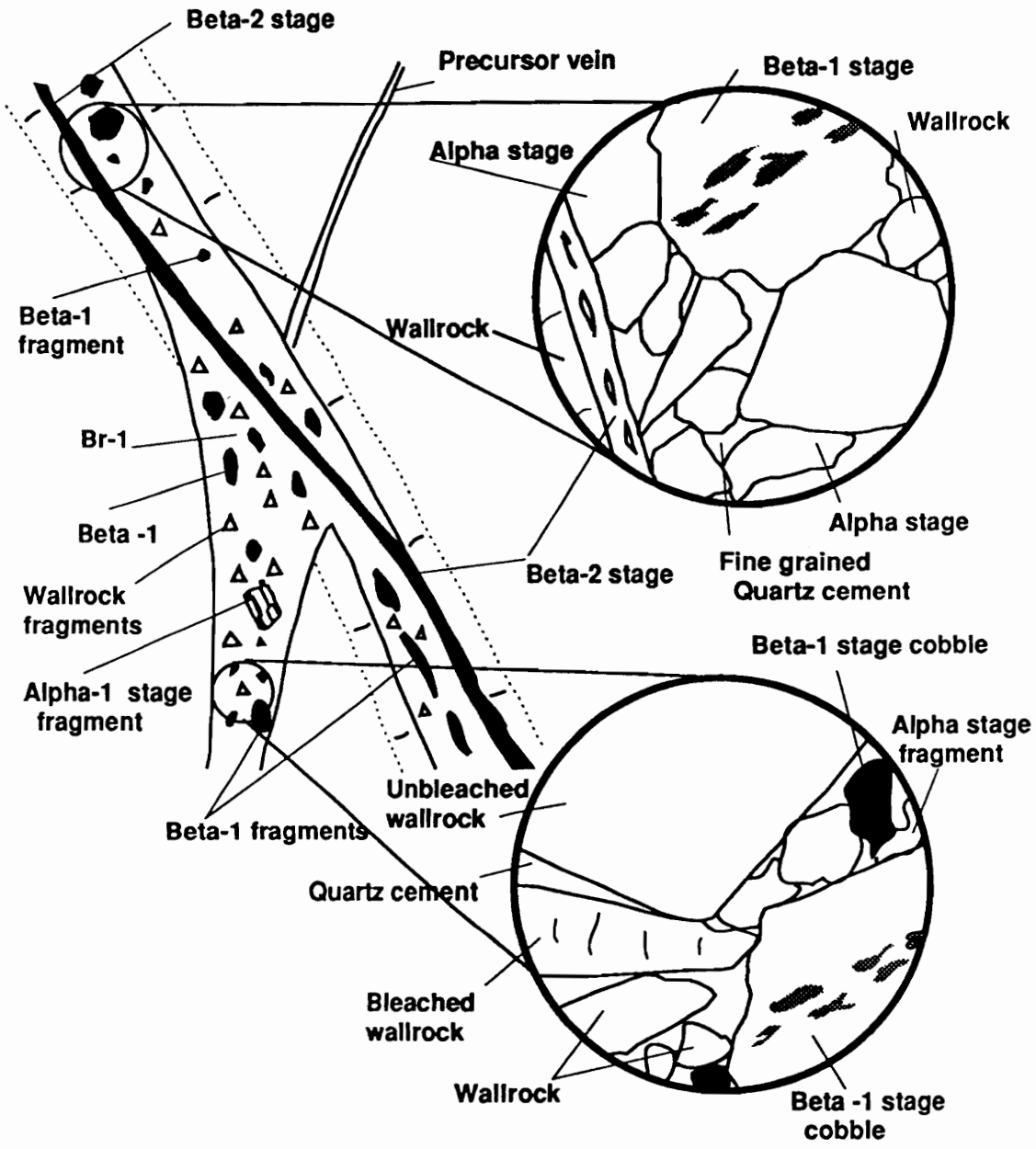

Figure 16. Relationship between beta-1 and beta-2 substages. Insets show development of breccia 1 (Br-1), which contains cobbles of beta-1 stage and is cut by a seam of beta-2.

Figure 12. The intergrowth of gangue, sulfides and sulfosalts shows that in general deposition within the beta-stage was initiated by precipitation of pyrite and sphalerite, followed by galena, chalcopyrite, electrum and other gold and silver minerals. Although the depositional sequence was interrupted by minor periods of dissolution (e.g., replacement of pyrite crystals, and chalcopyrite and tetrahedrite disease in sphalerite, corroded sphalerite crystals), beta-stage precipitation was generally continuous. Native silver, stromeyerite, etc., are found mainly in tiny late veinlets that cut the beta-stage seams or as rims on earlier phases, and may be supergene.

Beta-stage seams show a mineralogic zonation that is discontinuous along strike of the seams and irregularly distributed across the vein widths. Zinc, iron, and lead minerals occur across the width of all seams, while chalcopyrite and other copper-bearing minerals are concentrated towards the center of the seams. In general, electrum, and gold and silver sulfides and sulfosalts occur with, or are generally later than chalcopyrite.

The iron-oxide and -sulfide assemblage of beta-stage consists of magnetite, hematite, and pyrite. The assemblage occurs locally along the beta-stage seams and is most frequently found at depth in the system. The irregular distribution of the iron-oxide minerals, especially hematite, in contrast to the pervasive occurrence of pyrite may indicate local change from pyrite or pyrite-magnetite equilibria to a pyrite-magnetite-hematite buffer by an oxidative process such as boiling (Foley, 1990b).

The pyrite, hematite and magnetite are intergrown with fine zinc-, lead-, and copper-sulfides and abundant quartz. Electrum is the only precious metal mineral commonly found with the iron assemblage; it occurs intergrown with magnetite and pyrite and compositionally is similar to electrum in other assemblages. Euhedral magnetite occurs intergrown with pyrite and hematite in apparent equilibrium and magnetite also replaces hematite blades; the constrasting textures support a local change from pyrite-hematite-magnetite to pyrite-magnetite equilibria as noted above. Hematite appears, in some cases, to be altered to limonite; the texture probably is supergene in origin.

Transitional Breccias and Sediments

The transition between deposition of assemblages of the Mn-Au association and those of the Base metal - Silica association is marked by extensive brecciation of, and sedimentation in, the veins. The movement along the veins may have been a continuation, on a much larger-scale, of the fracturing that formed Breccia-1. Most of the breccias and sediments formed during this period are lumped together under Breccia-2, with the exception of one - the "black quartz breccia" - a matrix-supported, quartz-cemented breccia. The different breccias types record a short history of the transition period, from the initial dynamic hydrology that reworked fragments and deposited them as fragment-supported breccias in large shoots and sediment "dumps", to the hydrologic setting that resulted in graded bedding and chemically cemented, matrix-supported breccias.

Breccia-2

Breccias that are lumped together in this group have fragments that range in width from a few millimeters to 15 centimeters and in shape from angular to rounded (Figure 17). The fragments consists of all earlier stages of mineralization and wallrock; most were picked up close to the site of deposition.

Large breccia zones, resembling "shoots", of sedimented material with local graded bedding and quartz cement, formed as the fluids dumped their sediment load. The unsorted material forming the breccia zones consists mainly of subangular to rounded, bleached and unbleached fragments of volcanic wallrock, rounded and altered pieces of alpha-stage, rounded to subrounded cobbles up to 15 centimeters in width of sulfide-rich beta-stage and fragments of earlier breccias (Figure 17a, b). The pieces are held together with a muddy, quartz-rich cement. Interstitial sediment between larger fragments has graded bedding, soft-sediment deformation, and other textures indicating the material settled out of solution after the larger cobbles and blocks were dumped (Figure 17b).

In another area, silt-to-gravel sized fragments settled out in large graded beds of at least four cycles that extend for 30 meters along a vein wall and are greater than 10 feet in height (tops and bottoms were not visible; Figure 4g, 17c). The water-deposited beds show minor soft-sediment deformation, and an occasional sulfide-bearing cobble (up to 8 cm in width) fallen into fine graded sediment (Figure 4h). The graded beds are truncated at one end by a mineralized linking fault, at the other they appear to drape against hanging wall volcanics.

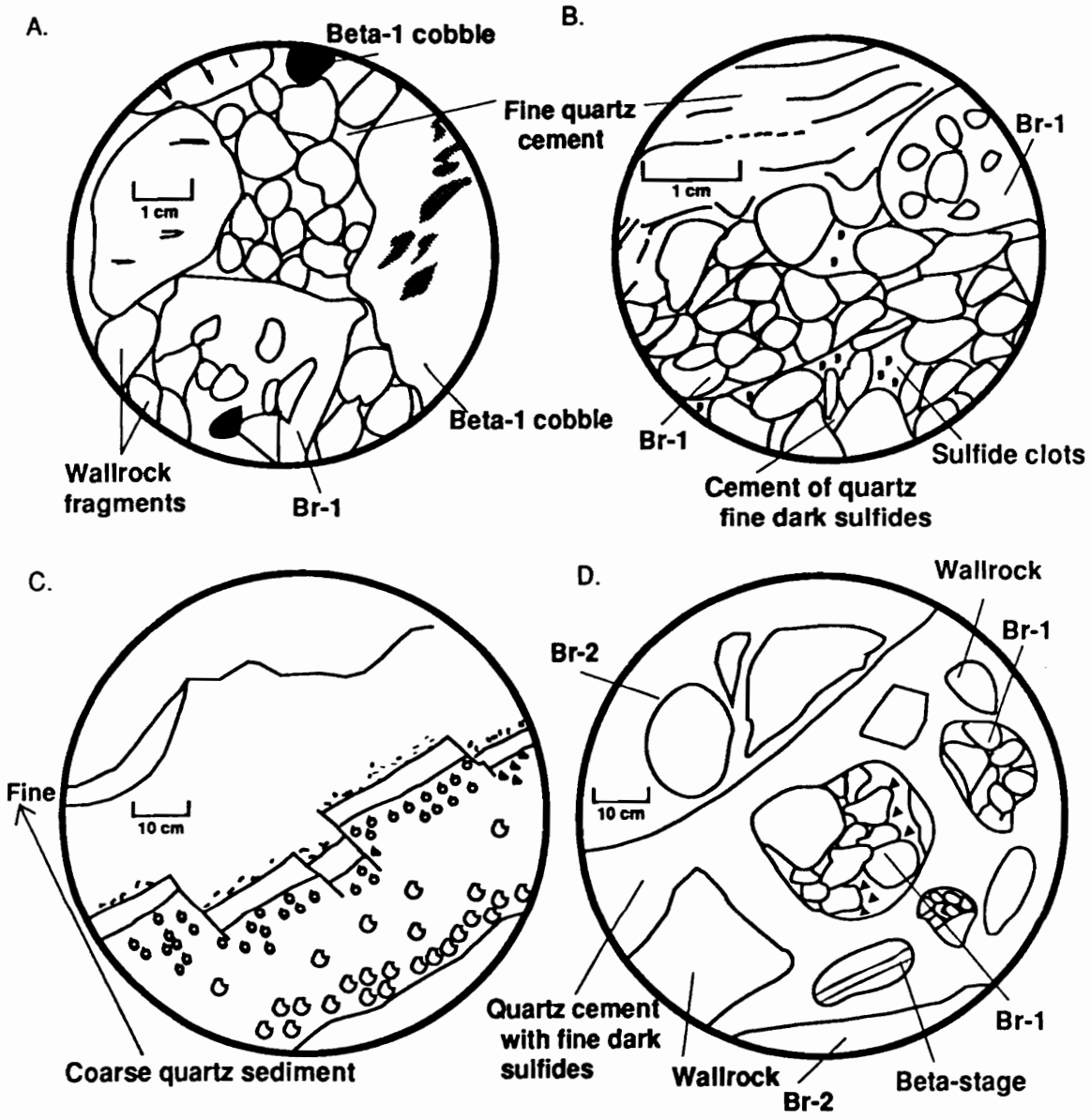

Figure 17. a) Breccia containing wallrock and sulfide cobbles cemented with a quartz slurry. b) Detail showing bedding in fine quartz cement surrounding breccia fragments. c) Graded bedding from fine quartz cement to coarser breccia fragments. d) Black quartz breccia (see text); breccia fragments in dark quartz cement colored by sulfide dust.

Beta-2 ore seams are reasonably intact in some areas, but most show minor offsets. In other areas, the seams are stretched and broken, and sulfide-rich pods are more strongly deformed. Minor development of boudin-like structures and of folding of the sulfide seams has occurred.

Black quartz breccia

Late in this transition period, along planes of movement, veins of "black quartz breccia" developed (Figure 17d). The black quartz breccias consist of 50-90 volume percent microcrystalline quartz-rich matrix, and 10-50% fragments of beta- and alpha-stage, earlier breccias, and wallrock. The cement is composed dominantly of microcrystalline quartz having a granular texture with sutured grain boundaries and are presumably is a chemical precipitate. The cements grade in color from light gray to black; apparently a function of the amount of fine sulfides and electrum contained therein. It has not been possible to ascertain whether the sulfide aggregates are clastic or if they formed as precipitates, but the shapes of the grains suggest that they were broken and ground. They may be fine ground dust from earlier beta-stage sulfide seams.

Base Metal - Silica Association

This association has three mineralogical stages that are characterized by (1) dominantly base-metal sulfides, iron-oxide, and quartz, (2) Ca-, Mn-, and Fe-bearing carbonates, fluorite, and quartz, and (3) Mn-calcite, quartz and pyrite. Thus, the association is named after the most common constituents - base-metal sulfides and quartz. Complete mineralogical listings of all stages are given in Table 3.

Stage 1

The first stage of the base metal - silica association (Figure 18) is characterized by abundant base-metal sulfides, argentian tetrahedrite, hematite, chlorite and quartz. Two mineralogically distinct substages are recognized: a chlorite, hematite, and quartz assemblage was deposited prior to, and concurrently with, the major period of base metal mineralization that resulted in a crustified sequence of sphalerite, galena, pyrite, chalcopyrite, and tetrahedrite.

The fine-grained chlorite, hematite, and quartz assemblage was deposited on blocks of earlier breccias, and in fractures cutting earlier assemblages of the Mn-Au association. Isolated crystals of sphalerite appear in the siliceous mixture. Some of the siliceous mixture was fragmented and recemented before the fluids began depositing relatively coarse base-metal sulfides. In other areas, the sulfides are intergrown with chlorite, hematite and quartz without obvious breaks suggesting a gradual shift in dominant mineralogy.

The coarse-grained sphalerite, galena, and pyrite, and chalcopyrite assemblage of Stage-1 contains interstitial quartz, chlorite, and hematite. Hematite flakes also are included in the sphalerite crystals. No clear-cut paragenetic relations are apparent among the minerals, with the exception that fluid reacted with sphalerite along fractures and grain boundaries to form chalcopyrite- and tetrahedrite-disease textures (e.g., Barton and Bethke, 1987). Sphalerite crystals are corroded, and thin sections show periods of dissolution and reprecipitation. Latest galena formed skeletal crystals in open vugs that were later filled with minerals of Stage 2 (Figure 18).

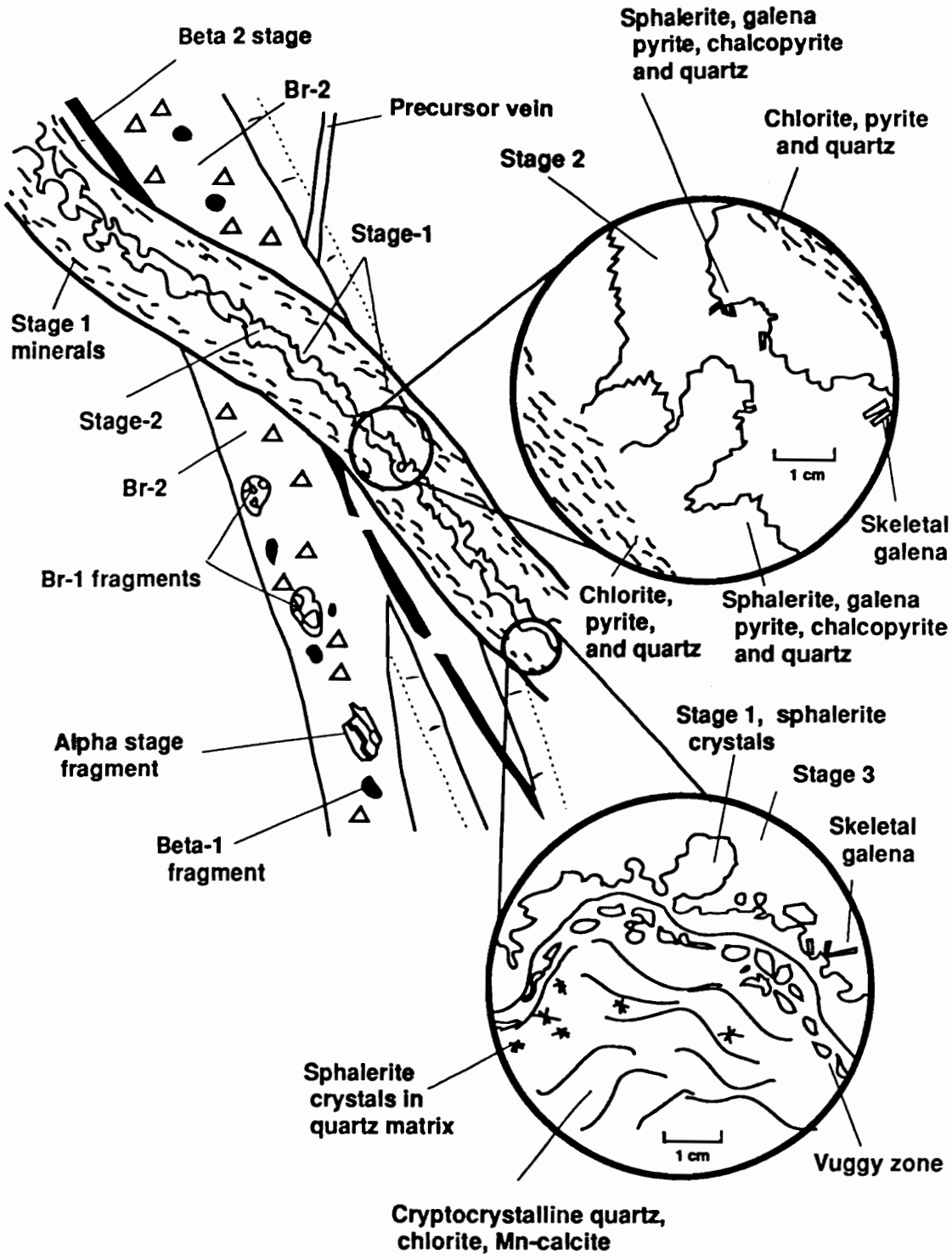

Figure 18. Schematic diagram showing relationship of stage-1 minerals to all preceding stages and breccias. Insets show textures typical of stage 1. See Fig. 5a-d.

Breccia 3

Continued local fracturing of Stage-1 mineralization formed a breccia that is characterized by fragments of coarse base-metal sulfide and chloritized wallrock cemented by a slurry of cryptocrystalline quartz, chlorite and pyrite (Figures 5f, 19). The chlorite gives the cement a green hue. Minor amounts of base-metal sulfides were deposited on this brecciated material. Fragments of the base metal sulfide are angular to subangular, and the wallrock fragments are rounded. The breccia is most frquently found locally where Stage-1 vein widths are greatest.

Stage 2

The second stage of mineralization in the Base-metal Silica association (Figure 20) is characterized by coarse-grained quartz, calcite, rhodocrosite, and fluorite, all intergrown with minor amounts of adularia, chlorite, and pyrite. Locally, manganosiderite occurs within the calcite. Stage 2 was deposited on Breccia 3 and Stage 1. The minerals are coarse-grained; quartz crystals grew up to 40 mm in length, while green fluorite cubes attained 13 mm on a side. Smaller octeheda of fluorite (<3 mm) are colorless or pale green or purple. In general, quartz, chlorite, and calcite were deposited before fluorite and additional quartz. Quartz crystals are zoned from colorless and white to amethystine, and contain solid inclusions of calcite, adularia, and fluorite. Occasionally a small amount of fine gray quartz sediment was deposited in vugs on crystals of Stage 2.

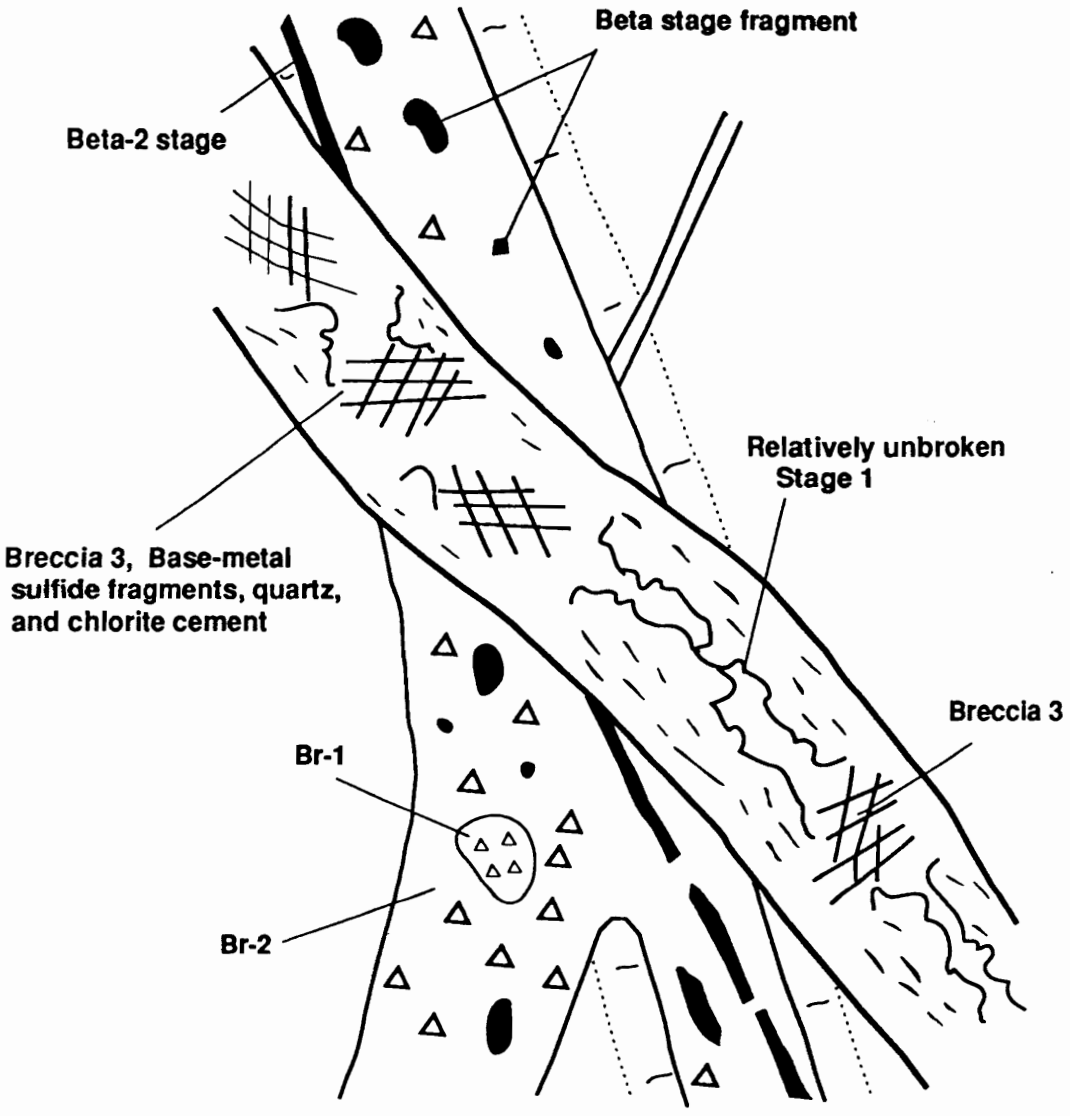

Figure 19. Local development of breccia 3, characterized by fragments of stage-1 sulfide and a green, chlorite-rich cement.

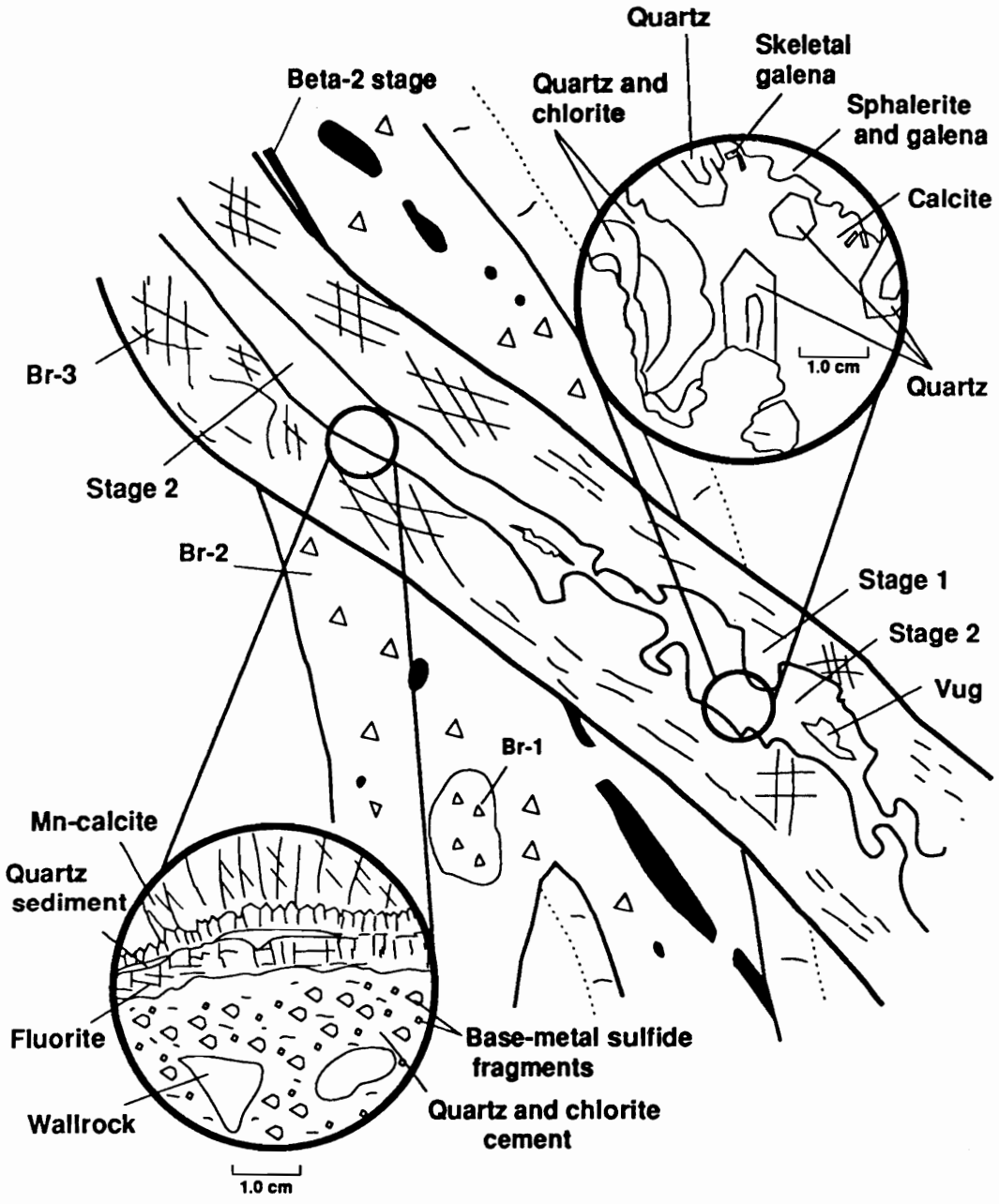

Figure 20. Reopening of vein and deposition of stage 2 minerals on preexisting mineral stages and breccias. Insets show textures of stage 2 minerals.

Quartz and adularia that fill barite (?) molds in alpha-stage probably crystallized from stage 2 fluids. The mineral are texturally identical to stage 2 minerals, and have fluid inclusion salinities and homogenization temperatures that are similar to other stage 2 mineralization (Foley, 1990b). Rhodonite crystals, up to 0.5 mm in length, that form selvedges and project into some of the quartz filled molds, and are intergrown with some rhodocrosite, may have formed from recrystallization of the finer-grained alpha-stage material.

Breccia-4

This breccia contains angular fragments of all earlier assemblages, some breccias, and broken crystals, and is cemented with a pale to light pink calcium carbonate having a composition of $Cc_{95}Rc_5$ (Figure 21). It is especially prevalent in the north parts of the vein system. The fragile and vuggy nature of the breccia suggest a late formation, probably concurrently with the development of Stage 3.

Stage 3

The last clearly defined mineralization in the paragenetic sequence was deposition of quartz or manganocalcite, with pyrite along the North Amethyst structure (Figure 22). Movement along the structure created vugs, cavities, and brecciated zones that cut all of the earlier stages. This movement was accompanied by, or followed by leaching of earlier vein material along the entire length of the North Amethyst workings.

In the northern part of the ore zone, extensive crusts of pink to pale-yellow colored, manganese-bearing calcite, interlayered with thin layers of crustiform pyrite were deposited in the vugs and on earlier leached material. The carbonate crusts ranged in total thickness from

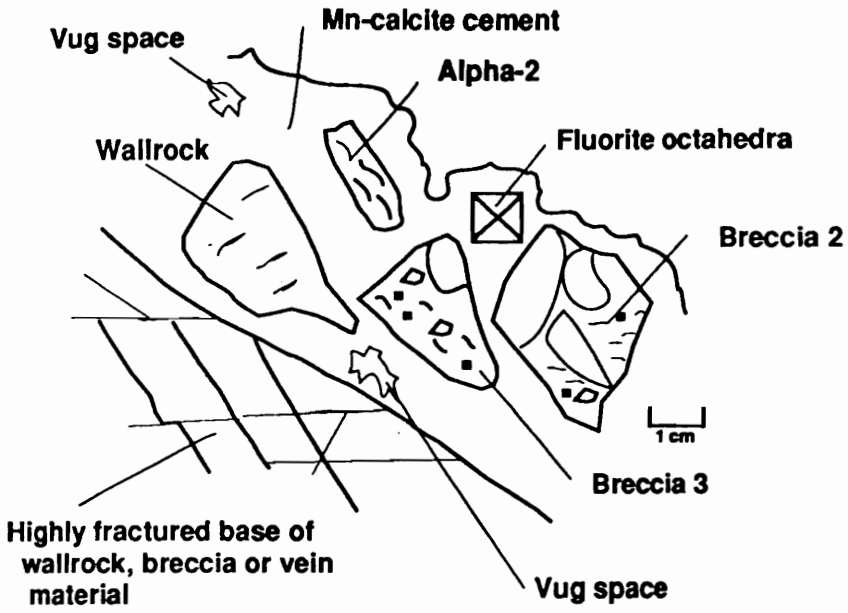

Figure 21. Development of breccia cemented by pink calcite just prior to, or concurrently with, stage 3 mineralization.

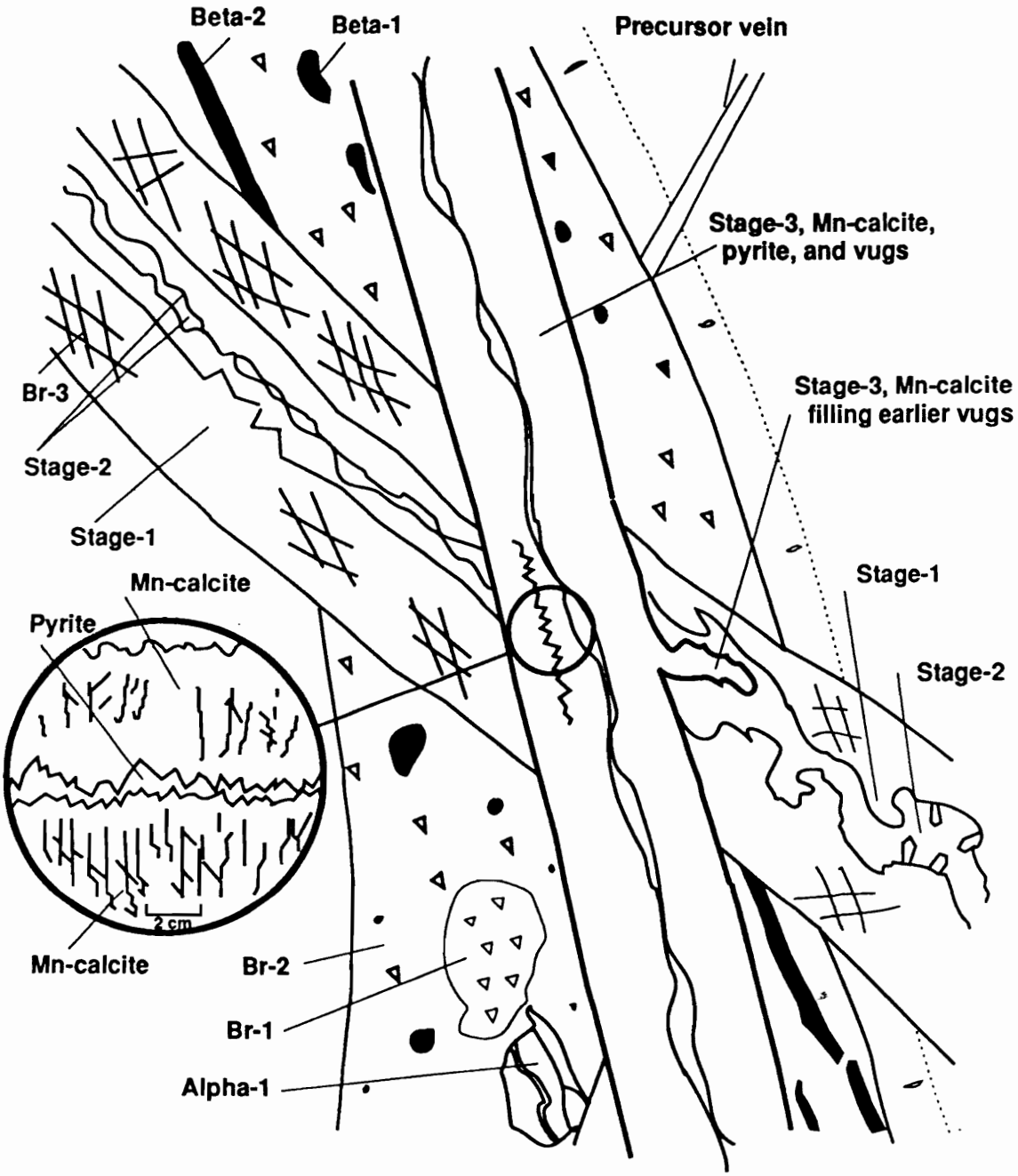

Figure 22. Stage 3 is marked by deposition of thick crusts of a coarse pink calcite, pyrite and quartz. Inset shows calcite and pyrite occurence.

millimeters to a meter. The carbonates were selectively leached later and now form large, open vuggy zones.

In the southern workings, leaching of earlier stages, especially the extensive breccias, was probably more extreme. A suite of samples of Breccia 2 selected to display gradations in the degree of leaching range from a speciman showing only bleaching of fragments and alteration to clay minerals, to samples that consist entirely of a foam-like "clinkery" siliceous material containing molds possibly of leached blocks of wallrock and rare specks of dark sulfides. Geochemical analysis of the most altered and leached material indicates that of the major elements, only SiO_2 (~94%), and minor Al_2O_3 (~3%) and K_2O (~1%) remain. Relatively high values of base- and precious-metals also persist (~90 ppm Au, 30 ppm Ag). This base of leached material is overgrown by large terminated crystals of quartz in the southern part of the ore zone. The quartz crystals are included in stage 3 because they overgrow the leached base, however, their formation may predate the manganocalcite. Minute cubes of pyrite dust the quartz surfaces; timing of this pyrite relative to the crustiform occurrence within manganocalcite is not clear.

CORRELATION OF MINERAL ASSEMBLAGES WITH OTHER VEIN SYSTEMS

The relation of the North Amethyst ores to those of the main Creede district five kilometers to the south is of great importance in assessing the nature, size, and timing of mineralization. The mineralogy, textures, and paragenetic sequences established in this study can be used to compare the North Amethyst mineralization to ores

of the main mining district at Creede. Paragenetic relations are summarized in Table 9, for the North Amethyst vein system and some veins of the main mining district. Mineral stages defined for the North Amethyst vein system can be correlated, in part, with mineral stages defined in previous studies for the southern Amethyst vein (Robinson, 1981; Robinson and Norman, 1984; and Guidice, 1981), the Bulldog Mountain vein system (Plumlee, 1989), and the OH and P veins (Bethke and Rye, 1979; Barton et al., 1977; P. Barton, Jr., pers. commun., 1989). Most of the corresponding stages are similar mineralogically and occur throughout the district, however, there are some important exceptions.

At present, the alpha, and beta stages of the Mn-Au association are found only in the North Amethyst area. The assemblages have not been described elsewhere within the boundaries of the Creede mining district. Manganese-silicates and uytenbogaardtite are not found south of the North Amethyst workings, although rare occurrences of electrum have been reported for a couple of localities. An occurrence of dark yellow gold with a high degree of fineness in a gangue of manganese oxides has been described by Emmons and Larsen (1913, 1923) for the Happy Thought and Amethyst mines of the mid-Amethyst vein. The gold occurred in cracks and veinlets cutting older ore and was said to be a common supergene occurrence in near-surface workings. Gold also has been reported as inclusions in pyrite, galena, sphalerite, and other minerals (Emmons and Larsen, 1923), however, no additional details are available. P.M. Bethke and P.B. Barton, Jr., (pers. commun., 1989) note the occurrence of abundant finely disseminated gold in early chalcopyrite (B-stage?) in a single sample from the OH vein. Galenas

Table 9. District-wide correlation of mineral assemblages and brecciation events.

North Amethyst vein (Foley, 1990)	Bulldog vein (Plumlee, 1989)	OH - P vein (Bethke and Rye, 1979)	Southern Amethyst (Robinson (1981)	Disseminated ore, OH-Amethyst (Guidice, 1980)
Mn-Cc + Qz + Py (3)	Py + Stib + Pyrar (V)	Py + Stib (E)	Absent?	Gel Py + Qz (2)
Breccia-4	Absent?	Absent?	Absent?	Absent?
Absent	Sp + Gn + Cpy Td + Pearc + Ac (IV)	Sp + Gn + Qz + Cpy +Hm (D)	Absent?	Absent?
Qz + Mn-Cc + Ad + Rc Ad + Mn-sid + Chl (2) +Py	Qz + Fl + Mn-sid + Sp + Gn (III)	Fl + Qz + Mn-sid (C)	Absent?	Included in (1)?
Breccia-3	Absent?	Absent?	Absent?	Absent?
Sp + Gn + Py + Cpy + Qz + Hm + Chl + Td (1)	Bar + Qz + Sp + Gn + Td (II)	Qz + Sp + Chl + Gn + Hm + Td-tn + Au (B)	Qz + Sp + Gn + Py + Td + Hm + Acan + Ag (2)	Sp + Gn + Py + Cp + Chl + Rc + Bar + Ag + Td + Ac + (1)
Breccia-2	Rc + Qz + Sp + Gn + Ad (I)	Qz + Ad (A)	Rc + Qz + Bar + Cc + Sp + Gn + Py + Ccp (1)	Absent?
Gn + Sp + Cpy + Py + Td + Ac + Uyten + Au (beta-2)	Absent?	Absent?	Absent?	Absent?
Breccia-1	Absent?	Absent?	Absent?	Absent?
Gn + Sp + Cpy + Py + Td + Ac + Uyten + Au (beta-1)	Absent?	Absent?	Absent?	Absent?
Rc + Qz + Mn-Cc + Rh + Px + Sp + Gn + Py + Ad (alpha)	Absent?	Absent?	Absent?	Absent?

Abbreviations: Ac, acanthite; Ad, adularia; Ag, silver; Au, electrum; Bar, barite; Cc, calcite; Chl, chlorite; Cpy, chalcopyrite; Fl, fluorite; Gn, galena,; Hm, hematite; Mn, manganese; Pearc, pearcite; Px, pyroxmangite; Py, pyrite; Pyrar, pyrargyrite; Qz, quartz; Rc, rhodocrosite; Rh, Rhodonite; Sp, sphalerite; Sid, siderite; Stib, stibnite; Td, tetrahedrite-tennantite. Stage designations for each vein are shown in parentheses. (After Foley and Vardiman, 1989)

from North Amethyst gold-bearing beta-stage are isotopically distinct from galenas from the southern and central mining district (Foley, 1990c), lending support to their unique occurrence in the north. However, compositions of alpha-stage galenas are ambiguous. Salinities of fluids in sphalerite from alpha- and beta-stage are lower than salinities of fluids in sphalerite from the central and southern districts (Foley, 1990b).

The three stages of the base metal - silica association of the North Amethyst vein system can be correlated directly with mineralogically similar stages of the OH and P veins (defined as stages A through E). The A stage of the northern OH and P veins consists primarily of massive quartz intergrown with rhombs of adularia. This stage is not found in the North Amethyst ores, although in the interval of brecciation and sedimentation between the two sulfide-rich North Amethyst stages (beta-stage and stage 1) quartz was deposited as cement in breccia. While not defined as a vein-filling stage, the quartz cement may correlate with OH vein A-stage mineralization indicating a district-wide period of silica deposition.

The B stage of the OH and P veins is dominated by finegrained base metal sulfides - sphalerite, galena, chalcopyrite and lesser amounts of silver-rich tetrahedrite - in a chlorite, pyrite, hematite, and quartz gangue assemblage. This stage correlates directly with stage 1 of the North Amethyst vein. Sphalerites of the North Amethyst, OH and P vein assemblages show extensive chalcopyrite-, and minor tetrahedrite-disease textures. Zoned sphalerites from the OH B-stage and North Amethyst stage 1 are compositionally similar; light zones have generally low iron

contents (<2 mole %) and dark bands are iron-rich (up to 8 mole % for North Amethyst stage-1, up to 16 mole % OH B-stage). Galenas (Stage 1, B) from all three veins also have similar lead isotopic compositions (Foley, 1990c). The OH and P vein tetrahedrite is variable, but generally silver-rich (L.B. Wiggins and T.L. Woods, unpublished data, 1980) like that of the North Amethyst ore.

Stage 2 of the North Amethyst vein correlates mineralogically with stage C of the OH and P veins. Both North Amethyst stage 2 and C stage contain fluorite, quartz, and carbonate. The North Amethyst stage 2 carbonate consists of intergrown calcite and mangano-siderite, whereas, the OH and P veins contain only mangano-siderite (Wetlaufer, 1977). The OH and P vein D-stage ores are apparently absent in the North Amethyst vein system. The D stage consists largely of coarsely crystalline sphalerite, galena, quartz, chalcopyrite and hematite. D-stage sphalerite is free of chalcopyrite disease and colorzoned from yellow-white to red-brown to yellow-white with iron-contents of less than 3 mole percent FeS (Barton et al., 1977).

Stage 3 of the North Amethyst vein system can be correlated with E stage of the OH and P veins mainly on the basis of the occurrence of late pyrite. Pyrite in North Amethyst stage 3 is volumetrically minor compared to E stage, and quartz and manganoan calcite occur in relatively greater proportions.

The sequence of mineral stages defined for the Bulldog Mountain (BM) vein system has been correlated with mineralization stages of the OH and P veins by Plumlee (1989). The comments and ideas presented in that study generally hold true for comparing the North Amethyst and

Bulldog Mountain paragenetic sequences because of the mineralogical similarities between the OH and North Amethyst assemblages. BM I stage contains rhodocrosite, chalcedony, barite, disseminated sulfides, adularia, and calcite, and is not correlated directly with any North Amethyst stage. However, as in the case of the OH vein, I stage may correpond to North Amethyst Breccia 2. BM II stage is composed of interbanded barite, base metal sulfides, native silver, acanthite, argentian tetrahedrite (G. Plumlee, pers. commun., 1990), and miscellaneous sulfosalts, and is zoned from sphalerite- and galena-rich, silver-poor assemblages with lesser barite, chlorite and hematite in the northern system to barite- and silver-rich assemblages in the southern half of the system. The North Amethyst stage 2 is more similar mineralogically to the northern BM stage II, with the exception of barite in BM stage II and abundant chlorite-pyrite-hematite-quartz gangue in North Amethyst stage 2. BM stages III, IV, and V are similar mineralogically to OH vein stages C, D, and E. Compositions of carbonate of North Amethyst 2 (Table 5), BM III (Wetlaufer, 1977), and OH C (Wetlaufer, 1977) are similar. Thus, BM III probably correlates directly with North Amethyst 2, and BM V with North Amethyst 3. As noted above, OH D stage, and the correlative BM IV stage, are not found in the North Amethyst area.

Correlations between mineralization of the North Amethyst vein system, the southern Amethyst vein, and disseminated ore in the hanging wall of the OH-Amethyst intersection are difficult because paragenetic relations for some of those areas are less well known. Robinson (1981) defined two main stages of mineralization along the southern Amethyst

vein system and correlated them with the A and B stages defined by Bethke and Rye (1979) for the OH vein. Stage 1 of the southern Amethyst vein is a sulfide-poor assemblage characterized by rhodocrosite, quartz, barite, and an absence of silver. Stage 2 is a complex period made up of three substages. Mineral of stage 2 include quartz, galena, tetrahedrite, covellite, acanthite, and native silver. This stage correlates relatively well with Stage 1 of the North Amethyst vein, B stage of the OH and P veins, and stages II and possibly III of the Bulldog Mountain vein (Plumlee, 1989).

Guidice (1981) described two main hypogene stages and a supergene stage for mineralization disseminated in wallrock between the OH and Amethyst veins. The first hypogene stage of mineralization appears to correlate with a combination of stages 1 and 2 of the North Amethyst vein, and, as described by Plumlee (1989), with a combination of stages A through C of the OH vein and stages I through III of the Bulldog Mountain vein. This lumping of stages probably reflects a lack of clear-cut paragenetic relationships in the disseminated ore. The second hypogene stage for the disseminated ore correlates well with stage 3 of the North Amethyst mineralization, E stage of the OH vein and stage V of the Bulldog Mountain system.

CONCLUSIONS

1. The ore minerals of the North Amethyst vein system can be divided into two associations. The earlier association has two stages and is characterized by high manganese and high gold contents. The later association has three stages that consist primarily of base-metal

sulfides, chlorite, quartz, carbonate, and fluorite, in varying proportions.

2. Complete assemblages of the earlier manganese - gold stages of the North Amethyst system are not found elsewhere in the central San Juan region. In contrast, mineralogical stages and breccias identified in the base metal - silica association can be correlated with paragenetic stages defined for veins of the central and southern Creede mining district.

3. The local and early occurrence of the manganese and gold assemblages may indicate that they formed in a small, locally restricted hydrothermal cell that predated the extensive hydrothermal system from which ores of the Creede district are proposed to have been deposited (e.g., Bethke, 1988). If similar early cells were present in the central and southern parts of the district, they may have been replaced or incorporated by later assemblages, or they remain to be discovered. Paragenetically early mineral assemblages may hold the greatest potential for vein-related gold mineralization in the central San Juan Mountains.

4. The correlations of mineral assemblages described above have important implications for hydrologic modelling of the northern, central and southern parts of the Creede district. The extensive correlation of base-metal-, silver-, and silica-rich assemblages suggests a similar source of fluids and metals for the ore mineralization, and implies that the minerals were deposited in the veins by similar mechanisms and under similar conditions of ore formation.

REFERENCES

Baars, D.L., and Stevenson, G.M., 1984, The San Luis uplift, Colorado and New Mexico - an enigma of the ancestral Rockies: The Mountain Geologist, v. 21, no. 2, p. 57-67.

Barton, Mark, 1978, The Ag-Au-S system: M.S. thesis, Virginia Polytechnic Inst. and State Univ.

Barton, M.D., Kieft, C., Burke, E.A.J., Oen, I.S., 1978, Uytenbogaardtite, a new silver-gold sulfide: Can. Min., v. 16, pp. 651-657.

Barton, P.B., Jr. and Bethke, P.M., 1987, Chalcopyrite disease in sphalerite: pathology and epidemiology: Am. Mineralogist, v. 72, p. 451-467.

Barton, P.B., Bethke, P.M., and Roedder, E., 1977, Environment of ore deposition in the Creeede mining district, San Juan Mountains, Colorado: Part III. Progress toward interpretation of the chemistry of the ore-forming fluid for the OH vein: Econ. Geol., v. 72, p. 1-24.

Bethke, P.M., 1988, The Creede, Colorado ore-forming system: a summary model: U.S. Geological Survey Open-file Report 88-408, 29p.

Bethke, P.M., and Lipman, P.W., 1987, Deep environment of volcanogenic epithermal mineralization: Proposed research drilling at Creede, Colorado: EOS, v. 68, p. 177, 187-89.

Bethke, P.M., Barton, P.B., Jr., Lanphere, M.A., and Steven, T.A., 1976, Environment of ore deposition of the Creede mining district, San Juan Mountains, Colorado: Part II. Age of mineralization: Econ. Geol., v. 71, p. 1006-1011.

Bethke, P.M., and Rye, R.O., 1979, Environment of ore deposition of the Creede mining district, San Juan Mountains, Colorado: Part IV. Source of fluids from oxygen, hydrogen, and carbon isotope studies: Econ. Geol., v.74, p. 1832-1851.

Bickford, M.L., 1988, The accretion of Proterozoic crust in Colorado: Igneous, sedimentary, deformational, and metamorphic history, in W.G. Ernst, ed., Metamorphism and crustal evolution of the western United States: Rubey volume 7, Prentiss Hall, New Jersey, p. 411-430.

Capobianco, C., and Navrotsky, A., 1987, Solid solution thermodynamics in $CaCO_3$-$MnCO_3$: American Mineralogist, v. 72, p. 312-318.

Craig, J.R., and Vaughan, D.J., 1981, Ore microscopy and ore petrography: John Wiley and Sons, New York, 406p.

de Capitani, C., and Peters, T., 1981, The Solvus in the system $MnCO_3$-$CaCO_3$: Contrib. Mineral. Petrol., v. 76, p. 394-400.

Djule, S., 1958, An x-ray study in the system Ag-Cu-S: Acta Chem. Scandinavica, v. 12, p. 1427-1436.

Emmons W. D. and Larsen, E. S., 1913, A preliminary report on the geology and ore deposits of Creede, Colorado: U.S. Geological Survey Bulletin 530, p. 42-65.

Emmons W.D. and Larsen, E.S., 1923, Geology and ore deposits of the Creede district, Colorado: U.S. Geological Survey Bulletin 718, 198p.

Foley, N.K., and Vardiman, D.M., 1988, Paragenesis and mineral chemistry of ores of the Au-. Ag-, and base-metal-bearing North Amethyst

property, San Juan Mountains, Colorado: Geol. Soc. Amer. [Abs.], v. 20, p. A276.

Foley, N.K., Bethke, P.M., and Rye, R.O., 1990, A reinterpretation of the δD_{H2O} of inclusion fluids in contemporaneous quartz and sphalerite, Creede mining district, Colorado: a generic problem for shallow orebodies?: Econ. Geol., v. 84, p. 1966-1977.

Foley, N.K., 1990b, Fluid inclusion thermometry and geochemistry of gold-, silver-, and base-metal ores of the North Amethyst vein system, San Juan Mountains, Mineral County, Colorado: PartII, unpublished Ph.D dissertation, Virginia Polytechnic Institute and State University, 75 p.

Foley, N.K., 1990c, Lead isotopic geochemistry of the North Amethyst vein system, and the Creede mining district and vicinity, San Juan Mountains, Colorado: Part III, unpublished Ph.D dissertation, Virginia Polytechnic Institute and State University, 90 p.

Goldsmith, J.R., and Graf, D.L., 1957, The system CaO-MnO-CO_2: solid solution and decomposition relations: Geochimica et Cosmochimica Acta, v. 11, p. 310-334.

Guidice, P.M., 1981, Mineralization at the convergence of the Amethyst and OH fault systems, Creede district, Mineral County, Colorado: Unpub. M.Sc. thesis, University of Arizona (Tucson), 95p.

Gries, R.R., 1985, San Juan Sag: Cretaceous rocks in a volcanic covered basin, south-central Colorado: The Mountain Geologist, v. 22, p. 167-179.

Haas, J.L., 1971, The effect of salinity on the maximum thermal gradient of a hydrothermal system at hydrostatic pressure: Econ. Geology, v. 66, no. 6, p. 940-946.

Heald, P.W., Foley, N.K., and Hayba, D.O., 1987, Comparative anatomy of volcanic-hosted epithermal deposits: Acid-sulfate and adularia-sericite: Econ. Geol., v. 82, p. 1-26.

Hayba, D.O., Bethke, P.M., Heald, P., and Foley, N.K., 1985, Geologic, mineralogic, and geochemical characteristics of volcanic-hosted epithermal precious-metal deposits: Reviews in Econ. Geology, v. 2, p. 129-167.

Hon, K., and Mehnert, H.H., Compilation of revised ages of volcanic units in th San Juan Mountains, Colorado: Recalculated K-Ar age determinations using IUGS constants: U. S. Geological Survey Open-file Report 83-668, 14p.

Horton, D.G., 1983, Argillic alteration associated with the Amethyst vein system, Creede mining district, Colorado: Unpub. Ph.D. thesis, University of Illinois (Urbana-Champaign), 337p.

Lanphere, M.A., 1987, High-resolution $^{40}Ar/^{39}Ar$ geochronology, central San Juan caldera complex, Colorado [abs]: Geol. Soc. America Abs. with Programs, v. 19, no. 5, p. 288.

Lanphere, M., 1988, High resolution $^{40}Ar/^{39}Ar$ chronology of Oligocene volcanic rocks, San Juan Mountains, Colorado: Geochimica cosmochimica acta, v. 52, pp. 1425-1434.

LeMaitre, R.W., 1984, Chemical classification of volcanic rocks: Australian Journal of Earth Science, v. 31, p. 245-255.

Lipman, P.W., and Sawyer, D.A., 1988, Preliminary geology of the San Luis Peak quadrangle, San Juan volcanic field, Southwestern Colorado: U.S. Geological Survey Open-file Report 88-359, 32p.

Lipman, P.W., Steven, T.A., and Mehnert, H.H., 1970, Volcanic history of the San Juan Mountains, Colorado, as indicated by potassium-argon dating: Geol. Soc. America Bull., v. 81, p. 2329-2352.

Lipman, P.W., Doe, B.R., Hedge, C.E., and Steven, T.A., 1978, Petrologic evolution of the San Juan volcanic field, southwestern Colorado: Pb and Sr evidence: Bull. Geol. Soc. Amer., v. 89, p. 59-82.

Maresch, W.V., and Mottana, A., 1976, The pyroxmangite-rhodonite transformation for the $MnSiO_3$ composition: Contributions to Mineralogy and Petrology, v. 55, p. 69-79.

Ohashi, Y., Kato, A., and Matsubana, S, 1975, Pyroxenoids: a variation in chemistry of natural rhodonites and pyroxmangites: Carnegie Inst. Wash. Year Book, v. 74, p. 561-564.

Peacor, D.R., Essene, E.J., Brown, P.E., and Winter, G.A., 1978, The crystal chemistry and petrogenesis of a magnesiun rhodonite: American Mineralogist, v. 63, pp. 1137-1142.

Peacor, D.R., Essene, E.J., and Gaines, A.M., 1987, Petrologic and crystal-chemical implications of cation order-disorder in kutnahorite [$CaMn(CO_3)_2$]: Am. Mineralogist, v. 72, p. 319-328.

Peters, T.J., Trommsdorff, V., and Sommerauer, J., 1978, Manganese pyroxenoids and carbonates: critical phase relations in metamorphic assemblages from the Alps: Contrib. Mineral. Petrol., v. 66, p. 383-388.

Peters, T.J., Valarelli, J.V., Coutinho, J.M., Sommerauer, J., and Von Raumer, J., The manganese deposits of Buritirama (Para, Brazil): Schweiz. Mineral. Petrog. Mitt. v. 57, p. 313-327

Plouff, D., and Pakister, L.C., 1972, Gravity study of the San Juan Mountains, Colorado: U.S. Geological Survey Prof. Paper 800-B, p. 183-190.

Plumlee, G.S., 1989, Processes controlling epithermal mineral distribution in the Creede mining district, Colorado: Unpub., Ph.D thesis, Harvard University, 378p.

Ramdohr, P., 1969, The ore minerals and their intergrowths: Pergamon Press, Braunschweig, West Germany, 1175p.

Robinson, R.W., 1981, Ore mineralogy and fluid inclusion study of the southern Amethyst vein system, Creede mining district, Colorado: Unpub. M.Sc. thesis, New Mexico Institute of Mining and Technology (Socorro), 85p.

Robinson, R.W., and Norman, D.I., 1984, Mineralogy and fluid inclusion study of the southern Amethyst vein system, Creede mining district, Colorado: Econ. Geol., v. 79, p. 439-337.

Roedder, E., 1977, Changes in ore fluid with time, from fluid inclusion studies at Creede, Colorado: Internat. Assoc. on the Genesis of Ore Deposits Proc. (IAGOD), 4th Symposium, Problems of ore deposition, Varna, Bulgaria, 1974, v. 2, p. 179-185.

Sawyer, D.A., Sweetkind, D., Rye, R.O.,Siems, D.F., Reynolds, R.L., Rosenbaum, J.G., et al., 1989, Potassium Metasomatism in the Creede mining district, San Juan volcanic field, Colorado: Continental Magmatism [Abs], International Association of

Volcanology and Chemistry of the Earth's Interior, New Mexico Bureau of Mines and Mineral Resources, Bulletin 131, p. 234.

Scarpalli, S., 1970, The Serro do Novio manganese deposit, Brazil: I. UNESCO (ed.) Genesis of Precambrian iron and manganese deposits, Proc. Kiev Symp. (Earth Science 9).

Skinner, B.J., 1966, The system Cu-Ag-S: Econ. Geol., v. 61, p. 1-26.

Skinner, B.J., Jambor, J.J., and Ross, M., 1966, Mckinstryite, a new copper-silver sulfide: Econ. Geol., v. 61, pp. 1383-1389.

Steven, T.A., 1975, Middle Tertiary volcanic field in the southern Rocky Mountains, in B.F. Curtis, ed., Cenozoic history of the southern Rocky Mountains: Geological Society of America Memoir 144, p. 75-94.

Steven, T.A., and Ratte, J.C., 1965, Geology and structural control of ore deposition in the Creede district, San Juan Mountains, Colorado: U.S. Geological Survey Prof. Paper 487, 90p.

Steven, T.A., and Ratte, J.C., 1960, Relation of mineralization to caldera subsidence in the Creede district, San Juan Mountains, Colorado: U.S. Geological Survey Prof. Paper 400-B, p. B14-B17.

Steven, T.A., 1968, Ore deposits in the central San Juan Mountains, Colorado, in J.D. Ridge, ed., Ore deposits of the United States 1933-1967, Graton-Sales volume, AIME, v. 1, p. 706-713.

Steven, T.A., and Eaton, 1975, Environment of ore deposition of the Creede mining district, San Juan Mountains, Colorado: Part I. Geologic, hydrologic, and geophysical setting: Econ. Geol., v. 70, P. 1023-1037.

Steven, T. A., and Lipman, P.W., 1976, Calderas of the San Juan volcanic field, southwestern Colorado: U.S. Geol. Survey Prof. Paper 958, 35p.

Van Loenen, R.E., 1980, Inesite, a new U.S. occurrence near Creede, Mineral County, Colorado: Mineralogical Record, v. 11, p. 35-36.

Vergo, N., 1987, Wallrock alteration at the Bulldog Mountain Mine, Creede, Colorado [abs.]:Geol. Soc. America Abs. with Programs, v. 19, no. 5, p. 340.

Wetlaufer, P.H., 1977, Geochemistry and mineralogy of the carbonates of the Creede mining district, Colorado: U.S. Geol. Survey Open-file Report 77-706, 134p.

Winter, G.A., Essene, E.J., and Peacor, 1981, Carbonates and pyroxenoids from the manganese deposit near Bald Knob, North Carolina: Am. Mineralogist, v. 66, p. 278-298.

PART 2:

Fluid inclusion thermometry and geochemistry of gold-, silver and base-metal ores of the North Amethyst vein system, San Juan Mountains, Mineral County, Colorado

LISTING OF CONTENTS

ABSTRACT

INTRODUCTION

GEOLOGIC SETTING

MINERALOGY AND PARAGENESIS

Conditions of ore formation

STABLE ISOTOPE SYSTEMATICS AND GAS CHEMISTRY

FLUID INCLUSION STUDY

Petrogaphy and thermometry

Precursor quartz veins

Mn - Au association

Base metal - silica association

Discussion of fluid inclusion data

Depth of ore formation

DEPOSITIONAL CONTROLS ON ORE MINERALIZATION

GENESIS OF NORTH AMETHYST MINERALIZING SYSTEM

CONCLUSIONS

REFERENCES

ABSTRACT

The North Amethyst vein system, a Au-, Ag-, and base-metal-rich deposit occurring at the northern edge of the historic Creede district in southwestern Colorado, formed approximately 25 million years ago in faults and fractures that cut Tertiary-aged volcanic rocks of the Nelson Mountain Tuff. Ore minerals of the North Amethyst vein system are distributed over a vertical interval of at least 600 meters and for over 600 meters along strike of the north-northwest-trending Amethyst fault. They are also found along upper elevations of the east-west-trending Equity fault.

The two North Amethyst vein mineral associations consist of 1) quartz, Mn-silicates, Mn-carbonates, K-feldspar, hematite, magnetite, electrum, sphalerite, galena, pyrite, chalcopyrite, Au-, and Ag-sulfides, and Ag-sulfosalts, and 2) quartz, calcite, sericite, chlorite, hematite, fluorite, adularia, sphalerite, galena, pyrite, chalcopyrite, and Ag-bearing tetrahedrite.

Fluid inclusion and paragenetic studies show that three distinct hydrothermal fluids contributed to mineralization of the North Amethyst veins. The fluids that deposited the finegrained early gold-bearing association ranged in temperature from >350^{o}C to 270^{o}C and contained less than 2 weight percent (NaCl equivalent) of dissolved components. Younger, generally cospatial fluids that deposited the slightly coarser-grained base-metal sulfides, and Ag-tetrahedrite were not boiling, ranged in temperature from 280^{o}C to 220^{o}C, and contained dissolved components equivalent to 5-11 weight percent NaCl. The youngest fluids deposited abundant thick crusts of pink calcite and large euhedral

quartz crystals in open spaces, especially along the northern Amethyst fault. Fluid inclusions contained in the latest quartz show copious evidence for formation in a boiling environment. The range of homogenization temperatures for the youngest fluids in quartz and calcite is 128-301 ^{o}C and salinities are generally less than 0.5 weight percent NaCl equivalent. CO_2 was not identified in any of the inclusions suggesting that CO_2 is below detection levels for standard crushing techniques.

Depth estimates of ~1000 meters and ~500 meters for Mn- Au-rich and base metal-silica-rich assemblages; respectively, based on periods of boiling identified in fluid inclusion studies are shallower than estimates from geologic reconstruction (~1500 m) supporting mineralogical evidence that CO_2 played an major role in depositional processes. However, if deposition of the later stages of mineralization occurred at a much later time than that of the earlier Au-rich stages, after a period of erosion that resulted in a topography similar to that of the present-day, CO_2-boiling may not have been a dominant control on mineral deposition.

INTRODUCTION

The North Amethyst vein system is located just south of the Continental Divide near the southern edge of the San Luis caldera in Mineral County, Colorado. The precious- and base-metal-bearing veins fill steeply dipping structures related to an extension of the Amethyst fault, a north-northwest-trending normal fault system that cuts rhyolitic and rhyodacitic volcanics of the central San Juan volcanic

complex, and to the east-west-trending reverse Equity fault (Fig. 1). The veins lie just inside the northern boundary of the historic Creede mining district and constitute the largest Au-rich vein deposit discovered in the Creede district to date.

The geochemistry and fluid inclusion systematics of the gold-, silver-, and base-metal-rich mineralization are presented in this report which draws heavily on the observational database presented in Foley (1990a). The data are incorporated into a model based on mineralogic, geochemical, and isotopic constraints and comparison is made with existing models for mineralization in the central and southern parts of the Creede district.

Mineralization in the central San Juan area has been the subject of numerous reports and papers since the early 1880's when the area around Creede was first prospected. The relationship of the mineralization to regional geologic setting was first described in detail by Steven and Ratte (1965) and Steven (1968). The area encompassing the Creede mining district has been the subject of continuing research since the late 1950's by P.M. Bethke, P.B. Barton, Jr., Robert O. Rye, Ed Roedder, and others of the U. S. Geological Survey (see Appendix A). Their work has been published in a series of papers on the Creede district (Steven and Eaton, 1975; Bethke et al., 1976; Roedder, 1977; Barton et al., 1977; Bethke and Rye, 1979; Hayba et al., 1985; Foley et al., 1990; Plumlee, 1989, and others to follow). A recent bibliograghy of the Creede mining district has been compiled by Hayba and Conte (1987).

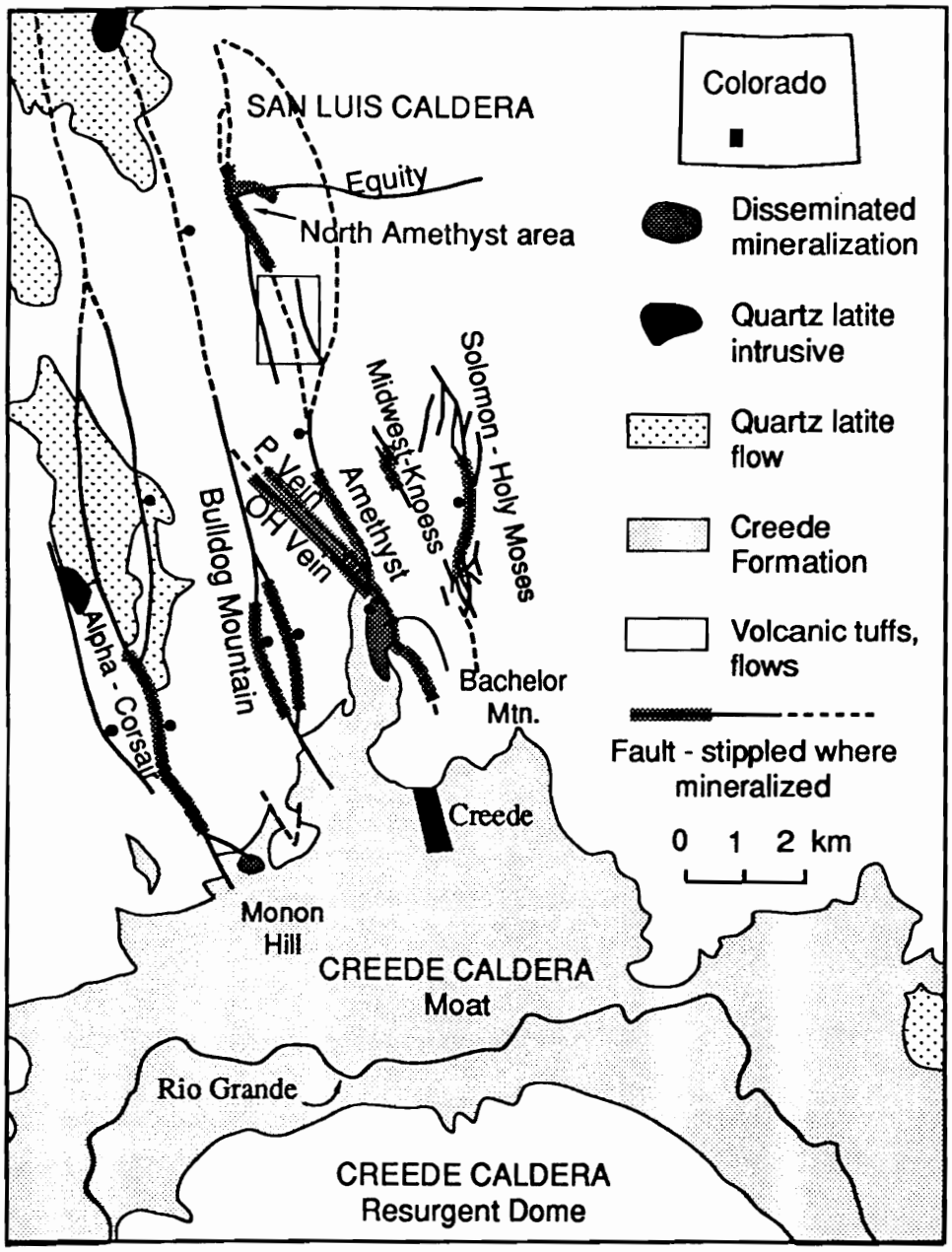

Figure 1. Generalized geologic map of the Creede mining district and vicinity. The graben structure formed by named faults is within the Bachelor caldera and links the San Luis and Creede calderas. North Amethyst vein system is at the intersection of the Equity and Amethyst faults. From Plumlee (1989), geology after Bethke and Lipman (1987) and Lipman and Sawyer (1988). Box shows location of study by Bazrafshan and Norman (1987); see text for discussion.

Mineralization in the North Amethyst area was discovered by Homestake Mining Company through an extensive drilling program in the area and they have developed exploratory workings along the veins. Historic accounts of ores of the Equity mine and some preliminary reports on the more recently discovered North Amethyst ores are described in Appendix A. Homestake Mining Company has delineated an extensive high-grade zone adjacent to old workings of the near-surface Equity mine. Permission to study the mineralization and logistical assistance from Homestake Mining Company are gratefully acknowledged. The fluid inclusion data collected for this study are compared to an extensive set of thermometric data on fluid inclusions from quartz, sphalerite, calcite, and fluorite collected by Bazrafshan and Norman (1987). Their work centered on minerals selected from core drilled in the north-central part of the Creede district in an area immediately south of the North Amethyst workings (Figure 1). Similar datasets for other veins of the Creede district have been compiled by Bethke et al. (1987) using data from Roedder (1977); Robinson (1981); Woods et al. (1982); Hayba (1984); Robinson and Norman (1984); and J. Goss, unpub. data (1987).

GEOLOGIC SETTING

The San Juan volcanic field is an erosional remnant of a much larger volcanic field that covered part of the southern Rocky Mountains in the middle Tertiary (Steven, 1975, Lipman et al., 1978). The volcanic field rests upon an eroded base consisting of Proterozoic crystalline metavolcanics, metasediments, and granitiod rocks, and,

possibly remnants of Paleozoic, Mesozoic and Tertiary sedimentary rock (summarized by Steven and Lipman, 1976, Lipman et al., 1978; Baars and Stevenson, 1984; and Gries, 1985). The composite volcanic field consisted dominantly of andesite-dacite lavas and associated volcaniclastic rocks erupted from precaldera volcanoes mainly between 35 and 30 million years ago. A large negative Bouguer gravity anomoly underlies much of the San Juan volcanic field and is believed to reflect a large composite batholith emplaced beneath the field (Plouff and Pakister, 1972). From about 28 to 26 million years, the central San Juan volcanic field experienced widespread, large volume, silicic ash-flow eruptions and related caldera subsidence (Lipman et al., 1970, Lipman et al., 1978; Lipman and Sawyer, 1988; Lanphere, 1988). The mineralization of the Creede district is located in a complex set of nested calderas formed by the pyroclastic eruptions.

Mid-Tertiary sediments accumulated locally within the San Juan field. The most voluminous sediments are those of the Creede Formation, which were deposited in the moat of the Creede caldera and in channels incised in the caldera wall. They consist of stream channel gravels, landslide breccias, travertines, bedded lacustrine sediments and water-lain tuffs (Steven and Ratte, 1965). Thin, local sediments interbedded with volcanic units have also been found in the north-central part of the district by mining companies. Bachelor caldera moat sediments consisting mainly of lacustrine sediments including bedded ash and fine siltstones and local lenses of sand and pebble conglomerates, some of which were reworked and locally argillized, have been identified by Chevron Resources, Inc, (O'Brient, pers. commun., 1982) and Homestake

Mining Company (S. Caddey and C. Byington, pers. commun., 1983). Near the caldera walls, the sediments include megabreccias, laharic breccias, and rare organic-rich lacustrine carbonates (S. Caddey, C. Byington, pers. commun., 1983; D. Sawyer, pers. commun., 1987). Within the San Luis caldera, fluvial and lake-bed sediments (few tens of meters thick) that accumulated in local basins overlie the main Equity dacite facies of the Nelson Mountain Tuff (Lipman and Sawyer, 1988).

The North Amethyst mineralization is located approximately at the intersection of the Equity fault and the probable northern extension of the Amethyst fault, just inside the southern topographic wall of the San Luis caldera (Fig. 1). The ores are hosted by rhyolitic to dacitic intracaldera tuff[1]. Lipman and Sawyer (1988) include this tuff as part of the Nelson Mountain Tuff, a unit with a total exposed thickness of more than 1.5 km and no base exposed in the thickest section (Lipman and Sawyer, 1988). As described by Lipman and Sawyer (1988), mapped units overlying the tuff in the vicinity of the mineralization include lavas and related rocks of Stewart Peak (0-500 m), and intracaldera sedimentary rocks (0-50 m); in the North Amethyst area these may have had a combined thickness of about 500 meters. The rocks are generally in the same attitude as they formed.

---

1 Volcanic units named in this text follow the terminology of Lipman and Sawyer (1988), however, P. Lipman (written commun., June, 1990) notes that new paleomagnetic data raise some questions as to whether the volcanic rocks hosting the North Amethyst mineralization are part of the Nelson Mountain Tuff or the Carpenter Ridge Tuff. The unit was originally correlated with the Carpenter Ridge Tuff by Steven and Ratte (1965) and C. Byington (written commun., 1982).

The total thickness of rocks above the mineralization in the North Amethyst area (~10000'-12000+' elev.) at the time of ore deposition is not well-constrained. The Nelson Mountain Tuff is exposed at an elevation of 13285 feet (4050 m) on Captive Inca Ridge, two kilometers northeast of the intersection of the northern Amethyst and Equity faults (Steven and Ratte, 1965). This suggests that at least a kilometer of lavas, tuff and related volcanic rocks of Nelson Mountain Tuff may have overlain the base of gold ore at the time of mineralization (10000' elev.). Depth estimates based the volcanic stratigraphy including the upper two-thirds of the exposed Nelson Mountain Tuff (~1000 m) and, possibly as much as 500 meters of overlying Stewart Peak lava flows and associated volcaniclastic rock (filling moat area of caldera) and sedimentary rock, suggest thicknesses on the order of 1500 meters. If the tuffs hosting ore mineralization are part of the Carpenter Ridge Tuff, the stratigraphic thicknesses described in Lipman and Sawyer (1988) will have to be reevaluated, however, this should not affect estimates of the total thickness of volcanic rocks in the area. Further constraints on depth of mineralization based on fluid inclusion data are discussed below. Depths to the base of gold mineralization from the present-day surface range from about 350 meters to around 750 meters due to the steep topography (Fig. 2).

The complex history of movement and reactivation along faults of the Creede graben has been described in detail by Steven and Ratte (1965). Normal faults are the dominant structural element controlling the location of mineralization in the central San Juan area and most are related to evolution of the Oligocene calderas (Figure 1). The reverse

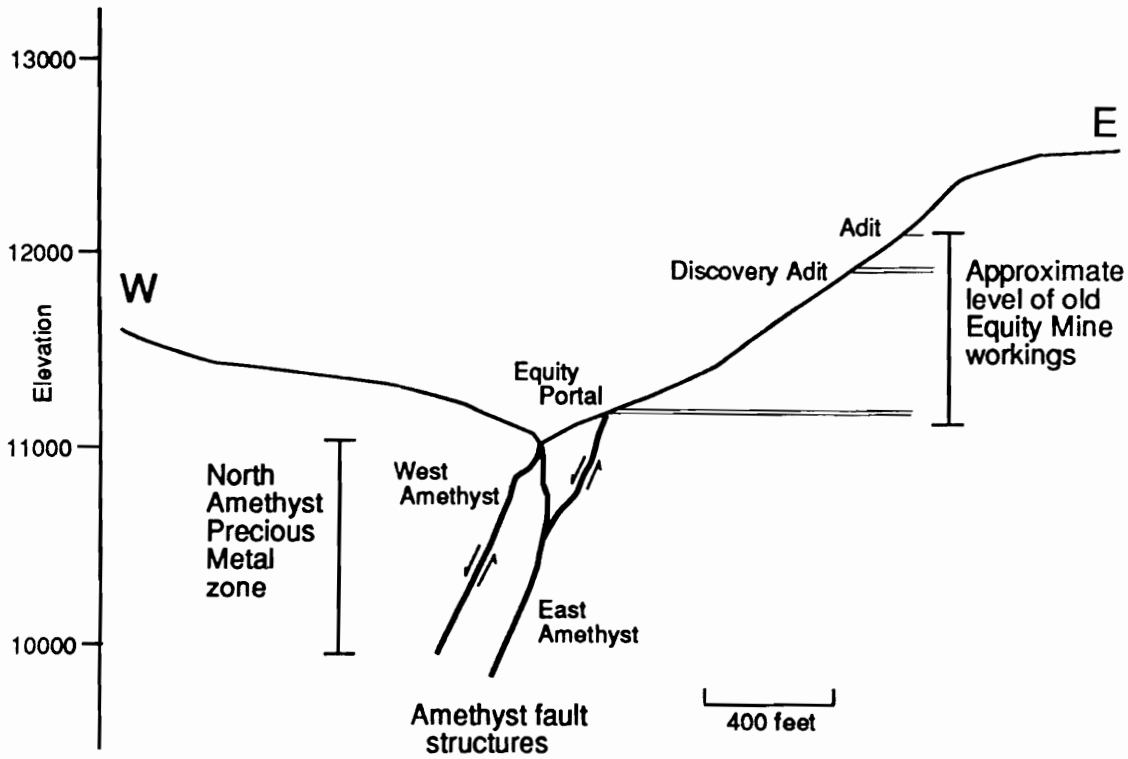

Figure 2. Cross-section view looking northward of the North Amethyst area. Levels of mineralization along northern Amethyst structure and Equity fault are identified.

Equity Fault, which formed by fault-bounded uplift of a triangular block presumably related to a shallow underlying intrusion (Lipman and Sawyer, 1988), is also mineralized. The dominant structural features are the well-formed caldera expressions and the north-northwest trending Creede graben which initially formed as a keystone graben in the Bachelor caldera (Figure 1). The major faults from west to east include the Alpha-Corsair, Bulldog Mountain, Amethyst, and Solomon-Holy Moses faults. The OH, P and other minor faults cut the central block of the graben, are nearly vertical, and had primarily strike-slip motion (S. Caddey, pers. commun., 1985).

Radiometric age determinations on adularia ($^{40}Ar/^{39}Ar$ incremental heating ages) from drillcore from the North Amethyst vein system indicate an age of 25.13 +/- .13 Ma (M. Lanphere, written commun., 1989). The adularia is associated with base-metal mineralization of the later hydrothermal event occurring along the North Amethyst vein system. The gold-bearing ores predate the base-metal mineralization (Foley and Vardiman, 1988; Foley, 1990a), and thus their age falls in the interval between that of the host rock (the Nelson Mountain Tuff) at 26.13 Ma and the vein adularia at 25.13 Ma. Radiometric age-dates on gangue associated with ore mineralization from the main Creede mining district indicate that the minerals were also deposited at about 25 Ma (Bethke et al., 1976).

MINERALOGY AND PARAGENESIS

The mineralogy, paragenesis, and mineral chemistry of the North Amethyst mineralization has been studied in detail (Foley and Vardiman,

1988; Foley, 1990a), and aspects relating to the interpretation of the petrology and the geochemical evolution of the mineralizing hydrothermal system are summarized below.

The earliest set of veins dominantly consists of quartz and calcite. Because these quartz veins are cut by all other stages defined for the North Amethyst mineralization they are termed precursor veins (Foley, 1990a).

The potentially economic mineralization of the North Amethyst vein system consists of two nearly coextensive associations (Table 1) having contrasting mineralogies, textures, and modes of formation (Foley, 1990a). The two associations are separated locally by a period of major brecciation and sedimentation. Both mineral associations are confined primarily to the same steeply dipping structures in silicified rhyolite. The ores are multiply brecciated and vein fillings locally show sedimentary textures. Intense sericitic alteration occurs at higher levels in the system; at depth the wallrock is potassium metasomatized (Sawyer et al., 1989).

The older, manganese- and gold-bearing association consists of two fine-grained ore substages, both of which contain electrum, uytenbogaardtite, tetrahedrite, Ag-sulfosalts, and Ag- and base-metal-sulfides (beta-1, and beta-2 stages, Table 1). The beta-1 stage occurs as rounded cobbles, pebbles and angular fragments of a range of sizes within an unsorted quartz-cemented breccia. The second fine-grained gold-bearing stage (beta-2) occurs as a fairly continuous seam or vein that cuts across the quartz-cemented breccia containing cobbles and angular fragments of the first fine-grained ore stage. The two stages

Table 1. Stages of mineralization and brecciation events of the North amethyst vein system.

STAGE	NORTH AMETHYST VEIN MINERAL ASSEMBLAGE
Late:	
Base metal - silicate association:	
3	Mn-calcite >> Quartz > Pyrite
Breccia-4	Mn-calcite cement, fragments of earlier assemblages, breccias and minerals, [wallrock]
2b	Quartz > Calcite > Adularia > Fluorite > Chlorite = Pyrite
Breccia-3	Quartz + chlorite cement, fragments of wallrock, and coarse stage 1 sulfides
1b	Sphalerite > Galena > Pyrite > Chalcopyrite > Tetrahedrite
1a	Quartz > Pyrite = Hematite > Chlorite
Breccia-2	Quartz cement, fragments of α-,and β-stages, wallrock, sedimented structures black quartz breccia
Mn - Au association:	
β-2	Galena > Sphalerite > Chalcopyrite > Pyrite > Tetrahedrite > Ag- and Au-minerals > Electrum {Magnetite, Hematite}
Breccia-1	Quartz cement, fragments of α- and β-1 stages
β-1	Galena > Sphalerite > Chalcopyrite > Pyrite > Tetrahedrite > Ag- and Au-minerals > Electrum {Magnetite, Hematite}
α	Rhodocrosite = Quartz > Mn-calcite = Pyroxmangite K-feldspar >> Sphalerite > Galena > Pyrite > [Barite]
Precusor veins:	Quartz > Calcite >> Barite
Early:	

Abbreviations: >>, much greater than; >, greater than; =, approximately equal; {} distribution unknown; [], molds.

are mineralogically identical and occur at the same localities. These ore stages cut a cryptocrystalline assemblage (alpha-stage) containing manganese-carbonate, manganese-silicate, and quartz. The alpha-stage assemblage primarily consists of rhodocrosite, manganocalcite, and kutnahorite (manganese analog to dolomite), rhodonite, pyroxmangite, and quartz. Minor amounts of sphalerite and galena (Table 1) occur within the manganese-rich assemblage. Fragments of the Mn-carbonate and - silicate assemblage also occur within the quartz-cemented breccia. The iron-oxide-sulfide assemblage found with this association is hematite + quartz + pyrite +/- magnetite.

The younger crosscutting base metal - silica association contains a coarse-grained base-metal sulfide assemblage (stage 1) that primarily consists of colorless to red-brown sphalerite showing extensive chalcopyrite disease (e.g., Barton and Bethke, 1988), galena, pyrite and chalcopyrite (Table 1). The base-metal stage contains an iron-bearing assemblage that consists of hematite + chlorite + pyrite + quartz. Later open-space filling minerals that are part of the association include calcite, adularia, fluorite, and quartz (stage 2). Local occurrences of quartz, manganocalcite, trace pyrite, rhodocrosite, and gypsum line late vugs and form crusts on earlier assemblages and breccias (stage 3).

During the periods of brecciation and sedimentation that separated associations and stages, chalcedonic quartz cement was deposited around some fragments and crystals. The cements vary in color from light gray to near black; the coloration is apparently related to the amount of sulfide dust carried by the cement (Foley, 1990a).

The complete manganese- and gold-bearing assemblages of the older association are not documented in the main district (Foley, 1990a). In contrast, the mineralogic and lead isotopic characteristics of the younger association are similar to those of ores of the main Creede district (Foley, 1990a; Foley, 1990c). These characteristics enabled Foley and Vardiman (1988) and Foley (1990a) to correlate the younger association of the North Amethyst area (Stages 1 through 3) with Stages B through E of the Creede district (Bethke and Rye, 1979), with Stages II through IV of the Bulldog vein system (Plumlee, 1989), and with mineralization occurring along the southern Amethyst vein and with disseminated mineralization.

Conditions of Ore Deposition

Broad limits can be placed on the temperatures of mineral formation of the Mn-Au association by the following observations: 1) The range of carbonate compositions found for alpha-stage (Foley, 1990a) indicate a formation temperature in excess of 350°C (proposed natural solvus of calcite-kutnahorite), and possibly in excess of 500°C (experimental solvus of kutnahorite-rhodocrosite). 2) The predominance of rhodonite over pyroxmangite is generally consistent with a formation temperature of greater than 350°C (Maresch and Mottana, 1976, see Foley 1990a for discussion). 3) The high Ag content of electrum coexisting with acanthite and uytenbogaardtite in beta-stage indicates a disequilibrium assemblage formed by the breakdown of a high-temperature gold-bearing argentite and silver-rich electrum, thus, the original assemblage must have formed at temperatures greater than 200°C. 4) The mole percent FeS in sphalerite of alpha-, and beta-stage (<2.0 mole %) can be used to

estimate log f_{S2} by the relation: log f_{S2} = 14.32 - 15460/T - 2logX_{FeS} (Barton and Toulmin, 1964; Barton and Skinner, 1979). Electrum compositions can also be used to estimate log f_{S2} by the relation log f_{S2} = 1/4.576T[-41980 + 16.52T - 18.296Tlog N_{Ag} + 4(1 - N_{Ag})^2(5650 - 1600(1 - N_{Ag}) - 1.375T)] (Barton and Toulmin, 1964; Barton, 1978). Lines defining the range of temperatures (~280-390^oC) and fugacities of S_2 (log f_{S2} ~ -8 to -12.5) consistent with three coexisting pairs of electrum and sphalerite are shown in Figure 3.

The occurrence of the assemblage hematite + pyrite + quartz + magnetite, and the absence of pyrrhotite places limits on the fugacities of S_2 and O_2 for the Mn-Au association at the temperature of formation. The assemblage rhodonite + rhodocrosite + quartz uniquely fixes the fugacity of CO_2 at a given temperature, pressure, and activity of SiO_2 (Abrecht, 1988). Other minerals used to place limits on conditions under which ore formed in the Mn - Au association include 1) the presence of galena and absence of anglesite, 2) presence of chalcopyrite and absence of bornite, and 3) the absence of hausmannite, alabandite, and graphite. Figure 4 was constructed based on these mineralogic constraints and shows stability fields for minerals of the Mn - Au association. Contour lines for the FeS and MnS contents of sphalerites are shown for sphalerites intergrown with magnetite, hematite, rhodocrosite, and pyrite. FeS is contoured from the relation FeS (in sphalerite) + 1/2S_2 = FeS_2 following the approach of Barton and Skinner (1979). MnS is contoured in the rhodocrosite field using the relations MnS (in sphalerite) + 1/2S_2 + CO_2 = $MnCO_3$ + 1/2S_2, and data from Robie

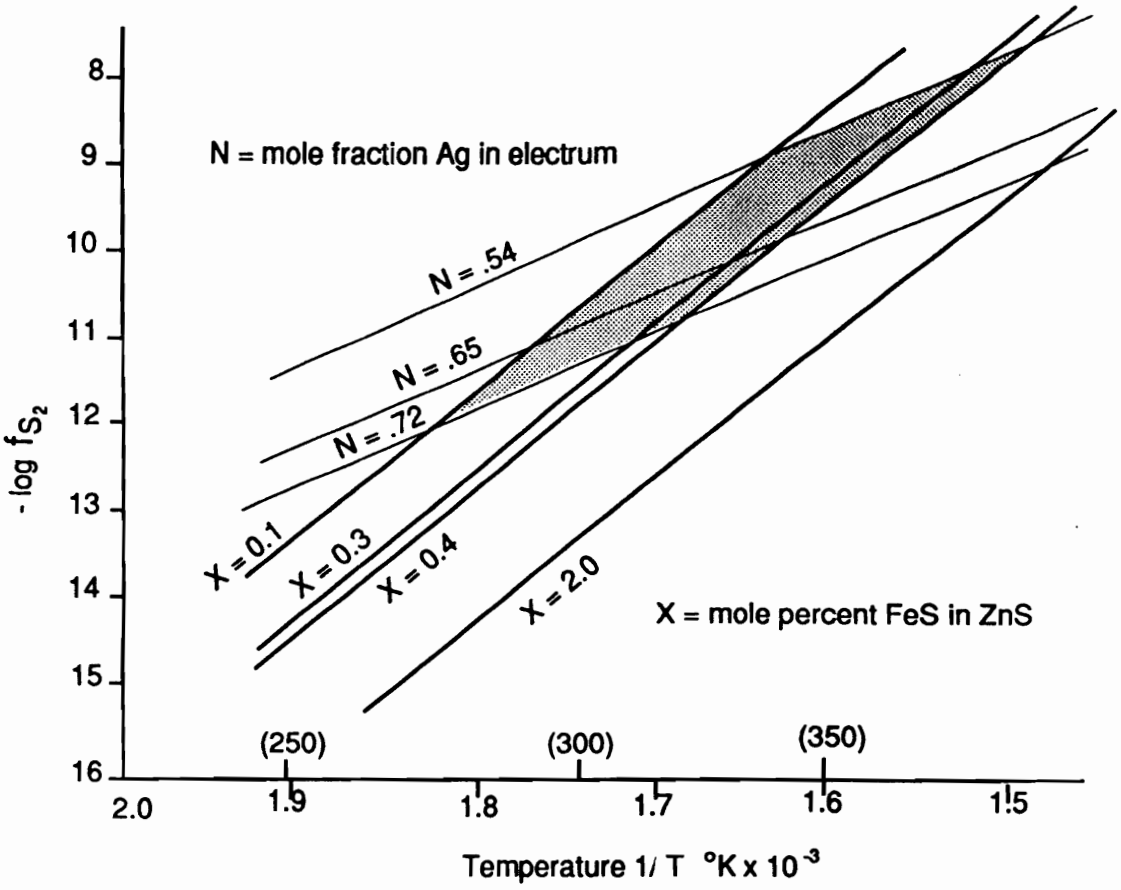

Figure 3. Compositions of three pairs of coexisting electrum and sphalerite used to define ranges of temperature and fugacity of sulfur consistent with gold-rich beta stage mineralization. Constructed using equations from Barton and Toulmin (1964, 1966), Barton and Skinner (1979), and Barton (1978).

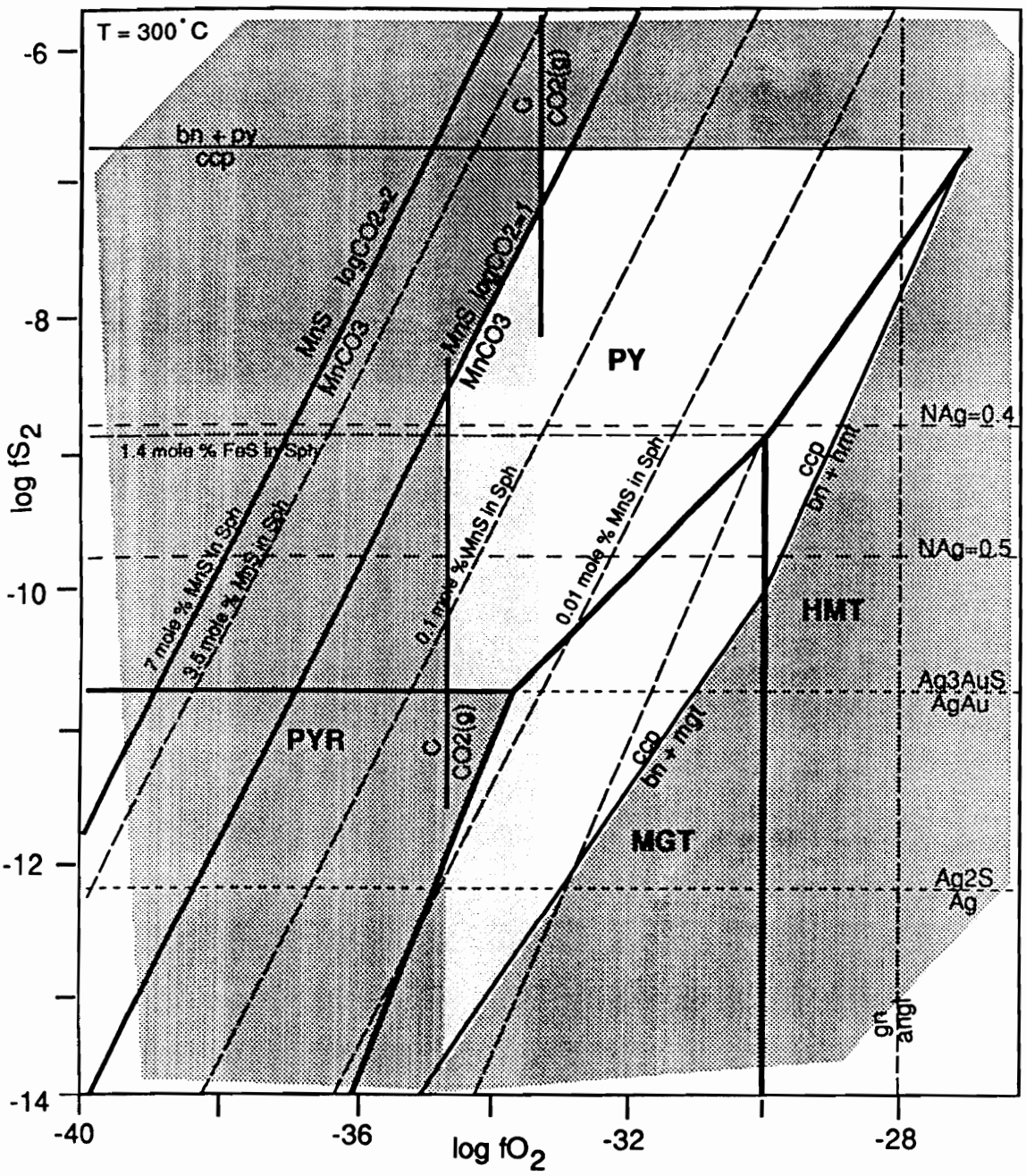

Figure 4. Stability fields of minerals of the Mn - Au association (Table 2) of the North Amethyst vein system. Area pertinent to ore asemblages is constructed using data from Barton and Skinner (1979), Vaughan and Craig (1978), and Robie et al. (1979). Shaded fields are inconsistent with mineralogical data.

et al. (1978), Bethke and Barton (1971), and Sombuthawee et al. (1978). A temperature of 300°C was chosen for the alpha- and beta-stage diagram based on fluid inclusion and mineralogical data.

None of the assemblages of the base metal - silica association can be used to estimate temperature[2], however, suitable material from each stage was available for fluid inclusion studies and the results are described below. The assemblages hematite + Fe-chlorite + pyrite + quartz and quartz + siderite + calcite restrict the fugacities of S_2 and O_2 of possible ore-fluids for stage 1 and 2 of the base metal - silica association. Additional mineralogic constraints on conditions of ore formation for the base metal- silica association include 1) the presence of galena and absence of anglesite, 2) presence of chalcopyrite and absence of bornite, 3) the absence of alabandite and graphite, and 4) the FeS content of sphalerite. Stability fields for minerals of the base metal - silica association are shown in Figure 5.

The similarity between Figure 5 and log a_{S2} - log a_{O2} diagrams constructed by Barton et al. (1977) for the OH vein of the central part of the Creede district is immediately apparent. The mineralogical constraints discussed by Barton et al. (1977) are virtually identical to those listed above for the North Amethyst base metal - silica association, with the exception that Barton et al. (1977) fixed FeS

---

2 The high concentration of Mn in chlorite of the North Amethyst area prohibited application of the chlorite geothermometer of Cathelineau (1988) and Cathelineau and Nieva (1985).

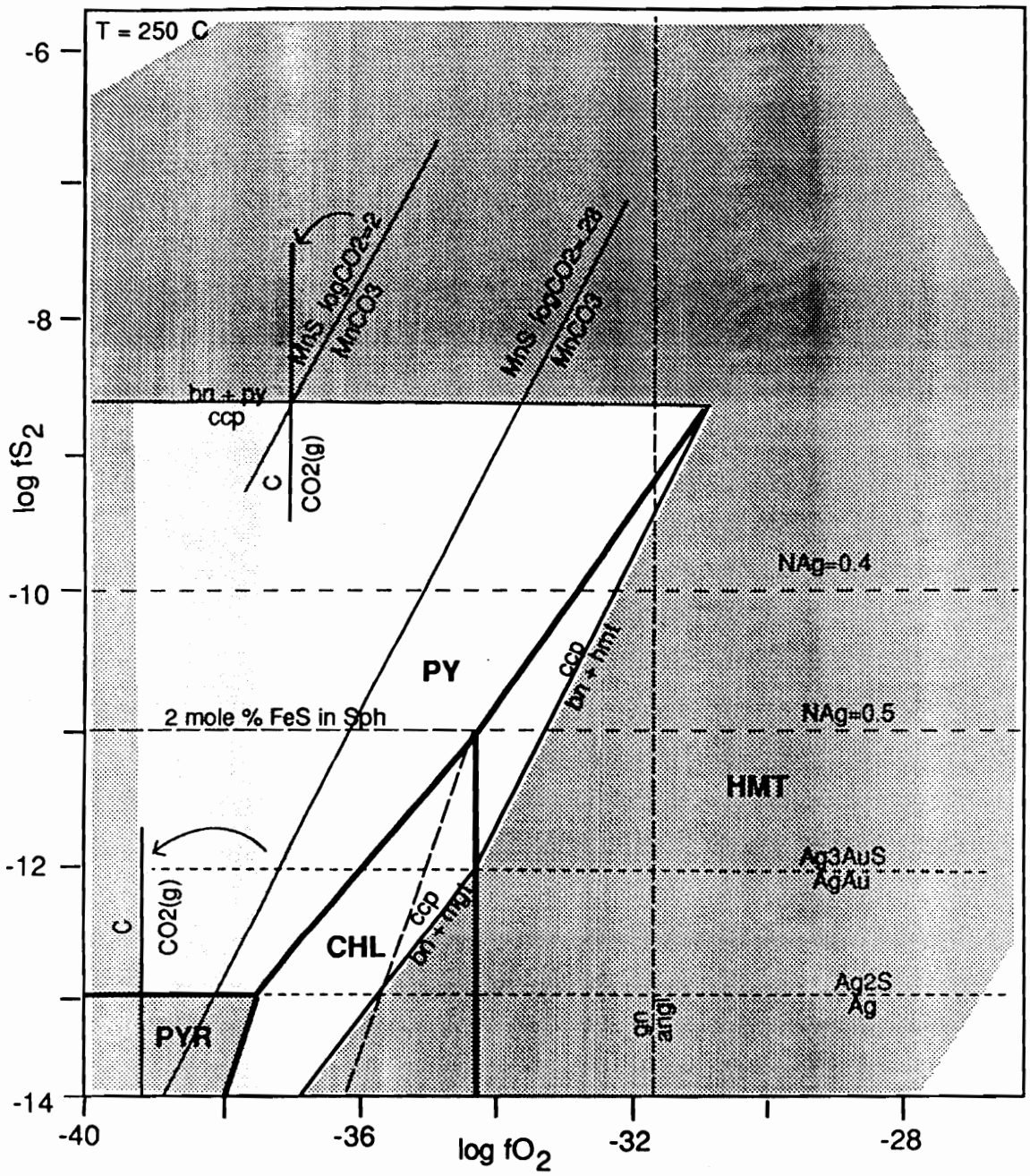

Figure 5. Stability fields of minerals of the base metal - silica association (Table 1) of the North Amethyst vein system. Area pertinent to ore asemblages is constructed using data from Barton and Skinner (1979), Vaughan and Craig (1978), and Robie et al. (1979). Shaded fields are inconsistent with mineralogical data.

contours by the common occurrence of 2 mole percent FeS-bearing sphalerite intergrown with chlorite and hematite along the OH vein. Figure 5 was constructed using a temperature of 250°C based on Stage-1 fluid inclusion data.

STABLE ISOTOPE SYSTEMATICS AND GAS CHEMISTRY

The stable isotope geochemistry of the Creede district has been studied extensively and Rye et al. (1988) recently summarized the results of fifteen years of work and over 1000 measurements. Most of their work has focussed on mineralization of the southern and central parts of the district, however, they have also completed initial work on the northern parts of the district including some of the ores examined in this study. Rye et al. (1988) have defined four end-member fluids that appeared at different times and places in the hydrology of the Creede hydrothermal system. These are shallow groundwater (δD--110°/oo, $\delta^{18}O$--16°/oo), a deep southern recharge fluid (δD--50, $\delta^{18}O$--2), a deep northern recharge fluid (δD--110, $\delta^{18}O$--2), and isotopically heavy fluids from Creede Formation sediments (travertines) (δD--80, $\delta^{18}O$-+8) (Rye et al., 1988). They summarized that saline fluids recharged from the Creede Formation sediments south of the district dominated main stage (B, C, and D stage of OH vein, Bethke and Rye, 1979) mineralization of the southern and central veins and coarse sphalerite (stage 1) mineralization of the North Amethyst vein system. Rye et al. (1988) also suggest that dilute $\delta^{18}O$ exchanged northern recharge fluids played a role in the North Amethyst mineralization, but they were unable to identify the extent of the fluids contribution to mineralization.

The entire Creede hydrothermal system was overlain by dilute unexchanged groundwater which flooded the veins when the system collapsed. These dilute meteoric-derived fluids mixed with the saline fluid, especially near the interface, throughout the life of the system. Additionally, isotopically heavy fluids from Creede Formation sediments were present in the southern parts of the district during pre-main-stage carbonate deposition (I stage of Bulldog vein, Plumlee, 1989). For samples from the North Amethyst vein system, Rye et al. (1988) found that sphalerite (stage 1, Foley, 1990a) formed from isotopically heavier fluids than did fluorite, adularia, and quartz (stages 2, 3, Foley, 1990a) which formed from fluids that contained a substantial component of isotopically light, northern recharge water.

Reconnaissance study of the gas chemistry of mineralization of the Creede district by Landis and Rye (1989) using quadrupole mass spectrometry has shown that each major stage of mineralization is characterized by a specific gas chemistry. Landis and Rye (1989) found that fluids from all minerals of the Creede district contain a complex, and as yet poorly characterized mixture of alkanes, alkenes, and aromatic hydrocarbons, in addition to varying proportions of H_2O, CO_2, H_2S, SO_2, Ar, N_2, and CH_4. For the North Amethyst vein system, they analysed inclusions in quartz, sphalerite, fluorite and adularia. Their data indicate that fluids in quartz, rhodocrosite, and calcite (probably stage 2, and 3, Foley, 1990a) had high CO_2 contents relative to fluid in sphalerite (stage 1). Sphalerite fluids apparently contain dominantly CH_4, and lack the more complex organic gases found in southern veins closer to moat sediments of the Creede Formation. This is attributed to

thermal pyrolysis of organics during transport within the hydrothermal system. Quartz and fluorite from the North Amethyst area contain abundant organics relative to H_2O. Stable isotope data suggest these fluids were derived locally (Rye et al., 1988), and Landis and Rye (1989) propose that these northern-derived organics survived pyrolysis due to shorter residence time within the hydrothermal system, or because the fluid was at lower temperatures. Greater amounts of N_2 are found in the North Amethyst samples relative to the central and southern parts of district and the North Amethyst samples have the highest HF contents of any samples in the entire district.

The CO_2 contents of individual inclusions reported by Landis and Rye (1989) for the North Amethyst mineralization range from 0.2 to 29 mole percent CO_2. 85% of the North Amethyst inclusions had CO_2 contents that were high enough to result in clathrate formation during freezing studies[2] or to cause visible expansion of the gas bubble during crushing under oil[3]. For minerals from the central and southern parts of the Creede mining district, CO_2 contents ranged from 0.1 to 54 mole percent and 71% of the inclusions analysed apparently had CO_2 contents that

---

3 Hedenquist and Henley (1985) have shown that if an inclusion has an internal CO_2 pressure of less than 10 bars at room temperature, the clathrate compound will not form. H_2O-CO_2 inclusions with a composition of 0.5 molal CO_2 trapped at 250°C, typical parameters for most epithermal deposits, will have internal pressures at 25°C of less than 9 bars (Bodnar et al., 1985).

4 Calculations by Bodnar et al. (1985) suggest that evidence of gases is almost never revealed during crushing tests on very small inclusions from epithermal deposits because such deposits generally have relatively low CO_2 contents that result in only slight expansion of the bubble. If the inclusion is large or individual inclusions are monitored during the crushing test the slight expansion of the bubble is usually visible.

should be detectable by clathrate formation or expansion of the gas bubble under oil. These results are surprising considering that the presence of CO_2 has never been identified visibly, during crushing tests, or by clathrate formation although over 3000 inclusions from Creede minerals have been studied by over a dozen analysts working in four different laboratories (Roedder, 1977; Woods et al, 1982; Guidice, 1981, Robinson, 1981; J. Goss, written commun. 1987; Hayba, 1986; Foley et al., 1990). CO_2 contents of inclusions in quartz and sphalerite from Creede analysed by crushing in a stream of helium, followed by high-sensitivity gas chromatography are about 80 ppm (Roedder and Andrawes, unpub. data, cited in Woods et al., 1982). Figure 6, modified from Bodnar et al. (1985), compares measured CO_2 contents from a number of geothermal and epithermal deposits. Typically, inclusions in epithermal deposits contain less than 3 mole percent CO_2.

Analyses of gases by mass spectrometry of fluid from inclusions can be complicated by several factors, the most important of which may be: 1) the decrepitation process (heating up to ~425^{o}C) could alter true gas abundances by decomposing or oxidizing minute sulfide inclusions and organic compounds and 2) water adsorbtion on fresh mineral surfaces and glass extraction lines may distort actual gas abundances relative to recovered water. Detailed work presently underway by D. Sweetkind and G. Landis (pers. commun., 1990) to compare quadropole mass spectrometry of samples from well-characterized inclusions from specific localities at Creede with results of gas compositions from other techniques may help to reconcile these observations.

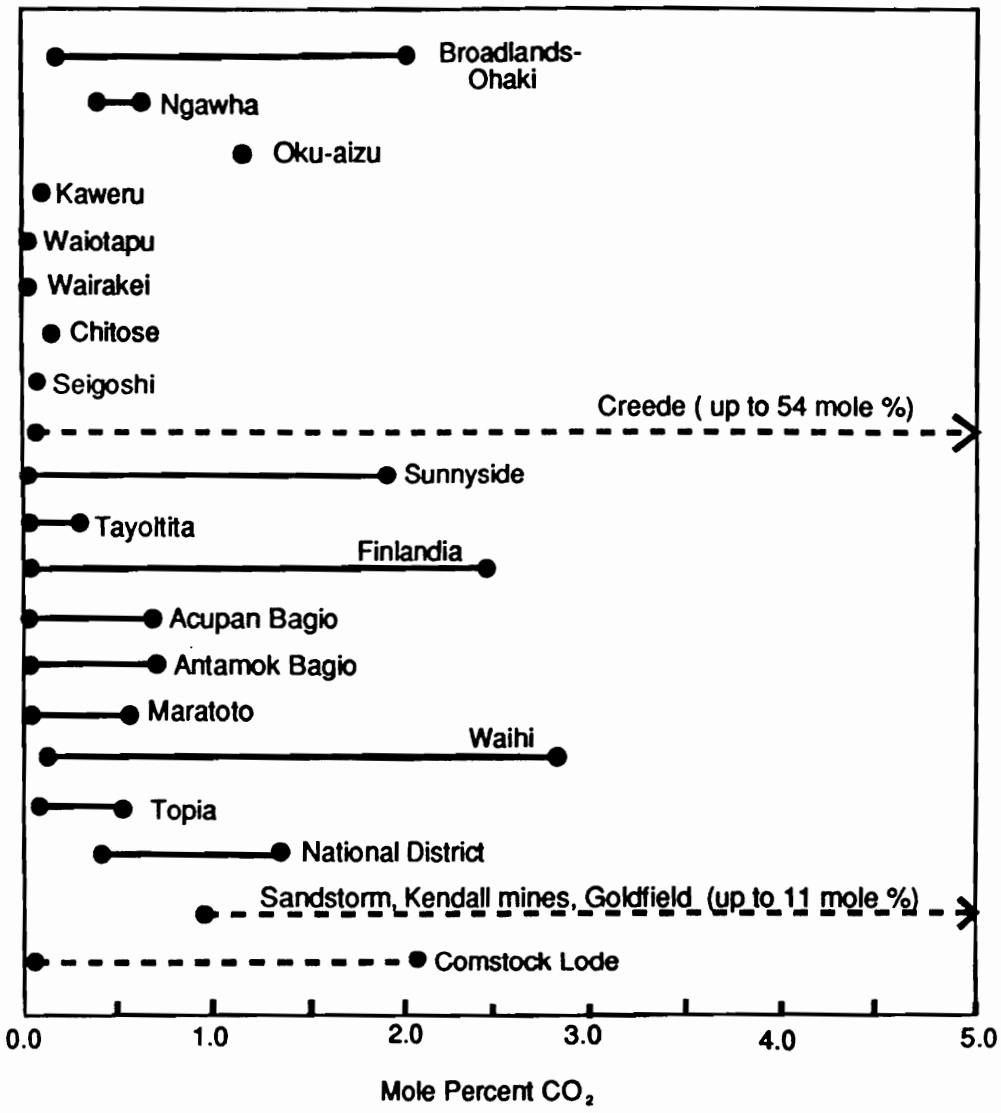

Figure 6. Summary of reported CO2 concentrations in hydrothermal fluids from some geothermal systems and epithermal precious-, and base-metal deposits. Compiled by Bodnar et al. (1985) from data given by Hedenquist and Henley (1985), Somner et al. (1985), and Vikre (1985), with additional data from Vikre (1990a, b), and Landis and Rye (1989). Dashed lines show data collected by mass spectrometry.

FLUID INCLUSION STUDY

A suite of vein minerals containing abundant fluid inclusions was selected from 15 sample localities along the North Amethyst vein system. Sample localities are shown in Figure 7 and descriptions of each are listed in Table 2. Thermometric determinations were made on 246 inclusions contained in quartz, sphalerite, fluorite, and calcite (Table 3). Minerals were chosen from samples showing clear paragenetic relationships as outlined by Foley (1990a). A detailed petrographic examination of the inclusions was done prior to thermometric analysis. The fluid inclusion data listed in Table 3 were collected using thermometry equipment made by Fluid, Inc. Precision associated with measurements of homogenization temperature is better than +/-2^{o}C in most cases; that associated with measurements of equivalent salinity is better than +/-0.2 weight percent. The stage was calibrated using SYN FLINC synthetic fluid inclusions (Sterner and Bodnar, 1984) and various standards of known melting point. Equivalent salinities are calculated using data of Hall et al. (1988) for the NaCl-KCl-H_2O system.

Petrography and Thermometry

Fluid inclusions suitable for at least partial thermometric analysis were found in all paragenetic stages documented for the North Amethyst vein. Textural relationships indicate, however, that the inclusions formed from a variety of mechanisms, not all of which yield

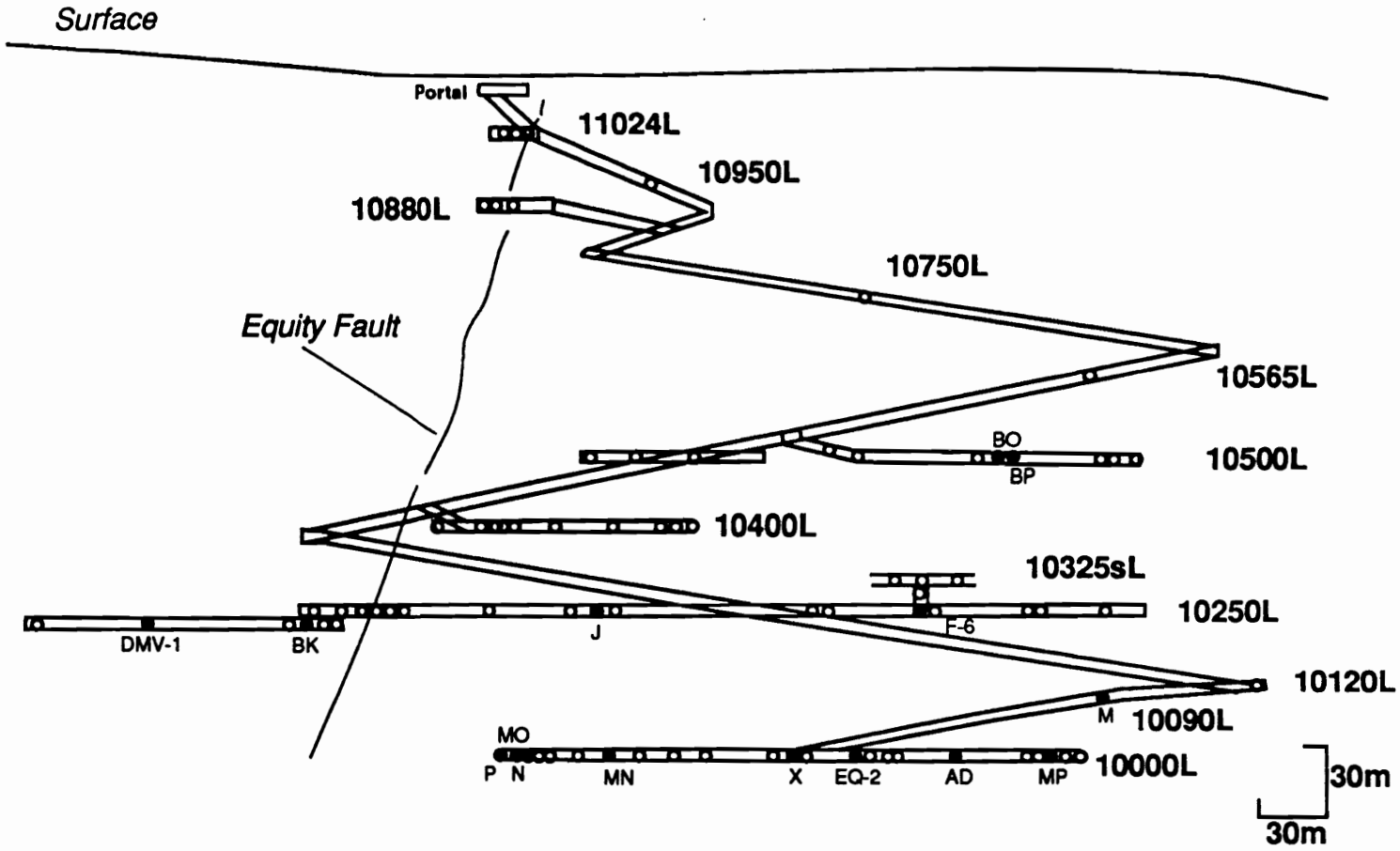

Figure 7. Cross-section view of mine workings, locations of samples used in fluid inclusion study are named. See Table 3 for sample descriptions.

Table 2. Descriptions of samples used in fluid inclusion study of the North Amethyst vein system.

Sample No.[1]	Location	Description
DMV-1	10250 level, E-125+75'N	Coarse-grained (up to 1 cm wide) Stage-1 lemon-yellow crystals of sphalerite intergrown with quartz, galena, and chalcopyrite in 0.2-1 cm wide veinlets cutting bleached volcanic rock.
EQ-2	10000 level	Large (4 cm in long dimension) singly terminated quartz crystals of stage 2 growing on sulfide base and engulfed in finegrained pink carbonate.
NKF-F-6-87	10250 level, E-84-10'S	Large (3 cm in length) singly terminated quartz crystal growing on leached base consisting of finegrained quartz, dusted with fine pyrite cubes and white clay, stage 3.
NKF-M-13-87	10090 level, E-120	Small (1-2 mm wide) rounded sphalerite grains of Alpha stage rimmed with chalcopyrite disease, contained in finegrained admixture of rhodonite, rhodocrosite and quartz.
NKF-N-14-87	10000 level, North end, face	Coarsegrained (up to 7 mm wide) lemon-yellow sphalerite of stage 1 with red-brown chalcopyritized rims, intergrown with galena, chalcopyrite, carbonate, and quartz. In fractures at north face of level.
NKF-P-16-87	10000 level, North end, footwall.	Similar to NKF-N-14-87, in footwall fractures.
NKF-X-24-87	10000 level, below 1SOB	Yellow to red-brown sphalerite intergrown with other stage 1 minerals, overgwown by quartz, fluorite, and calcite of stage 2.
NKF-AD-30-87	10000 level, E-120+30'N	Finer-grained (<2 mm) fluorite, quartz and sphalerite (dominantly stage 2) intergrown with calcite.
NKF-BK-63-87	10250 level, No. 2 dogleg	Finegrained minerals of alpha stage cut by late veins containing red-brown to yellow sphalerite of stage 1, pyrite, chalcopyrite, and quartz and calcite gangue. Sphalerite was analysed.

NKF-BO-67-87	10500 level, E-61	Large irregular pieces of cloudy quartz broken out of precursor veins in hanging wall.
NKF-BP-68-87	10500 level, E-61	Large irregular pieces of cloudy quartz broken out of precursor veins in hanging wall.
GSP-MN-87	10000 level, E-125+35'N	Large (up to 1cm wide) colorbanded crystals of sphalerite of stage 1 intergrown with quartz and chlorite, coated by stage 3 pink calcite.
GSP-MO-87	10000 level, E-126+50'N	Large (up to 1.5 cm wide) colorzoned crystals of sphalerite having yellow cores and dark overgrowths, some dark crystals have yellow overgrowths of sphalerite, intergrown with pyrite.
GSP-MP-87	10000 level	2-4 mm-wide banded redbrown to colorless crystals of sphalerite of stage 1.
GSP-MM-87	10000 level, E-125	Rounded grains of sphalerite, with chalcopyritized rims, intergrown with chalcopyrite, galena, electrum and other precious- and base-metal minerals of Beta stage.

1. First characters denote sample collector: NKF, Nora K. Foley; GSP, Geoffrey S. Plumlee, EQ and DMV, David M. Vardiman.

Table 3. Fluid inclusion data for sphalerite, fluorite, and quartz from the North Amethyst vein system.

Locality[1]	No.	Min[2]	Type[3]	Stage[4]	Color[5]	Th	Tm	Salinity[6]
DMV-1	1-3	S	P	1	y	261.2	-5.3	8.26
DMV-1	1-3	S	P	1	y	278.2	-6.2	9.46
DMV-1	1-3	S	P	1	y	262.1	-5.5	8.53
DMV-1	1-2	S	P	1	y	277.6	-7.3	10.8
DMV-1	1-2	S	P	1		262.1	-5.3	8.26
DMV-1	2-1	Q	P	1		240.9	-4.2	6.72
DMV-1	2-1	Q	P	1		239.1	-3.8	6.14
DMV-1	2-1	Q	P	1		240.8	-5.6	8.67
DMV-1	2-1	Q	P	1		240.8	-3.9	6.28
DMV-1	2-1	Q	P	1		245.1		
NKF-P-16-87	1-1	S	P	1	yb	258	-6.5	9.85
NKF-P-16-87	1-2	S	P	1	yb	260	-6.6	9.98
NKF-P-16-87	1-3	S	P	1	yb	260	-6.4	9.72
NKF-P-16-87	1-4	S	P	1	yb	259	-6.6	9.98
NKF-P-16-87	1-5	S	P	1	yb	255	-6.5	9.85
NKF-P-16-87	1-7	S	P	1	yb	256	-6.3	9.59
NKF-P-16-87	1-8	S	P	1	yb	255	-5.9	9.07
NKF-P-16-87	2-1	S	P	1	yb	256	-5.8	8.94
NKF-P-16-87	2-2	S	P	1	yb	257	-5.8	8.94
NKF-P-16-87	2-3	S	P	1	yb	262	-6	9.20
NKF-P-16-87	2-4	S	P	1	yb	260	-5.9	9.07
NKF-P-16-87	2-5	S	P	1	yb	260	-5.9	9.07
NKF-P-16-87	2-6	S	P	1	yb	257	-5.8	8.94
NKF-P-16-87	2-7	S	P	1	yb	258	-5.8	8.94
NKF-P-16-87	2-8	S	P	1	yb	260	-5.8	8.94
NKF-P-16-87	2-9	S	P	1	yb	256	-5.8	8.94
NKF-P-16-87	2-10	S	P	1	yb	255	-5.8	8.94
NKF-P-16-87	2-11	S	P	1	yb	258	-5.7	8.80
NKF-P-16-87	2-12	S	P	1	yb	257	-5.7	8.80
NKF-P-16-87	2-13	S	P	1	yb	255	-5.6	8.67
NKF-P-16-87	3-2	S	P	1	yb	261	-5.7	8.80
NKF-P-16-87	3-3	S	P	1	yb	256	-5.6	8.67
NKF-P-16-87	3-5	S	P	1	yb		-3.5	5.69
NKF-N-14-87	2A-1	S	P	1	r	271	-4.5	7.15
NKF-N-14-87	2A-2	S	P	1	r	270	-4.5	7.15
NKF-N-14-87	2A-3	S	P	1	r	271	-4.3	6.86
NKF-N-14-87	2A-4	S	P	1	r	268	-4.4	7.01
NKF-N-14-87	2A-5	S	P	1	r	270	-4.5	7.15
NKF-N-14-87	2B-1	S	P	1	c	260	-6.5	9.85

NKF-N-14-87	2B-2	S	P	1	c	262	-6.5	9.85
NKF-N-14-87	2C-1	S	P	1	y	255	-6.1	9.33
NKF-N-14-87	2C-2	S	P	1	y	253	-6.5	9.85
NKF-N-14-87	2C-5	S	P	1	y	254	-6.2	9.46
NKF-N-14-87	2C-6	S	P	1	y	256	-6.4	9.72
NKF-N-14-87	2C-7	S	P	1	y	256	-6.4	9.72
NKF-N-14-87	1A-1	S	s	1		215	-4.3	6.86
NKF-N-14-87	1A-2	S	s	1		215	-4.1	6.57
NKF-N-14-87	1A-3	S	s	1		215	-4.1	6.57
NKF-N-14-87	3-1	S	P	1	r	251	-4.3	6.86
NKF-N-14-87	3-2	S	P	1	r	252	-4.3	6.86
NKF-N-14-87	3-3	S	P	1	r	250	-4.1	6.57
NKF-N-14-87	3-4	S	P	1	c	260	-5	7.85
NKF-N-14-87	3-5	S	P	1	c	255	-4.4	7.01
NKF-N-14-87	3-6	S	P	1	c	255	-4.4	7.01
NKF-N-14-87	3-7	S	P	1	c	255	-4.4	7.01
GSP-MP-86	1-1	S	P	1	y	240	-4.2	6.72
GSP-MP-86	1-2	S	P	1	y	237	-4.2	6.72
GSP-MP-86	1-3	S	P	1	y	237	-4.2	6.72
GSP-MP-86	1-4	S	P	1	y	236	-4.3	6.86
GSP-MP-86	2-1	S	P	1	y	246	-5.5	8.53
GSP-MP-86	2-2	S	P	1	y	250	-5.8	8.94
GSP-MP-86	2-3	S	P	1	y	251	-5.8	8.94
GSP-MP-86	3-1	S	P	1	y	245	-5.7	8.80
GSP-MP-86	3-2	S	P	1	y	246	-5.6	8.67
GSP-MP-86	3-3	S	P	1	y	243	-5.6	8.67
GSP-MP-86	4-1	S	P	1	y	255	-4.8	7.57
GSP-MP-86	4-2	S	P	1	y	256	-4.8	7.57
GSP-MP-86	4-3	S	P	1	y	255	-4.6	7.29
GSP-MP-86	4-4	S	P	1	y	251	-4.4	7.01
GSP-MP-86	4-5	S	P	1	y	245	-4.5	7.15
GSP-MP-86	4-6	S	P	1	y	244	-4.5	7.15
GSP-MP-86	5	S	P	1	y	260	-6	9.20
GSP-MP-86	6	S	P	1	y	245	-5.3	8.26
GSP-MP-86	7	S	P	1	y	245	-5.3	8.26
GSP-MP-86	8	S	P	1	y			0
GSP-MP-86	9	S	P	1	y			0
NKF-BK-63	1-8-1	S		1	c	257	-5.8	8.94
NKF-BK-63	1-7-1	S		1	c	255	-5.5	8.53
NKF-BK-63	1-8-2	S		1	c	257	-5.8	8.94
NKF-BK-63	1-8-3	S		1	c	261	-6.1	9.33
NKF-BK-63	1-8-4	S		1	c	261	-5.9	9.07
NKF-BK-63	1-8-5	S		1	c	255	-5.8	8.94
NKF-BK-63	1-8-6	S		1	c		-5.7	8.80
NKF-BK-63	1-2-1	S		1	c	260	-5.7	8.80
NKF-BK-63	1-2-2	S		1	c	255	-5.4	8.40

NKF-BK-63	1-2-3	S	1	c	255	-5.4	8.40
NKF-BK-63	1-2-4	S	1	c	257	-5.8	8.94
NKF-BK-63	1-2-5	S	1	c	260	-5.8	8.94
NKF-BK-63	1-1	S	1	c	260	-6.1	9.33
NKF-BK-63	1-2	S	1	c	260	-6.1	9.33
NKF-BK-63	1-3	S	1	c	257	-5.8	8.94
NKF-BK-63	1-4	S	1	c	257	-5.8	8.94
NKF-BK-63	1-5	S	1	c	257	-5.8	8.94
NKF-BK-63	1-6	S	1	c	259	-5.9	9.07
NKF-BK-63	1-7	S	1	c	260	-6.1	9.33
GSP-MO	2-1-1	S	1	y	260	-5.5	8.53
GSP-MO	2-1-2	S	1	y	260	-5.4	8.40
GSP-MO	2-1-3	S	1	y	257	-5.6	8.67
GSP-MO	2-2-1	S	1	y	262	-4.5	7.15
GSP-MO	2-2-2	S	1	y	262	-4.7	7.43
GSP-MO	2-2-5	S	1	y	261	-5.9	9.07
GSP-MO	2-2-6	S	1	y	262	-5.8	8.94
GSP-MO	2-2-7	S	1	y	260	-5.8	8.94
GSP-MO	4-1-1	S	1	y	264	-6.3	9.59
GSP-MO	4-1-2	S	1	y	264	-6.3	9.59
GSP-MO	4-2-1	S	1	y	266	-5.7	8.80
GSP-MO	4-2-2	S	1	r	265	-6	9.20
GSP-MO	4-2-3	S	1	r	266	-6.1	9.33
GSP-MO	4-2-4	S	1	r	265	-6.3	9.5
GSP-MO	4-2-5	S	1	r	264	-6.3	9.59
GSP-MO	4-3-1	S	1	r	259	-5.7	8.80
GSP-MO	4-3-2	S	1	r	258	-5.7	8.80
GSP-MO	1-1	S	1	y	261	-6	9.20
GSP-MO	1-2	S	1	y	261	-5.8	8.94
GSP-MO	1-3	S	1	y		0	0
GSP-MO	2	S	1	y	250	-5.8	8.94
GSP-MO	3-1	S	1	y	259	-6.2	9.46
GSP-MO	3-2	S	1	y	260	-6.2	9.46
GSP-MO	3-3	S	1	y	261	-6.2	9.46
GSP-MO	3-4	S	1	y	259	-6.1	9.33
GSP-MO	3-5	S	1	y	259	-6.3	9.59
GSP-MO	3-6	S	1	y	259	-6.2	9.46
GSP-MO	3-7	S	1	y	259	-6.1	9.33
GSP-MO	3-8	S	1	y	258	-6	9.20
GSP-MO	3-9	S	1	y	261	-5.9	9.07
GSP-MO	4-1	S	1	y	255	-5.8	8.94
GSP-MO	4-2	S	1	y	257	-5.8	8.94
GSP-MO	3-1-1	S	1	y	262	-6.1	9.33
GSP-MO	3-1-2	S	1	y	263	-6.2	9.46
GSP-MO	3-1-3	S	1	y	262	-6.1	9.33
GSP-MO	3-1-4	S	1	y	263	-6.2	9.46

GSP-MO	3-1-5	S		1	y	263	-6.2	9.46
GSP-MO	3-1-6	S		1	y	265	-6	9.20
GSP-MO	3-2-2	S		1	r	260	-6.1	9.33
GSP-MO	3-2-3	S		1	r	260	-6.2	9.46
GSP-MO	3-3-1	S		1	y	260	-4.5	7.15
GSP-MO	3-3-2	S		1	y	260	-4.5	7.15
NKF-AD	f-1	F	P/S	2		218	-3.5	5.69
NKF-AD	f-2	F	P/S	2		240	-3.5	5.69
NKF-AD	f-3	F	P/S	2		256	-3.5	5.69
NKF-AD	q-1	Q	P?	2		231	0	0
NKF-AD	s-1	S	P	2		250	-5.2	8.12
NKF-AD	s-2	S	P	2		245	-5.9	9.07
NKF-F-6	1-1	Q	P	3		239.5	0	0
NKF-F-6	1-2	Q	P	3		242.6	-0.1	0.17
NKF-F-6	1-3	Q	P	3		241.6	0	0
NKF-F-6	2-1	Q	P	3		216.8	0	0
NKF-F-6	2-2	Q	P	3		266.9	-0.1	0.17
NKF-F-6	2-3	Q	P	3		266.9	-0.1	0.17
NKF-F-6	3-1	Q	P	3		238.5	0	0
NKF-F-6	3-2	Q	P	3		242.6	0.1	-0.1
NKF-F-6	3-3	Q	P	3		251.6	0	0
NKF-F-6	3-4	Q	P	3		270.4	0	0
NKF-F-6	3-5	Q	P	3		300	0	0
NKF-F-6	3-6	Q	P	3		300.7	-0.1	0.17
NKF-F-6	3-7	Q	P	3		193.7	0	0
EQ-2-87	Ca	Q	P	2			-5	7.85
EQ-2-87	Cb	Q	P	2			-5	7.85
EQ-2-87	B1a	Q	P	2		220	-1.5	2.56
EQ-2-87	B1b	Q	P	2		274.1	-1.3	2.22
EQ-2-87	B1c	Q	P	2		275.1	-1.1	1.89
EQ-2-87	B1d	Q	P	2		268.3	-1.3	2.22
EQ-2-87	B1e	Q	P	2		238.7	-0.7	1.21
EQ-2-87	B1f	Q	P	2		266.7	-0.5	0.87
EQ-2-87	B1g	Q	P	2		254.3	-1.1	1.89
EQ-2-87	B1h	Q	P	2		271.6	-0.7	1.21
EQ-2-87	B1i	Q	P	2		245	-1.2	2.06
EQ-2-87	B1j	Q	P	2		264	?	?
EQ-2-87	B1k	Q	P	2		258	?	?
EQ-2-87	B1l	Q	P	2		268.3	-1.6	2.72
EQ-2-87	B1m	Q	P	2		256.5	-1.5	2.56
EQ-2-87	B1n	Q	P	2		231.5	-1.7	2.88
EQ-2-87	A-1	Q	P	2		277.4	0	0
EQ-2-87	A-2	Q	P	2		244	0.2	0.35
EQ-2-87	A-3	Q	P	2		256	0	0
EQ-2-87	A-4	Q	P	2		271.3	0	0
EQ-2-87	A-5	Q	P	2		251.1	0	0
EQ-2-87	A-6	Q	P	2		244.4	-0.1	0.17
EQ-2-87	A-7	Q	P	2		268.3	0	0

EQ-2-87	A-8	Q	P		2	261.1	-0.1	0.17
EQ-2-87	A-1a	Q	P		2	271.5	-4.2	6.72
EQ-2-87	A-2a	Q	S		2	300.8	-3.8	6.14
EQ-2-87	A-3a	Q	S		2	279.1	-2.1	3.53
EQ-2-87	A-4a	Q	S		2	281.7	0	0
EQ-2-87	A-9	Q	P		2	240	0	0
EQ-2-87	A-10	Q	P		2	256.1	0	0
EQ-2-87	A-11	Q	P		2	266.3	0.2	0.35
EQ-2-87	A-12	Q	P		2	248.7	0	0
EQ-2-87	A-13	Q	P		2	251.1	-0.1	0.17
EQ-2-87	A-14	Q	P		2	253.4	0	0
EQ-2-87	A-15	Q	P		2	266	0	0
EQ-2-87	A-16	Q	P		2	278	0	0
EQ-2-87	A-17	Q	P		2	264	-0.5	0.87
EQ-2-87	A-18	Q	P		2		0	0
EQ-2-87	A-19	Q	P		2		0	0
EQ-2-87	A-20	Q	P		2		0	0
EQ-2-87	A-v	Q	P		2	321	0	0
EQ-2-87	1a	Q	P		2	254	-6.1	9.33
EQ-2-87	1b	Q	P		2	256	-5.6	8.67
EQ-2-87	1c	Q	P		2	266.1	-6	9.20
EQ-2-87	1d	Q	P		2	273.1	0	0
EQ-2-87	1e	Q	P		2	268.1	0	0
EQ-2-87	g-1	Q	P		2	268.1	-3.2	5.24
EQ-2-87	g-2	Q	P		2	261.3	-3.1	5.09
EQ-2-87	g-3	Q	P		2	252.1	-3.2	5.24
GSP-MN-B	A-1	Q	P		1	263	-6.5	9.85
GSP-MN-B	A-2	Q	P		1	245	-6	9.20
GSP-MN-B	A-3	Q	P		1	253	-6	9.20
GSP-MN-B	A-4	Q	P		1	255.9	-6.2	9.46
GSP-MN-B	A-5	Q	P		1	249	-6.2	9.46
GSP-MN-B	A-6	Q	P		1	271	-6.1	9.33
GSP-MN-B	A-7	Q	P		1	268	-6.4	9.72
N2F-X-24	S-1	S	P		1	253	-6.2	9.46
N2F-X-24	S-2	S	P		1	261	-5.8	8.94
N2F-X-24	S-3	S	P		1	259	-5.8	8.94
N2F-X-24	S-4	S	P		1	252	-6.1	9.33
N2F-X-24	S-5	S	P		1	262	-6.2	9.46
N2F-X-24	F-1	F	P		1	250	-5.2	8.12
N2F-X-24	F-2	F	P		1	249	-5.1	7.99
NKF-M-13	B-1	S	PS	α		261	0	0
NKF-M-13	B-2	S	PS	α		265	-1	1.72
NKF-M-13	A-1	S	PS	α		278	0.2	-0.3
NKF-M-13	A-3	S	PS	α		283	0.2	-0.3
NKF-M-13	C-2	S	PS	α		282	-1	1.72
NKF-M-13	D1	S	PS	α		288	-5.5	8.53

NKF-BP	1	Q	PS	P			0	0
NKF-BP	2	Q	PS	P			0.2	-0.3
NKF-BP	3	Q	PS	P			0	0
NKF-BP	4	Q	PS	P		265	-0.1	0.17
NKF-BP	5	Q	PS	P		270	0	0
NKF-BP	6	Q	PS	P		280	0.1	-0.1
NKF-BP	7	Q	PS	P		281	0	0
NKF-BP	8	Q	PS	P		294	0	0
NKF-BO	1	Q	PS	P		270	0	0
NKF-BO	2	Q	PS	P		268	0.1	-0.1
NKF-BO	3	Q	PS	P		250	0	0
NKF-BO	4	Q	PS	P		254	0.2	-0.3
NKF-BO	5	Q	PS	P		255	0	0
NKF-BO	6	Q	PS	P		260	0.2	-0.3
NKF-BO	7	Q	PS	P		245	0	0
NKF-J-10	1	C	S		3	180	0	0
NKF-J-10	2	C	S		3	151	0	0
NKF-J-10	3	C	S		3	175	0	0
NKF-J-10	4	C	S		3	128	0	0
NKF-J-10	5	C	S		3	153	0	0
NKF-J-10	6	C	S		3	173	0	0

1. Sample collector: EQ, DMV, David M. Vardiman; NKF, Nora K. Foley
2. Min, Mineral: S, sphalerite; Q, quartz; F, fluorite; C, calcite.
3. Inclusion type: P, primary; PS, Pseudosecondary; S, secondary.
4. Paragenetic stage: see Table 2.
5. Color: y, yellow; yb, yellow-brown; r, red; c, colorless.
6. Calculateds using data of Hall et al. (1988).

interpretable results. Many of the problems involved in interpreting fluid inclusions that form in a shallow, epithermal environment have been described in detail by Bodnar et al. (1985); others are outlined below.

Data from primary, pseudosecondary, and secondary inclusions in sphalerite, quartz, fluorite, and calcite are used in this study to constrain the evolution path of the ore fluid. Primary inclusions place limits on the temperature and salinity of the hydrothermal fluid during the development of a given mineralogic stage, and, as such, characterize the fluid at a specific point in time, easily related to mineral paragenesis. Pseudosecondary and secondary inclusions, on the other hand, characterize the temperature and composition of the fluid at some later point in time during the evolutionary cycle. For example, pseudosecondary inclusions in sphalerite attacked by chalcopyrite disease may yield data on the composition of the fluid involved in the dissolution and replacement process leading to the disease texture. Secondary inclusions are used only in a general manner to identify post-mineralization fluids present in the vein system that may complicate the interpretation of results.

Sphalerite (Figure 8a-e) was found to contain fewer inclusions than other minerals, and the origins of most sphalerite inclusions could be readily identified. Sphalerite was most useful for determining fluid parameters at a given point in time. In contrast, quartz (Figure 8f-i) contains abundant inclusions that formed from fluids of different composition by a number of mechanisms. Many of the inclusions in quartz

Figure 8. a) Isolated group of inclusions in alpha stage sphalerite, note chalcopyritized rim, b) Planar arrangement of inclusions in sphalerite of alpha stage, c) Inclusions decorating mineral fibers in stage 1 sphalerite, d) relatively large primary inclusions in color zoned sphalerite of stage 1, e) Colorzoned sphalerite of stage 1, inclusions aligned along growth zones, f) Fluid and solid carbonate (C) inclusions aligned along growth zones in stage 2 quartz, g) Group of relatively large vapor-rich and liquid + vapor inclusions in clear quartz of stage 2, h) Growth-zone of fluid inclusions in quartz, note fluorite octehedra (F), i) core of stage 3 quartz crystal containing fibers decorated with vapor-rich and vapor + liquid inclusions.

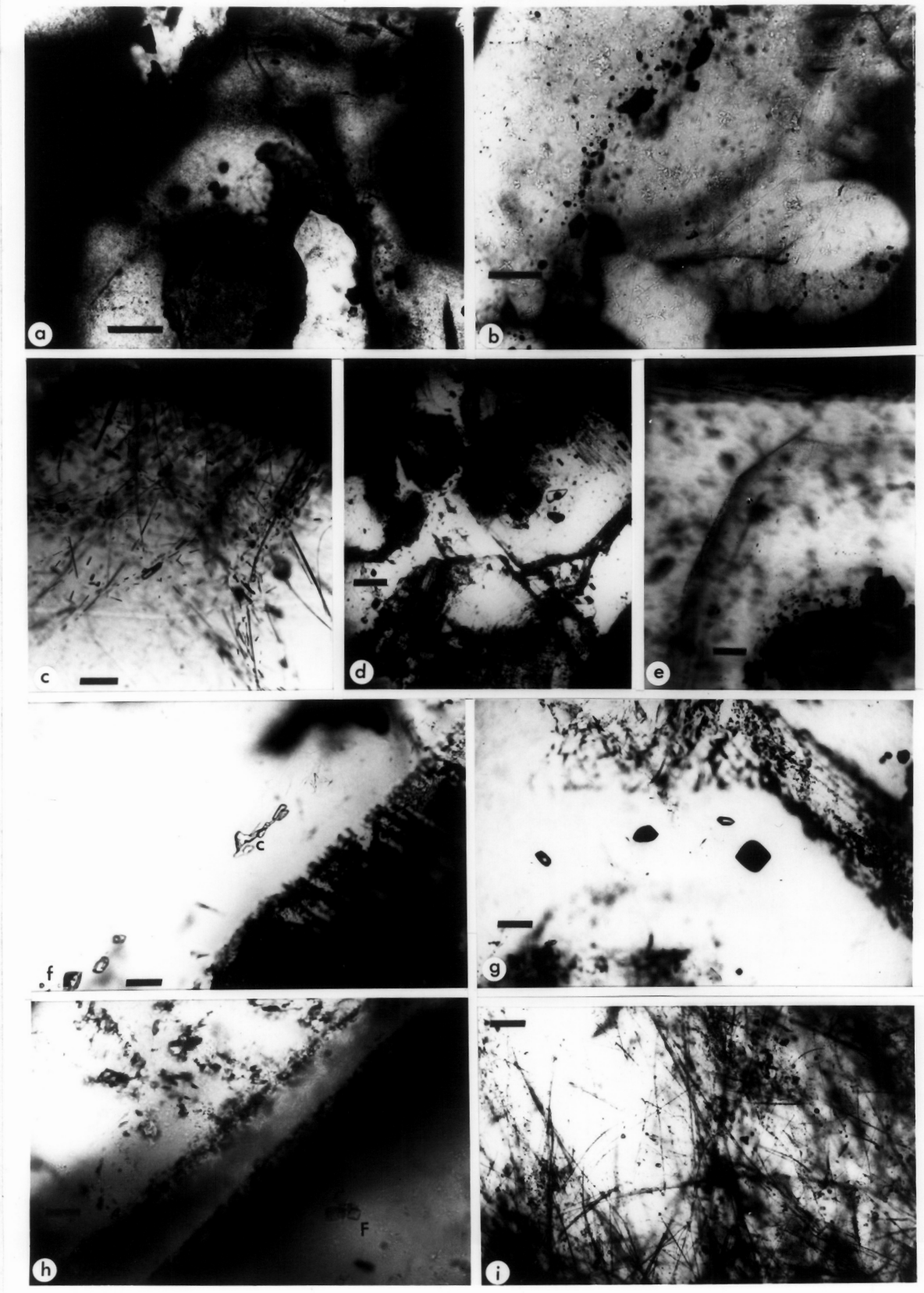
a
b
c
d
e
C
f
g
h
F
i

changed after formation by necking down. In spite of, or perhaps because of these complexities, inclusions in quartz proved to be invaluable for identifying change in the salinity of the hydrothermal fluid.

Visible CO_2 was not seen in any inclusions studied and none exhibited clathrate formation. When the inclusions chips were crushed in oil, the bubbles did not appear to expand indicating that CO_2, if present, is below detectibility for that technique (as noted above and in Bodnar et al., 1985).

Precursor quartz veins Quartz was selected from two localities identified by D. Vardiman of Homestake Mining Company (pers. commun., 1988) as among the best sites for collecting precursor vein minerals (NKF-BO, NKF-BP, Figure 7; Tables 2, 3). The data are plotted on histograms in Figure 9 and in Figure 10a by stage and in Figure 10b by mineral. The intergrown crystals are cloudy-to-white and contain numerous fluid inclusions, the majority of which are secondary in origin. It was not possible to identify any inclusions of clearly primary origin. Large areas of quartz containing numerous inclusions were examined to ascertain the salinity and temperature range of the fluids. All measured inclusions contain fluids having salinities of less than 0.3 weight percent NaCl equivalent and temperatures of less than 300°C. Vapor-rich (V) and irregularly-shaped mixed liquid-vapor (L-V) inclusions coexist in some areas suggesting that either the quartz trapped boiling fluids at some point in time or the inclusions necked down. These inclusions mainly occur strung out along healed fractures

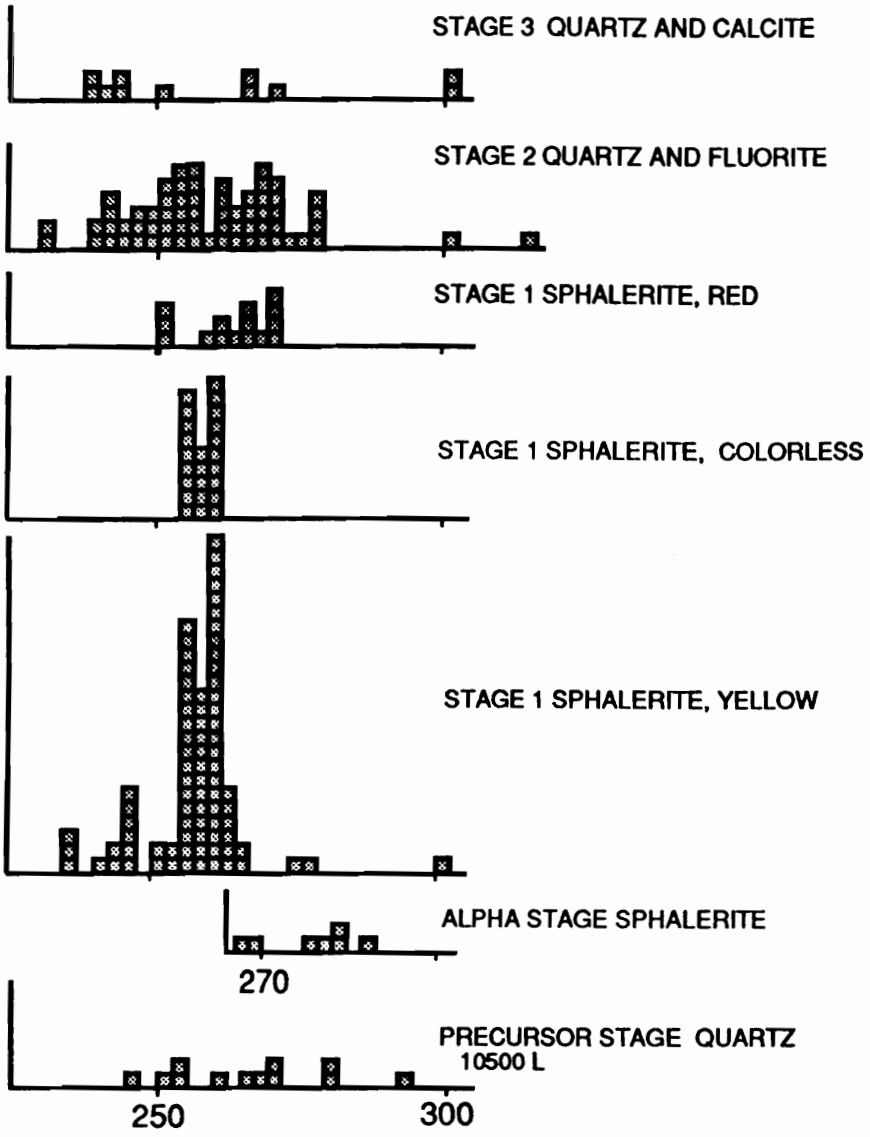

Figure 9. Temperature relations in the North Amethyst vein system. Fluid inclusion histograms for sphalerite, quartz, fluorite and calcite plotted by mineral and stage (see Table 1). Number of inclusions is too small to establish distribution patterns for most stages.

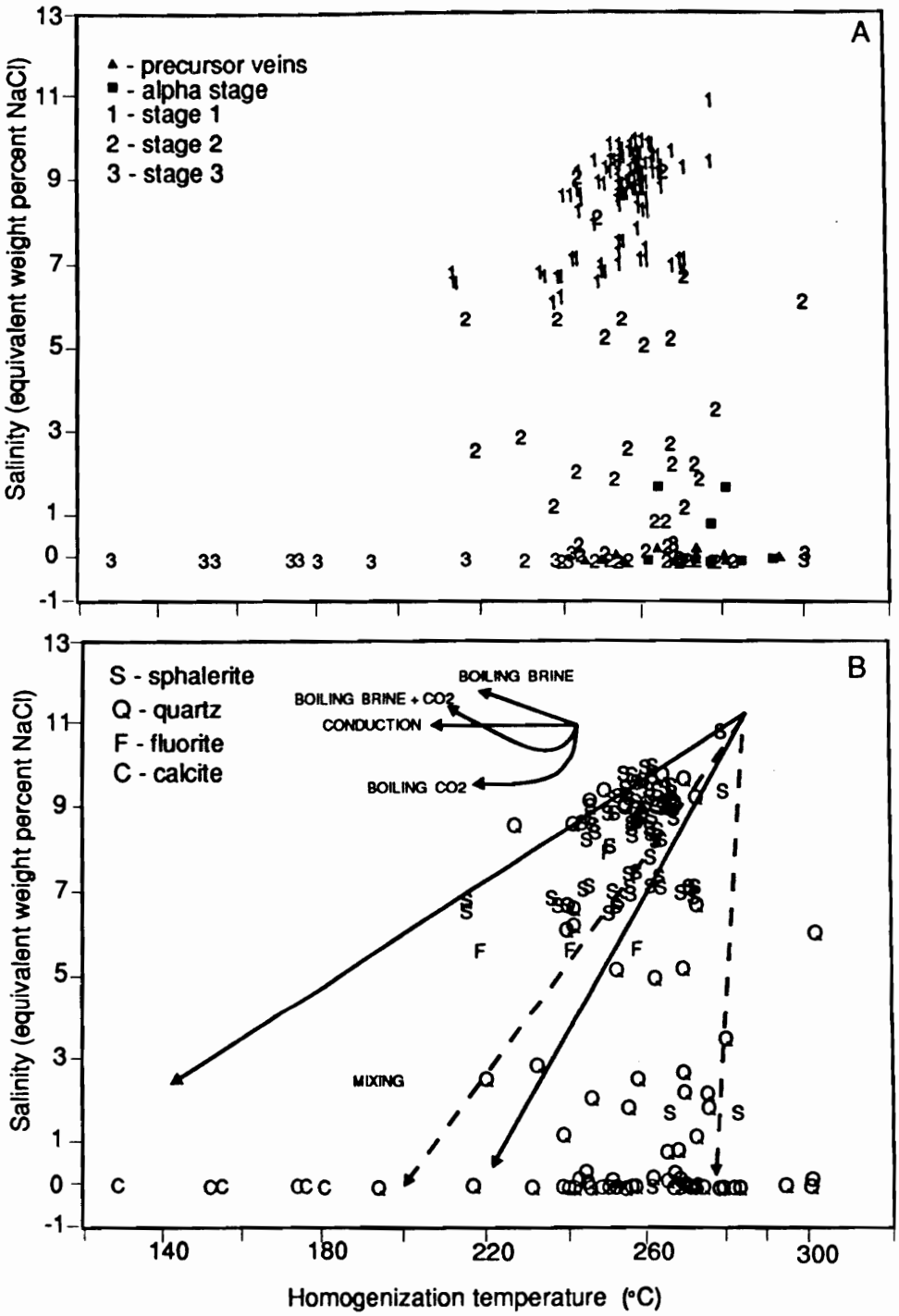

Figure 10. Temperature-salinity relations for North Amethyst ores. Fluid inclusion data on sphalerite, quartz, fluorite, and calcite are plotted by stage (A) and mineral (B). See Table 1 for description of stages; text for discussion of solid and dashed lines showing mixing, boiling, and conduction relations.

and in three dimensional arrays. A few microfractures appear to contain only vapor-rich inclusions. L-V inclusions coexisting with V-rich inclusions yielded homogenization temperatures ranging from 245°C to 294°C and salinities of .3 to 0 equivalent weight percent NaCl. Measured salinities of the V-rich inclusions are approximately 0 equivalent weight percent NaCl.

Mn - Au association Sphalerite from alpha-, and beta-stages (Tables 2, 3) contains relatively few measurable inclusions. The 2 to 10 micrometer-diameter rounded inclusions (Figure 8a, b) occur in isolated groups and in microfractures that cut across the crystals. The sphalerite grains are rounded and rimmed with chalcopyrite disease. Room temperature phase relations show liquid coexisting with vapor in consistent volumetric ratios for all visible inclusions. The inclusions homogenize over the range of 271 to 288°C (Figure 9), and have equivalent salinities that range from of 1.8 to 0 weight percent NaCl. The data are plotted in Figure 10a by stage and in Figure 10b by mineral. The inclusions occur in small islands of apparently disease-free sphalerite surrounded by chalcopyritized sphalerite. Because of their proximity, however, it is possible that the salinity and temperature ranges for these inclusions reflect the parameters of the fluid involved in chalcopyritization rather than those of the primary sphalerite-depositing fluid. Mineralogical and paragenetic studies suggest that intergrown sphalerite, chalcopyrite, electrum, and other precious and base metal minerals of this stage are generally coeval (Foley, 1990a). Thus, the data derived for this association are probably representative of the latest mineral deposition.

Base metal - silica association The coarse-grained, crustiform and open-space filling minerals of the base metal - silica association (Table 2) yielded numerous inclusions suitable for thermometric measurements (Figure 8c, d, e). Fluid inclusions were studied from sphalerite and quartz of Stage 1, quartz and fluorite of Stage 2, and calcite and quartz of Stage 3.

Sphalerite from Stage 1 contains a large number of inclusions having fairly regular L-V ratios and no daughter minerals. Most of the inclusions range in size up to 50 micrometers in long dimension and are generally regular in shape. Most primary and pseudosecondary inclusions in Stage 1 sphalerite yielded salinity values in the range 6 to 10 equivalent weight percent NaCl. Homogenization temperatures in these inclusions ranged from 237 to 278 C. Inclusions in quartz intergrown with sphalerite from Stage 1 have homogenization temperatures of about 239^{o}C to 249^{o}C (Figure 9) and corresponding values of salinity ranging from 6.1 to 8.7 weight percent NaCl.

Many of the crystals show dissolution features that transect the colorbanding. They demonstrate that fluids temporarily undersaturated in zinc sulfide corroded the crystals at times during the growth history of Stage-1 sphalerite. Overgrowths of sphalerite trapped ore fluid in some of the reentrants and, thus, the inclusions fall into primary and pseudosecondary categories. The sphalerite is chalcopyrite-diseased (Foley, 1990a), and the some of the inclusions may have formed by dissolution and replacement of sphalerite by chalcopyrite, however, no differences in temperature and salinity were noted for primary versus pseudosecondary inclusions. A small portion of inclusions in sphalerite

are truly secondary in origin, occuring mainly in partially healed curved planar arrays. Temperatures of these inclusions vary widely but are generally less than 150°C.

Only slight differences in salinity and homogenization temperature were found for inclusions in different colored sphalerite. Inclusions in yellow sphalerite, the most common variety, span the entire temperature and salinity range. Colorless sphalerite has a more restricted temperature range of 255°C to 263°C, but a similar salinity range. Individual clusters of inclusions in red-brown sphalerite have relatively uniform temperature and salinity values, but these vary without discernable pattern from group to group even within a single crystal of sphalerite.

Both quartz and fluorite yielded measurable inclusions for Stage 2 mineralization (Figure 8f, g, h). As a group, the inclusions from stage 2 mineralization have salinities that range from 8 to 0 weight percent NaCl equivalent and homogenization temperatures that vary from 300°C to 218°C (Figure 10a, b).

Primary inclusions in fluorite are rare; most fluorite, especially coarse grained crystals, contains only secondary inclusions. The finer grained (>2mm) octahedra of fluorite intergrown with amethystine quartz contained a small number of inclusions; these homogenized over the interval from 218-256 C, and had salinities ranging from 5.5 to 8 weight percent NaCl equivalent.

Quartz from stage 2 contains a myriad of inclusions and the history mapped by the inclusion populations is complex. Inclusions types include isolated groups of primary L-V and V-rich inclusions, primary L-

V inclusions defining former growth surfaces, secondary inclusions along healed microfractures, and L-V, and V-, and L-rich inclusions in groups and along healed microfractures.

Textures definitive of boiling (isolated groups of coexisting L-V and V-rich inclusions) only occur infrequently, however, in many cases boiling textures may have been obscured by subsequent necking down of L-V inclusions, a common phenomenon in epithermal deposits (Bodnar et al, 1985). Within growth zones in the quartz, many L-V inclusions occur intermixed with relatively large V-rich inclusions, and smaller and irregularly shaped L-rich inclusions. The presence of the L-rich inclusions indicates that necking down occurred at some point in the history of the inclusions. Whether the inclusions originally formed from boiling fluids (coexisting V-rich and L-V inclusions) or from nonboiling fluids (L-V inclusions that underwent necking-down after formation of the vapor bubble resulting in V-rich, L-V, and L-rich inclusions) cannot be determined unequivocally. Most inclusions along growth zones yielded similar salinities (L-rich, V-rich and L-V inclusions), but widely ranging temperatures (Figure 10). Isolated groups of V-rich and L-V inclusions yielded the most unambiguous evidence for boiling. L-V inclusions had salinities in the range 0-3.0 weight percent NaCl, while coexisting V-rich inclusions had apparent salinities of 0 weight percent NaCl.

The evidence for boiling indicated here is complicated by the fact that salinity changes strikingly during deposition of stage 2. Primary inclusions in the bases of some quartz crystals contain relatively saline (~5 wt.%) nonboiling inclusions, while inclusions in later quartz

overgrowths, both in isolated group and in growth zones, contain much less saline fluids (<<3wt.%). Secondary and pseudosecondary inclusions in bases of such crystals invariably contain nonsaline fluids (0 wt% NaCl). Some secondary inclusions in quartz overgrowths contain higher salinity fluids. These may reflect partial opening and leaking of fluid from large primary inclusions trapped in the cores of the quartz crystals.

Quartz and manganoan calcite were studied from Stage 3 of the base metal - silica association. Most inclusions found in calcite are aligned along cleavage traces and appear secondary in nature; the inclusions are uniformly nonsaline (~0 wt% NaCl equiv.) and contain widely variable L-V ratios (measured Th = 128-180^{o}C; Figure 9). Many one-phase liquid inclusions were also present in the samples. Inclusions in quartz yielded a wider temperature range, from 216-301^{o}C, and low salinities (<1.2 wt% NaCl equiv.; Figure 10), however, the wide Th range of the few inclusions measured may be suspect if there was extensive necking-down after the fluids were trapped. Necking down of L-V inclusions would cause a spread in Th, as would necking down of L-rich inclusions formed from a boiling solution after generation of a vapor bubble. The size of the Th spread would be related to the temperature and timing of necking down.

The bases of stage 3 quartz crystals contain numerous solid and fluid inclusions. Solid inclusions include octahedra of fluorite, irregular grains of carbonate, and acicular fibers of an unidentified mineral (Figure 8i). Coexisting V-rich and L-V inclusions decorate the fibrous needles.

Discussion of Fluid Inclusion Data

The data collected in this study encompass a wide range of temperatures and salinities that can best be interpreted by considering the paragenetic position of the host phase. The evolution of the fluid dictated by this dataset is compared to those for other veins of the Creede district (Bethke et al., 1987) and used to substantiate correlations of mineral assemblages presented by Foley and Vardiman (1988) and Foley (1990a).

The vapor-rich and vapor + liquid inclusions aligned along healed microfractures in precursor quartz veins may have resulted from either continued healing of the microfractures after nucleation of the bubble, or they may be indicative of boiling. These textures may be distinguished if the mineral-depositing fluid was saline (salinity of vapor-rich inclusions), but are ambiguous if the original fluid was nonsaline. The presence of a few microfractures that contain only vapor-rich inclusions does suggest that at some point in time fluids were boiling at or below the 10500' elevation of the mine. The boiling could occurred any time after the quartz was deposited and may be related to a later stage of mineralization.

Inclusion data for the manganese and gold assemblages are sparse but they indicate that the minerals were deposited from relatively high temperature (>~270^{o}C?), low salinity solutions. The temperatures from the inclusions are somewhat lower than those derived from mineralogical studies (Foley, 1990a), but they reflect conditions of chalcopyritization (e.g. Barton and Bethke, 1989) which occurred late in beta-stage, at the end of Mn-Au mineralization. The finegrained

textures of ore and gangue minerals of the alpha-, and beta-stages are consistent with rapid nucleation and precipitation that might accompany boiling making that a viable mechanism for deposition of these stages.

The temperature and composition of the fluid in the veins during the extensive period of brecciation and sedimentation that began concurrently with the later part of the Mn-Au association can not be derived by fluid inclusion data. The clastic and chemical sediments are similar to those described by Schieber and Katsura (1986) for the Bohemia Au district, Oregon and by Vikre (1989) for the Sandstorm and Kendall Au mines near Goldfield, Nevada, epithermal deposits. Unsorted breccias, chemical sediments and pockets of chalcedonic vein sediments similar to those prevalent along the North Amethyst vein system (Foley, 1990a) have been attributed to rapid changes in temperature that substantially affect silica saturation levels and accompany fracturing, pressure release, and boiling (Schieber and Katsura, 1986; Vikre, 1989). Boiling is cited as an important mechanism leading to the formation of the breccias and sedimented zones in both of these districts and may account for the sedimented breccies of the North Amethyst vein system. Similar clastic and chemical sediments have been found at the Happy Thought mine dump, on the Amethyst vein at the northern edge of the central mining district (P.B. Barton, pers. commun., 1990)

The first stage (Stage 1) of the base metal-silica association was deposited from fluids with salinities in excess of 9 weight percent NaCl equivalent, and temperatures probably only slightly in excess of 260^{o}C. No textures indicative of boiling are present in the sphalerite. Later stages (Stages 2 and 3) of this association formed from a solution whose

salinity dropped sharply as quartz and other minerals continued to be deposited. The dramatic change in salinity reflects a fundamental change in the composition of fluid input into the hydrothermal system, as is discussed later. The temperature of the fluid during this later period is more uncertain because of boiling, necking down, and leaking along microfractures, etc.

Quartz in both stages 2 and 3 contains inclusions showing ample evidence for boiling at the 10000' and 10250' elevations. These inclusions are similar to inclusions described by Bodnar et al. (1985) in quartz from the 12450' elevation of the Equity vein that demonstrated excellent evidence for boiling. The inclusions are aligned along well-defined growth zones and liquid + vapor inclusions coexist with vapor-rich inclusions. Bodnar et al. (1985) cite several important characteristics that indicate that the vapor-rich inclusions were the result of entrapment of a vapor phase, rather than the result of later healing (necking) processes: 1) the absence of one-phase liquid-filled inclusions 2) the consistent liquid-to-vapor ratios, and consistent homogenization temperatures 3) the vapor-rich inclusions are large relative to liquid-rich inclusion. Similar inclusions populations were found in stage 2 and 3 quartz from both the 10000' and 10250' elevations in this study. Healed microfractures containing all vapor-rich inclusions were also found in stage 3 quartz from the southern end of the 10250 level.

Depth of ore formation

Estimates of the minimum depth of ore formation can be obtained using Haas' (1971) boiling-point-with-depth curves for $NaCl-H_2O$

solutions (Figure 11). The estimated depths correspond to the height of a column of liquid exerting a load pressure equal to P_{H2O} of the vapor-saturated solution at the temperature of interest for hydrostatic conditions, and assume no contribution to freezing point measurements from other dissolved species (e.g., CO_2). As has been discussed in detail by Roedder and Bodnar (1980), such depth determinations are generally accurate only to the extent that the actual geologic setting conforms to the assumptions upon which the estimates are based. In this case the most questionable assumptions are 1) that the fluid consists of only NaCl and H_2O - the abundance of calcite would argue otherwise, 2) that the fluid composition (integrated density) was uniform - an overlying low salinity fluid present at the time of ore deposition has been documented in other parts of the Creede district (Foley et al., 1990), and 3) that the system was open to the surface and approximated hydrostatic conditions during mineral deposition.

For manganese and gold mineralization of alpha-stage and beta-stage, the estimated formation temperature based on fluid inclusion data is greater that 270°C and fluid salinity is less than 2 equivalent weight percent NaCl. Mineralogical data indicate that temperatures may have exceeded 300°C during formation of alpha-stage, but are consistent with about 280°C for the Au-rich beta-stage. A pure H_2O solution at that temperature range corresponds to a P_{H2O} of 64.2 to 85.9 bars; a more saline solution (2.0 weight percent NaCl) would correspond to a P_{H2O} range of 63.4-84.9 (Haas, 1971). Thus, minimum depth estimates for alpha- and beta-stages may be 785-1090 meters and 760-1040 meters;

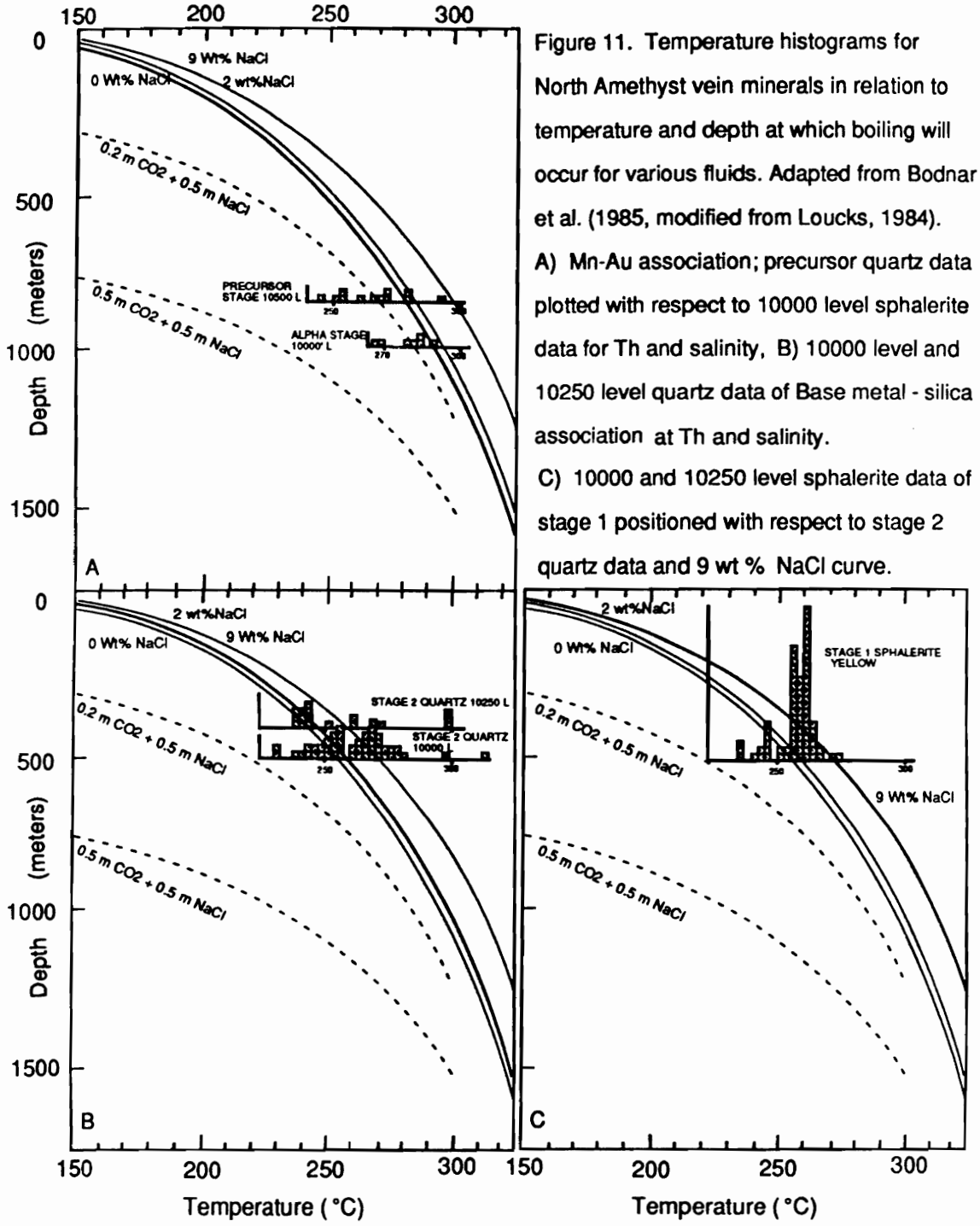

Figure 11. Temperature histograms for North Amethyst vein minerals in relation to temperature and depth at which boiling will occur for various fluids. Adapted from Bodnar et al. (1985, modified from Loucks, 1984). A) Mn-Au association; precursor quartz data plotted with respect to 10000 level sphalerite data for Th and salinity, B) 10000 level and 10250 level quartz data of Base metal - silica association at Th and salinity. C) 10000 and 10250 level sphalerite data of stage 1 positioned with respect to stage 2 quartz data and 9 wt % NaCl curve.

respectively. The finegrained nature of minerals of alpha-stage and beta-stage is permissive of boiling, so these depth estimates may approximate minimum depths from water table to mineralization (Figure 11). The depths are about 500 meters shallower than maximum estimates by geologic reconstruction.

During Stage 1, the major period of Ag-, and base-metal mineralization, the fluid had a mean temperature of 260°C and a mean salinity of 9 weight percent NaCl (Figure 10). These values correspond to a P_{H2O} of about 44 bars and a minimum depth of 480 meters. The minerals of stage 1 show no evidence for deposition from a boiling solution, so clearly the actual depth from water table to mineralization is greater than 480 m (Figure 11).

Inclusions in minerals of stage 2 and 3 show a sharp decrease in salinity and an apparent decrease in temperature as well. Minerals deposited early in stage 2 contain inclusions having temperatures and salinities that are virtually identical to those of stage 1 mineralization. Stage 2 quartz records a relatively sharp decrease in salinity, and quartz precipitated later in stage 2 has measured salinities of less than 3 equivalent weight percent NaCl. Fluids were boiling during the later part of stage 2 and continued boiling during deposition of stage 3 quartz and calcite. Stage 3 minerals were deposited from fluids having salinities of less than 1 weight percent NaCl (Figure 10). Homogenization temperatures during stage 2 and stage 3 vary widely because of boiling and later healing (necking) processes; the data are consistent with either no change in temperature or allow for a decrease in temperature from 260°C to 220°C. These data imply a

P_{H2O} range from about 44 to 46.5 bars and corresponding depths of 480-540 meters. Modal values of 260°C and 240°C estimated for boiling solutions of stage 2 and later stage 2 and 3 are based on the empirical Th frequency histogram method of Irish and Luocks (1987). As shown on Figure 11, the data are clearly inconsistent with depth estimates based on fluid inclusion data from earlier mineralogical stages and with estimates based on geologic reconstruction that suggest greater depths.

The apparent shallow depths estimated for late stage 2 and stage 3 mineralization could be accounted by the presence of CO_2 in ore-fluids of the North Amethyst mineralization. Loucks (1984) has graphically described the relationship between temperature and the depth at which boiling occurs for simple H_2O-NaCl solutions compared to two H_2O-NaCl-CO_2 solutions (0.2 molal CO_2 + 0.5 molal NaCl; 0.5 molal CO_2 + 0.5 NaCl). Figure 11 shows that the addition of even small amounts of CO_2 to an NaCl-H_2O solution dramatically affects the position of the boiling curve. As calculated by Bodnar et al. (1985), for example, the addition of 0.5 mole percent CO_2, a value well within the range of CO_2 contents for most epithermal deposits, including Creede, (Figure 6), to a 2.8 weight percent NaCl solution at 250°C raises the vapor pressure from 69 to 108 bars and changes the estimated depth from 450 to 1120 - a two-and-a-half-fold increase in estimated depth (Figure 11). The range in CO_2 contents cited by Landis and Rye (1989) preclude calculation of reasonable depth estimates based on CO_2 content at this time.

An alternative explanation for the striking differences in depth of formation calculated for different stages of North Amethyst mineralization is that a period or periods of erosion of up to 500

meters of volcanic rock occurred prior to deposition of much of the later base metal - silicate association (Table 1). Minerals of the Mn - Au association, which were clearly deposited at depths greater than 750 meters, and possibly as deep as 1500 meters, formed at some time prior to base-metal - silica mineralization dated at 25.13 Ma (M. Lanphere, written commun., 1989), but after the host Nelson Mountain Tuff at 26.13 Ma. Substantial amounts of erosion could have taken place before or after deposition of stage 1 minerals (base-metal mineralization) because their depth is relatively unconstrained (>480 m, Figure 11). Minerals of the later part of stage 2 and stage 3 may have been deposited after erosion to near present-day levels (~400-500 meters). The base metal - silica mineralization is contemporaneous with mineralization in the central and southern Creede district that was deposited at depths of about 480 meters (Steven and Eaton, 1975). Calcite and quartz of stage 3 also could have been deposited at a significantly later period of time, but probably formed prior to the regional uplift of the southern Rocky Mountains at about 5 Ma[5].

Without more precise analyses of the dissolved gas content of individual inclusions whose thermometry and pedigree is well characterized, or conversely, better constraints on the ages of different stages of mineralization and erosion levels in the central part of the San Juan Mountains, neither of these alternatives can be

---

5 The regional uplift of the southern Rocky Mountains occurred in latest Cenozoic time (Steven, 1968). The event, which presumably raised the Creede orebodies above the water table, has been related to formation of alunite and supergene minerals dated at 3.5-5.0 Ma (M. Lanphere, pers. commun., 1981, cited in Hayba et al., 1985) in veins of the central Creede district (Rye et al., 1988).

discounted. At this time, the second alternative, i.e., erosion, is favored as the dominant external control on depth of mineralization for later stages because of the abundance of nonsaline (ice melting temperatures of 0 to -0.2°C) L-V inclusions in quartz and calcite intergrown with V-rich inclusions indicative of boiling during stage 3. CO_2 contents high enough to allow for an additional ~500 meters of overburden (~0.5 molal CO_2) would result in a measurable lowering of the freezing point for all L-V inclusions. Because nonsaline fluids attributed to overlying groundwater are well-documented in secondary and pseudosecondary inclusions at Creede for the OH vein (Foley et al., 1990), the possibility remains that the lowest salinity inclusions reflect an influx of overlying fluid unrelated to ore mineralization. Salinities of most fluids of stage 2, and earlier, could mask CO_2 contents high enough to suppress boiling curves to greater pressures, allowing for greater estimates of depth of mineralization. However, the fact remains that evidence of CO_2 was not obtained by crushing studies.

COMPARISON WITH CENTRAL AND SOUTHERN CREEDE DISTRICT

Detailed knowledge of the geochemical environment of the Creede hydrothermal system has been developed through integrated fluid inclusion (cited below), light-stable isotope (Bethke and Rye, 1979; Rye et al., 1988; Plumlee, 1989), and lead-isotope studies (Doe et al., 1979; Foley, 1990c), coupled with thermochemical analysis of the ore and gangue mineral asssemblages (Barton et al., 1977; Plumlee, 1989). Fluid inclusion homogenization measurements have defined a temperature range of 120° to 280°C for central and southern Creede ore-forming fluids

(Hayba et al., 1985; Figure 12). Most measurement were made on sphalerite, quartz and fluorite from C and D stage mineralization (Barton et al., 1977) of the OH-Amethyst vein system (Woods et al, 1982; Robinson and Norman, 1984; Hayba, 1986; J. Goss, written commun., 1987; Foley et al., 1990) and on barite from a mineralized stream channel of the Creede Formation (Rice, 1984). There is a clear trend from higher temperatures in the north (OH vein) to lower temperatures in the south (southern Amethyst vein and Creede Formation) although temperature ranges for minerals of each vein overlap (Hayba et al., 1985).

The Creede ores were deposited from relatively concentrated NaCl brines. Data from freezing, crushing, and leaching studies (Roedder, 1963; 1965) indicate that ore fluid salinity ranged from about 4 to 12 weight percent NaCl equivalent and had average atomic ratios of Na:K:Ca of 9:1:1. The salinity of the central and southern Creede ore fluids is much higher than most other adularia-sericite-type deposits evaluated by Heald et al. (1987).

Fluid inclusion studies have also shown that the fluid at times was boiling near the top of the OH vein. Crushing studies indicate that the fluid inclusions have a uniformly low gas content. The pressure at the top of the ore body was approximately 40 bars based on the boiling point of a 250^{o}C, 1 molal fluid (Haas, 1971). The pressure must have been slightly greater than this during deposition of most ore because boiling appears to have occurred infrequently. A depth of 450 meters is estimated for the ores based on the pressure estimate, and this is in excellent agreement with the geologic reconstruction by Steven and Eaton (1975).

Figure 12. Temperature - salinity plots showing fluid inclusion data collected in previous studies of veins of the Creede mining district and Creede Formation-hosted mineralization on Bachelor Mountain. The plots present all data from all localities and stages of each vein system and, thus, are composites of temperatures and salinity variations within time and space. Fluid inclusion data were presented by Bethke et al. (1978) and compiled from studies by Roedder (1977); Robinson (1981); Woods et al. (1982); Hayba (1984); Robinson and Norman (1984); Misantoni (1985); Bazrafshan and Norman (1987); and J. Goss, unpub. data (1987).

CREEDE FM DEPOSIT (BACHELOR MTN)

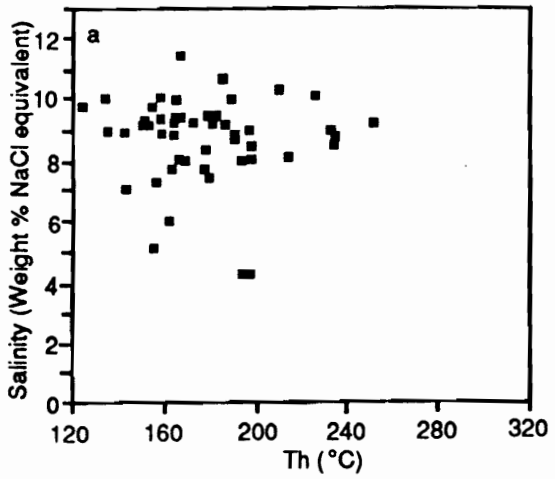

SOUTHERN AMETHYST VEIN SYSTEM

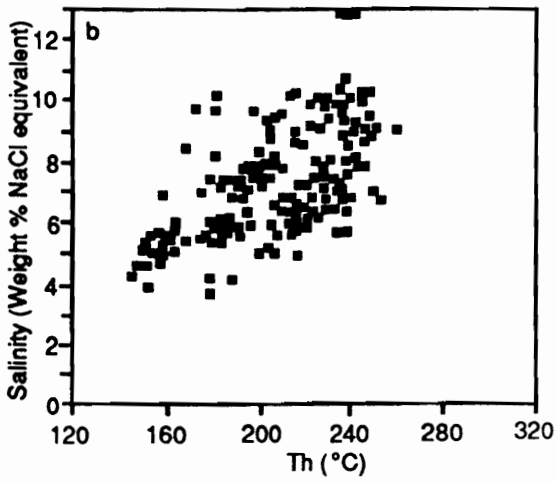

BULLDOG MOUNTAIN VEIN SYSTEM

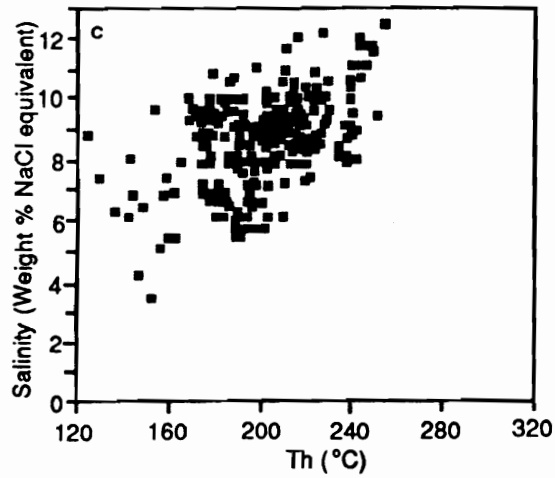

OH VEIN

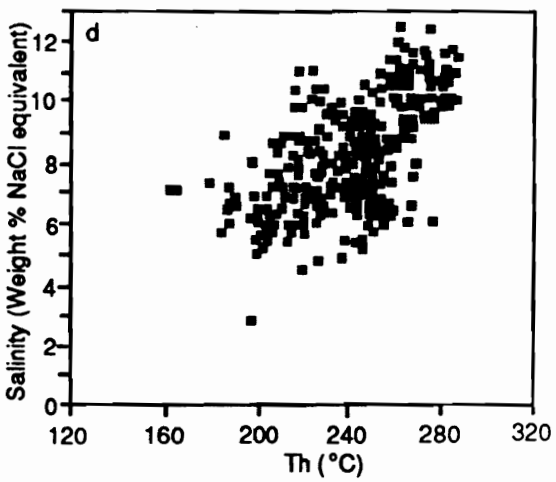

MIDWEST VEIN SYSTEM

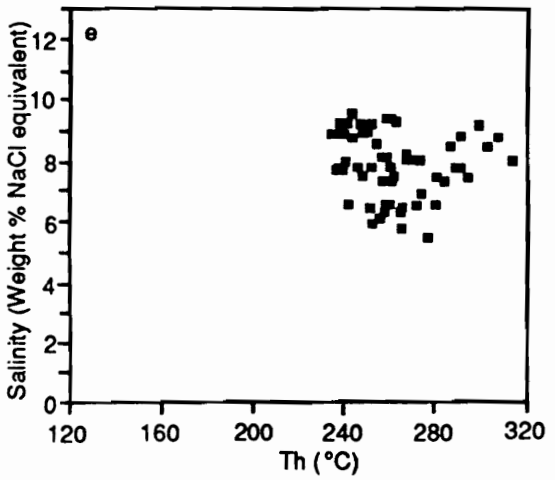

NORTHERN VEIN SYSTEMS

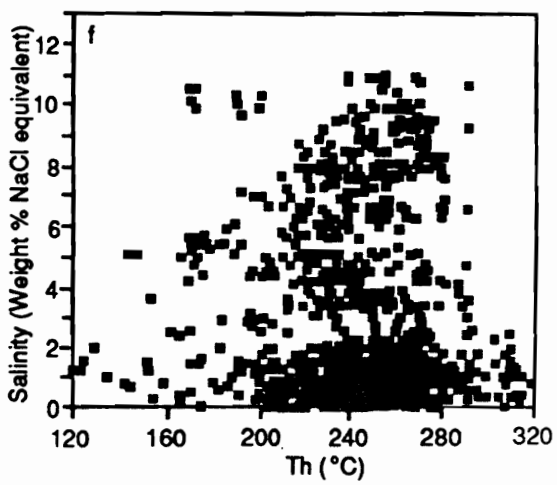

The central and southern Creede ores are thought to be deposited along the top of a saline, deeply circulating hydrothermal system, charged primarily with waters derived from the Creede basin to the south and which displaced the regional ground water flow (Bethke, 1988). An intrusion underlying the district at a depth of 3-5 kilometers is speculated to have been the heat source which provided bouyancy of the brine plume (Steven and Eaton, 1975). In the upper part of the system fluid movement was fracture controlled and nearly horizontal, travelling from north to south. The ore zone was overlain by a zone of fresh water approximately 500 meters thick which flowed southward down the regional hydraulic gradient. The base of the ground water zone was heated to temperatures of about 160^{o}C by heat transfer from the underlying brine. Precipitation of the ores at the interface between the deep brine and the overlying ground water appears to have resulted from the dual processes of boiling and mixing (Hayba et al., 1985).

Primary fluid inclusion data compiled for veins in the southern and central parts of the Creede district (Bethke et al., 1987) are shown in Figure 12a-e. Data for alpha-stage and beta-stage of the North Amethyst mineralization are too limited for comparison, however, clearly there is no inclusion evidence that any minerals in the southern and central parts of the district were deposited from high temperature, low salinity boiling fluids (Figure 12a-e). The temperature and salinity range obtained for stage 1 minerals of the base metal - silica association corresponds to ranges obtained from minerals of the central and southern parts of the Creede district.

Fluid inclusion data from the area immediately south of the North Amethyst workings (Bazrafshan and Norman, 1987) show ranges similar to those seen in North Amethyst stage 2 and stage 3 mineralization (Figure 10). The data for sphalerite, fluorite, quartz and calcite, plotted in Figure 12f, show virtually identical ranges in temperature and salinity for like minerals from stages 1, 2, and 3 of the North Amethyst vein. This similarity suggests that the North Amethyst base metal - silicate association was deposited over a larger area than that considered by this study, supporting conclusions by Foley (1990a) that the hydrothermal system depositing the base metal- silicate association extended further to the south. The absence of detailed paragenetic descriptions of the samples analysed by Bazrafshan and Norman (1987) limits further discussion, with the exception that similar mechanisms were probably involved in mineral deposition for both areas.

DEPOSITIONAL CONTROLS ON MINERALIZATION

Mn-carbonates, Mn-silicate, quartz and minor sulfides of the alpha-stage of the North Amethyst vein system were probably deposited during boiling of hot, relatively dilute fluids. The finegrained nature of the carbonate-rich stage indicates very sudden deposition, or dumping, that might have resulted from a sudden release of pressure due to tectonic adjustments or a rupture in a seal capping an overpressured zone, leading the hydrothermal eruption. Numerous breccias with chalcedonic cements occurring in the veins provide ample direct evidence for explosive brecciation that may be due to overpressuring (Hedenquist and Henley, 1985). However, there is little evidence to constrain

speculation as to the probable cause of the pressure release. Electrum and base metal mineralization of beta-stage also precipitated from a hot, relatively dilute fluid. The timing of brecciation and sedimentation coincident with gold-rich beta-stage mineralization as documented in Foley (1990a) is also indicative of boiling due to pressure release by explosive brecciation. The vertical extent of mineralization and documented boiling horizons (10000, 10400, 12450' levels) suggests extensive mineralization possibly along temperature-depth curves related to CO_2 content. Such an interpretation also is speculative because it hinges on the presence, and abundance, of CO_2 which is not well constrained at this time. The curves cannot be quantified at present without additional data defining the temperatures of fluids boiling at the highest levels and the concentrations of CO_2 in primary inclusions at each horizon.

Following boiling during alpha and beta-stages, lateral mixing of hydrothermal brines having salinities greater than 11 wt% NaCl with heated dilute groundwater may have triggered deposition during stage 1 mineralization. Hydrothermal brines carrying up to 11 weight percent NaCl equivalent precipitated base metal sulfides, fluorite and some quartz during stage 1 and early stage 2 of the base metal - silicate association. The minerals show no evidence for boiling as a depositional mechanism. Inclusion data for stage 1 show a correlation between decreasing temperature and salinity of the ore fluid (Figure 10) as is seen for base metal mineralization of the central and southern parts of the Creede district (Figure 12).

A number of previous studies have demonstrated the important of mixing between hydrothermal brines and shallow dilute groundwater as as ore deposition mechanism for D- stage mineralization of the central and southern parts of the Creede district (Roedder, 1977; Woods et al., 1982; Hayba, 1984; Robinson and Norman, 1984; and Foley et al., 1990). Plumlee (1989) has recently applied chemical reaction path modelling to show that boiling followed by mixing may be a viable mechanism for deposition of II- (and B) stage ores of the central and southern part of the district.

Histograms of inclusion temperatures in different colored sphalerite indicate that most yellow and colorless sphalerite was deposited over an interval from 250-265^{o}C and paragenetically later red sphalerite formed from 250-275^{o}C. Although the available data are few in number, in general, in contrast to yellow sphalerite, decreasing salinities of red sphalerites are not correlated with decreasing temperatures. These observations suggest that towards the end of stage 1 the ore fluids did not change in a regular and systematic manner. Perturbations in temperature and salinity of the ore fluid occurred during deposition of late stage 1 red sphalerites probably as a result of changes in the relative proportions of saline brine and dilute groundwater in the ore fluid. Data for the stage 1 fluids indicate two end-members, an ~11 wt% NaCl, 280^{o}C fluid and an ~0 wt% NaCl fluid having a temperature of less than ~200^{o}C (Figure 10, solid lines).

In contrast, the spread in Th values shown for the intermediate salinity fluids of stage 2 (Figure 10, dashed lines) indicates that mixing between saline ore fluid and a dilute end-member during this

stage may have been virtually isothermal. Later mineralization of stage 2 and stage 3 was deposited from boiling fluids whose temperature-depth profile for mine levels corresponds to <2 wt% NaCl boiling curves (Figure 11) and depths of about 450 meters. The change in orientation of the mixing profile (Figure 10, dashed lines) may indicate an influx of heat (ie., hotter northern recharge water) into the hydrothermal system. This may be the best evidence available to document the extent of the contribution to ore mineralization in the North Amethyst vein system of the isotopically light, hot, northern recharge water identified by Rye et al. (1988).

It is tempting to propose that the hot isotopically light recharge water identified in late stage 2 and stage 3 mineralization is the same fluid responsible for gold-rich alpha-, and beta-stage mineralization. Accordingly, during stage 2 and 3, this fluid re-established itself as the dominant fluid in the North Amethyst hydrothermal system. In this case, the fluids of stage 1 may represent a periodic influx of saline fluid derived from the extensive hydrothermal system to the south. The bulk of the fluid inclusion, mineralogic and geologic evidence, however, is suggestive of a more substantial temporal break between deposition of the Mn-Au association and the base metal - silica association during which extensive tectonic adjustments, brecciation and sedimentation, and possibly erosional unroofing occurred. Mn-Au association assemblages may have been deposited from a fluid that has not previously been defined for Creede mineralization.

GENESIS OF NORTH AMETHYST VEIN SYSTEM

1. Manganese-carbonate + Mn-silicate + and quartz veins were deposited at depths equal to or greater than 1000 meters by boiling of >300^{o}C fluids. The fluids precipitated a microcrystalline "mush" in fractures. The pressure release was due to sudden tectonic adjustments that possibly resulted from CO_2 overpressuring.

2. High-grade gold, silver, and base-metal sulfides and sulfosalts were introduced into narrow seams cutting the "mush" of Mn-carbonate, -silicate, and quartz, following fracturing of the earlier vein material. The occurrences of unsorted breccias, chemical sediments, and pockets of chalcedonic vein sediments attest to an extensive period of hydrothermal brecciation and sedimentation that began concurrently with gold mineralization and continued for some time after deposition of most gold ore. The age of Mn - Au mineralization (Foley, 1990a) is constrained between 26.13 Ma (age of host rock) and 25.13 (age of stage 2 adularia, base metal -silica association).

3. During the period of time following deposition of the Mn - Au association, erosion of up to 500 meters of volcanic rock may have commenced. Erosional unroofing would have altered substantially the hydrology of the North Amethyst vein system, and may have been a contributing factor in the development of the sediments and breccias. However, if CO_2 rather than erosion is called upon to account for the difference in estimated depth for the two associations, the major factor in the development of the sediments and breccias may have been hydrothermal brecciation related to to CO_2 overpressuring.

4. At about 25.13 Ma, an influx of saline (11 wt% NaCl), ~280°C fluid into the hydrothermal system initiated precipitation of a relatively simple suite of base metal sulfides, chlorite, and quartz. The dominant mechanism for deposition was probably mixing with dilute, cooler overlying groundwaters. The bulk of the evidence suggests that the ores formed at about 500 meters depth from fluids initially just below the boiling curve. This depth estimate requires a depositional mechanism involving continued dilution coupled with influx of heat (ie., isothermal mixing of a more saline end-member and an isotopically light hot rechange fluid) to precipitate quartz, fluorite, and carbonate along boiling surfaces at different levels in the ore body.

5. Textures, mineralogy, and fluid inclusion data suggest that the extensive crusts of pink calcite, thin crustifications of pyrite, and coarse quartz draped with paler calcite were deposited from fluids in the waning stages of the hydrothermal system. Deposition from fluids flowing down the sides of vapor-filled fractures in a vapor-dominated hydrothermal system has been proposed for correlative mineralization of the central and southern parts of the Creede district (Plumlee, 1989).

REFERENCES

Abrecht, J., 1988, Experimental evaluation of the $MnCO_3$ + SiO_2 = $MnSiO_2$ + CO2 equilibrium at 2 kilobars: American Mineralogist, v. 77 no. 11-12, p. 1285-1295.

Baars, D.L., and Stevenson, G.M., 1984, The San Luis uplift, Colorado and New Mexico - an enigma of the ancestral Rockies: The Mountain Geologist, v. 21, no. 2, p. 57-67.

Barton, M.D., 1980, The Ag-Au-S system: Economic Geology, v. 75, p. 303-316.

Barton, P.B., Jr., and Toulmin, P., III, 1966, Phase relations involving sphalerite in the Fe-Zn-S system: Econ. Geology, v. 61, p. 815-849.

Barton, M.D., 1978, The Ag-Au-S system: M.Sc. thesis, Virginia Polytecchnic Institute and State University.

Barton, M.D., Kieft, C., Burke, E.A.J., Oen, I.S., 1978, Uytenbogaardtite, a new silver-gold sulfide: Can. Min., v. 16, pp. 651-657.

Barton, P.B., and Bethke, P.M., 1987, Chalcopyrite disease in sphalerite: pathology and epidemiology: Amer. Mineralogist, v. 72, p. 451-467.

Barton, P.B., Jr. and Skinner, B.J., 1979, Sulfide mineral stabilities: in H.L. Barnes, ed., Geochemistry of Hydrothermal Ore Deposits, second edition: J. Wiley and Sons, New York, p. 278-403.

Barton, P.B., Jr., and Toulmin, P., III, 1964, The electrum-tarnish method for determination of the fugacity of sulfur in laboratory systems: Geochim. et Cosmochim. Acta, v. 28, p. 619-640.

Barton, P.B., Jr., Bethke, P.M., and Roedder, E., 1977, Environment of Ore Deposition in the Creede mining district, San Juan Mountains, Colorado: Part III. Progress toward interpretation of the chemistry of the ore-forming fluid for the OH vein: Econ. Geol., v. 72, p. 1-24.

Bazrafshan, K., and Norman, D.I., 1987, Fluid inclusion study of the northern Amethyst vein system [abs]: Geol. Soc. America, Abstracts with programs, v.19, no. 5, p. 259.

Bethke, P.M., and Barton, P.B., Jr., 1971, History of filling of the OH vein, Creede, Colorado [abs]: Economic Geology, v. 66, p. 1265.

Bethke, P.M., Barton, P.B., Jr., Lanphere, M.A., and Steven, T.A., 1976, Environment of ore deposition in the Creede mining district, San Juan Mountains, Colorado: Part II. Age of mineralization: Econ. Geol., v. 71, p. 1006-1011.

Bethke, P.M., and Lipman, P.W., 1987, Deep environment of volcanogenic epithermal mineralization: proposed research drilling at Creede, Colorado: EOS, v. 68, p. 177, 187-89.

Bethke, P.M., and Rye, R.O., 1979, Environment of ore deposition in the Creede mining district, San Juan Mountains, Colorado: Part IV. Source of fluids from oxygen, hydrogen, and carbon isotope studies: Economic Geology, v. 74, p. 1832-1851.

Bethke, P.M., 1988, The Creede, Colorado ore-forming system: a summary model: U.S. Geological Survey Open-file Report 88-408, 29p.

Bethke, P.M., Lipman, P.W., Barton, P.B., Jr., Daniels, J.J., Foley, N.K., Hayba, D.O., 1987, Research drilling in the mineralizaed hydrothermal system at Creede, Colorado: A research proposal submitted to DOSECC, Inc., 129p.

Bodnar, R.J., Reynolds, T.J., and Kuehn, C.A., 1985, Fluid inclusions systematics in epithermal systems: in B.R. Berger and P.M. Bethke, eds., Geology and geochemistry of epithermal systems: Reviews in Econ. Geology, v. 2, p. 73-97.

Cathelineau, M., 1988, Cation site occupancy in chlorites and illites as a function of temperature: Clay minerals, v. 23, p. 471-485.

Cathelineau, M., and Nieva, D., 1985, A chlorite solid solution geothermometer: The Los Azufres (Mexico) geothermal system: Contrib. Mineral., Petrol., v. 91, p. 235-244.

Foley, N.K., and Vardiman, D.M., 1988, Paragenesis and mineral chemistry of ores of the Au-, Ag-, and base-metal-bearing North Amethyst property, San Juan Mountains, Colorado: Geol. Soc. Amer. [Abs.], v. 20, p. A276

Foley, N.K., 1990a, Mineralogy, paragenesis, and mineral chemistry of gold-, silver-, and base-metal-bearing ores of the North Amethyst vein system, Mineral County, Colorado: Part I, unpublished Ph.D dissertation, Virginia Polytechnic Institute and State University, 103p.

Foley, N.K., Bethke, P.M., and Rye, R.O., 1990, A reinterpretation of the δD_{H2O} of inclusion fluids in contemporaneous quartz and sphalerite, Creede mining district, Colorado: a generic problem for shallow orebodies?: Econ. Geol., v. 84, p. 1966-1977.

Gries, R.R., 1985, San Juan Sag: Cretaceous rocks in a volcanic-covered basin, south-central Colorado: The Mountain Geologist, v. 22, p. 167-179.

Giudice, P.M., 1981, Mineralization at the convergence of the Amethyst and OH fault systems, Creede district, Mineral County, Colo.: Unpub. M.Sc. thesis, University of Arizona (Tucson), 95p.

Haas, J.L., 1971, The effect of salinity on the maximum thermal gradient of a hydrothermal system at hydrostatic pressure: Econ. Geol., v. 66, no. 6, p. 940-946.

Hall, D.L., Sterner, S.M., Bodnar, R.J., 1988, Freezing point depression of NaCl-KCl-H_2O solutions: Econ. Geology, v. 83, p. 197-202.

Hayba, D.O., Bethke, P.M., Heald, P., and Foley, N.K., 1985, Geologic, mineralogic, and geochemical characteristics of volcanic-hosted epithermal precious-metal deposits: in B.R. Berger and P.M. Bethke, eds., Geology and geochemistry of epithermal systems: Reviews in Econ. Geology, v. 2, p. 129-167.

Heald, P.W., Foley, N.K., and Hayba, D.O., 1987, Comparative anatomy of volcanic-hosted epithermal deposits: Acid-sulfate and adularia-sericite types: Econ. Geol., v. 82, p. 1-26.

Hayba, D.O., 1984, Documentation of thermal and salinity gradients and interpretation of the hydrologic conditions in the OH vein, Creede, Colorado [abs.]: Geol. Soc. America Abstracts with Programs, v. 16, no. 6, p. 534.

Hayba, D.O., 1986, District-wide fluid mixing during precious/base-metal epithermal mineralization at Creede, Colorado [abs.]: Geol. Soc. America Abstracts with Programs, v. 18, no. 6, p. 632.

Hayba, D.O., 1987, Fluid-inclusion evidence for hydrologic and hydrothermal processes in the Creede mineralizing system, Colorado [abs.]: Geol. Soc. America Abstracts with Programs, v. 19, no. 5, p. 282.

Hayba, D.O., and Conte, C., 1987, Bibliography and index of the geology of the Creede mining district and vicinity: U.S. Geological Survey Open-file Report 87-371, 48p.

Hedenquist, J.W., and Henley, R.W.,1985, The importance of CO_2 on freezing point measurements of fluid inclusions: Evidence from active geothermal systems and implications for epithermal ore deposition: Economic Geology, v. 80, no. 5, p. 1379-1406.

Irish, N.F., and Loucks, R.R., 1987, High-precision thermometry from inclusions that trapped boiling solutions [abs]: American Current Research on Fluid Inclusions Conference, Socorro, New Mexico, January 5-7, 1987, Abstracts with Programs, p. 29.

Landis, G.P., and Rye, R.O., 1989, Reconnaissance gas chemistry of the Creede, Colorado, hydrothermal system: U.S. Geological Survey Open-file Report 89-84, 49p.

Lanphere, M.A., 1988, High resolution $^{40}Ar/^{39}Ar$ chronology of Oligocene volcanic rocks, San Juan Mountains, Colorado: Geochimica cosmochimica acta, v. 52, p. 1425-1434.

Lipman, P.W., Steven, T.A., and Mehnert, H.H., 1970, Volcanic history of the San Juan Mountains, Colorado, as indicated by potassium-argon dating: Geol. Soc. America Bull., v. 81, p. 2329-2352.

Lipman, P.W., Doe, B.R., Hedge, C.E., and Steven, T.A., 1978, Petrologic evolution of the San Juan volcanic field, southwestern Colorado: Pb and Sr evidence: Bull. Geol. Soc. Amer., v. 89, p. 59-82.

Lipman, P.W., and Sawyer, D.A., 1988, Preliminary geology of the San Luis Peak quadrangle and adjacent areas, San Juan volcanic field,

southwestern Colorado: U.S. Geological Survey Open-file report 88-359, 32p.

Loucks, R.R., 1984, Zoning and ore genesis, Topia, Durango, Mexico: Unpub. Ph.D dissertation, Harvard Univ., 329p.

Maresch, W.V., and Mottana, A., 1976, The pyroxmangite-rhodonite transformation for the $MnSiO_3$ composition: Contributions to Mineralogy and Petrology, v. 55, p.69-79.

Plouff, D., and Pakiser, L.C., 1972, Gravity study of the San Juan Mountains, Colorado: U.S. Geological Survey Prof. Paper 800-B, p. 183-190.

Plumlee, G.S., 1989, Processes controlling epithermal mineral distribution in the Creede mining district, Colorado: unpublished Ph.D, Harvard University, 379p.

Potter, R.W., II, Clynne, M.A., and Brown, D.L., 1978, Freezing point depression of aqueous sodium chloride solutions: Econ. Geology, v. 73, p. 284-285.

Rice, J.A., 1984, Controls on silver mineralization in the Creede Formation, Creede, Colorado: Unpub. M.Sc. thesis, Colorado State University (Ft Collins), 135p.

Robie, T.A., Hemingway, B.S., and Fisher, J.R., 1979, Thermodynamics of minerals and related substances at 298.15K and 1 bar (10^5 pascals) and at higher temperatures: U.S. Geological Survey Bulletin 1452, 456p.

Robinson, R.W., 1981, Ore mineralogy and fluid inclusion study of the southern Amethyst vein system, Creede mining district, Colorado:

Unpub. M.Sc. thesis, New Mexico Institute of Mining and Technology (Socorro), 85p.

Robinson, R.W., and Norman, D.I., 1984, Mineralogy and fluid inclusion study of the southern Amethyst vein system, Creede mining district, Colorado: Econ. Geol., v. 79, p. 439-337.

Roedder, E., 1977, Changes in ore fluid with time, from fluid inclusion studies at Creede, Colorado: Internat. Assoc. on the Genesis of Ore Deposits Proc. (IAGOD), 4th Symposium, Problems of ore deposition, Varna, Bulgaria, 1974, v. 2, p. 179-185.

Roedder, E., and Bodnar, R.J., 1980, Geologic pressure determinations from fluid inclusion studies: Ann. Rev. Earth Planet. Sci., v. 8, p. 263-301.

Rye, R.O., Plumlee, G.S., Bethke, P.M., and Barton, P.B., Jr., 1988, Stable isotope geochemistry of the Creede, Colorado, hydrothermal system: U.S. Geological Survey Open-file Report 88-356, 40p.

Sawyer, D.A., Sweetkind, D., Rye, R.O., Siems, D.F., Reynolds, R.L., Rosenbaum, J.G., 1989, Potassium metasomatism in the Creede mining district, San Juan volcanic field, Colorado: Continental Magmatism [Abs], International Association of Volcanology and Chemistry of the Earth's Interior, New Mexico Bureau of Miners and Mineral Resources, Bulletin 131, p. 234.

Schieber, J., and Katsura, K.T., 1986, Sedimentation in epithermal veins of the Bohemia mining district, Oregon, USA: Interpretations and significance: Mineralium Deposita, v. 21, no. 4, p. 322-329.

Sombuthawee, C., Bonsall, S.B., and Hummel, F.A., 1978, Phase equilibria in the systems ZnS-MnS, ZnS-$CuInS_2$, and MnS-$CuInS_2$: Journal of Solid State Chemistry, v. 25, p. 391-399.

Sommer, M.A, II, Yonover, R.N., Bourcier, W.L., and Gibson, E.K., 1985, Determination of H_2O and CO_2 concentrations in fluid inclusions in minerals using laser decrepitation and capacitance manometer analysis: Analytical Chemistry, v. 57, p. 449-453.

Sterner, S.M., and Bodnar, R.J., 1984, Synthetic fluid inclusions in natural quartz I. Compositional types synthesized and applications to experimental geochemistry: Geochim. Cosmochim. Acta., v. 48, p. 2659-2668.

Steven, T.A., 1968, Critical review of the San Juan peneplain, southwestern Colorado: U.S. Geological Survey Professional Paper 594-I, p. I1-I19

Steven, T. A., 1975, Middle Tertiary volcanic field in the southern Rocky Mountains, in B.F. Curtis, ed., Cenozoic history of the southern Rocky Mountains: Geological Society of America Memoir 144, p. 75-94.

Steven, T.A., and Ratte, J.C., 1965, Geology and structural control of ore deposition in the Creede district, San Jaun Mountains, Colorado: U.S. Geological Survey Prof. Paper 487, 90p.

Steven, T.A., and Ratte, J.C., 1973, Geologic map of the Creede quadrangle, Mineral and Saguache Counties, Colorado: U.S. Geological Survey Map GQ-1053.

Steven, T.A., and Eaton, G.P., 1975, Environment of ore deposition in the Creede mining district, San Juan Mountains, Colorado: I.

Geologic, hydrologic, and geophysical setting: Econ. Geol., v. 70, p. 1023-1037.

Steven, T.A. and Lipman, P.W., 1976, Calderas of the San Juan volcanic field, southwestern Colorado: U.S. Geological Survey Professional Paper 958, 35p.

Woods, T.L., Roedder, E., and Bethke, P.M., 1982, Fluid inclusion data on samples from Creede, Colorado, in relation to mineral paragenesis: U.S. Geological Survey Open-file Report 82-313, 77p.

Vaughan, D.J., and Craig, J.R., 1978, Mineral chemistry of metal sulfides: Cambridge Earth Science Series, Cambridge University Press, 493p.

Vikre, P.G., 1989, Ledge formation at the Sandstorm and Kendall Gold Mines, Goldfield, Nevada: Economic Geology, v. 84, p. 2115-2138.

Vikre, P.G., 1989, Fluid - mineral relations in the Comstock Lode: Economic Geology, v. 84, p. 1574-1613.

PART 3:

Pb isotopic geochemistry of the North Amethyst vein system, and the Creede mining district and vicinity, San Juan Mountains, Colorado

LISTING OF CONTENTS

ABSTRACT

INTRODUCTION

GEOLOGIC SETTING

Age of mineralization

MINERALIZATION IN THE CENTRAL SAN JUAN VOLCANIC FIELD

The North Amethyst Vein Mineralization

Deposits of the Central and Southern Creede district

Prospects of the Bondholder district

Prospects of the Spar City district

PB EVOLUTION IN CENTRAL SAN JUAN VOLCANIC FIELD

Elementary Systematics

The Western United States

The San Juan Volcanic Field

Ore Deposits of the San Juan Volcanic Field

Sources of Pb

SAMPLE PREPARATION AND ANALYTICAL TECHNIQUES

RESULTS AND DISCUSSION OF PB ISOTOPIC DATA

Pb Isotope Data

The North Amethyst vein system

Alpha - Corsair vein system, Creede district

Amethyst Vein System, Creede district

Bulldog Vein System, Creede district

OH and P Veins, Creede district

Cascade Prospect, Bondholder district

Other veins in the area

Isotopic composition of volcanic hostrocks

Discussion

Pb Isotopic Evolution of the System

Comparison with Oligocene volcanics and basement rocks of Colorado

MODEL FOR THE NORTH AMETHYST VEIN MINERALIZATION

PB ISOTOPIC SIGNATURES AS A TOOL FOR EXPLORATION

REFERENCES

ABSTRACT

Pb isotopic compositions of 32 galenas, one adularia, and two K-feldspars were determined from ore deposits and volcanic wallrock in the North Amethyst area, and from the central and southern parts of the Creede mining district in the central San Juan Mountain caldera complex of southwestern Colorado. Paragenetically early galenas from Au, silver and base-metal mineralization of the North Amethyst vein system have isotopic compositions that vary in $^{206}Pb/^{204}Pb$ from 18.826 to 18.881, in $^{207}Pb/^{204}Pb$ from 15.588 to 15.602, and in $^{208}Pb/^{204}Pb$ from 37.790 to 37.926. Galenas formed later in the North Amethyst area, during the overprinting by silver and base-metal mineralization, range in $^{206}Pb/^{204}Pb$ from 19.041 to 19.115, $^{207}Pb/^{204}Pb$ from 15.627 to 15.672, and $^{208}Pb/^{204}Pb$ from 37.829 to 38.057. Galenas and adularia of the main mining district at Creede and from the Bondholder district range from about 18.97 to 19.11 in $^{206}Pb/^{204}Pb$, 15.62 to 15.66 in $^{207}Pb/^{204}Pb$, and 37.81 to 38.02 in $^{208}Pb/^{204}Pb$. Galenas of the Alpha - Corsair vein system range from 18.816 to 18.868, from 15.612 to 15.635, and from 37.942 to 38.019.

Pb isotopic results indicate that Au mineralization of the North Amethyst area may represent a separate, and relatively local, hydrothermal system distinct from that of younger base-metal and silver-rich mineralization found throughout the vicinity. The fluids may not have interacted extensively with radiogenic Precambrian rocks at depth. Instead they may have derived their isotopic composition by a greater degree of interaction with shallow relatively less radiogenic volcanic wallrocks. The silver-, and base-metal-rich mineralization overprints

the Au mineralization in the North Amethyst area. This type of mineralization formed as part of a much larger hydrothermal system than that which produced the gold mineralization. The hydrothermal system was composed of a large convecting cell or a series of interconnected cells that resulted in relatively uniform Pb isotopic compositions derived mainly from interaction with Precambrian basement rocks.

Pb isotopic data of the North Amethyst vein system and the Creede mining district generally define two isotopically distinct groups. Both groups are isotopically more radiogenic than the enclosing volcanics of the central San Juan volcanic field. The galenas are also depleted in thorogenic Pb relative to uranogenic Pb, consistent with previously published conclusions that the lower crust and continental lithosphere in this region were never raised to granulite facies metamorphism.

INTRODUCTION

This paper presents the first detailed account of the Pb isotope composition of recently discovered Au-, silver-, and base-metal mineralization that occurs along the North Amethyst vein system in Mineral County, Colorado, as well as Pb isotope data on the silver-, and base-metal mineralization of the main mining district at Creede. The principal objective of this study is to establish the nature of the source of the Pb contributed to the ores of the North Amethyst vein system and the main mining district at Creede. This information can also be used to infer genetic relationships between the different types of mineralization in the central San Juan Mountains, the extent of local control imposed by the associated volcanic rocks on the ore fluid, and

the role of Proterozoic and Phanerozoic rocks in the mid- and upper-crust in the development of the Pb isotopic composition of the ore fluid.

Precious and base metal veins of the North Amethyst system are located along the southern topographic margin of the 26 Ma-old San Luis caldera, a part of the San Juan volcanic field in the southern Rocky Mountains (Figure 1). The veins are found near the intersection of the northern extension of the Amethyst fault and the Equity fault (Figure 2). The main mining district at Creede is 5-7 kilometers to the south, in a zone of recurrent faulting just north of the Creede caldera. The Bondholder district is located approximately 7 kilometers to the north of the North Amethyst mineralization within the San Luis caldera; the Spar City district is located approximately 15 kilometers to the south of the Creede district along the southern margin of the Creede caldera.

The results of this study improve our understanding of the evolution of the Pb signatures of economically important precious and base-metal mineralization in the central San Juan volcanic field. In addition, the Pb isotope compositions help to distinguish the source of Pb contributed to the ores of the North Amethyst system relative to the main mining district at Creede. The data also suggest an isotopic method by which high-Au mineralizing systems might be distinguished from low-Au mineralizing systems in the central part of the San Juan volcanic field.

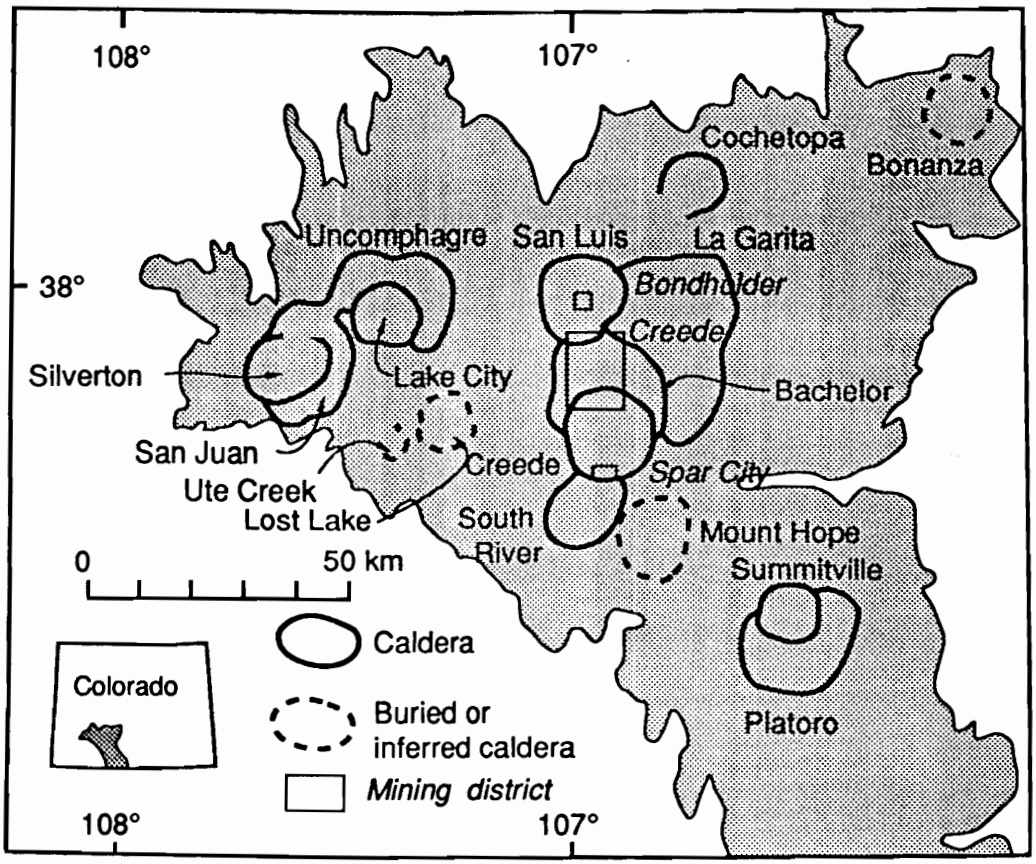

Figure 1. Map of the San Juan volcanic field in southwestern Colorado showing the extent of major ash flow tuffs and associated calderas. From Plumlee (1989), after Steven and Lipman (1976), and incorporating changes suggested by Lipman and Sawyer (1988). Boxes outline mining districts discussed in text: Bondholder, Creede, and Spar City. Creede box shows location of Figure 2.

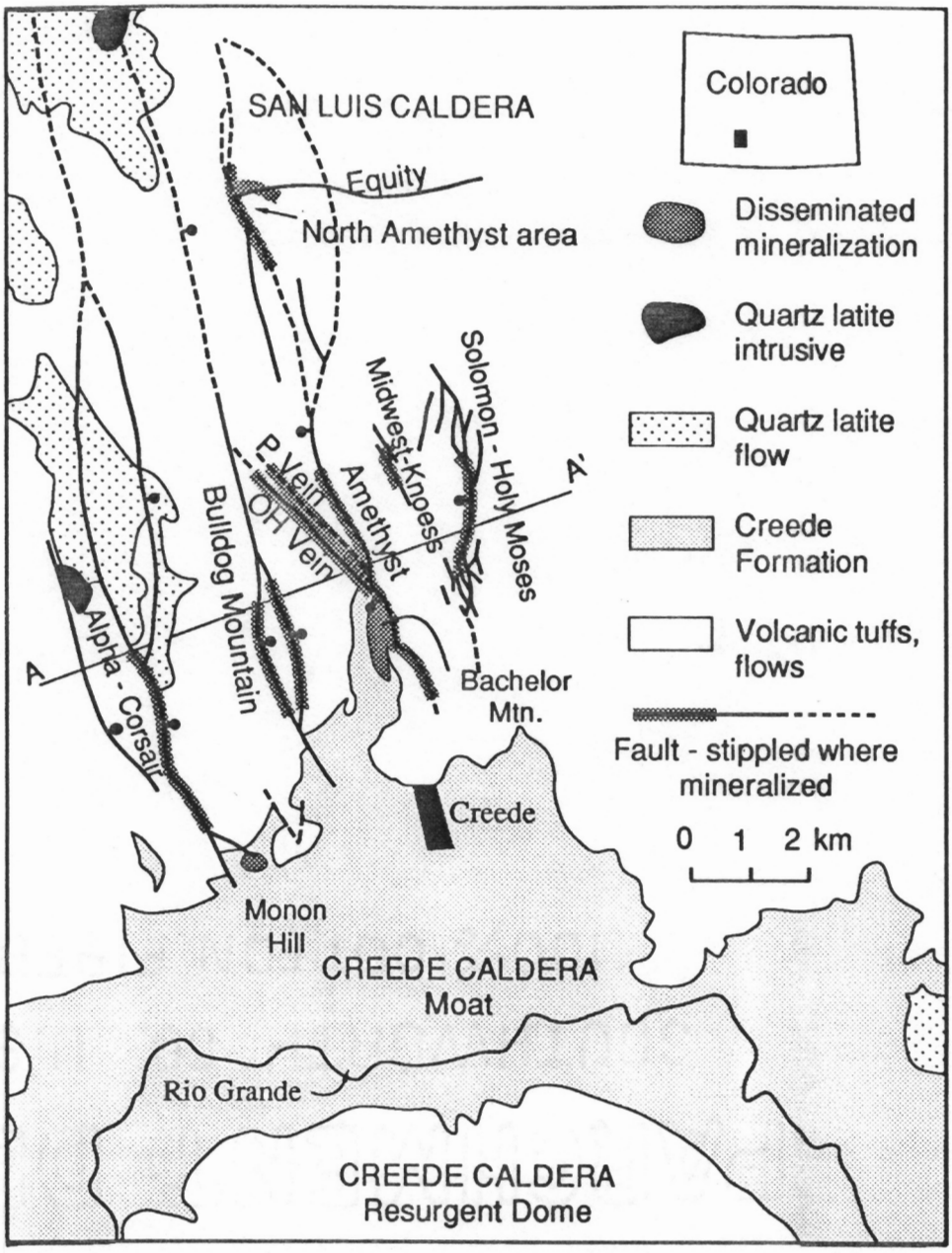

Figure 2. Generalized geologic map of the Creede mining district and vicinity. The graben structure formed by named faults is within the Bachelor caldera and links the San Luis and Creede calderas. North Amethyst vein system is at the intersection of the Equity and Amethyst faults. From Plumlee (1989), geology after Bethke and Lipman (1987) and Lipman and Sawyer (1988). Line A-A' drawn at right angle to veins shows orientation of Figure 13.

GEOLOGIC SETTING

The San Juan volcanic field is an erosional remnant of a much larger volcanic field that covered part of the southern Rocky Mountains in the middle Tertiary (Steven, 1975, Lipman et al., 1978). The present extent of the major ash-flow tuffs and their associated calderas are shown in Figure 1. The volcanic field rests upon an eroded base consisting of Proterozoic crystalline metavolcanic rocks, metasedimentary rocks, and granitic rocks, and possibly on remnants of Paleozoic, Mesozoic and Tertiary sedimentary rock (summarized by Steven, 1975, Lipman et al., 1976, Lipman and Mehnert, 1975, Lipman et al., 1978, Afifi, 1981, Barker, 1969, Bickford and Boardman, 1984, Baars and Stevenson, 1984, and Gries, 1985). The composite volcanic field consists dominantly of andesite-dacite lavas and associated volcaniclastic rocks erupted from Oligocene precaldera volcanoes, mainly between 35 and 30 million years ago. A large negative Bouguer gravity anomaly underlies much of the San Juan volcanic field and is believed to reflect a large composite batholith emplaced beneath the field (Plouff and Pakister, 1972). From about 28 to 26 million years (Table 1), the central San Juan volcanic field experienced widespread silicic ash-flow eruptions and related caldera subsidence (Lipman et al., 1970, Lipman et al., 1978; Lipman and Sawyer, 1988; Lanphere, 1988). The mineralization of the northern, central and southern parts of the Creede district is contained in a set of generally north-south striking vertical faults sited within nested calderas formed by the pyroclastic eruptions.

Table 1. Radiometric ages of lavas, ash-flow sheets, and mineralization of the central San Juan Mountains.

Caldera	Ashflow	Age (Ma)	Ref.
San Luis	Quartz latite of Baldy Cinco (Stewart Peak)	25.72 +/- 0.13	2
San Luis	Nelson Mountain	26.13 +/- 0.08	1
San Luis	Rat Creek Tuff	26.45 +/- 0.06	1
Creede	Snowshoe Mountain Tuff	26.80 +/- 0.10	1
South River	Wason Park Tuff	27.15 +/- 0.12	1
Bachelor	Campbell Mountain Tuff	27.2 +/- 0.2	4
Bachelor	Carpenter Ridge Tuff	27.61 +/- 0.21	1
La Garita	Fish Canyon Tuff	27.80 +/- 0.2	1
Mount Hope	Masonic Park Tuff	28.25 +/- 0.2	1
Regional K-metasomatic event		26.4 +/- 1.3	4

Caldera	Mineralization	Age (Ma)	
San Luis	Northern Amethyst vein adularia	25.13 +/- 0.13	1
Bachelor	OH vein		
	adularia	25.1 +/- 0.6	3
	sericite,	25.7 +/- 1.2	3
	sericite,	25.5 +/- 0.8	3
	sericite	25.3 +/- 1.4	3
	illite-smectite	24.8 +/- 1.3	4

References: 1, Lanphere (1987, 1988); 2, M. Lanphere, written commun. (1989); 3, Bethke et al. (1976), revised by Hon and Mehnert (1983) using new IUGS constants; 4, Vergo (1987).

Mid-Tertiary sediments accumulated locally within the San Juan volcanic field. The most voluminous sediments are those of the Creede Formation, which were deposited in the moat of the Creede caldera and in channels incised in the caldera wall. They consist of stream channel gravels, landslide breccias, travertines, bedded lacustrine sediments and water-lain tuffs (Steven and Ratte, 1965). Thin, local sediments interbedded with volcanic units have also been found in the north-central part of the district by mining companies. Bachelor caldera moat sediments consisting mainly of lacustrine sediments including bedded ash and fine siltstones and local lenses of sand and pebble conglomerates, some of which have been reworked and locally argillized, have been identified by Chevron Resources, Inc, (O'Brient, pers. commun., 1982) and Homestake Mining Company (S. Caddey and C. Byington, pers. commun., 1983). Near the caldera walls, the sediments include megabreccias, laharic breccias, and rare organic-rich lacustrine carbonates (S. Caddey, C. Byington, pers. commun., 1983; D. Sawyer, pers. commun., 1987). Within the San Luis caldera, fluvial and lake-bed sediments (few tens of meters thick) that accumulated in local depositional basins overlie the main Equity dacite facies of the Nelson Mountain Tuff which hosts the North Amethyst ores (Lipman and Sawyer, 1988).[1]

[1] Volcanic units named in this text follow the terminology of Lipman and Sawyer (1988), however, Lipman notes (P. Lipman, written commun., May, 1990) that new data on the positions of paleomagnetic reversals raise some questions as to whether volcanic rocks in the vicinity of the Equity mine are part of the Nelson Mountain Tuff or Carpenter Ridge Tuff.

The complex history of movement and reactivation along faults of the Creede graben has been described in detail by Steven and Ratte (1965). Normal faults are the dominant structural element controlling the location of mineralization in the central San Juan area and most are related to evolution of the Oligocene calderas (Figure 2). The reverse Equity Fault, which formed by fault-bounded uplift of a triangular block presumably related to a shallow underlying intrusion (Lipman and Sawyer, 1988), is also mineralized. The dominant structural features are the well-formed caldera expressions and the north-northwest trending Creede graben which initially formed as a keystone graben in the Bachelor caldera (Figure 2). The major faults from west to east include the Alpha-Corsair, Bulldog Mountain, Amethyst, and Solomon-Holy Moses faults. The OH, P and other minor faults cut the central block of the graben, are nearly vertical, and had primarily strike-slip motion (S. Caddey, pers. commun., 1985).

A radiometric age determination by $^{40}Ar/^{39}Ar$ (Table 1) of adularia associated with base-metal mineralization from a drillcore from the North Amethyst vein system indicates an age of 25.13 +/- 0.13 Ma (M. Lanphere, written commun., 1989). The Au-bearing ores have been shown to predate the base-metal mineralization (Foley and Vardiman, 1988), and thus their age falls in the interval between that of the host rock (the Nelson Mountain Tuff) at 26.13 Ma and the vein adularia at 25.13 Ma. At least three volcanic units were deposited as part of the San Luis caldera complex after the Nelson Mountain Tuff (tuff of Cathedral Peak, rhyolite of Mineral Mountain, and volcanics of Stewart Peak). The youngest volcanic rock dated in the area is the quartz latite of Baldy

Cinco at 25.72 Ma, a unit that is equivalent to the volcanics of Stewart Peak in the San Luis quadrangle (Lipman and Sawyer, 1988). Radiometric age information on gangue minerals associated with ore mineralization from the main Creede mining district indicate that they were deposited at about 25 Ma (Table 1) generally concurrent with mineralization of the North Amethyst ores.

MINERALIZATION IN THE CENTRAL SAN JUAN VOLCANIC FIELD

Galena-bearing mineralization in the central part of the San Juan volcanic field is found primarily in three mining districts (Figure 1). The Bondholder district is located within the San Luis caldera. The Spar City district is found along the southern flank of the Creede caldera. The Creede district is the largest, and the most economically important, of the three. The combined total production at the Bondholder and Spar City districts is only a small fraction of the estimated 85,000,000 oz. of Ag, 150,000 oz. of Au, 350,000,000 lbs. of Pb, 83,000,000 lbs. of zinc, and 5,000,000 lbs. of copper taken out of the Creede district from 1891 to 1986 (Bethke and Lipman, 1989). The historic Creede district can be divided into two parts, the central and southern Creede district (main mining district), and the northern Creede district (North Amethyst vein system), which are separated by about 5 kilometers distance of relatively unexplored area.

The North Amethyst Vein Mineralization

The mineralogy, paragenesis, and mineral chemistry of the North Amethyst mineralization has been studied in detail, and aspects relating directly to the interpretation of the Pb isotopic variations will be

summarized in this section. More detailed information can be found in Foley and Vardiman (1988), and Foley (1990a, 1990b), and in Appendices A-C.

Preliminary study of a limited drillcore and hand sample collection initially indicated that the ores of the North Amethyst mineralization might represent a more Au-rich northern facies relative to the main Creede mining district. Preliminary studies of gas chemistry, stable isotope systematics and chemical modelling (Rye et al., 1988; Plumlee et al., 1988) were based on the belief that the Au ores of the North Amethyst vein system and the ores at Creede were genetically identical. Detailed textural, mineralogical, and chemical observations reported on here, and in Foley and Vardiman (1988), and Foley (1990a), however, indicated that mineralization of the North Amethyst vein system consists of at least two partially coextensive associations having contrasting mineralogies (Table 2), textures, and modes of formation. These two associations are separated locally by a period of major brecciation and sedimentation. Both mineral associations are confined primarily to steeply dipping structures in silicified rhyolite. The ores are multiply brecciated and vein fillings locally show sedimentary textures. Intense sericitic alteration occurs at higher levels in the system; at depth the wallrock is potassium metasomatized. The two contrasting associations suggest a major shift with time in the chemistry of the mineralizing fluid, whereas changes within associations probably reflect local control on the composition of the hydrothermal fluid (Foley, 1990b).

Table 2. Stages of mineralization and brecciation events of the North amethyst vein system.

STAGE	NORTH AMETHYST VEIN MINERAL ASSEMBLAGE
YOUNGEST	
Base metal - silica association:	
3	Mn-calcite >> Quartz > Pyrite
Breccia-4	Mn-calcite cement, fragments of earlier assemblages, breccias and minerals, [wallrock]
2b	Quartz > Calcite > Rhodocrosite > Adularia > Fluorite > Chlorite = Pyrite
Breccia-3	Quartz + chlorite cement, fragments of wallrock, and coarse stage 1 sulfides
1b	Quartz > Sphalerite > Galena > Pyrite > Chalcopyrite > Tetrahedrite
1a	Quartz > Pyrite = Hematite > Chlorite
Breccia-2	Quartz cement, fragments of α-,and β-stages, wallrock, sedimented structures black quartz breccia
Mn - Au association:	
β-2	Sphalerite > Galena > Chalcopyrite > Pyrite > Tetrahedrite > Ag- and Au-minerals > Electrum {Magnetite, Hematite}
Breccia-1	Quartz cement, fragments of α- and β-1 stages
β-1	Sphalerite > Galena > Chalcopyrite > Pyrite > Tetrahedrite > Ag- and Au-minerals > Electrum {Magnetite, Hematite}
α	Rhodocrosite = Quartz > Mn-calcite = Rhodonite > K-feldspar > Sphalerite > Pyrite > Galena > [Barite]
OLDEST	

Abbreviations: >>, much greater than; >, greater than; =, approximately equal; {} distribution unknown, local occurrence; [], molds

Table 3. District-wide correlation of mineral assemblages and brecciation events.

North Amethyst vein (Foley, 1990)	Bulldog vein (Plumlee, 1989)	OH - P vein (Bethke and Rye, 1979)	Southern Amethyst (Robinson (1981)	Disseminated ore, OH-Amethyst (Guidice, 1980)
Mn-Cc + Qz + Py (3)	Py + Stib + Pyrar (V)	Py + Stib (E)	Absent?	Gel Py + Qz (2)
Breccia-4	Absent?	Absent?	Absent?	Absent?
Absent	Sp + Gn + Cpy Td + Pearc + Ac (IV)	Sp + Gn + Qz + Cpy +Hm (D)	Absent?	Absent?
Qz + Mn-Cc + Ad + Rc Ad + Mn-sid + Chl +Py (2)	Qz + Fl + Mn-sid + Sp + Gn (III)	Fl + Qz + Mn-sid (C)	Absent?	Included in (1)?
Breccia-3	Absent?	Absent?	Absent?	Absent?
Sp + Gn + Py + Cpy + Qz + Hm + Chl + Td (1)	Bar + Qz + Sp + Gn + Td (II)	Qz + Sp + Chl + Gn + Hm + Td-tn + Au (B)	Qz + Sp + Gn + Py + Td + Hm + Acan + Ag (2)	Sp + Gn + Py + Cp + Chl + Rc + Bar + Ag + Td + Ac + (1)
Breccia-2	Rc + Qz + Sp + Gn + Ad (I)	Qz + Ad (A)	Rc + Qz + Bar + Cc + Sp + Gn + Py + Ccp (1)	Absent?
Gn + Sp + Cpy + Py + Td + Ac + Uyten + Au (beta-2)	Absent?	Absent?	Absent?	Absent?
Breccia-1	Absent?	Absent?	Absent?	Absent?
Gn + Sp + Cpy + Py + Td + Ac + Uyten + Au (beta-1)	Absent?	Absent?	Absent?	Absent?
Rc + Qz + Mn-Cc + Rh + Px + Sp + Gn + Py + Ad (alpha)	Absent?	Absent?	Absent?	Absent?

Abbreviations: Ac, acanthite; Ad, adularia; Ag, silver; Au, electrum; Bar, barite; Cc, calcite; Chl, chlorite; Cpy, chalcopyrite; Fl, fluorite; Gn, galena,; Hm, hematite; Mn, manganese; Pearc, pearcite; Px, pyroxmangite; Py, pyrite; Pyrar, pyrargyrite; Qz, quartz; Rc, rhodocrosite; Rh, Rhodonite; Sp, sphalerite; Sid, siderite; Stib, stibnite; Td, tetrahedrite-tennantite. Stage designations for each vein are shown in parentheses. (After Foley and Vardiman, 1989)

the association include calcite, adularia, fluorite, and quartz. Local occurrences of quartz, Mn-rich calcites, trace pyrite, and gypsum line late vugs and form crusts on earlier assemblages and breccias.

The Au-rich beta-1 and beta-2 assemblages of the Mn-Au association are not documented in the main district, and manganese-silicate is absent. In contrast, mineralogic and fluid inclusion characteristics of the younger base metal-silica association are similar to those of ores of the main Creede district (Foley, 1990a, b). These characteristics enabled Foley and Vardiman (1988) and Foley (1990a) to correlate the base metal - silica association of the North Amethyst area (Table 3, Stages 1 through 3) with Stages B through E of the Creede district (Bethke and Rye, 1979), and Stages II through IV of the Bulldog vein system (Plumlee, 1989). The correlation of the stages suggests that the ores of the later North Amethyst association formed as part of a large hydrothermal cell or series of interconnected, open hydrothermal cells that deposited mineralization along the lengths of the North Amethyst, Amethyst, Bulldog, OH, and P vein structures.

Deposits of the Main Creede district

The epithermal Ag and base-metal ores of the main mining district at Creede occur as open space fillings in a N-S graben system which cuts ash flow tuffs of middle Tertiary age that comprise the Bachelor caldera (Figure 2). The mineralization is hosted by a thick intracaldera accumulation of rhyolitic tuff designated the Bachelor Mountain Member (Steven and Eaton, 1975) that is now interpreted as an intracaldera part of the Carpenter Ridge Tuff. The structures which have contributed significantly to the production history of the district include the

Amethyst, OH, P, and Bulldog Mountain vein systems. Mineral assemblages include pyrite, hematite, chlorite, quartz, K-feldspar, sericite, sphalerite, galena, chalcopyrite, and tetrahedrite-tennantite, acanthite and various sulfosalts (Barton et al., 1977). The paragenesis of the OH-vein is summarized by Bethke and Rye (1979). They identify five mineralogical stages: A through E. Sphalerite and galena occur predominantly in the B- and D-stages (Table 3). The Bulldog vein system has recently been studied in detail by Plumlee (1989) who describes five stages (I through IV) that correlate directly with Bethke and Rye's district-wide conclusions (Table 3). The ores are of the adularia-sericite type (Heald et al., 1987) and are postulated to have been deposited 300-500 meters below the water table in a sub-horizontal zone of mixing between a deeply convecting brine plume and overlying ground water (Hayba et al., 1985; Bethke, 1988).

Prospects of the Bondholder district

The geology and mineral resources of the Bondholder district were examined by Steven and Bieniewski (1977) as part of a mineral resource appraisal of the La Garita Wilderness area. The Bondholder district is located within the San Luis caldera on slopes adjacent to Bondholder Meadow, a relatively large flat stream valley situated three to six kilometers north of the Continental Divide (Figure 1). The mineralization is hosted by by rhyolitic and transitional rhyolitic-dacitic intracaldera Nelson Mountain Tuff. Lipman and Sawyer (1988) describes a possible northwesterly continuation of the Amethyst structure in this area: an up-to-the-east fault concealed beneath surficial deposits in upper Cascade Creek. Numerous pits and small mine

workings were dug in the late 1800's when the area was extensively prospected. Many of the workings expose small mineralized fractures having encouraging assays for Pb, Zn, and Ag associated with quartz and fluorite, and anomalous Cu and Au (<0.1 to 0.35 ppm) values. The highest grade material is located around Cascade mine near the mouth of Cascade Creek, and in the vicinity of the Woodmansee mine along the east side of Spring Creek, 0.8 kilometers to the north.

Wallrock along the mineralized fractures of the Cascade mine is irregularly silicified and the rock locally contains pyrite, and sparse galena and sphalerite. Pyrite, galena, and sphalerite are irregularly distributed along the fractures and locally is sufficiently abundant to be of ore grade. The mineralized fractures commonly split and die out, or link irregularly with subparallel minor fractures.

Mineralization in the Woodmansee mine area is more widespread (Steven and Bieniewski, 1977). The prospects extend over an area more than 300m across and over a vertical range of at least 240 meters. The vein material is visible in small fractures, none of which can be traced laterally due in part to generally poor exposures on the talus covered slope. Samples from Woodmansee mine area indicate Pb, Zn, and Ag values approaching ore grade, as well as anomalous Cu and Au values, occur throughout the area.

Deposits of the Spar City district

The Spar City district (Steven, 1964) is a small mineralized area located along the southern flank of the Creede caldera in the central San Juan Mountains in southwestern Colorado (Figure 1). The district has been explored sporadically since the early 1900's. The mineralized

area is near the intersection of two differently trending structures active during volcanic activity and the known veins appear to be along minor faults associated with this intersection. Mineralization took place late in the sequence of volcanic and structural events and was either associated with or later than the last main period of faulting. The exposed veins were deposited in a near-surface environment and consist mainly of galena, sphalerite, barite, manganese oxides, and jaspery to amethystine quartz. Gold has not been reported for the Spar City district.

PB EVOLUTION IN THE CENTRAL SAN JUAN VOLCANIC FIELD

Elementary Systematics

The isotopic composition of Pb reflects the incorporation of primordial Pb originating when the solar system formed about four and a half billion years ago and Pb derived from the final decay product of thorium and uranium. Thorium primarily exists as a single long-lived radioactive isotope, ^{232}Th, which decays to ^{208}Pb with a half-life of about 14.008×10^{9} years (LeRoux and Glendenin, 1963). Uranium has two isotopes, ^{238}U and ^{235}U which decay by emission of alpha and beta particles to ^{206}Pb and ^{207}Pb; respectively, with half-lives of 4.468×10^{9} and 0.7038×10^{9} (Jaffey et al., 1971). A fourth Pb isotope, ^{204}Pb, is not the product of any known decay and, thus, the earth's endowment of ^{204}Pb has remained relatively constant through time. ^{204}Pb is very weakly radioactive and decays to stable ^{200}Hg with a half-life of 1.4e17 years (Holden and Walker, 1972), so for all purposes it can be treated as a stable reference isotope. The primordial Pb isotopic composition

was estimated to be 29.476 for $^{208}Pb/^{204}Pb$, 10.294 for $^{207}Pb/^{204}Pb$, and 9.307 for $^{206}Pb/^{204}Pb$ (Stacey and Kramers, 1975). The integrated half-lives of the intermediate decay products are practically instantaneous in the geological sense, so that for most applications the intermediate decay steps can be overlooked and treated as a single step in the evolution of Pb isotopes for most applications (Faure, 1977).

Thorium and uranium are generally similar in their geochemical behavior and are accommodated in the accessory minerals (esp. zircon, sphene, apatite, allanite, monazite, etc.) of igneous and metamorphic rocks. Under granulite-facies metamorphism thorium and uranium may become decoupled and in this case uranium will become depleted relative to thorium. It is also well known that under oxidizing conditions (especially at lower temperatures) uranium becomes more soluble than thorium and can thus be separated from thorium and concentrated to yield uranium-rich rocks. In contrast, Pb either follows potassium into a major rock-forming mineral, such as alkali feldspar, or it fractionates into a hydrothermal phase and, may eventually be deposited as a thorium and uranium-free sulfide, galena.

Pb isotopic signatures are effective in characterizing plutonic source rocks because, assuming no subsequent comtamination, melts that derive their isotopic signatures directly from a source region have lead isotopic compositions whose primary differences are a function of the contrasting geochemical behavior of parental elements (U and Th) and of their half-lives (Ayuso and Bevier, 1990). As a result of the control imposed by the half-lives of radiogenic parents on daughter products, different regions of the crust and mantle display a degree of similarity

in daughter isotopic ratios that relates directly to the effective U/Pb and Th/U ratios during evolution. Because of the relatively short half-life of ^{235}U compared to ^{238}U and ^{232}Th, recent changes in U/Pb do not as strongly affect the variation in $^{207}Pb/^{204}Pb$. Thus, a Proterozoic crustal region affected by high-grade metamorphism shortly after its formation will evolve along an evolution path controlled by lower U/Pb ratios and this will result in lower $^{207}Pb/^{204}Pb$ values than if the crustal region were affected by high grade metamorphism much later. The identification of major differences in $^{207}Pb/^{204}Pb$ and $^{206}Pb/^{204}Pb$ values in groups of galenas may provide a clear indication of long-lived and distinct isotopic evolution trends for the components in the source regions for these groups (e.g., Ayuso and Bevier, 1990). Differences in $^{208}Pb/^{204}Pb$ can also be used to identify source regions that contain granulites and to differentiate between continental crust and mantle sources (e.g., Ayuso and Bevier, 1990). For example, high grade metamorphism of potential source rocks results in variations in Th/U, $^{238}U/^{204}Pb$, and $^{232}Th/^{204}Pb$ values, so that in general in granulite facies rocks the Th/U ratio is increased (e.g., Heier, 1973) and the U/Pb ratio is decreased relative to the same rocks at lower grade.

The Western United States

Regional Pb isotopic differences have been recognized in rocks of the western United States in a number of studies including Doe (1967, 1968), Doe et al. (1979), Zartman and Stacey (1971), and Doe and Delevaux (1973). Zartman (1974), however, first recognized that the Pb isotopic compositions of Mesozoic and Cenozoic igneous rocks and related hydrothermal ore deposits could be used to define three discrete Pb

isotopic provinces in the western United States. The Pb isotopic composition of each of these provinces is believed to reflect the source material from which the Pb was derived.

Zartman's (1974) three geographically distinct provinces are characterized as follows: I, Pb derived from Precambrian crystalline basement; II, isotopically homogeneous Pb derived from a sedimentary pile eroded from adjacent Precambrian rocks; and III, Pb derived from young plutonic, volcanic, and sedimentary rocks. Area I is further subdivided into Ia, which characterizes a terrane underlain by 2.7 b.y. and older basement rock, and Ib, a terrane underlain by 1.4 to 1.8 b.y. old basement rock. The Proterozoic crust in the southwestern United States was recently studied in more detail by Wooden et al. (1988) who summarized four crustal age and isotopic provinces: 1, the Mojave desert; 2, an area with variable but high contributions of Pb from an Archean (>2.5 Ga) age source; 3, a terrane with a MORB-like (Mid-Ocean Ridge Basalt) mantle Pb isotopic signature, which was further subdivided into 1.78-1.69 Ga and 1.68-1.61 Ga basement rock; and 4, the group III terrane of Zartman (1974).

The San Juan volcanic field, on the eastern edge of the Colorado Plateau, falls within Zartman's area Ib and Wooden et al.'s area 3 (Figure 3). To the northeast, in central and northern Colorado, the Colorado Mineral Belt was found to has a composite 1.75 Ga lower crustal Pb source for Laramide-Tertiary magmatism (Table 4; Stein, 1985). South and west of the San Juan region, the Pb source for rocks and ore is about 1.60-1.70 Ga (Table 4; Stacey and Hedlund, 1983, Wooden et al., 1988). Detailed studies by Lipman et al. (1978) and Doe et al. (1979)

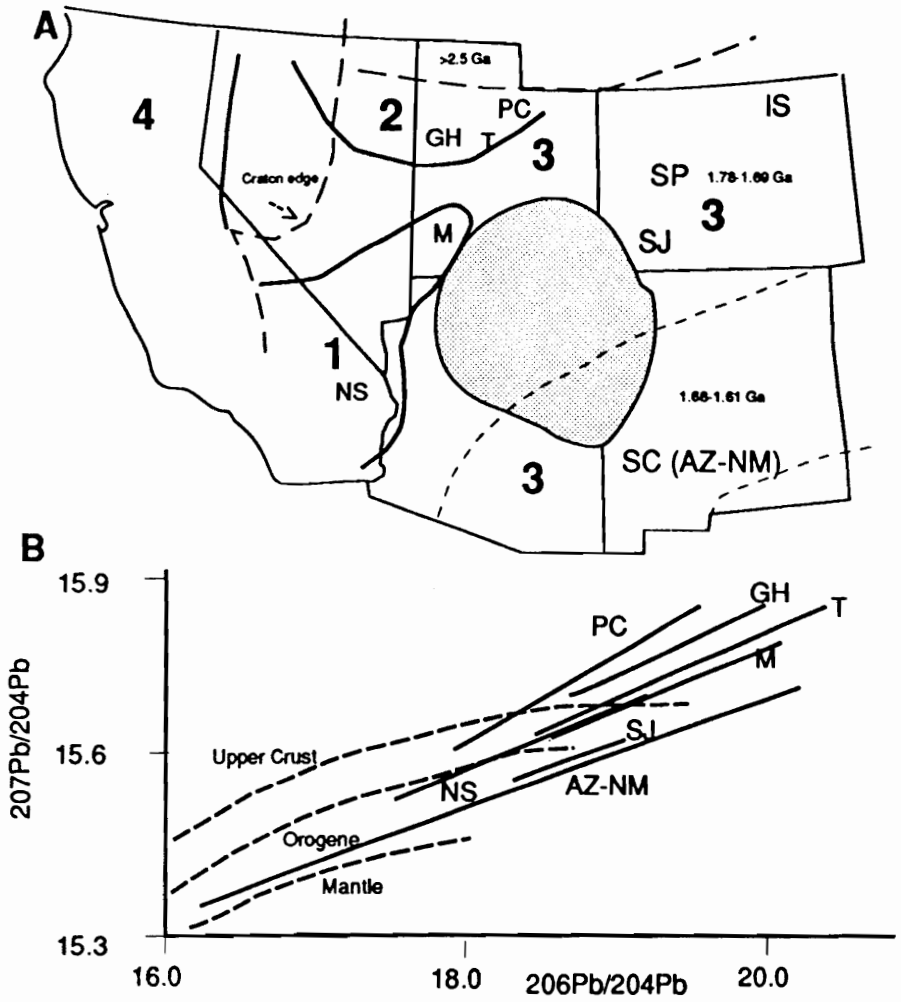

Figure 3. A) Map of the western United States showing lead provinces as defined by Wooden et al. (1988). Lead isotopic studies of Precambrian rocks referred to in this study (Table 4): SC, Silver City (Stacey and Hedlund, 1983); SJ, San Juan area (Lipman et al., 1978; Doe et al., 1979); SP, Silver Plume (Stein, 1985); IS, Idaho Springs Formation (Stein, 1985). Others studies include PC, Park City; B, Bingham; T, Tintic; GH, Gold Hill; M, Milford; NS, Needles sheet (as described by Stacey and Hedlund, 1983). Shaded area is of the Colorado Plateau. B) Lower figure shows summary diagram of lead data compiled in Wooden et al. (1988), abbreviations as above. Dashed lines are average growth curves from the model of Zartman and Doe (1981). The orogene curve approximately overlaps the uranogenic two-stage model curve of Stacey and Kramers (1975).

Table 4. Whole rock and potassium feldspar sample descriptions, locations, and lead isotope data of Precambrian rocks of Colorado and New Mexico.

Description	$^{206}Pb/^{204}Pb$	$^{207}Pb/^{204}Pb$	$^{208}Pb/^{204}Pb$	References
Eolus Granite, Needle Mountains, Colo. (1.4 Ga)				
Whole rock	25.402	16.208	41.867	Doe (1976)
K-feldspar	16.64	15.41	35.97	Doe (1976)
Biotite Granite, Bullard Peak Series, Silver City, New Mexico (1.45 to 1.55 Ga)				
Gold Hill, K-Feldspar	16.22	15.353	35.866	Stacey and Hedlund (1983)
Gold Hill, Whole rock	17.276	15.441	38.97	Stacey and Hedlund (1983)
Gold Hill, K-Feldspar	16.323	15.358	36.22	Stacey and Hedlund (1983)
Gold Hill, K-Feldspar	16.412	15.378	36	Stacey and Hedlund (1983)
Gold Hill, Whole rock	26.543	16.354	46.58	Stacey and Hedlund (1983)
Silver Plume Granite, Colorado (1.4 Ga.)				
HS-82-53K, K-feldspar	16.19	15.377	36.297	Stein (1985)
HS-82-69WR, Whole rock	17.345	15.49	53.408	Stein (1985)
GSP-1, Whole rock	17.998	15.546	47.053	Doe (1976), Stein (1985)
St. Kevin Granite, northern Sawatch Range, Colo. (1.4 Ga)				
K-feldspar	16.61	15.48	36.36	Doe (1976)
K-feldspar	16.61	15.58	36.61	Doe (1976)

suggested that Proterozoic basement rocks of the San Juan region were not raised above granulite-facies metamorphism because thorium and uranium are not decoupled. This contrasts with central and northern Colorado where the source material for Laramide-Tertiary magmatism was mostly cratonized Proterozoic lower crust containing small and variable amounts of Archean detritus (Stein, 1985).

The San Juan Volcanic Field

Lipman et al. (1978) first examined the petrologic evolution of the San Juan volcanic field by applying the U-Th-Pb isotope system. They showed that the Pb isotopic range of the Oligocene volcanics is large, requiring a relatively heterogeneous source for the magmas, and that the volcanic rocks were less radiogenic than most upper-crustal Precambrian rocks of North America (Figure 4). Geographic variations in $^{208}Pb/^{204}Pb$ and $^{206}Pb/^{204}Pb$, for the western, eastern and central San Juan provinces were related to lateral compositional variations in the source region of the magmas. The results showed that all of the San Juan volcanic rocks plotted below the single-stage evolution curve for $^{208}Pb/^{204}Pb$ requiring relatively low Th/U values in the source reservoir; probably ranging from 3.6 (western San Juan) to 2.6 (central San Juan) and 2.7 (southwestern San Juan). Pb isotope secondary-isochron ages calculated by Lipman et al. (1978) for source rocks of the volcanics of the San Juan region were 1.4 +/-.50 Ga for southeastern, 1.97 +/-.25 Ga for central; 1.71 +/-.32 Ga for western parts of the region. If all of the data were treated together the secondary isocron age is 1.86 +/-.11 Ga.

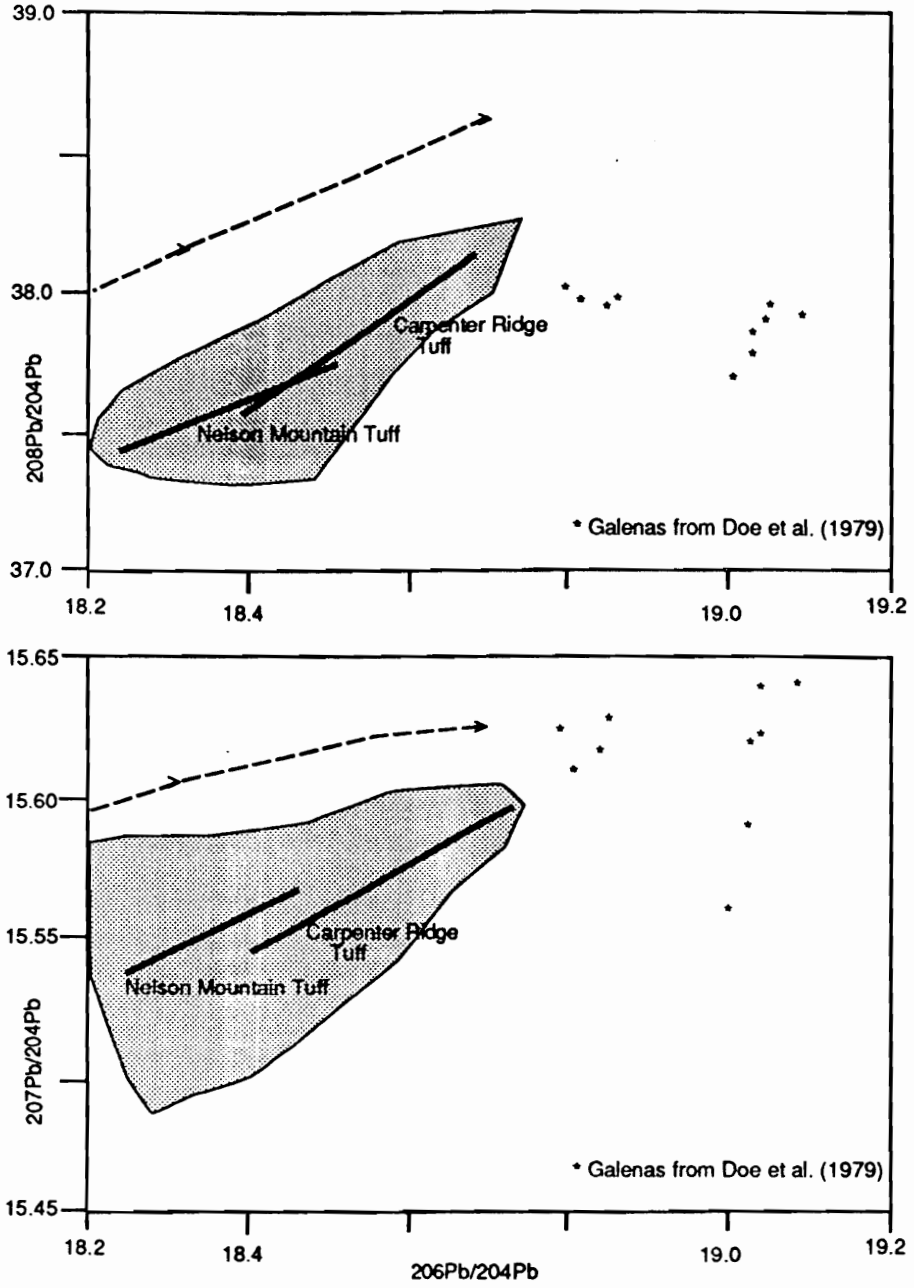

Figure 4. Lead isotopic composition of Oligocene volcanics of the central San Juan region from Lipman et al. (1978); Matty et al. (1987); and D. Matty, written commun., (1987). Galena data from Doe et al. (1979) are also shown. Dashed line for reference is model curve of Stacey and Kramers (1975). Heavy lines show general trend of field of data for named tuffs (D. Matty, pers. commun., 1989).

Matty et al. (1987) and D. Matty (written commun., 1987) examined in detail the common Pb isotopic compositions of individual ash-flow tuffs and related volcanic rocks of the central San Juan field (Figure 4). The Nelson Mountain Tuff which hosts mineralization of the North Amethyst vein system and the Bondholder district, has $^{206}Pb/^{204}Pb$ values from 18.231 to 18.374, $^{207}Pb/^{204}Pb$ from 15.540 to 15.563, and $^{208}Pb/^{204}Pb$ from 37.464 to 37.581 (Matty et al., 1987; D. Matty, unpub. data, 1987). The Carpenter Ridge Tuff, which hosts ores of the main mining district at Creede and the Alpha-Corsair vein system, has $^{206}Pb/^{204}Pb$ values from 18.501 to 18.742, $^{207}Pb/^{204}Pb$ from 15.564 to 15.607, and $^{208}Pb/^{204}Pb$ from 37.886 to 38.183 (Lipman et al., 1978; Matty et al., 1987; D. Matty, unpub. data, 1987). Common Pb determinations of two K-feldspar separates (Table 6) from welded and unwelded Carpenter Ridge Tuff (host rocks to the mineralization in the main mining district at Creede), were also determined during this study to supplement published Pb data. Matty et al.'s (1987) data yielded a secondary isochron age of 1.78 +/- .18 Ga when combined with previously published data for all the San Juan volcanic rocks, and the associated reservoir of $^{238}U/^{204}Pb$ (μ) is 9.52. This age agrees with Precambrian crustal ages in the area (Lipman et al., 1978; DePaolo, 1981).

Ore Deposits of the San Juan Volcanic Field

Pb isotope compositions of the ore deposits of the San Juan volcanic field were studied by Doe et al. (1979) to determine the source of the metal in the mining districts. They proposed that a significant part of the ore lead in the San Juan Mountains was scavenged by deeply circulating meteoric hydrothermal waters in convection cells driven by

magmatic heat. The fluids acquired Pb at depth by leaching of Precambrian rocks or sediments derived from Precambrian rocks, and deposited the Pb as galena in base-metal-rich veins in the Cenozoic igneous rocks.

Doe et al. (1979) analysed five galenas from the main mining district at Creede, two galenas from the Monon Hill mine (Alpha-Corsair fault), and one each from the Sonota mine (Alpha - Corsair fault system), the Solomon-Holy Moses vein, and the Spar City (Emma mine) and Bondholder (Cascade mine) districts (Figure 4). Pb isotopic compositions for the Creede district and for other ore deposits in the central San Juan Mountains were found to be more radiogenic than any known Mesozoic or Cenozoic igneous rocks in the entire Rocky Mountain region. Galenas from the main mining district (OH, Bulldog, and Amethyst veins) and the Solomon-Holy Moses vein were found to have nearly identical isotopic compositions implying that galena was precipitated from a large, well-mixed reservoir of mineralizing solution that did not undergo significant modification during transport to the site of deposition (Doe et al., 1979). At least two separate convecting cells of mineralizing solutions each with its own unique Pb isotopic composition were proposed to account for local differences in the Creede district.

Sources of Lead

Ore-leads for the central San Juan region analysed by Doe et al. (1979) plot below the average orogene curve and are thought to reflect mixing between upper-mantle Pb and upper-crustal Pb in circulating volcanic hydrothermal systems. The ores plot below the two-stage

evolution curve (Stacey and Kramer, 1975) for thorogenic Pb, consistent with the assumption that the lower crust and continental lithosphere were never raised above granulite facies metamorphism (Lipman et al., 1978). The controlling influence on the isotopic composition of Pb in the mining districts in the central part of the San Juan volcanic field was related by Doe et al. (1979) to the age and Th/U value of underlying Precambrian basement rock. They suggested that the rocks and galena contain a significant component of Pb derived from 1400 to 1500 m.y. old and 1700 to 1800 m.y. old source materials. The proportion of lead from each source contributed to the galenas and rocks was related to the Th/U value of the source material. A low Th/U value of 0.7 indicated greater involvement of 1.4 to 1.5 b.y. old source material, whereas a larger Th/U value of 2.3 to 3.3 was thought to characterize the 1,700 to 1800 m.y. old source. The Pb may also have been derived from a combination of sources of both ages.

SAMPLE PREPARATION AND ANALYTICAL TECHNIQUES

Galena crystals 0.1 to 1.0 millimeters on edge were cleaved from samples whose mineralogy, location and identification number are listed in Table 5. Sample locations for North Amethyst vein are shown in Figure 5, except for NA-11-1698 which was selected from drillcore. The cleavage fragments of galena were washed in 7N nitric acid and then dissolved in 14N nitric acid (Foley et al., 1981). After evaporization to dryness on a hot plate, the Pb was analysed using the single filament, silica gel-phosphoric acid method of Cameron et al. (1969) on a 12-inch NBS-type mass spectrometer and a Finnigan MAT 261 mass spectrometer at the U. S. Geological Survey, Branch of Isotope Geology,

Reston, Virginia. Repeat analyses and separate dissolutions were made for selected samples on both machines.

The alkali feldspars were separated with heavy liquids from bulk rock samples. Pure potassium feldspar concentrates were then obtained by hand-picking inclusion-free unaltered grains using a binocular microscope. Following the method outlined by Ayuso et al. (1988), the feldspars were leached with HF and HCl, rinsed in water and dried overnight. Feldspar samples were then dissolved in a mixture of HF-HNO_4 and processed through ion-exchange chemistry using AG-1-X8 anion exchange resin and HBr and HCl solutions. Pb was analysed using the single-filament surface emission (silica-gel) technique of Cameron et al. (1969) on a 12-inch NBS-type mass spectrometer at the U.S. Geological Survey. The runs were corrected for fractionation by comparison with repeat analyses of NBS SRM-982. The isotopic ratios produced using these techniques have an uncertainty of less than 0.15 percent (2τ).

RESULTS AND DISCUSSION OF PB ISOTOPIC DATA

Pb Isotope Data

Pb isotope results from ore deposits of the central San Juan volcanic complex are listed in Table 6. The data are compared to previously published data (Doe et al., 1979, Lipman et al., 1978, Matty et al., 1987) on ores and volcanics of the central San Juan complex in the section that follows.

Table 5. Locations and descriptions of galena and feldspar samples from the North Amethyst vein, the main mining district at Creede mining district, and vicinity.

Sample No.[1]	Location	Description
Amethyst vein system:		
NKF-12-81	P&E 150 level	Bleached Bachelor wallrock with disseminated mineralization (galena, sphalerite, and silver sulfide).
PBB194-3-79	Last Chance, 5 level, where Pittsburgh drift intersects Amethyst	Underground dump sample, banded amethyst quartz and chalcedony containing galena, and sphalerite crystals and native silver. Galena taken from amethystine quartz band.
PMB-PU-740-75	Commodore 5 level, Daylight turn.	Amethystine quartz, sphalerite and galena of D-stage.
GS/682-62[2]	5 level	D-stage galena (Doe et al., 1979).
Bondholder district:		
GS6-76	Cascade	Galena from small base-metal veinlet.
GS4-76	Cascade	Galena from small base-metal veinlet.
66SD-3[2]	Cascade	Galena selected from a quartz-pyrite-galena-sphalerite vein (Doe et al., 1979).
Bulldog vein system:		
PBB139-19-74-1	9360 level, E-vein	Late galena grown on pale sphalerite and drusy quartz (IV-stage).
PBB139-19-74-2	9360 level, E-vein	Fine-grained sulfide (galena) of II-stage overgrown by quartz druse, pale sphalerite pueblo to lamellar galena and trace late gel pyrite and marcasite.
PBB139-19-74-2b	9360 level, E-vein	Fine-grained sulfide (galena) of II-stage overgrown by quartz druse, pale sphalerite cubic to lamellar galena and trace late gel pyrite and marcasite.
PBB139-19-74-3	9360 level, E-vein	Late galena grown on pale sphalerite and drusy quartz of IV-stage.

PBB180-19-78	9360 level, West Strand, 186 X-cut, N-vein	Fine-, to medium -grained sphalerite and galena crystals lining vugs and as crusts on fragments of wallrock breccia.
PMB-KB-543-71-1	9360 level, A-vein, A205 xcut	Late galena (IV-stage) on drusy quartz on top of quartz and fine-grained sulfide.
PMB-KB-543-71-3	9360 level, A-vein, A205 xcut	Late galena on drusy quartz on top of quartz and fine-grained sulfide containing galena.
PMB-KG-549-71	9360 level, at Spad A212	Coarse galena and sphalerite on drusy quartz coatingn fine-grained sulfides on honey-combed quartz.
66SD-1[2]	Puzzel vein	Coarse galena (Doe and other, 1979).

Equity area (North Amethyst vein system):

GSP-MM-10-86	10000 level, E-125	20-cm-wide seam of gold-bearing fine-grained sulfides of β-stage in fracture cutting vein of Mn-carbonate, and Mn-silicate and quartz.
GSP-MO-2-86	10000 level, E-126+ 50' N, in scram off vein structure	Coarse veins of honey-brown sphalerite, galena, chalcopyrite, pyrite, and quartz of stage-1 cutting meter-wide brecciated vein of Mn-carbonate and -silicate, and quartz.
NA-11-1698	Diamond drill hole NA-11, 1698 footage.	Coarse galena, sphalerite, quartz, chlorite, and later carbonate in vein cutting chloritized wallrock (probably stage-1).
NKF-G-7-87	10250 level, S2 ore body, E-83+45'S	Massive sample of Mn-carbonate and silicate with seam of fine-grained sulfides containing galena (β stage), sphalerite, pyrite, chalcopyrite, electrum, and other gold and silver minerals.
NKF-Q-17-87	10000 level	Meter-wide vein of Mn-carbonates and silicates containing disseminated galena (α-stage), sulfides, quartz and rhodocrosite.
NKF-R-18-87	10000 level, E-126+25'S	Banded hematite, magnetite, sulfides, quartz, and electrum (α stage). Cut by later fractures containing coarse-grained sulfides of stage 1.

NKF-X-24-87	10000 level, below 1S ore body, 30'N of borehole x-cut.	Coarse-grained sulfides, quartz and late carbonate on chlorite + pyrite alteration. (stage-1).
NKF-AA-24-87	10000 level, E-125	15 cm-wide seam of high-grade ore in vein of Mn-carbonates and silicates. Galena taken from gold-bearing zone (beta stage).
NKF-AE-31-87	10250 level, E-127 +155'N,	Stage-1 galena, sphalerite, and pyrite in quartz matrix.
NKF-AG-33-87	10400 level, north end of scram, 35'N of road to level.	Thin vein of coarse quartz + galena + sphalerite (all stage-1) in face.
NKF-AV-48-87	10500 level, E-58+ 40'S, mid-upper 2S ore body.	Fine-grained ore stringers in altered wall-rock (beta stage).
NKF-BK-63f-87	10250 level, No. 2 dogleg.	Disseminated sulfides in recrystallized Mn-carbonates and silicates.
NKF-BM-65-87	10250 level, S2 raise.	Rounded cobble of fine-grained sulfide (beta stage) in breccia.
NKF-S2R-71-87	10250 level, 20' S of S2 raise.	Seam of fine-grained sulfide at contact of volcanic wallrock with breccia (beta stage).
<u>OH vein:</u>		
PBB1-1-59	30' below Commodore 5 level, Sybil winze	Coarse-grained galena (up to 1 cm) and sphalerite (D-stage), pyrite-hematite-quartz gangue.
PBB-25-83-59	12 level, 15'S of NW R-3	Etched galena perched on sphalerite (D-stage.
PBB-44-159-59	Amy 5 level, 20'N of 17 raise	Puebloid shaped galena (3.5 cm) with chalcopyrite overgrowths, light sphalerite overgrows galena. (D-stage).
PBB83-59[2]	Northwest drift 15' S of Volunteer Raise	D-stage (Doe et al., 1979).
PBB0-57[2]	Near 8 raise, 5 level	D-stage galena (Doe et al., 1979).
PBB1-59[2]	Sybil Winze, 5 level	D-stage galena (Doe et al., 1979).

PMB-J	20'N of 10 raise 11 level	Rhombs of adularia separated from adularia + mixture of A stage.
<u>P vein:</u>		
PMB-EC-003-67	220 level, 170' N of Spad 1927	Large galena crystals of D-stage from breccia rubble, galena appears to sit on sphalerite and quartz.
PMB-JF-509-71	320 level, Slusher drift between P3S and P4S	Coarse, late sphalerite, and galena of D-stage, grown on green fluorite and euhedral quartz, with latest gel pyrite.
PMB-JF-509-71-2	320 level, Slusher drift between P3S and P4S	Earlier medium-grained galena and sphalerite of B-stage with hematite and quartz cement.
<u>Alpha-Corsair system:</u>		
PMB-WD-943-78	Cowboy-Johnson dump	Euhedral sphalerite, pyrite, galena (2-4 mm) and quartz coating wallrock fragment.
66SD-4[2]	Silver Horde tunnel Monon Hill mine	Replacement ore, Doe et al. (1979)
PHW-E-75[2]	Kreutzer-Sonata mine dump	Doe et al. (1979)
66SD-5[2]	Vein under Monon Hill mine	Doe et al. (1979)
<u>Solomon-Holy Moses</u>		
PBB159-59[2]	#2 Winze	Doe et al. (1979)
<u>Emma Mine, Spar City district:</u>		
66SD-1[2]	Dump sample	Doe et al. (1979)

1. First two or three characters denote sample collector: NKF, Nora K. Foley; PBB, Paul B. Barton, Jr.; PMB, Philip M. Bethke; GSP, Geoffrey S. Plumlee; PHW, Pamela Heald, SD, ; GS, Geological Survey.

2. Identifies samples analysed for and described in Doe et al. (1979)

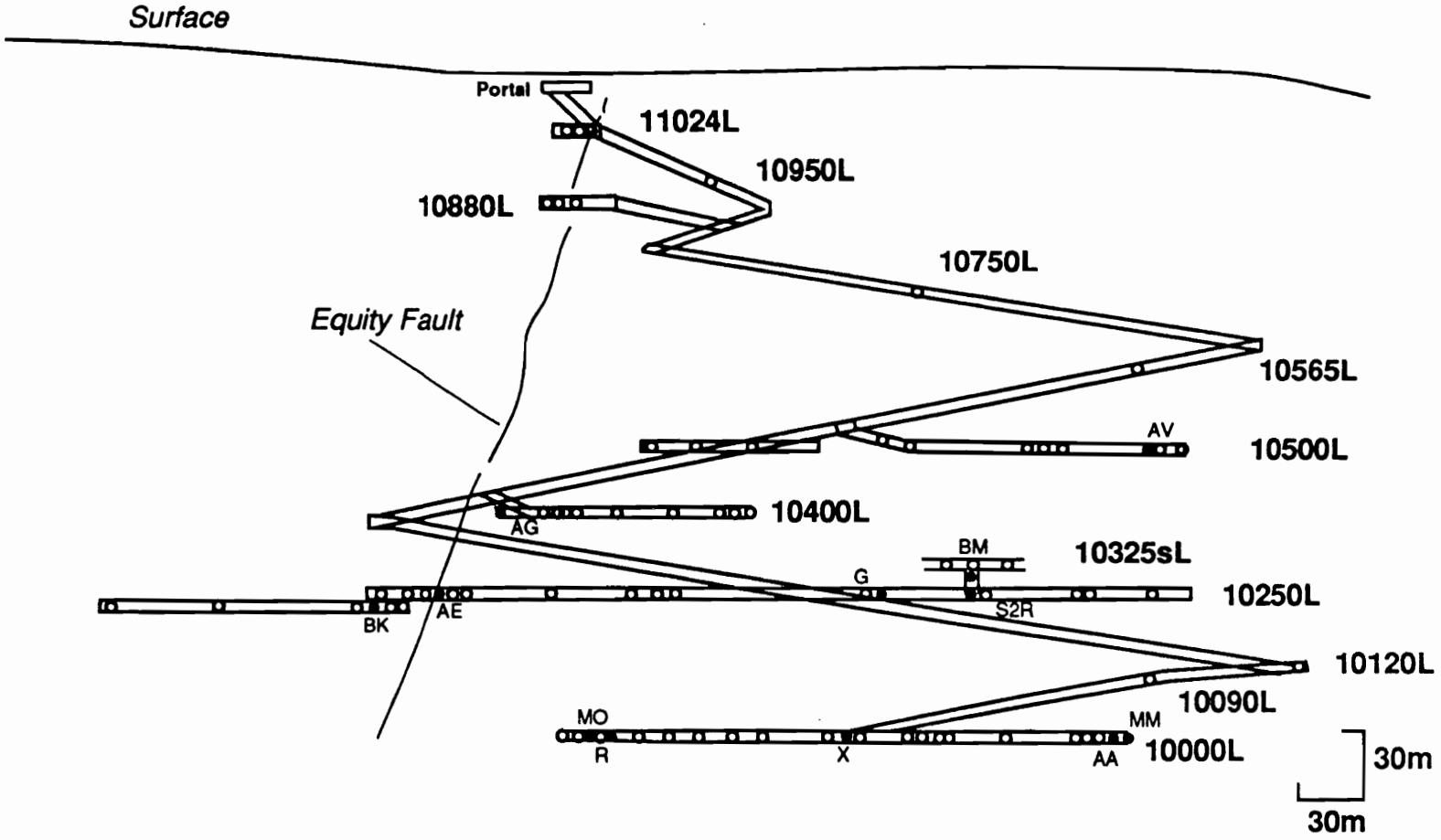

Figure 5. Cross-section view of mine workings, sample locations of galenas used in Pb isotope study are named. See Table 5 for sample descriptions.

The North Amethyst vein system

The Pb isotopic compositions of fourteen galenas from the North Amethyst vein mineralization are plotted in conventional Pb isotope diagrams in Figure 6. Galenas from North Amethyst ores can be divided into three distinct groups on the basis of their isotopic compositions.

North Amethyst galenas from Stage-1 of the base metal - silica association (Figure 6) have values of $^{206}Pb/^{204}Pb$ that are greater than 19.04 and define the most radiogenic field of Pb isotopic compositions. In this field, $^{206}Pb/^{204}Pb$ ranges from 19.041 to 19.115, $^{207}Pb/^{204}Pb$ from 15.627 to 15.672 and $^{208}Pb/^{204}Pb$ from 37.829 to 38.057 (Table 6).

Galenas from the North Amethyst mineralization with values of $^{206}Pb/^{204}Pb$ less than 18.9 belong to the early beta-stage (beta-1 and beta-2) associated with Au, Ag and base-metal mineralization (Figure 6). Of those samples, one was selected from a breccia containing the beta-1 precious metal assemblage and five were selected from the beta-2 assemblage. The less radiogenic group has $^{206}Pb/^{204}Pb$ from 18.826 to 18.881, $^{207}Pb/^{204}Pb$ from 15.588 to 15.602, and $^{208}Pb/^{204}Pb$ ranging from 37.790 to 37.926 (Table 6).

A small but analytically discrete compositional gap in $^{206}Pb/^{204}Pb$ from about 18.9 to 19.04 separates these two groups. Relative to $^{207}Pb/^{204}Pb$, one radiogenic group has values greater than about 15.62 and the less radiogenic group has values consistently less than 15.61.

Table 6. Lead isotopic analyses of galenas and feldspar from the North Amethyst vein, Creede mining district, and vicinity, Colorado.

Sample No.[1]	Mineral[3]	Stage[3]	$^{208}Pb/^{204}Pb$	$^{207}Pb/^{204}Pb$	$^{206}Pb/^{204}Pb$
NKF-12-81	G	D	37.905	15.631	19.104
PBB-194-3-79	G	D	37.815	15.613	19.113
PMB-PU-740-75	G	D	37.805	15.617	19.042
GS/682-62[2]	G		37.884	15.623	19.047
6-76	G		37.906	15.618	19.060
4-76	G		37.818	15.619	18.975
66SD-3[2]	G		37.906	15.641	19.092
PBB139-19-74-1	G	IV	37.780	15.591	18.997
PBB139-19-74-2b	G	II	37.872	15.622	18.971
PBB139-19-74-2	G	II	37.841	15.622	18.971
PBB139-19-74-3	G	IV	37.902	15.612	19.030
PBB-180-19-78	G	IV	37.843	15.642	19.068
PMB-KB-543-71-1	G	IV	37.916	15.636	19.048
PMB-KB-543-71-3	G	IV	37.826	15.610	19.029
PMB-KG-549-71	G	IV	37.882	15.625	19.044
66SD-1[2]	G	IV?	37.85	15.62	19.03
GSP-MM-10-86	G	β	37.843	15.602	18.892
GSP-MO-2-86	G	1	37.878	15.651	19.102
NA-11-1698	G	1	38.057	15.671	19.041
NKF-G-7-87	G	β	37.925	15.595	18.825
NKF-Q-17-87	G	α	37.709	15.584	19.047
NKF-R-18-87	G	1	38.051	15.668	19.115
NKF-X-24-87	G	1	37.828	15.626	19.040
NKF-AA-27-87	G	β	37.919	15.616	18.905
NKF-AE-31-87	G	1	37.959	15.651	19.046
NKF-AG-33-87	G	1	37.985	15.650	19.080
NKF-AV-48-87	G	β	37.918	15.616	18.880
NKF-BK-63-87	G	α	37.698	15.572	18.955
NKF-BM-65-87	G	β	37.790	15.587	18.880
NKF-S2R-71-87	G	β	37.913	15.615	18.904
PBB-25-83-59	G	D	37.861	15.623	19.038
PBB-44-159-59	G	D	37.813	15.605	19.035
PBB83-59[2]	G	D	37.68	15.56	19.01
PBB0-51[2]	G	D	37.888	15.638	19.038
PBB1-59[2]	G	D	37.94	15.64	19.05
PMB-J	Ad	A	38.001	15.664	18.987

PMB-EC-003-67	G	D	37.994	15.659	18.965
PMB-JF-509-71	G	D	37.952	15.652	19.059
PMB-JF-509-71-2	G	B	37.927	15.647	19.069
PMB-WD-943-78	G		38.019	15.635	18.868
66SD-4 2	G		37.942	15.617	18.847
PHW-E-75[2]	G		37.967	15.612	18.816
66SD-5[2]	G		37.96	15.63	18.86
PBB159-59[2]	G		37.77	15.59	19.03
66SD-1[2]	G		38.018	15.626	18.802
NKF-1[4]	K		37.971	15.607	18.688
NKF-2[4]	K		37.959	15.594	18.693

1. Samples are listed in same order as in Table 5.
2. Published analysis of galena from the Creede district by Doe at al. (1979).
3. G, galena; Ad, adularia; K, K-feldspar; see Table 2 for key to stage designations, omitted if unknown.

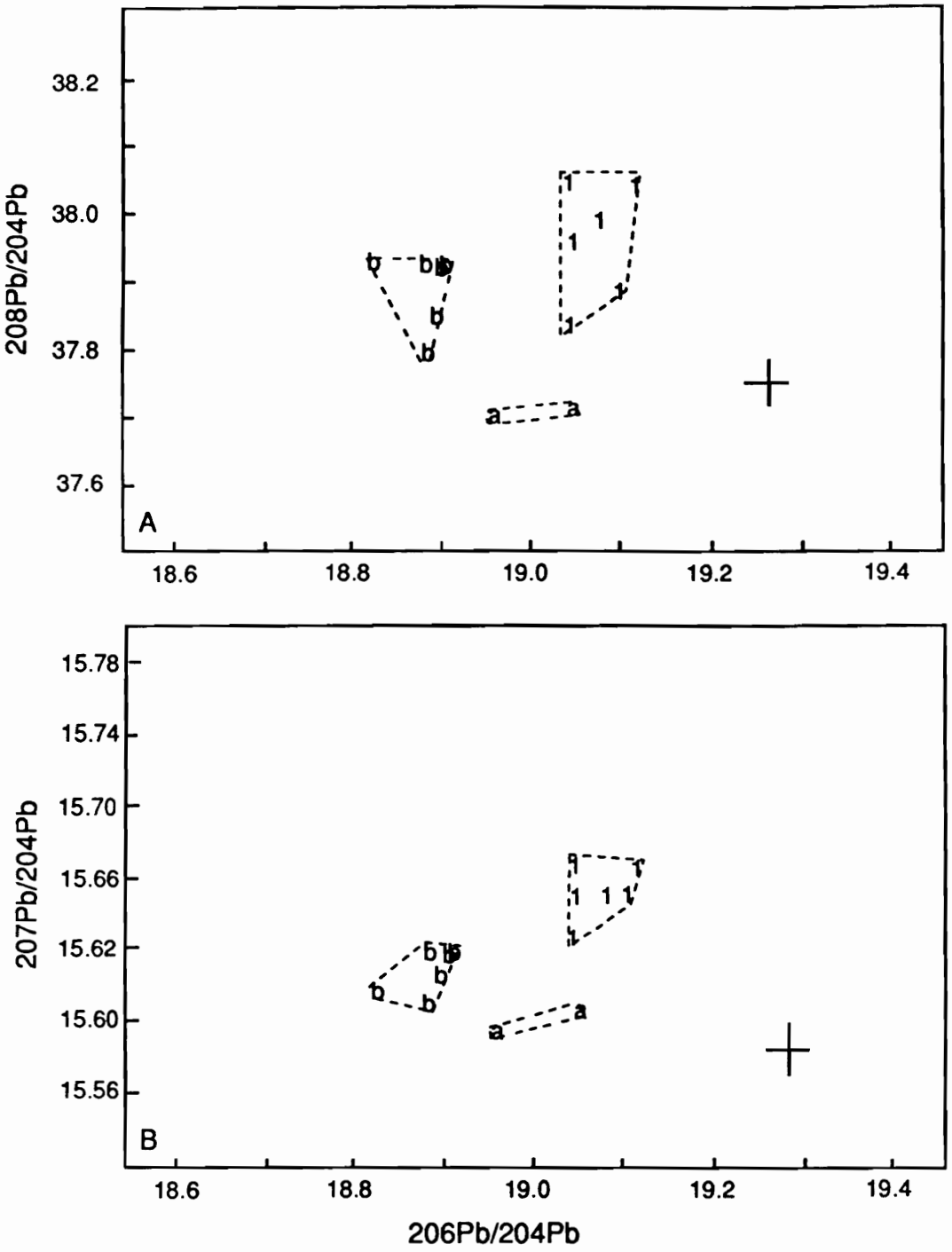

Figure 6. 208Pb/204Pb vs. 206Pb/204Pb (A) and 207Pb/204Pb vs. 206Pb/204Pb (B) diagrams showing galenas compositions for the North Amethyst vein system: a, alpha stage; b, beta stage; 1, stage 1 (see text for descriptions of each). All samples, this study.

Two additional galenas were selected from small sulfide clots, predominantly composed of sphalerite, galena, and pyrite, in a metasomatic reaction zone consisting of Mn-carbonate, Mn-silicate, quartz and minor potassium feldspar (alpha-stage). These samples (NKF-Q-17 and NKF-BK-63) have lower values of $^{207}Pb/^{204}Pb$ than other samples from the North Amethyst vein deposits.

Alpha - Corsair vein system

Pb isotopic compositions of four galenas from the Monon Hill mine and the Cowboy Johnson and Kreutzer-Sonota mine dumps of the Alpha-Corsair fault system (PMB-WD, this study, and Doe et al., 1979) located at the southern end of the Alpha-Corsair fault (Figure 7) range from 18.816 to 18.868 in $^{206}Pb/^{204}Pb$, from 15.612 to 15.635 in $^{207}Pb/^{204}Pb$, and from 37.942 to 38.019 in $^{208}Pb/^{204}Pb$ (Table 6, Figure 7). The four samples form a tight cluster and are indistinguishable within the analytical error of the technique. The Alpha - Corsair galenas occur with honey-colored sphalerite, pyrite and quartz as coatings on wallrock fragments. They are less radiogenic in $^{206}Pb/^{204}Pb$ than galenas from the stage-1 association of the North Amethyst vein paragenesis (Figure 7). The $^{206}Pb/^{204}Pb$, $^{207}Pb/^{204}Pb$, and $^{208}Pb/^{204}Pb$ values in the Alpha-Corsair are similar to the beta-stage group from the North Amethyst mineralization.

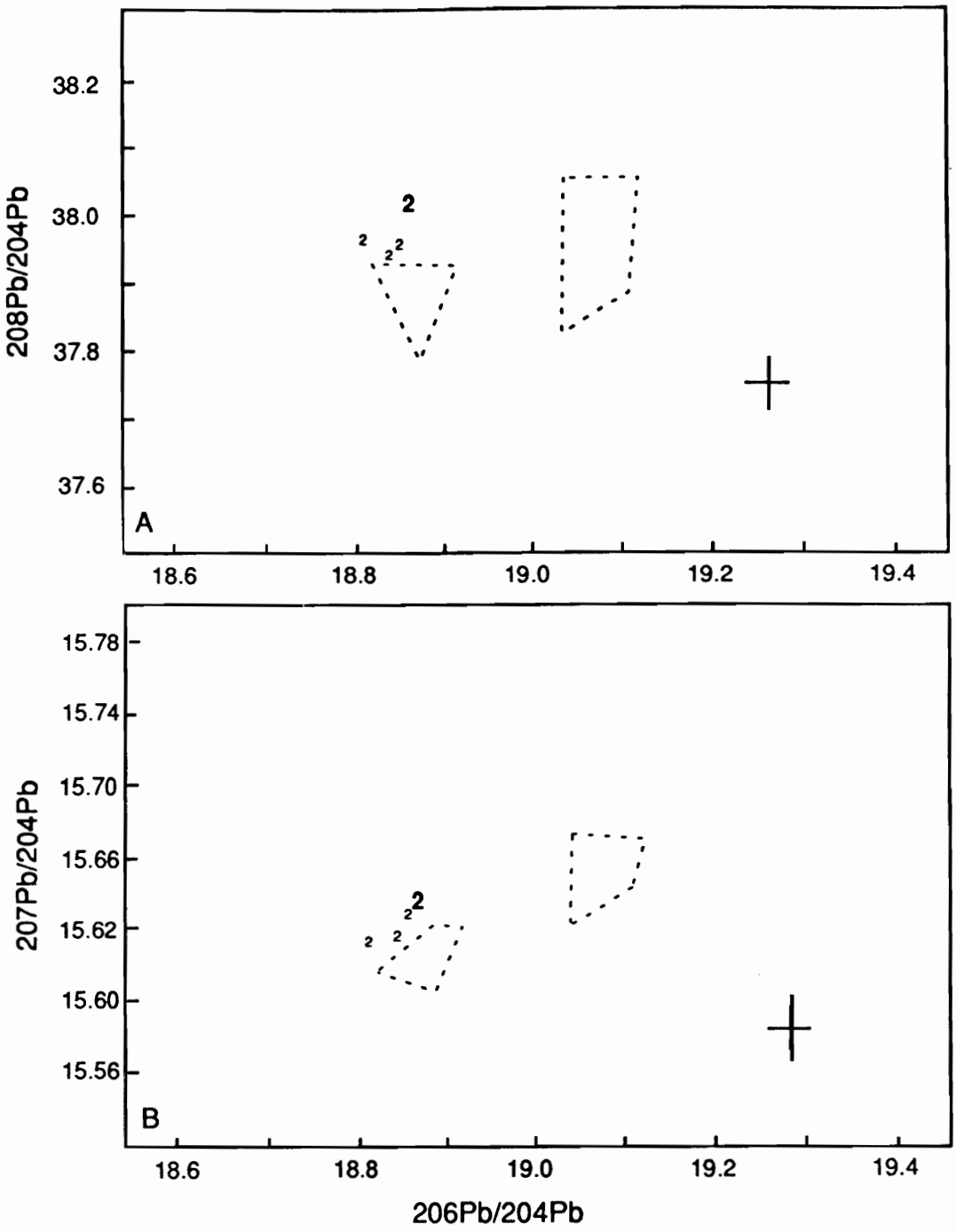

Figure 7. 208Pb/204Pb vs. 206Pb/204Pb (A) and 207Pb/204Pb vs. 206Pb/204Pb (B) diagrams showing galena compositions for the Alpha - Corsair vein system (2) ; North Amethyst stage 1 and beta stage are shown on this and subsequent diagrams for comparison. Bold type, this study; small regular type, Doe et al., (1979).

Amethyst vein system

Galenas from two samples from the southern end of the Amethyst vein system are predominantly of banded amethystine quartz that contains sphalerite and native Ag (PBB194-3-79, PMB-PU-740-74); a third sample of bleached wallrock contains disseminated sphalerite, galena and argentite (NKF-12-81). The galenas range in $^{206}Pb/^{204}Pb$ from 19.042 to 19.114, in $^{207}Pb/^{204}Pb$ from 15.613 to 15.631, and in $^{208}Pb/^{204}Pb$ from 37.806 to 37.905 (Table 6, Figure 8). Samples analysed for this study and by Doe et al. (1979) are virtually identical (Figure 8). Galenas from the southern end of the Amethyst vein system have values of $^{206}Pb/^{204}Pb$ indistinguishable from galenas from the Stage-1 ore of the North Amethyst vein system, and overlapping values of $^{207}Pb/^{204}Pb$ and $^{208}Pb/^{204}Pb$.

Bulldog vein system

Nine galenas were analysed from the Bulldog vein system (Figure 9). Two galenas were selected from II-stage and seven from IV-stage assemblages that are described in detail by Plumblee and Heald (1989). IV-stage galena occurs as late crystals intergrown with pale sphalerite and drusy quartz. II-stage galena occurs in a fine grained mix of sphalerite and chalcopyrite overgrown by the IV-stage assemblage. Pb isotopic compositions of Bulldog galena range from 18.972 to 19.068 for $^{206}Pb/^{204}Pb$, from 15.591 to 15.642 for $^{207}Pb/^{204}Pb$, and from 37.781 to 37.916 for $^{208}Pb/^{204}Pb$ (Table 6, Figure 9). The two galenas from II-stage have slightly lower values of $^{206}Pb/^{204}Pb$ for a given value of $^{207}Pb/^{204}Pb$ or $^{208}Pb/^{204}Pb$. Galenas from the Bulldog vein system are slightly less radiogenic than galenas from Stage-1 ores of the Northern

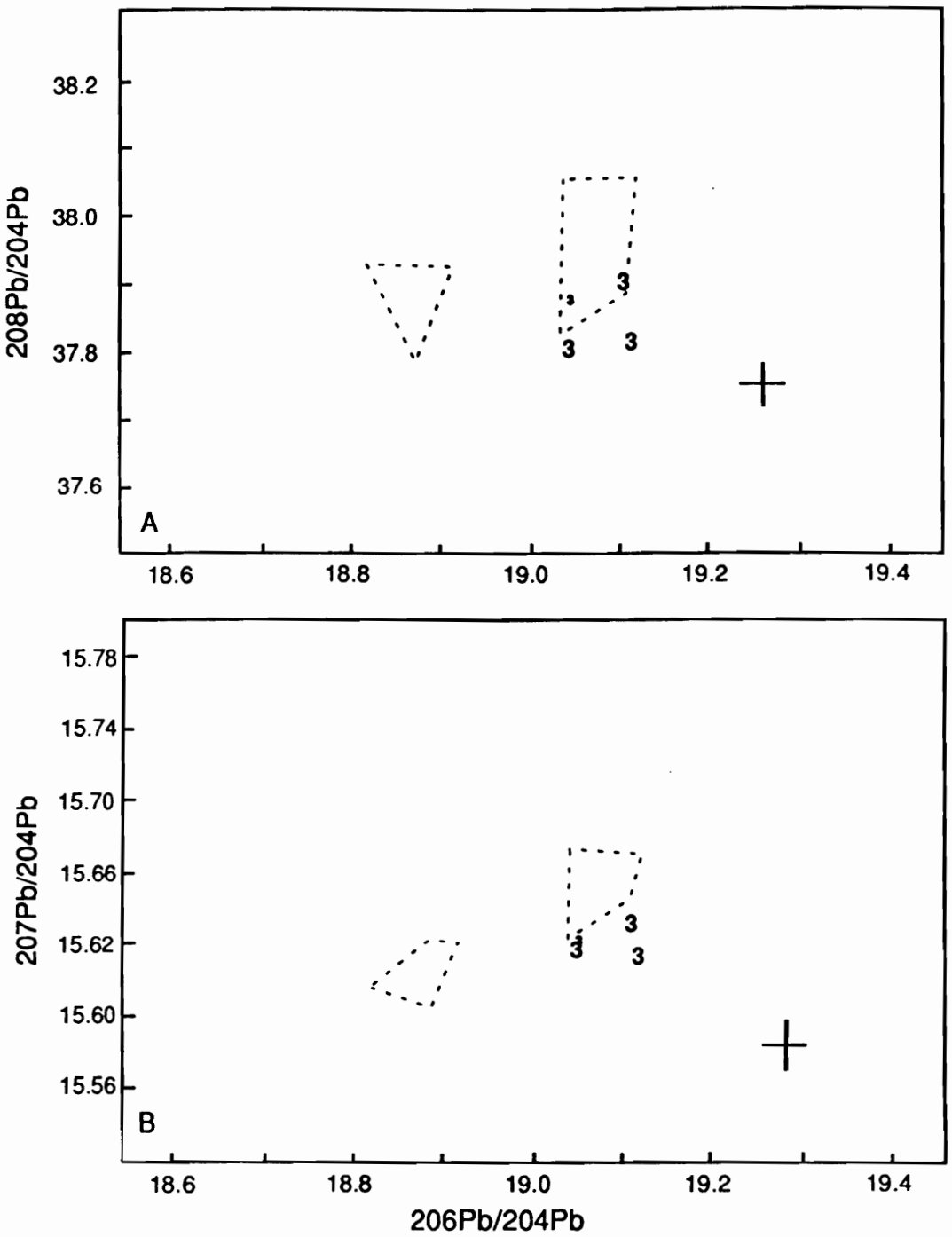

Figure 8. 208Pb/204Pb vs, 206Pb/204Pb (A) and 207Pb/204Pb vs. 206Pb/204Pb (B) diagrams showing galena data (3) for the southern Amethyst vein. North Amethyst stage 1 and beta stages shown for reference. Bold type, this study; small, regular type, Doe et al. (1979).

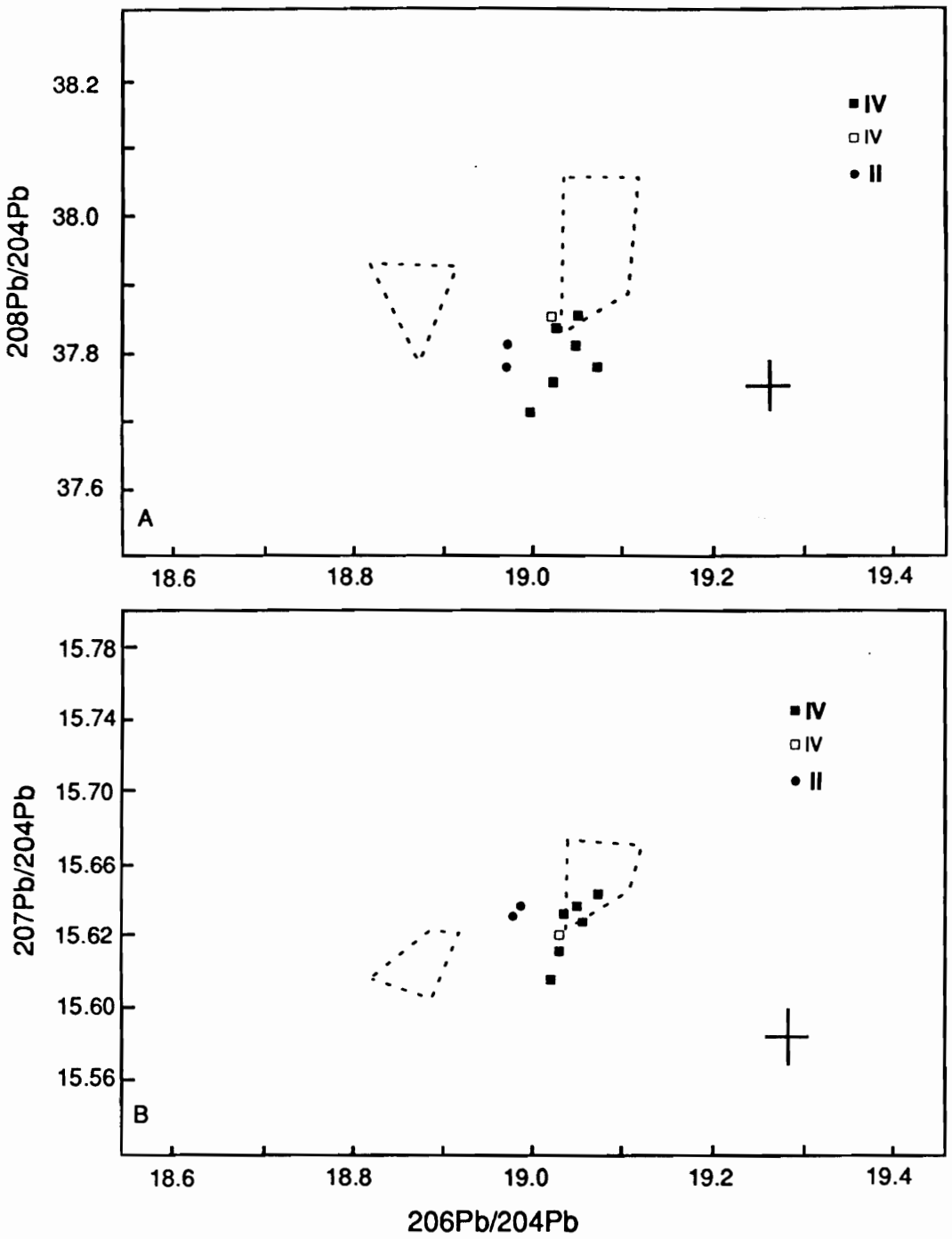

Figure 9. 208Pb/204Pb vs. 206Pb/204Pb (A) and 207Pb/204Pb vs. 206Pb/204Pb (B) diagrams showing galena data for the Bulldog vein system. North Amethyst stage 2 and beta stages shown for reference. Bold type, this study; small regular type , Doe et al. (1979).

Amethyst vein mineralization. The analyses partly bridge the gap between early Au-rich and late Au-poor associations of the North Amethyst vein (especially II-stage galenas), however, the Bulldog vein is Ag-rich and Au-poor (Plumlee, 1989).

OH and P veins

The OH and P veins (Figure 10) occur as cross faults that cut diagonally between the Bulldog and Amethyst veins, although they are not known to intersect either structure. Two galenas and one adularia were analysed from the OH vein to supplement the three galena samples of Doe et al. (1979). All sulfide samples analysed consisted of coarse grained D-stage galena intergrown with sphalerite. Four galenas have almost identical Pb isotopic compositions: 19.01 to 19.039 for $^{206}Pb/^{204}Pb$, 15.605 to 15.64 for $^{207}Pb/^{204}Pb$, and 37.813 to 37.94 for $^{208}Pb/^{204}Pb$ (Table 6, Figure 10). A fifth galena (PBB83-59) was analysed by Doe using the less precise PbS-NH_4NO_3 surface emission technique and is similar to the others considering the larger errors of that technique.

Three galena samples were analysed from the P vein (Table 6, Figure 10). One sample of coarse galena (D-stage) resting on sphalerite and quartz yielded ratios very similar to those of adularia from the OH vein. The other two samples were of early, medium-grained galena and sphalerite (B-stage), and late, coarse sphalerite and galena overgrowing fluorite and euhedral quartz (D-stage). The Pb isotopic composition of these samples is identical to those of the D-stage OH vein galenas.

OH and P vein galenas are thus for the most partanalytically indistinguishable from the later North Amethyst stage of base-metal mineralization (Figure 10). There is apparently no isotopic difference

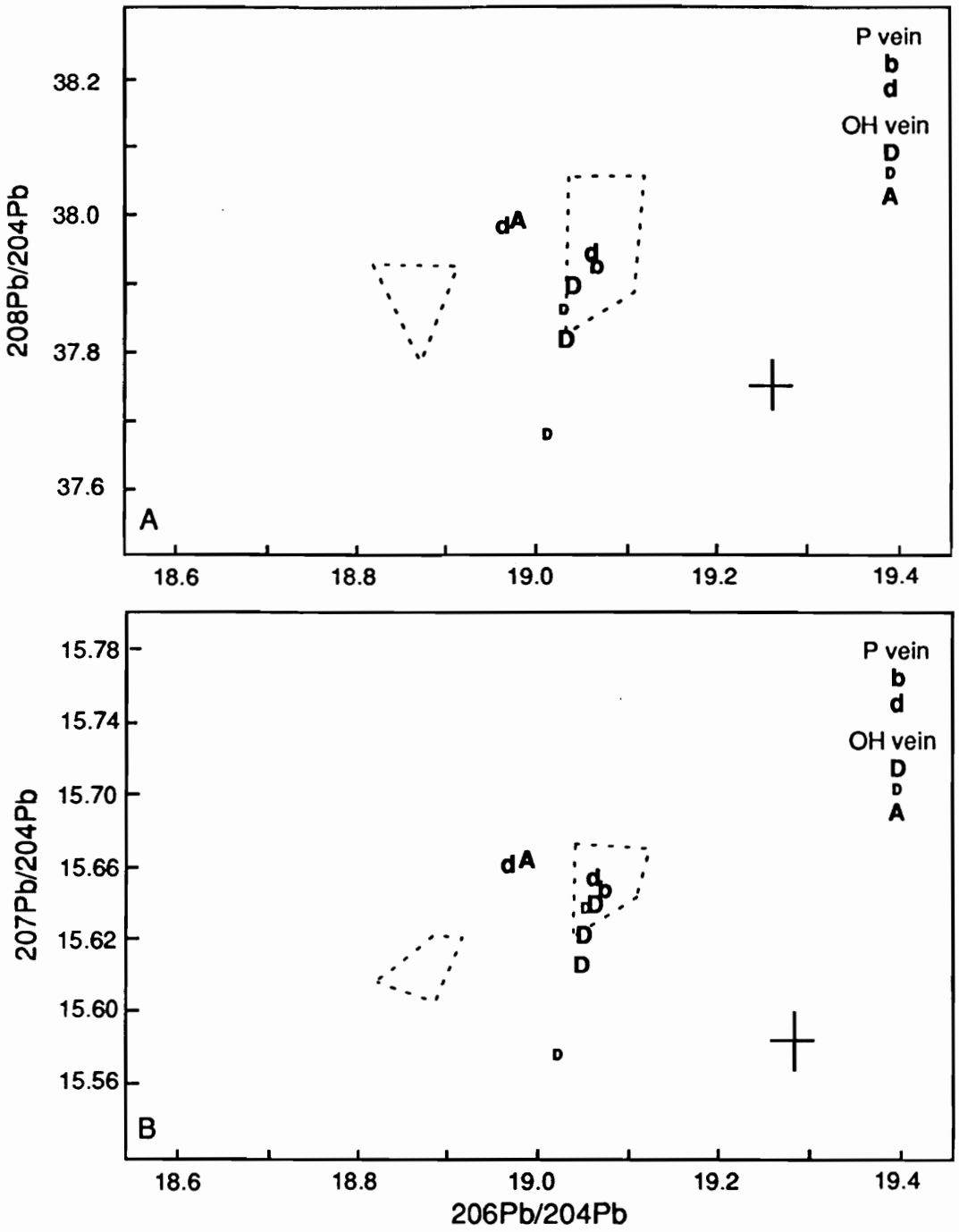

Figure 10. 208Pb/204Pb vs. 206Pb/204Pb (A) and 207Pb/204Pb vs. 206Pb/204Pb (B) diagrams for galena data for the OH (Bold type, this study; small type, Doe et al., 1979) and P vein (lower case type). North Amethyst stage 1 and beta stage fields shown for reference. A, A-stage; D, D-stage mineralization (Barton et al., 1977).

between B-stage and D-stage mineralization of the P-vein. Adularia from a mineralized OH vein sample is slightly less radiogenic in $^{206}Pb/^{204}Pb$ than galena from the base-metal association (Stage-1) of the North Amethyst mineralization (Figure 10). The adularia data point is plotted as measured, uncorrected for U/Pb decay in the ~25 m.y. since formation.

Cascade mine, Bondholder district

Three galena samples were analysed from the Cascade mine of the Bondholder district (Figure 11). Two samples (66SD-3, Doe et al., 1979; 6-76, this study) have virtually indistinguishable Pb isotopic compositions that fall within the more radiogenic field of North Amethyst galena compositions; a third sample is slightly less radiogenic.

Other veins in the area

A galena selected from the Holy Moses mine of the Solomon - Holy Moses vein (Figure 11) and analysed by Doe et al. (1979) yielded a value of $^{206}Pb/^{204}Pb$ of 19.03, of $^{207}Pb/^{204}Pb$ of 15.59, and of $^{208}Pb/^{204}Pb$ of 37.77. The values are identical within analytical error to galenas of Stage-1 mineralization and of the main mining district.

Doe et al. (1979) also analysed a galena from the Emma mine dump of the Spar City district along the southern margin of the Creede caldera. The analysis yielded a value of 18.802 for $^{206}Pb/^{204}Pb$, of 15.626 for $^{207}Pb/^{204}Pb$, and of 38.018 for $^{208}Pb/^{204}Pb$ (Figure 11). Although similar in $^{207}Pb/^{204}Pb$ and $^{206}Pb/^{204}Pb$ to gold-rich samples of the North Amethyst system, the galena from the Emma mine has a relatively high value of $^{208}Pb/^{204}Pb$ compared to all other galenas.

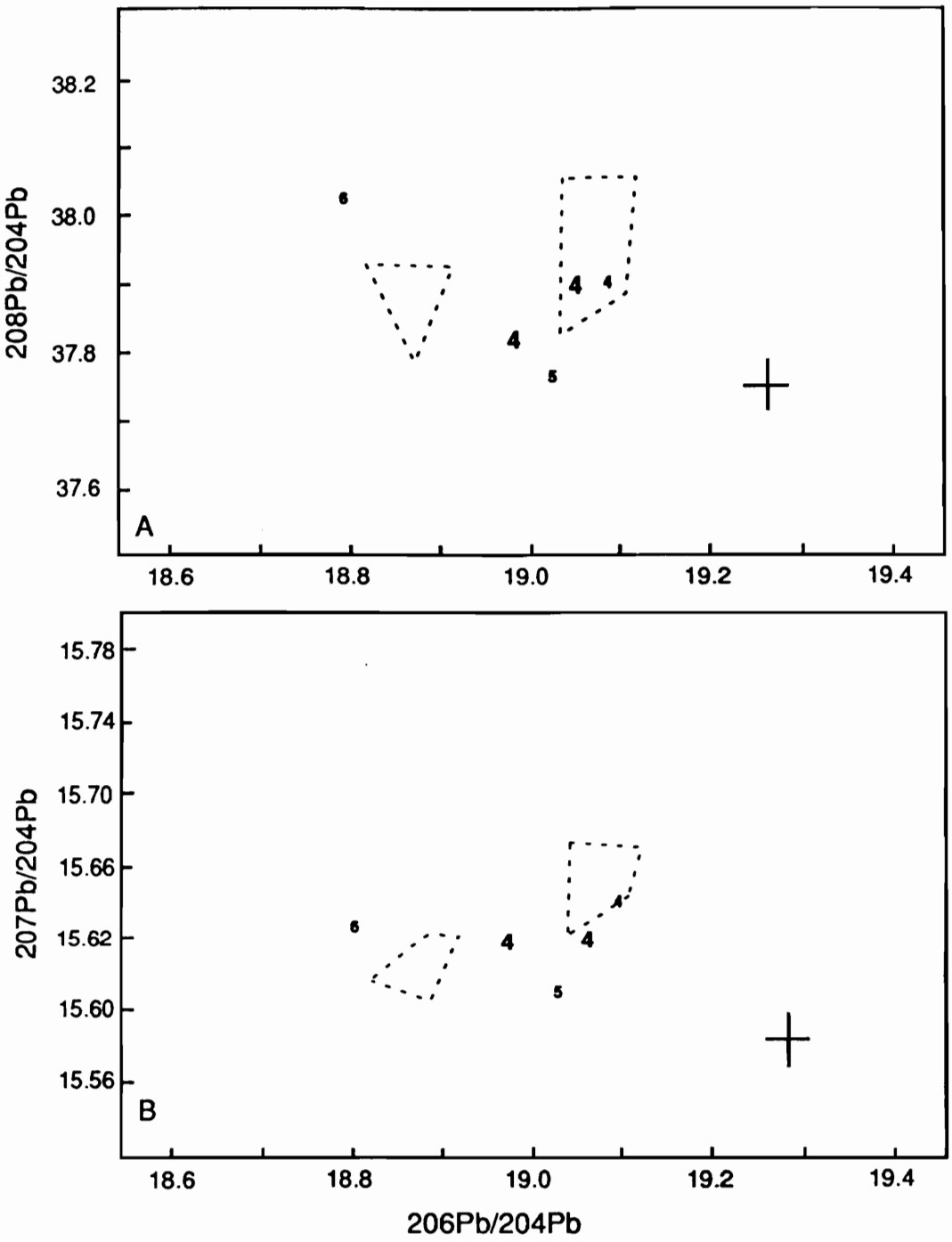

Figure 11. 208Pb/204Pb vs. 206Pb/204Pb (A) and 207Pb/204Pb vs. 206Pb/204Pb (B) diagrams showing galena data for the Cascade mine, Bondholder district (4), the Solomon -Holy Mose mine, Creede district (5), and the Emma mine, Spar City district (6). Bold face type, this study; small regular type, Doe et al. (1979).

Isotopic composition of volcanic hostrocks

The Nelson Mountain Tuff and the Carpenter Ridge Tuff, hosts to ore in the Creede district, are distinctly less radiogenic than most galenas of the North Amethyst area or the southern and central Creede district. Figure 12 shows Pb isotopic compositions of feldspars derived from volcanics of the central San Juan field. The field and datapoints are uncorrected for decay of U since formation. Although U/Pb ratios were not measured for the feldspars analysed in this study, D. Matty (written commun., 1987) has shown that U/Pb values of central San Juan volcanics are so small that the correction would not change the positions of the points significantly given the half-life of $^{238}U/^{235}U$. Thus, the data from K-feldspars can be treated as initial Pb ratios.

The least radiogenic group of galenas, from the beta-stage Au ore, has higher values of $^{206}Pb/^{204}Pb$ than either the Nelson Mountain Tuff or the Carpenter Ridge Tuff, and values of $^{207}Pb/^{204}Pb$ and $^{208}Pb/^{204}Pb$ that overlap those of the Carpenter Ridge Tuff. Galenas from Stage-1 of the North Amethyst mineralization, the main mining district at Creede, and from the Bondholder district have even higher values of $^{206}Pb/^{204}Pb$ relative to the Carpenter Ridge Tuff, and they have overlapping and higher values of $^{207}Pb/^{204}Pb$ and overlapping values of $^{208}Pb/^{204}Pb$.

The Carpenter Ridge Tuff is one of the most radiogenic volcanic units in the central San Juan Mountains. Lipman et al. (1978) suggested that the Carpenter Ridge Tuff acquired its radiogenic nature by contamination with old Precambrian basement and Whitney et al., (1988) and Whitney and Stormer, (1988) suggested that the Carpenter Ridge Tuff can be related to primary magma of the older Fish Canyon Tuff (Table 1)

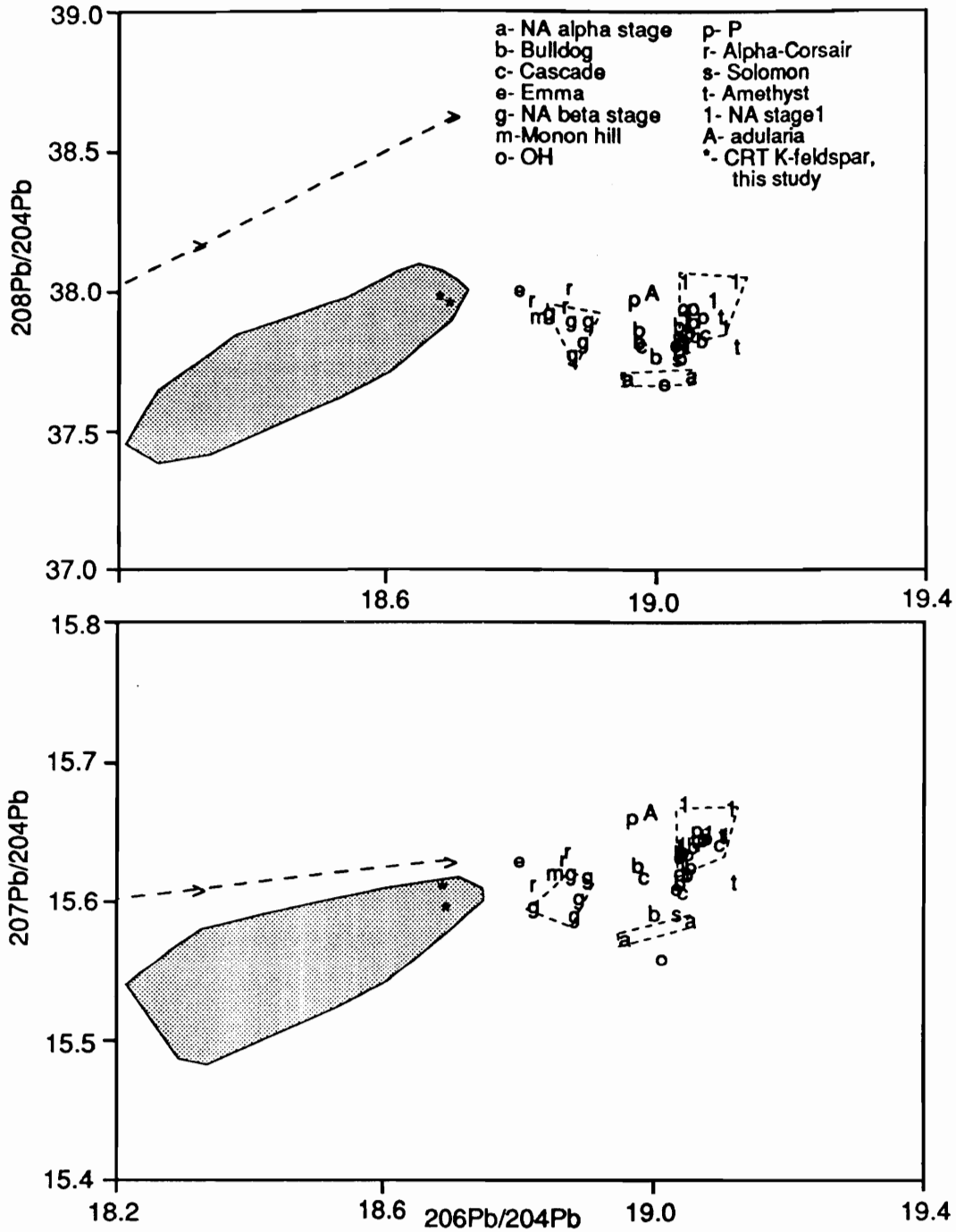

Figure 12. 208Pb/204Pb vs. 206Pb/204Pb (A) and 207Pb/204Pb vs. 206Pb/204Pb (B) diagrams showing galena data relative to field of volcanics of central San Juan region as defined by Lipman et al. (1978); Doe et al. (1979); D. Matty (written commun., 1987). Feldspars are uncorrected. Compare with Figure 4. See table 4 for descriptions of mines and districts. Orogene curve of Stacey and Kramers (1975) for comparison.

of the La Garita caldera. Intracaldera Carpenter Ridge Tuff is potassium-metasomatized in the vicinity of the main mining district (Steven and Ratte, 1965). The radiogenic nature of the Carpenter Ridge Tuff is not the result of the pre-ore metasomatism because unmetasomatized samples of the tuff (outflow units) are also radiogenic.

The Nelson Mountain Tuff is slightly less radiogenic than both the Fish Canyon Tuff and the Carpenter Ridge Tuff (Lipman et al., 1878; Matty et al., 1987). The Nelson Mountain Tuff is potassium-metasomatized at depth in the underground workings of the North Amethyst area (Sawyer et al., 1989; Foley, unpub. data), however, surface exposures of the Nelson Mountain Tuff are probably not potassium-metasomatized (Sawyer et al., 1989). No K-metasomatized wallrock samples were analysed to ascertain the effect of the metasomatism on the lead isotopic composition of the feldspar because the samples are associated with mineralization and probably contain galena.

Discussion

Pb isotopic analyses of galenas from the North Amethyst mineralization form three general groups on conventional Pb-Pb diagrams (a, g, 1, Figure 12). Two of the groups separate the relatively unradiogenic North Amethyst galenas formed early during the period of Au mineralization (beta-stage; g, Figure 12), from more radiogenic galenas produced during a subsequent event that overprinted the Au mineralization (Stage-1; 1, Figure 12). Silver- and base-metal mineralization related to the later event has been correlated regionally (Foley and Vardiman, 1988; Foley, 1990), and is referred to as the base-metal association in the discussion that follows. Mineralogical stages

related to the earlier Au-rich mineralization are referred to as the Mn-Au association (Table 3). The third group of galenas has $^{206}Pb/^{204}Pb$ values that are similar to the more radiogenic North Amethyst galenas, but lower values of $^{207}Pb/^{204}Pb$ and $^{208}Pb/^{204}Pb$ (a, Figure 12).

Galenas from the beta-stage that are associated with Au-mineralization in the North Amethyst area are among the least radiogenic ore samples analysed from the central San Juan Mountains. They are isotopically similar to galenas from the mines along the Alpha-Corsair vein system to the west of the main mining district at Creede (m, r, Figure 12), but are less radiogenic than galenas from most galeas obtained from the vein systems comprising the central and southern Creede district (b, o, p, A). In contrast, the most radiogenic galena group (Stage-1; 1, Figure 12) from North Amethyst shows considerable overlap in $^{206}Pb/^{204}Pb$ with galenas from the main mining district at Creede (b, p, o, Figure 12), as well as with galenas from the Solomon-Holy Moses vein system (s, Figure 12) and from the Bondholder district (c, Figure 12).

Pb isotopic compositions of galenas from the central San Juan region may reflect local isotopic control depending on individual vein systems and on the paragenetic stage containing the galena. Galenas collected along the different faults are projected onto an west-east traverse in Figure 13 for comparison. The lowest $^{206}Pb/^{204}Pb$ values are generally found in the west, within the Alpha-Corsair fault system, but also in the earliest stages of the North Amethyst vein. Galenas from the Bulldog vein system and the OH and P cross faults are similar, and are more radiogenic than Alpha-Corsair galenas. North Amethyst (Stage-

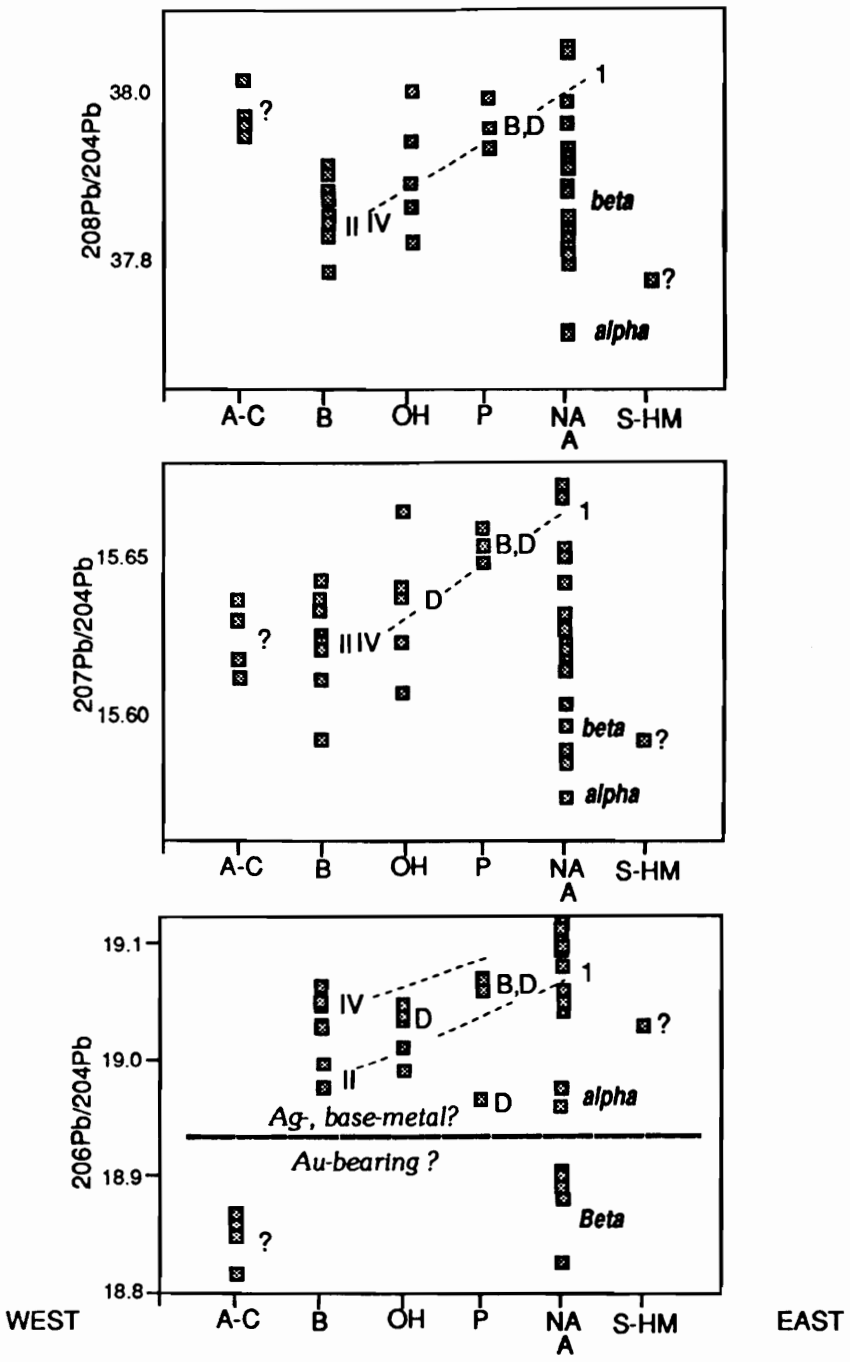

Figure 13. Bar diagram comparing lead isotopic ratios in a west to east traverse across the main part of the Creede district (see text for discussion). Veins are as follows: A-C, Alpha-corsair; B, Bulldog; OH, OH vein; P, P vein; A, Amethyst; NA, northern Amethyst; S-SH, Solomon - Holy Moses. See Table 3 for stage designations. Short dashed lines connect equivalent paragenetic stages.

1) and Amethyst galenas have slightly higher $^{206}Pb/^{204}Pb$ values relative to the Bulldog, OH and P vein galenas. Galena from the eastern-most Solomon-Holy Moses vein is isotopically similar to the North Amethyst and Amethyst galenas. The general trend toward more radiogenic compositions in the North Amethyst area is not straightforward because paragenetically earlier galenas tend to less radiogenic values (Figure 13).

These small but consistent isotopic variations may have developed as a result of differences in the composition of the fluids affected by hydrothermal cells that developed along each fault structure. Minor variations in the Pb isotopic composition of the fluid in each hydrothermal cell was probably controlled locally by the amount and isotopic composition of pre-existing mineralization, extent of dissolution and reprecipitation of the minerals, and especially by the variations in Pb isotopic composition of the host volcanics and volcaniclastic sediments. Variations in isotopic composition of the volcanics, as noted earlier, have been related to lateral compositional variations in the source region of the magmas (Lipman et al., 1978). Detailed paragentic studies (Barton et al., 1977; Plumlee, 1989; Foley, 1990a) demonstrated that base-metal mineralization of the B-, II-, and 1-stages in the OH, P, Bulldog and North Amethyst veins is the most widely distributed and persistent mineralogical stage, occurring in all veins. Later stages of mineralization are more local and were interrupted by periods of dissolution.

Paragenetically early galenas from the P and Bulldog veins have similar or slightly less radiogenic values than galenas formed later in

the same veins. For the Bulldog vein system (Figure 9), the difference between the early II-stage and later IV-stage galenas is only about 0.36% in $^{206}Pb/^{204}Pb$; they overlap in $^{207}Pb/^{204}Pb$ and $^{208}Pb/^{204}Pb$. The isotopic similarity is consistent with petrologic studies which have found no major breaks in the paragenetic sequence (Plumlee, 1989). B- and D-stage galenas from the P-vein have similar values (Figure 10), and, likewise, there are no major breaks in the paragenetic sequence (Barton et al., 1977). Thus, the isotopic variation in galenas associated with the base-metal association in the central and southern Creede district is consistent generally with a fluid with isotopically homogeneous Pb.

Galenas from the North Amethyst vein show the widest range in lead isotopic compositions for all paragenetic stages (Figure 13). The North Amethyst vein has the most complete record of the changing lead isotopic composition of the hydrothermal fluids. This may be, in part, because the North Amethyst vein retains the most complete record of mineralogical stages deposited anywhere in the central San Juan area. In some of the other veins, only certain mineralogical stages are well-developed, and many stages are absent or unrecognized.

The isotopic uniqueness of paragnetically early (beta-stage) relative to later (stage-1) galenas is best exemplified in the North Amethyst area. $^{206}Pb/^{204}Pb$ values in beta-stage galena relative to Stage-1 galena differ by about 1.2%; $^{207}Pb/^{204}Pb$ values differ by about 0.45%. This difference, coupled with the fact that the two associations of the North Amethyst area are paragenetically distinct, showing crosscutting relationships and separation by a period of extensive

brecciation and hydrothermal sedimentation, suggests a more complex origin for the isotopic variations in the North Amethyst area than in the central and southern Creede district to the south. In this case, the isotopic distinctions are not easily explained by a regular and progressive change in the fluid composition.

Pb Isotopic Evolution of the System

An isotopic model to explain the differences in Pb isotopic composition between the Au-rich (Mn-Au association) and the base-metal-rich (base metal association) ores must also explain the following:

1) The regional similarities in Pb isotopic composition among main Creede district galenas, galenas of stage-1 mineralization of the North Amethyst vein system, and galenas of the Bondholder district. These ore zones are separated by a distance of over 11 kilometers along strike and suggest a large-scale reservoir for lead.

2) The temporal differences in Pb isotopic composition between the earlier manganese (alpha) stage and Au (beta) stage ores, and the later stage-1 ores of the North Amethyst vein system.

3) The similarity in the $^{206}Pb/^{204}Pb$ values between the Au (beta) stage of the North Amethyst vein system and the Alpha-Corsair ores.

The similarity in Pb isotopic composition among later ores (Stage-1) of the North Amethyst area, all ores of the main vein systems at Creede, and galenas from the Bondholder district, strongly suggests a large-scale Pb isotopic reservoir so that the ore-forming fluids developed in a convecting system of regional dimensions or in a series of relatively open interconnected cells that tapped the same Pb source. This suggests that the ores of the later base metal association at North

Amethyst probably formed as part of the large mineralizing system described by Bethke (1988) for the main Creede district. The fluid was characterized by a relatively homogeneous Pb source. Mixing within the hydrothermal cell also contributed to the relative homogeneity of the Pb. Dissolution and reprecipitation of galena, documented in paragenetic studies of the central and southern parts of the district (Barton et al., 1977; Plumlee, 1989; P. Barton and P. Bethke, pers. commun., 1990) also may have contributed to the relative homogeneity of the galenas. The isotopic composition of the galenas from the base metal association (Stage 1) is consistent with derivation, as suggested by Doe et al. (1979) for galenas from the main mining district, from the interaction of a large convecting hydrothermal cell with Precambrian basement rocks or their sedimentary equivalents.

Mineralogical and paragenetic data (Foley, 1990a) suggest that beta-stage ores of the North Amethyst area are more areally restricted than are ores of the base metal association which are found throughout the district. The restricted occurrence of the beta-stage Au ore suggests that this stage formed in a smaller, more local hydrothermal cell than Stage-1 ores and that the heat-source for this hydrothermal cell may be the relatively shallow, ring-fault intrusion beneath the hill northeast of the Equity fault.

Fluid inclusion data on beta-stage sphalerites (~270-300^{o}C) and compositional data on rhombohedral carbonates of alpha-stage (>350^{o}C) indicate temperatures for the early North Amethyst ores that are well in excess of 250^{o}C, the temperature proposed for ores of southern and central base metal mineralization (Foley, 1990b). Textural evidence

indicating that Mn-Au association fluids reacted with wallrock feldspars in the North Amethyst vein (Foley, 1990a) also suggests hotter temperatures for those fluids than for the later base-metal-silica fluids because, in the southern part of the district, ore fluids did not interact to any appreciable degree with wallrock (Barton et al., 1977; Plumlee, 1989). If the hydrothermal cell of the Mn-Au association was hotter than that of the base metal association, the Au-rich system may have interacted to a greater degree with a less radiogenic Pb reservoir as represented by volcanic wallrock feldspar than did the later base-metal-rich system. The Pb isotopic composition of the resulting fluid would be much less radiogenic than a fluid that derived a Pb composition solely from Precambrian basement sources.

With evolution of the mineralizing system, Au-rich hydrothermal cells located on the ring fault of the San Luis caldera may have started to cool and equilibrate thermally with the regional hydrologic system, gradually becoming part of the district-wide hydrothermal system proposed by Bethke (1988). The extensive hydrothermal system may have been composed of a series of interconnected cells rather than the single, 7 kilometer long system described by Bethke (1988). A series of cells accounts more readily for the isotopic variations between veins and mineralogical stages. This hydrothermal system probably leached Pb extensively from the Tertiary - Proterozoic Pb reservior at depth as suggested by Doe et al. (1979). The changes in Pb isotopic compositions with successive mineralized stages and for each structure might reflect a gradual increase in reaction of the fluid with a Pb reservior containing a larger proportion of Proterozoic rocks or their sedimentary

equivalents. This explanation does not account for the relatively radiogenic $^{206}Pb/^{204}Pb$ values of the alpha-stages galenas, although, it explains the general increase in radiogenic Pb isotopic composition with time (Figure 13).

The similarity in Pb isotopic composition between the Au-stage ore of the North Amethyst vein system and the Alpha - Corsair system may indicate that the Alpha - Corsair system also formed early from a hotter fluid in a localized hydrothermal cell. If smaller and hotter systems are more favorable sites for Au mineralization, then the Alpha - Corsair structure may be a promising target for Au exploration.

An alternative explanation for the lead isotopic variations is that the initial Pb isotopic compositions of the Stage 1, and alpha- and beta-stage ore fluids were identical and approximately equal to the most radiogenic stage 1 galena. This would require a larger initial hydrothermal system for the Au mineralization, one that could interact with the Tertiary - Proterozoic rock reservoir at depth, or a subsurface geometry that would allow for the shallower occurrence of Precambrian rock. The isotopic compositions of alpha-stage mineralization would reflect the initially more radiogenic fluid composition. Leaching of wallrock K-feldspar by beta-stage fluids may have changed the bulk isotopic composition of the fluids toward less radiogenic K-feldspar compositions resulting in less radiogenic galena compositions for beta-stage minerals. Later fluids from which Stage 1 ores were deposited were prevented from significant reaction with the volcanic wallrock because the volcanic rocks were armored by Mn-silicate-carbonate and Au-rich assemblages, thus decreasing the porosity and permeability of the

wallrocks. The wallrocks may also have become depleted gradually, but, in this case, one would expect to see a wider range of intermediate values. In this way, these stage-1 fluids may have retained the initial Pb composition inherited from a Precambrian-Tertiary Pb reservior as proposed by Doe et al. (1979).

The second of the two alternatives described above is preferred because it better accounts for the change in Pb isotopic composition with paragenetic position indicated by alpha-, and beta-stage minerals of the Mn-Au association, and stage-1 minerals of the base-metal association. Temporal changes in the Pb isotopic composition may not be regular because they result from local addition of Pb from volcanic rocks by reaction with wallrock. The degree of interaction of ore fluid with wallrock probably varied with time and space across the district, and cannot be quantified at present, however, geochemical investigations of mass transfer (Foley, unpub. data) may help elucidate this process, and explain more clearly the changes in Pb isotopic composition between successive stages.

This second alternative has important implications for Au exploration in the district. If mineralization from both associations formed from the same evolving hydrothermal system, early Mn-Au association could have been deposited throughout the district in an area possibly as widespread as the later base-metal mineralization. The occurrence of minor Au with manganese oxides in the Amethyst vein (Emmons and Larsen, 1923), and the occurrence of small blebs of electrum in early chalcopyrite in the OH vein (Bethke, pers. commun., 1989) lends support to this interpretation. Less radiogenic values of galena in a

vein may then indicate deposition early in the development of the vein systems from hotter fluids that interacted to a greater degree with host volcanics. Thus, less radiogenic values may be used as an exploration index for the occurrence of Au-bearing mineralization, an idea that is discussed in detail below.

Comparison with Oligocene Volcanics and Basement Rocks of Colorado

The North Amethyst galena Pb isotope values generate $^{207}Pb/^{206}Pb$ model ages, using either the Stacey and Kramers (1975) two-stage model or a single-stage model, that are much younger than the age of the ore as obtained by $^{40}Ar/^{39}Ar$ geochronology using vein adularia (Table 1). These "future" ages are characteristic of ore deposits having complex histories of Pb isotope evolution that do not conform to simple Pb evolution models. Common Pb isotope studies of such deposits usually do not yield useful data on the age of ore mineralization, although, the data can often be used to trace the source of the Pb-metal, to explore for ore bodies that are concealed by overburden, or for deposits that have a subtle surface expression (Gulson, 1986). Results of this study indicate that, Pb isotope values may also be used to differentiate ores that occur in the same vein structure but that formed from different hydrothermal fluids, separating Au-rich mineral associations from Ag- and base-metal mineralization.

Pb isotopic data for all galenas in this study plot on and near the 1.47 Ga secondary isochron (Figure 14) defined by Doe et al. (1979) for galena from the Embargo district of the Baughman Creek area, eastern San Juan mountains. The Baughman trend describes the effect of a net

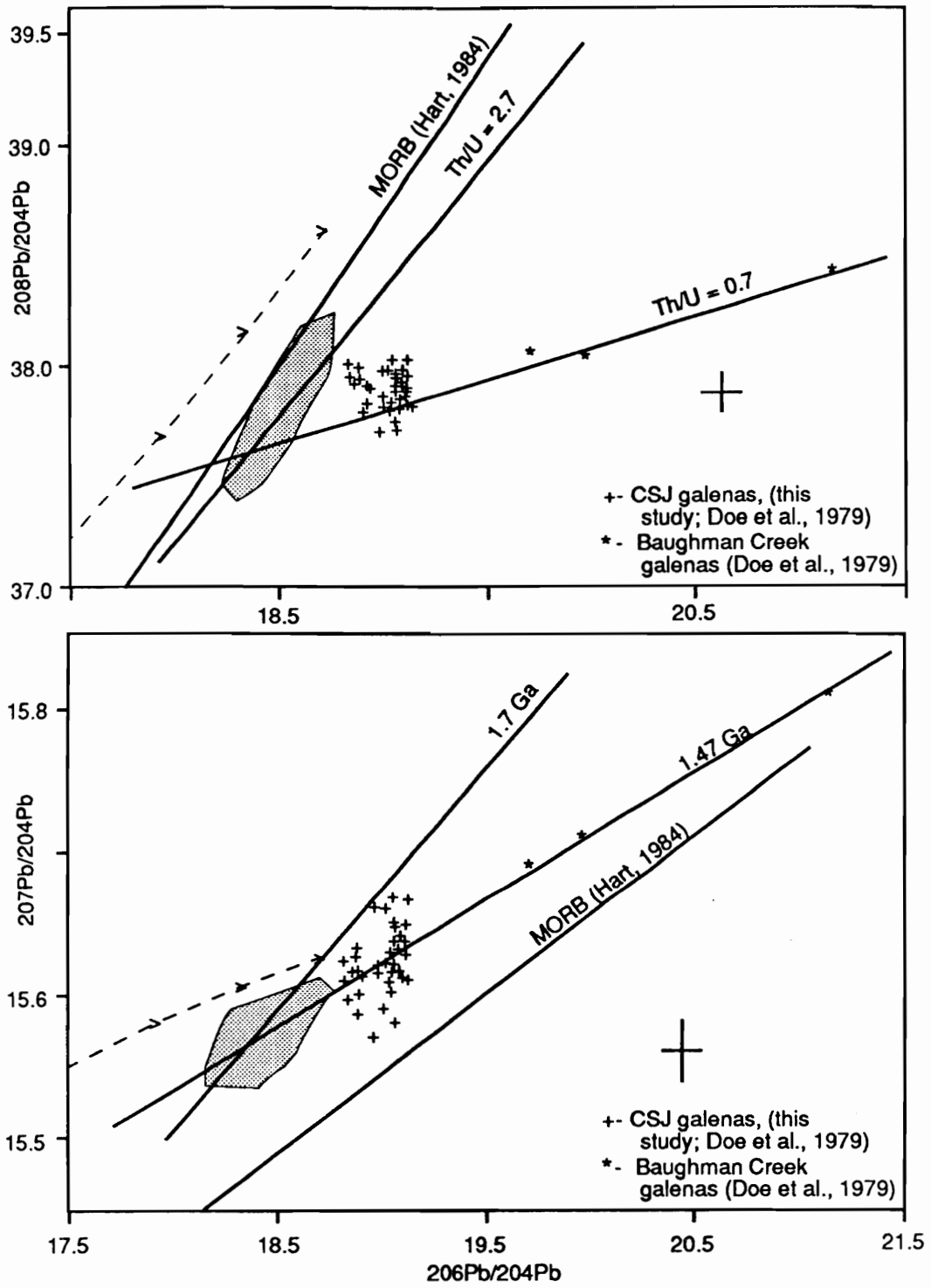

Figure 14. Summary diagram showing possible lead sources for galenas from central San Juan area (CSJ), see text for discussion.

addition of Pb from a 1.4 to 1.5 Ga-old source material having a Th/U ~ 0.7 to a Tertiary volcanic - Proterozoic Pb reservoir (Doe et al., 1979). The secondary isochron is consistent with the probable age of plutonic (granitoids) basement rocks in this area (Doe, 1976; Stein, 1985; Stacey and Hedlund, 1983; Table 2). The isotopic composition of a fluid obtaining its Pb at about 25 Ma from 1.47 Ga-old source material must lie on that line. Figure 14 shows that the spread in $^{207}Pb/^{204}Pb$ for the galenas is much larger than can be accounted for by derivation of the central San Juan Mountaina galenas from 1.47 Ga source material. Other sources of Pb must be considered. As described above, secondary isochron regression lines by Doe et al. (1979) and Lipman et al. (1978) for volcanics of the central part of the San Juan province yield ages of 1.78 Ga and 1.97 Ga, and Th/U ~ 2.6. There is ample evidence for a 1.7 Ga regional plutonic event in southwestern Colorado, for example, Barker (1969) has dated the Irving Formation, the earliest known igneous activity in Colorado, at about 1.78 Ga and Bickford and Boardman (1984) have dated granitic rocks in the Gunnison and Salida areas at 1.67-1.76 Ga. Source material having a Th/U~2.6 and a secondary isocron age of about 1.7 Ga is thus another possible Pb source for galenas in the central San Juan area.

Most of the galena analyses, except galenas from the north Amethyst area metasomatic zone (a, Figure 12), plot between the regression lines for Th/U~ 0.7 and Th/U ~ 2.7 on Figure 14. Thus, as originally proposed by Doe et al. (1979), different proportions of Pb from 1.7 and 1.4 Ga source material can explain much of the variation seen in the Pb composition of the ores. Other explanations are possible, for example

leaching of Pb from a more heterogeneous basement, but at present there are not enough data to consider them in detail.

Doe et al. (1979) also suggested that the contribution of Pb to galena from the main mining district at Creede could have been entirely derived from Proterozoic rocks. This is unlikely for the district as a whole, however, given the variations in Pb isotopic composition for the North Amethyst data.

Calculations aimed at estimating the minimum and maximum allowable percentages of material derived from a 1.47 Ga Precambrian source cannot be rigorously tested because they are strongly dependent on the assumed bulk isotopic composition of the Pb, and on the assumption that the Pb isotopic composition is relatively uniform. This last assumption may be considered for ores of the Creede district because most of the spread in the data is along the 1.47 Ga isochron; only the North Amethyst alpha-stage and Stage-1 galenas show significant spread in $^{207}Pb/^{204}Pb$ as a group. Galenas from North Amethyst stage 1 having the highest $^{207}Pb/^{204}Pb$ values lie on the 1.7 Ga secondary isochron. The composition of Pb derived directly from a 1.7 Ga-old source would lie on the isochron line. Pb generated from both 1.7 Ga and 1.4 Ga sources and mixed at 25 Ma during of formation of the ore mineralization would lie in the field bounded these two lines on Figure 13. The fraction of Pb contributed from each source to the ore fluid at 25 Ma was probably widely variable and contributions of the 1.7 Ga Pb source material to the stage 1 galenas of North Amethyst may have been 100%. The spread in $^{207}Pb/^{204}Pb$ below the 1.47 Ga secondary isochron line is slighly larger than can be accounted for by the analytical error of the technique. A

source for leads of this composition is at this time unknown. Likely candidates to account for the low values of $^{207}Pb/^{204}Pb$ involve basaltic rocks and the northern hemisphere reference line for mid-ocean ridge basalts (Hart, 1984; Hart, 1988) is shown for comparison on Figure 14. Leads derived from such a source would not, however, have values of $^{208}Pb/^{204}Pb$ as low as those of the central San Juan galenas.

Pb leached from 1.47 Ga source material having a bulk composition equal to that of the most radiogenic Creede ores (D-stage), would result in contributions of Pb from the Precambrian that varied from 100% for the most radiogenic D-stage fluids, to about 66% for the least radiogenic Au-rich fluids when mixed with Pb derived from the volcanic rocks. The intermediate values of II-stage galenas of the Bulldog vein system can be derived by mixing ~90% of Pb having an isotopic composition equal to the D-stage galenas with ~10% of the Pb derived from the Carpenter Ridge Tuff. The beta-stage galenas of the North Amethyst mineralization would require, however, a much higher percentage of Pb derived from volcanic rocks. A mixture consisting of ~66% of Pb from the Precambrian and up to ~34% of Pb derived from the Nelson Mountain Tuff could account for the beta-stage values. The amount of Pb required from the Tuff depends in part to its less radiogenic nature. If Pb was also contributed from the more radiogneic Carpenter Ridge Tuff, the percentage required from the volcanic rocks would be greater.

For ore deposits of the San Juan Mountains, Doe et al. (1979) have shown that the addition of lead from crustal sources has always resulted in more radiogenic signatures for galenas. Galenas defining the Baughman trend represent the most radiogenic values thought to have been

derived from a Precambrian source known in the San Juan Mountains. If a fluid similar in Pb isotopic composition to the most radiogenic galena of the Baughman trend mixed with Pb derived from the Carpenter Ridge to produce the North Amethyst mineralization, the Creede ores, and the Bondholder mineralization, then only 14 % of the Pb is required to have been derived from the Precambrian basement. Considering the size of the Carpenter Ridge volcanic field (~1000 cubic kilometers, Lipman, 1976) at 26 m.y. ago, the probable size of the solidified magma chamber, and the minimum estimates of its Pb content (about 20 ppm), an ore deposit the size of Creede (~150,000 tons of Pb) could be derived from the Carpenter Ridge Tuff or volcanics at depth even at a relatively low extraction efficiency (<<25%).

SUMMARY MODEL FOR THE NORTH AMETHYST VEIN MINERALIZATION

A model for the North Amethyst area requires that galenas were deposited from metal-bearing fluids which obtained their Pb isotopic composition primarily from interaction of hydrothermal fluid with Tertiary volcanics and Precambrian basement.

The earliest galenas, those of alpha-stage, may reflect Pb derived directly from a Tertiary - Proterozoic reservior at depth. Leaching of Pb from wallrock K-feldspar by Au-bearing beta-stage fluids and mixing at the site of deposition may have changed the bulk isotopic composition of the Au-rich fluids towards the isotopic composition of the less radiogenic wallrock K-feldspar, resulting in a less radiogenic composition of galena deposited with electrum. The restricted occurrence of the beta-stage Au ore suggests that this stage may have

formed from a small hydrothermal cell possibly related to a relatively shallow ring fault intrusion, however the fluids must have interacted with a Precambrian source at depth.

Stage-1 ores probably formed from the large mineralizing system that deposited base-metal mineralization along structures throughout the central San Juan Mountains. This suggestion is supported by mineralogical and Pb isotopic similarities among later ores of the North Amethyst area, all ores of the main vein systems at Creede, and ores from the Bondholder district. The hydrothermal system must have tapped a relatively homogeneous Pb source and/or contributed to the relative homogeneity of the Pb throughout the district by mixing within the hydrothermal cell.

Stage 1 ores are armored from reaction with the volcanic wallrock by earlier assemblages. Ores of the main mining district at Creede show no evidence for extensive wallrock replacement, except for intense sericitization along the top of the present workings, and locally are shielded from reaction with the wallrock by earlier assemblages (Plumlee, 1989, Barton et al., 1977). Thus, the mineralizing fluids retained an initial Pb isotopic composition generated at depth in a Precambrian - Tertiary Pb reservior as proposed by Doe et al. (1979).

The similarity in Pb isotopic composition between the Au ores of the North Amethyst vein system and the ores of the Alpha - Corsair system may indicate that fluid of the latter system also reacted with wallrock to a greater degree than the ore fluid of the main mining district. This may indicate hotter average fluid temperatures for the

Alpha-Corsair system, and, possibly, a system more like that of the Au mineralization of the North Amethyst area.

PB ISOTOPE SIGNATURES AS A TOOL FOR EXPLORATION

Pb isotopic signatures have been shown to be an effective tool for identifying and discriminating economically important ore deposits from less economic mineral occurrences (Doe and Zartman, 1979, Foley et al., 1981, Ayuso et al., 1987, Gulson, 1986, and Gulson and Mizon, 1979, Stacey and Hedlund, 1983). In the central San Juan Mountains, Pb isotopic signatures may be useful in distinguishing smaller, hotter, and more localized hydrothermal systems that have a higher Au potential from later, Ag-, and base-metal-rich mineralization.

Doe and Zartman (1979), in developing a model for Pb evolution in the Phanerozoic, recognized that among magmatothermal deposits within a rejuvenated craton setting, the largest and richest base-metal epithermal deposits are nonradiogenic for their age. Small deposits, or ones formed on the periphery of a larger system, tend to be more radiogenic. They proposed that the circulating systems in magmatic hydrothermal deposits may be too small or too hot to form major base-metal deposits with radiogenic isotopic compositions like those of some low-temperature, lateral-secretion ores. Thus, their work suggested that large base-metal deposits like Butte, Montana, Climax, Colorado, Leadville/Gilman, Colorado, and Park City, Utah, exist within rejuvenated cratons and that such mineralized areas have Pb isotopic signatures for $^{206}Pb/^{204}Pb$ of less than 18.8. Production from most of these large and relatively nonradiogenic deposits has been in the

hundreds and thousands of millions of dollars; as stated succinctly by Doe and Zartman (1979), the category includes the "nation savers". Stacey and Hedlund (1983) found a similar relationship between $^{206}Pb/^{204}Pb$ value and ore deposit size in southwestern New Mexico. Their study indicated that Pb isotopic signature may be used as a criteria for mineral exploration because $^{206}Pb/^{204}Pb$ values for larger deposits related to Laramide activity are <18.6. Similarly the largest deposits related to mid-Tertiary activity also have the lowest values of $^{206}Pb/^{204}Pb$.

The ores of the main mining area of the Creede district, including the Stage-1 ore of the North Amethyst mineralization, appeared to be an exception to Doe and Zartman's model for magmatothermal ores because the deposits are both economically important and among the most radiogenic of the magmatothermal type ($^{206}Pb/^{204}Pb$~19.1). This apparent exception in Pb isotopic composition may be explained by examining the model for the hydrologic evolution of the Creede district (Bethke, 1988). The Creede district, in contrast to many magmatothermal deposits, developed within an extensive system of northwest-trending faults that possibly extend for over 11 kilometers across three caldera structures (Lipman and Sawyer, 1988). These faults forced the ore-forming fluids to develop an extensive lateral-flow regime confined by the fault geometry (Steven and Eaton, 1975; Bethke, 1988). Such extensive lateral flow regimes characterize many adularia-sericite type epithermal deposits (Heald et al., 1987). The Creede-type ore-forming fluids created a large cell or a series of relatively open interconnected cells that either tapped a homogeneous Pb source (unlikely given what is known

about the source materials) or contributed to the relative homogeneity of the Pb isotopic composition by mixing. The extensive lateral flow-regime and large hydrothermal cell development probably allowed for lengthy interaction with Precambrain source material as initially suggested by Doe et al. (1979) to develop the radiogenic nature of the ores. The radiogenic nature of the main-stage base metal mineralization of the Bondholder district, the later association at the North Amethyst vein system, and the main mining district may be a result, in part, of the extensive deep lateral-flow regime dictated by the structural geometry. In contrast, hydrothermal cells responsible for mineralization in magmatothermal systems such as Butte, Montana, were hotter, less saline, and mainly confined to the densely fractured carapace of the pluton.

Pb isotopic signatures can be used as an index of the relative size of hydrothermal cell and to identify potential for Au mineralization in the central San Juan volcanic cluster. The Au ores of the North Amethyst vein system are probably not unique to the region and may reflect a period of hydrothermal activity in the interval between the waning stages of volcanic activity and the development of large-scale open hydrothermal cells that characterize the ores of the main mining district at Creede. The hotter and possibly more restricted hydrothermal cells of this intervening period are potentially the most favorable targets for Au exploration in the central San Juan province.

REFERENCES

Afifi, A.M., 1981, Precambrian geology of the Iris area, Gunnison and Saguache Counties, Colorado: Unpublished M.S. thesis, Colorado School of Mines, Boulder, Colorado, 197p.

Ayuso, R.A., and Bevier, M.L., 1990, Regional differences in Pb isotopic compositions of feldspars in plutonic rocks of the northern Appalachian Mountains, USA and Canada: A geochemical method of terrane correlation: Tectonics (in press) 57p.

Ayuso, R.A., Foley, N.K., and Brown, C,E., 1987, Source of Pb and mineralizing brines for Rossie-type Pb-Zn veins in the Frontenac axis area, New York: Economic Geology, v. 82, pp. 489-496.

Ayuso, R.A., Horan, M.F., and Criss, R.E., 1988, Pb and O isotopic geochemistry of granitic plutons in northern Maine: American Journal of Science, v. 288-A, p. 421-460.

Baars, D.L., and Stevenson, G.M., 1984, The San Luis uplift, Colorado and New Mexico - an enigma of the ancestral Rockies: The Mountain Geologist, v. 21, no. 2, p. 57-67.

Barker, F., 1969, Precambrian geology of the Needle Mountains, southwestern Colorado: U.S. Geological Survey Prof. Paper 644-A, 35p.

Barton, P.B., Jr. and Bethke, P.M., 1987, Chalcopyrite disease in sphalerite: pathology and epidemiology: Am. Mineralogist, v. 72, p. 451-467.

Barton, P.B., Jr., Bethke, P.M., and, Roedder, E., 1977, Environment of Ore Deposition in the Creede mining district, San Juan Mountains, Colorado: Part III. Progress toward interpretation of the

chemistry of the ore-forming fluid for the OH vein: Econ. Geol., v. 72, p. 1-24.

Bethke, P.M., 1988, The Creede, Colorado ore-forming system: a summary model: U.S. Geological Survey Open-file Report 88-408, 29p.

Bethke, P.M., and Lipman, P.W., 1987, Deep environment of volcanogenic epithermal mineralization: Proposed research drilling at Creede, Colorado: EOS, v. 68, p. 177, 187-89.

Bethke, P.M., Barton, P.B., Jr., Lanphere, M.A., and Steven, T.A., 1976, Environment of ore deposition in the Creede mining district, San Juan Mountains, Colorado: Part II. Age of mineralization: Econ. Geol., v. 71, p. 1006-1011.

Bethke, P.M., and Lipman, P.W., 1987, Deep environment of volcanogenic epithermal mineralization: proposed research drilling at Creede, Colorado: EOS, v. 68, p. 177, 187-89.

Bethke, P.M., and Rye, R.O., 1979, Environment of ore deposition in the Creede mining district, San Juan Mountains, Colorado: Part IV. Source of fluids from oxygen, hydrogen, and carbon isotope studies: Economic Geology, v. 74, p. 1832-1851.

Bickford, M.L., and Boardman, S.J., 1984, A Proterozoic volcano-plutonic terrane, Gunnison and Salida areas, Colorado: J. Geology, v. 92, p. 657-666.

Cameron, A.E., Smith, D.H., and Walker, R.L., 1969, Mass spectrometry of nanogram-size samples of Pb: Anal. Chem., v. 41, p. 525-526.

DePoalo, D.J., 1981, Neodymium isotopes in the Colorado Front Range and crustal-mantle evolution in the Proterozoic: Nature, v. 291, pp. 193-196.

Doe, B.R., Steven, T.A., Delevaux, M.H., Stacey, J.S., Lipman, P.W., and Fisher, F.S., 1979, Genesis of ore deposits in the San Juan volcanic field: Econ. Geol., v. 74, pp. 1-26.

Doe, B.R., 1967, The bearing of Pb isotopes on the source of granitic magma: J. Petrology, v. 8, p. 51-83.

Doe, B.R., 1968, Pb-isotope studies of Cenozoic volcanic rocks in the Rocky Mountain region - a summary [abs.]: Colo. School of Mines Quarterly, v. 63, p. 149-174.

Doe, B.R., and Delevaux, M., 1973, Variations in lead isotopic compositions in Mesozoic granitic rocks of California: A preliminary investigation: Bull. Geol. Soc. Amer., v 84, p3513-3526.

Doe, B.R., and Zartman, R.E., 1979, Plumbotectonics, the Phanerozoic, in H.L. Barnes, ed., Geochemistry of hydrothermal ore deposits, Second edition: John Wiley and Sons, New York, p. 22-70.

Emmons W.D. and Larsen, E.S., 1923, Geology and ore deposits of the Creede district, Colorado: U.S. Geological Survey Bulletin 718, 198p.

Faure, G., 1977, Principles of Isotope Geology: Smith-Wyllie Intermediate Geology Series, John Wiley and Sons, New York, 464p.

Foley, N.K., Sinha, A.K., and Craig, J.R., 1981, Isotopic composition of lead in the Austinville-Ivanhoe Pb-Zn district, Virginia: Econ. Geol., v. 76, p. 2012-2017.

Foley, N.K., 1986, Fluid inclusion study of ores from the Fukazawa Mine, Hokuroku district, Akita Prefecture, Japan: Mining Geology, v. 36, P. 11-20.

Foley, N.K., and Vardiman, D.M., 1988, Paragenesis and mineral chemistry of ores of the Au-, Ag-, and base-metal-bearing North Amethyst property, San Juan Mountains, Colorado: Geol. Soc. Amer. [Abs.], v. 20, p. A276.

Foley, N.K., 1990a, Mineralogy, paragenesis, and mineral chemistry of Au-, Ag-, and base-metal-bearing ores of the North Amethyst vein system, Mineral County, Colorado: Part I, unpublished Ph.D dissertation, Virginia Polytechnic Institute and State Univ., 103p.

Foley, N.K., 1990b, Fluid inclusion thermometry and geochemistry of Au, Ag, and base-metal ores of the North Amethyst vein system, San Juan Muntains, Mineral County, Colorado: Part II, unpublished Ph.D dissertation, Virginia Polytechnic Institute and State Univ., 75p.

Gries, R.R., 1985, San Juan Sag: Cretaceous rocks in a volcanic-covered basin, south-central Colorado: The Mountain Geologist, v. 22, p. 167-179.

Gulson, B.L., 1986, Lead isotopes in mineral exploration: Developments in Ecomonic Geology, v. 23, Elsevier, Amsterdam, 245p.

Gulson, B.L., and Mizon, K.J., 1979, Lead isotopes as a tool for gossen assessment in base metal exploration: J. Geochem. Explor., v. 11, pp. 299-320.

Hart, S.R., 1984, A large-scale isotope anomaly in the Southern Hemisphere mantle: Nature, v. 309, p. 753-757.

Hart, S.R., 1988, Heterogeneous mantle domains: signatures, genesis, and mixing chronologies: Earth and Planetary Science Letters, v. 90, p. 273-296.

Hayba, D.O., Bethke, P.M., Heald, P., and Foley, N.K., 1985, Geologic, mineralogic, and geochemical characteristics of volcanic-hosted epithermal precious-metal deposits: Rev. Econ. Geology, v. 2, p. 129-167.

Heald, P.W., Foley, N.K., and Hayba, D.O., 1987, Comparative anatomy of volcanic-hosted epithermal deposits: Acid-sulfate and adularia-sericite types: Econ. Geol., v. 82, p. 1-26.

Heier, K.S., 1973, Geochemistry of granulite facies rocks and problems of their origin: Phil. Trans. R. Soc. London A., v. 273, p. 429-442.

Holden, N.E., and Walker, F.W., 1972, Chart of the nuclides: 11th edition, Educational Relations, General Electric Co., Schenectady, N.Y.

Hon, K., and Mehnert, H.H., Compilation of revised ages of volcanic units in the San Juan Mountains, Colorado: Recalculated K-Ar age determinations using IUGS constants: U. S. Geological Survey Open-file Report 83-668, 14p.

Jaffey, A.H., Flynn, K.F., Glendenin, L.E., Bentley, W.C., and Essling, A.M., 1971, Precision measurements of half-lives and specific activities of U^{235} and U^{238}: Phys. Rev., C4, p. 1889-1906.

Krause, K.W., Stormer, J.C., Jr., and Whitney, J.A., 1986, Magmatic conditions of the Wason Park Tuff, central San Juan volcanic field, Colorado (abs): EOS, v. 67, p. 1269.

Lanphere, M.A., 1987, High-resolution $^{40}Ar/^{39}Ar$ geochronology, central San Juan caldera complex, Colorado [abs]: Geol. Soc. America Abs. with Programs, v. 19, no. 5, p. 288.

Lanphere, M., 1988, High resolution $^{40}Ar/^{39}Ar$ chronology of Oligocene volcanic rocks, San Juan Mountains, Colorado: Geochimica cosmochimica acta, v. 52, pp. 1425-1434.

LeRoux, L.J., and Glendenin, L.E., 1963, Half-life of thorium-232: Nat. Conf. Nucl. Energy Appl. Isotop. Radiat. Proc. 1963, p. 77-88.

Lipman, P.W., Steven, T.A., and Mehnert, H.H., 1970, Volcanic history of the San Juan Mountains, Colorado, as indicated by potassium-argon dating: Geol. Soc. America Bull., v. 81, p. 2329-2352.

Lipman, P.W., Fisher, F.S., Mehnert, H.H., Naeser, C.W., Luedke, R.G., and Steven, T.A., 1976, Multiple ages of mid-Tertiary mineralization and alteration in the western San Juan Mountains, Colorado: Economic Geology, v. 71, p. 571-588.

Lipman, P.W., Doe, B.R., Hedge, C.E., and Steven, T.A., 1978, Petrologic evolution of San Juan volcanic field, southwestern Colorado: Pb and Sr evidence: Bull. Geol. Soc. Amer., v.89, pp. 59-82.

Lipman, P.W., and Mehnert, H.H., 1975, Late Cenezoic basaltic volcanism and development of the Rio Grande depression in the southern Rocky Mountains: in B.F. Curtis, ed., Geologic history of the southern Rocky Mountains, Geological Society of America Memior 144, p. 119-154.

Lipman, P.W., and Sawyer, D.A., 1988, Preliminary geology of the San Luis Peak quadrangle and adjacent areas, San Juan volcanic field, southwestern Colorado: U.S. Geological Survey Open-file report 88-359, 32p.

Matty, D.M., Lipman, P.W., and Stormer, J.C., 1987, Common-Pb isotopic characteristics of central San Juan ash flow tuffs [abs]: Geol. Soc. America Anstracts with Programs, v. 19, no. 5, p. 319.

Plouff, D., and Pakiser, L.C., 1972, Gravity study of the San Juan Mountains, Colorado: U.S. Geological Survey Prof. Paper 800-B, p. 183-190.

Plumlee, G.S., 1989, Processes controlling epithermal mineral distribution in the Creede mining district, Colorado: unpublished Ph.D, Harvard University, 379p.

Plumlee, G.S. and Rye, R.O., 1988, Extreme sulfur isotope, As, Sb, Ag variations in late-stage botroidal pyrite from Creede, Colorado: vestiges of a waning hydrothermal system [abs.]: Geol. Soc. America Abstracts with Programs, v. 16, no. 6, p.719.

Rye, R.O., Plumlee, G.S., Bethke, P.M., and Barton, P.B., 1988, Stable isotope geochemistry of the Creede, Colorado, hydrothermal system: U.S. Geological Survey Open-file Report 88-356, 40p.

Sawyer, D.A., Sweetkind, D., Rye, R.O.,Siems, D.F., Reynolds, R.L., Rosenbaum, J.G., and others, 1989, Potassium Metasomatism in the Creede mining district, San Juan volcanic field, Colorado: Continental Magmatism [Abs], International Association of Volcanology and Chemistry of the Earth's Interior, New Mexico Bureau of Mines and Mineral Resources, Bulletin 131, p. 234.

Stacey, J.S., Zartman, R.E., and Nkomo, I.T., 1968, A lead isotope study of galenas and selected feldspars from mining districts in Utah: Econ. Geol., v.63, p. 796-814.

Stacey, J.S., and Hedlund, D.C., 1983, Lead-isotopic compositions of diverse igneous rocks and ore deposits from southwestern New Mexico and their implications for early Proterozoic crustal evolution in the western United States: Geol. Soc. Amer. Bull., v. 94, p. 43-57.

Stacey, J.S., and Kramers, J.D., 1975, Approximation of terrestrial lead isotope evolution by a two-stage model: Earth Plan. Sci. Lett., v. 26, p. 207-221.

Stein, H., 1985, A lead, strontium, and sulfur isotope study of Laramide-Tertiary intrusions and mineralization in the Colorado Mineral Belt with emphasis on Climax-type porphyry molybdenum systems plus a summary of other newly acquired isotopic and rare earth element data: Unpub. dissertation, Univ. of North Carolina, 493p.

Steven, T.A., 1964, Geologic setting of the Spar City district, San Juan Mountains, Colorado: U.S. Geological Survey Professional Paper 475-D, Article 146, p. 123-127.

Steven, T. A., 1975, Middle Tertiary volcanic field in the southern Rocky Mountains, in B.F. Curtis, ed., Cenozoic history of the southern Rocky Mountains: Geological Society of America Memoir 144, p. 75-94.

Steven, T.A., and Ratte, J.C., 1965, Geology and structural control of ore deposition in the Creede district, San Juan Mountains, Colorado: U.S. Geological Survey Prof. Paper 487, 90p.

Steven, T.A., and Ratte, J.C., 1973, Geologic map of the Creede quadrangle, Mineral and Saguache Counties, Colorado: U.S. Geological Survey Map GQ-1053.

Steven, T.A., and Eaton, G.P., 1975, Environment of ore deposition in the Creede mining district, San Juan Mountains, Colorado: I. Geologic, hydrologic, and geophysical setting: Econ. Geol., v. 70, p. 1023-1037.

Steven, T.A., and Bieniewski, C.L., 1977, Mineral resources of the La Garita Wilderness, San Juan Mountains, south-western Colorado: U.S. Geological Survey Bulletin 1420, 65p.

Steven, T. A., and Lipman, P.W., 1976, Calderas of the San Juan volcanic field, southwestern Colorado: U.S. Geol. Survey Prof. Paper 958, 35p.

Vergo, N., 1987, Wallrock alteration at the Bulldog Mountain mine, Creede, Colorado: Geol. Soc. Ameerica [abs.], v. 19, p. 340.

Whitney, J.A., and Stormer, J.C., 1985, The Carpenter Ridge Tuff: the development of chemical and thermal gradients through magma mixing in a periodically replenished magma chamber: American Journal of Science

Whitney, J.A, Dorais, M.J., Stormer, J.C., Jr., Kline, S.W., and Matty, D.J., 1988, Magmatic conditions and development of chemical zonation in the Carpenter Ridge Tuff, central San Juan volcanic field, Colorado: American Journal of Science Spec. V. 288-A, pp. 16-44.

Williams, D.L., and Abrams, G.A., 1987, Preliminary results of gravity and aeromagnetic studies in the central San Juan caldera complex, Colorado: Geol. Soc. America [abs.], v. 19, p. 342.

Wooden, J.L., Stacey, J.S., Howard, K.A., Doe, B.R., and Miller, D.M., 1988, Pb isotopic evidence for the formation of the Proterozoic crust in the southwestern United States, in W.G. Ernst, ed., Metamorphism and crustal evolution of the western United States: Rubey volume 7, Prentiss Hall, New Jersey, p. 69-86.

Zartman, R.E., 1974, Lead isotopic provinces in the cordillera of the western United States and their geologic significance: Econ. Geol., v. 69, pp. 792-805.

Zartman, R.E., and Stacey, J.S., 1971, Lead isotopes and mineralization ages in the Belt supergroup rocks, northwestern Montana andd northern Idaho: Econ. Geol., v. 66, pp. 849-860.

Zartman, R.E., and Doe, B.R., 1981, Plumbotectonics - the model: Tectonophysics, v. 75, pp. 135-162.

APPENDIX A: A SHORT SUMMARY OF THE CREEDE MINING DISTRICT

The historic Creede mining district is located in the central San Juan Mountains of Colorado. The geology of the district is described by Steven and Ratte (1965) and Steven and Eaton (1975). The veins have been the subject of extensive study over the past 35 years by P.B. Barton, Jr., P.M. Bethke, P. Lipman, E. Roedder, R.O. Rye, and others of the U. S. Geological Survey. The results of this work have been published in a number of papers describing the geology, mineralogy, geochemistry, and hydrology of the main mining district. Important contributions to the development of a summary model of the Creede hydrothermal system presented by Bethke (1988) are identified below. For additional information, the reader is directed to an extensive bibliography of the Creede mining district, including regional and historic studies, compiled by Hayba and Conte (1987).

The Central and Southern Creede Mining District:

Silver and base-metal ores of the main mining district at Creede formed 24.6 m.y. ago, approximately 1 m.y. later than the youngest known volcanism in the immediate area (Bethke et al., 1976). The mineralization occurs as open space fillings in a N-S graben system which cuts ash flow tuffs of middle Tertiary age (Figure 1, Foley, 1990a). The central and southern parts of the district include mineralized extents of the Bulldog Mountain, OH, P, and southern Amethyst, Alpha-Corsair, and Solomon-Holy Moses faults. Structural

aspects of the mining district have been summarized by Steven and Ratte (1965). Detailed structural studies of individual vein systems are underway by various mining company personnel (S. Caddey and C. Byington, pers. commun., 1985, 1987). The host rock for the veins in the southern and central parts of the district is mainly intracaldera fill of the Bachelor caldera (Bachelor Mountain rhyolite), although minor disseminated mineralization occurs in sedimentary rocks of the Creede Formation. The structures which have contributed significantly to the production history of the central and southern district include the Amethyst, OH, P, and Bulldog Mountain vein systems. Lesser amounts of ore were produced from the Solomon - Holy Moses and Alpha - Corsair veins, and from zones of disseminated mineralization in Creede Formation sediments. Substantial reserves of low-grade mineralization have been identified in highly fractures volcanics in the hanging wall of the Amethyst vein near its intersection with the OH vein (Giudice, 1981) and in sediments of the Creede Formation channel intersected by the Amethyst vein (Smith, 1981; Wason, 1983; Rice, 1984).

A zone of intense sericitic alteration marks the top of the productive zone of the OH vein and similar alteration caps the Amethyst and Bulldog Mountain vein systems, although the lower level of alteration fluctuates over several hundred feet. The clays are mixed-layer illite-smectites and have been studied extensively by Horton (1987) and Vergo (1984, 1987) and Bethke (pers. commun., 1988). Compositional variations in the clays (Vergo, 1987) may provide important constraints on the thermal history of Creede system. Most of the veins are hosted by potassium-feldspar stable wallrock. The ores

are of the adularia-sericite type (Heald et al., 1987) and are postulated to have been deposited between 300-500 meters below the water table in a sub-horizontal zone of mixing between a deeply convecting brine plume and overlying ground water (Steven and Ratte, 1965; Bethke and Rye, 1979; Bethke, 1988; Barton et al., 1977, and Hayba et al., 1985).

In the deeper and more northern parts of the main district, the ores consist dominantly of sphalerite, galena, and chalcopyrite (Bethke and Rye, 1979; Barton et al., 1977), and are termed the "OH assemblage". Silver-bearing tetrahedrite and minor amounts of other sulfosalts, all hosted by sphalerite, galena or chalcopyrite, were mined from paragenetically early, fine-grained ores of the "OH" type. A gangue of quartz, chlorite, pyrite, and hematite is associated with the sulfide ore. The "OH assemblage" is divided in 5 mineralogical stages, labelled A through E and listed in Table 9 (Foley, 1990a).

In the southern part of the district and higher in the veins, the ore is composed of abundant early rhodochrosite, cut by banded barite and sulfide ore, and quartz (Plumlee, 1989; Heald and Plumlee, 1987). The sulfide bands consist mainly of sphalerite, galena, and minor chalcopyrite. The paragenetically early barite-sulfide ore was mined for silver occurring in tetrahedrite, miscellaneous sulfosalts, acanthite, and native silver. Later in the paragenesis, minor silver occurs in a complex suite of Cu-, and Ag-sulfides and sulfosalts. Ores of this type are termed the "Bulldog assemblage", and Plumlee (1989) has defined mineralogical stages (I through II) that correlate with the "OH assemblage" (Table 9, Foley, 1990a).

Mineralogical stages were correlated across the central and southern Creede district by Plumlee (1989) based on work of Bethke and Rye (1979), Barton et al. (1977), Robinson (1981), Plumlee (1989), and Giudice (1981). This correlation documents a facies relationship between stages of the "OH" and "Bulldog" assemblages. The zoning relationship between the two assemblages records the dominant direction of fluid movement in the ore zone from north to south (Bethke, 1988).

Barton et al. (1977) proposed that the "OH assemblage" buffered the oxygen and sulfur activities of the ore fluid near a pyrite-chlorite-hematite triple point for much of the depositional history of the veins. Plumlee (1989) has used this Creede reference environment to model chemical controls on mineral deposition and mineral zoning patterns for the central and southern mining district.

Studies of chemical, thermal, and isotopic variations in the ore zone of the main mining district have contributed to the development of a model for the evolution of the ore fluid. The model presented by Bethke (1988), integrates data from a extensive number of geologic, fluid inclusion, stable isotope, lead isotope, and chemical modelling studies.

Fluid inclusion and stable isotope data suggest that two meteoric fluids having distinct isotopic and chemical signatures contributed to the hydrothermal system. An isotopically and chemically evolved fluid entered the system form the Creede caldera moat to the south of the district and a dilute fluid entered from highlands to the north. These fluids circulated deeply and were heated by a causitive pluton; they also probably interacted with magmatic fluids given off by the

crystalling magma. Lead isotopic evidence (Doe et al., 1979; Foley et al., 1987; Foley, 1990c) suggests the fluids interacted with Precambrian basement, or sediment derived from basement, and Tertiary volcanics or subvolcanic plutons. The hydrothermal fluids carried dissolved metals, sulfur, carbon, and other constituents from depth to the top of the system. Mineral deposition occurred within a zone of mixing (Hayba, 1987) between the brine and overlying fresh waters and, locally, boiling was an important process leading to mineral deposition (Roedder, 1977; Plumlee, 1989). In response to the north-to-south topographic gradient and structural controls, the fluids flowed laterally southward through the main mining district. The southward-flowing hydrothermal fluids mixed with overlying steam-heated groundwaters, and in the southernmost ore zones may have mixed with sulfate- and organic-rich pore fluids from Creede caldera moat sediments (Rye et al., 1988; Plumlee, 1989).

The Northern Creede district, North Amethyst vein:

The gold, silver and base-metal mineralization of the North Amethyst vein system was only recently discovered by extensive subsurface drilling in the general area of the historic Equity mine. The site of the old Equity mine, located on West Willow Creek about 7 miles northwest of Creede, was first investigated in the early 1900's (Emmons and Larsen, 1913, 1923). On the surface above the mine, Emmons and Larsen (1923) describe a great ledge of decomposed silicified "Willow Creek rhyolite" stained with iron oxides. The rhyolite was cut by thin fracture seams containing limonite, manganese oxides, and some barite. About 50 feet above the creek, a 725 foot long tunnel was

driven east-southeast into the "Campbell Mountain rhyolite". At about 715 feet, a drift was driven north and south along a one-to-three inch seam of sulfide ore carrying gold and silver. The drift to the north cut a fractured zone 10 to 20 feet wide about 30 feet north of the tunnel, an underground exposure of the reverse Equity fault.

The highly silicified rhyolite contained pyrite, sphalerite and galena and locally carried considerable gold and silver. Total production of the mine reported prior to closing in 1930 (due to the sharp drop in the price of silver) was $88,000 (Steven and Ratte, 1965).

The area around the Equity mine was extensively drilled by Homestake Mining Company, and, in 1983 a finding of gold-rich ore near the intersection of the northern extension of the north-trending Amethyst fault and the east-west-trending Equity fault was announced. Extensive underground exploratory workings developed along the Amethyst fault were made available for this study which focussed on the mineralization in the North Amethyst area. Reconnaisance studies of the mineralization by mining companies indicated that it differed substantially from southern district ores in metal abundances and mineralogy (S. Caddey, pers. commun., 1987).

The results of initial studies of the new mineralization by personnel of the Homestake Mining Company and the U. S. Geological Survey were presented at the annual meeting of the Rocky Mountain Section of the Geological Society of America meeting in Boulder, Colorado in May of 1987, and are enumerated below:

1). Adularia from North Amethyst vein mineralization dated by Lanphere (1987) using high-resolution $^{40}Ar/^{39}Ar$ geochronology indicated that some

mineralization of the North Amethyst area is contemporaneous in age with mineralization of the southern and central Creede district.

2). Foley et al. (1987) showed that some galenas from the North Amethyst area are isotopically similar to galenas from the southern and central Creede mining district. A more detailed study of the character of common lead in galenas from the northern, central and southern mining areas at Creede is presented in Foley (1990c).

3). Fluid inclusion study of quartz, sphalerite, fluorite and calcite from drillcore just south of the study area (Figure 1, Foley, 1990b) and north of the main mining distrtct by Bazrafshan and Norman (1987) indicated that fluids having a wide range in salinities (0 to 11 weight percent NaCl equivalent) and homogenization temperatures (150 -310 C) deposited mineralization throughout the area. Plumlee et al. (1987) and Hayba (1987) incorporated these data into models of chemical and hydrologic processes. Hayba (1987) proposed that saline fluids entering the Creede hydrothermal system at depth from the south and mixed with dilute fluids northern fluids. He listed deep mixing, shallow mixing and boiling as important processes leading to mineral deposition. Plumlee suggested that under wallrock buffered conditions, the dilute northern fluids were more enriched in bisulfide- and oxy-complexed metals (Au, Ag, As, Sb, Cu), whereas, the southern brines picked up and transported from depth large amounts of chloro-complexed metals (Pb, Zn, Ag, Cu).

4). Rye et al. (1988) presented stable isotope evidence to suggest that fluids responsible for coarse-grained sulfide and chlorite stages of the North Amethyst ores were similar to those depositing all ore stages in

the main Creede district. They also showed that some quartz was deposited from fluids with a dominant component of meteoric water that had been shifted to heavier values by interactions with wallrocks at depth in the system.

5). Landis and Rye (1987) have examined the gas chemistry of some mineralization of the North Amethyst vein system as part of a district-wide study by quadrupole mass spectrometry of the gas chemistry of fluids in major stages of the Creede district. They found that fluids from all minerals of the Creede district, including the North Amethyst vein system, contain varying proportions of H_2O, CO_2, H_2S, SO_2, Ar, N_2, and CH_4, in addition to a complex, and as yet poorly characterized mixture of alkanes, alkenes, and aromatic hydrocarbons.

6). Bethke (1988) presented an summary model of the Creede ore-forming system and discussed possible relationships between ores of the main mining district and the North Amethyst ores based on available data listed above. He described a scenario where brines, whose salinity was acquired in playa lakes in the moat of the Creede caldera, entered a hydrothermal system from the south through fractures of the Creede graben interacted with regional groundwaters. Both waters circulated deeply, were heated by a causitive intrusion, and rose in the northern part of the district beneath the North Amethyst area. Mixing of the brine and fresh water occured at their interfaces, especially along the top of the system.

References:

Barton, P.B., Jr., Bethke, P.M., and Roedder, E., 1977, Environment of Ore Deposition in the Creede mining district, San Juan Mountains,

Colorado: Part III. Progress toward interpretation of the chemistry of the ore-forming fluid for the OH vein: Econ. Geol., v. 72, p. 1-24.

Bazrafshan, K., and Norman, D.I., 1987, Fluid inclusion study of the northern Amethyst vein system [abs]: Geol. Soc. America, Abstracts with programs, v.19, no. 5, p. 259.

Bethke, P.M., 1988, The Creede, Colorado ore-forming system: a summary model: U.S. Geological Survey Open-file Report 88-408, 29p.

Bethke, P.M., and Rye, R.O., 1979, Environment of ore deposition in the Creede mining district, San Juan Mountains, Colorado: Part IV. Source of fluids from oxygen, hydrogen, and carbon isotope studies: Economic Geology, v. 74, p. 1832-1851.

Bethke, P.M., Barton, P.B., Jr., Lanphere, M.A., and Steven, T.A., 1976, Environment of ore deposition in the Creede mining district, San Juan Mountains, Colorado: Part II. Age of mineralization: Econ. Geol., v. 71, p. 1006-1011.

Doe, B.R., Steven, T.A., Delevaux, M.H., Stacey, J.S., Lipman, P.W., and Fisher, F.S., 1979, Genesis of ore deposits in the San Juan volcanic field, southwestern Colorado - lead isotope evidence: Econ. Geology, v. 74, p. 1-26.

Emmons, W.H. and Larsen, E.S., 1913, A preliminary report on the geology and ore deposits of Creede, Colorado: U.S. Geological Bulletin 530, p. 42-65.

Emmons, W.H. and Larsen, E.S., 1923, Geology and ore deposits of the Creede district, Colorado: U.S. Geological Survey Bulletin 718, 198p.

Foley, N.K, Barton, P.B., Jr., Bethke, P.M., and Doe, B.R., 1987, The isotopic composition of ore lead of the Creede mining district and vicinity, San Juan Mountains, Colo. [abs]: Geol. Soc. America, Abstracts with Programs, v. 19, no. 5, p. 275.

Giudice, P.M., 1981, Mineralization at the convergence of the Amethyst and OH fault systems, Creede district, Mineral County, Colo.: Unpub. M.Sc. thesis, University of Arizona (Tucson), 95p.

Hayba, D.O., 1987, Fluid-inclusion evidence for hydrologic and hydrothermal processes in the Creede mineralizing system, Colorado [abs.]: Geol. Soc. America Abstracts with Programs, v. 19, no. 5, p. 282.

Hayba, D.O., and Conte, C., 1987, Bibliography and index of the geology of the Creede mining districtand vicinity: U.S. Geological Survey Open-file Report 87-371, 48p.

Hayba, D.O., Bethke, P.M., Heald, P., and Foley, N.K., 1985, Geologic, mineralogic, and geochemical characteristics of volcanic-hosted epithermal precious-metal deposits: in B.R. Berger and P.M. Bethke, eds., Geology and geochemistry of epithermal systems: Reviews in Econ. Geology, v. 2, p. 129-167.

Heald-Wetlaufer, P. and Plumlee, G.S., 1984, Significance of mineral variations in time and space along the Bulldog Mountain vein system with respect to the district-wide hydrology, Creede district,

Heald, P.W., Foley, N.K., and Hayba, D.O., 1987, Comparative anatomy of volcanic-hosted epithermal deposits: Acid-sulfate and adularia-sericite types: Econ. Geol., v. 82, p. 1-26.

Horton, D.G., 1983, Argillic alteration associated with the Amethyst vein system, Creede mining district, Colorado: Unpub. Ph.D thesis, University of Illinois (Urbana-Champaign), 337p.

Lanphere, M.A., 1988, High resolution 40Ar/39Ar chronology of Oligocene volcanic rocks, San Juan Mountains, Colorado: Geochimica cosmochimica acta, v. 52, p. 1425-1434.

Landis, G.P., and Rye, R.O., 1989, Reconnaissance gas chemistry of the Creede, Colorado, hydrothermal system: U.S. Geological Survey Open-file Report 89-84, 49p.

Plumlee, G.S., 1989, Processes controlling epithermal mineral distribution in the Creede mining district, Colorado: unpublished Ph.D, Harvard University, 379p.

Plumlee, G.S., Barton, P.B., Jr., and Rye, R.O., 1987, Diverse chemical processes in the Creede, Colorado, epithermal system: a progress report [abs]: Geol. Soc America, Abstracts with Programs, v. 19, no. 5, p. 327.

Rice, J.A., 1984, Controls on silver mineralization in the Creede Formation, Creede, Colorado: Unpub. M.Sc. thesis, Colorado State University (Ft Collins), 135p.

Robinson, R.W., 1981, Ore mineralogy and fluid inclusion study of the southern Amethyst vein system, Creede mining district, Colorado: Unpub. M.Sc. thesis, New Mexico Institute of Mining and Technology (Socorro), 85p.

Roedder, E., 1977, Changes in ore fluid with time, from fluid inclusion studies at Creede, Colorado: Internat. Assoc. on the Genesis of

Ore Deposits Proc. (IAGOD), 4th Symposium, Problems of ore deposition, Varna, Bulgaria, 1974, v. 2, p. 179-185.

Rye, R.O., Plumlee, G.S., Bethke, P.M., and Barton, P.B., Jr., 1988, Stable isotope geochemistry of the Creede, Colorado, hydrothermal system: U.S. Geological Survey Open-file Report 88-356, 40p.

Smith, J.W., 1981, Bachelor Mountain silver deposit, Mineral County, Colorado: Denver Region Exploration Geologist' Society, Field Trip Guidebook, Creede mining district, p. 11-18.

Steven, T.A., and Eaton, G.P., 1975, Environment of ore deposition in the Creede mining district, San Juan Muntains, Colorado: I. Geologic, hydrologic, and geophysical setting: Econ. Geol., v. 70, p. 1023-1037.

Steven, T.A., and Ratte, J.C., 1965, Geology and structural control of ore deposition in the Creede district, San Jaun Mountains, Colorado: U.S. Geological Survey Prof. Paper 487, 90p.

Vergo, N., 1984, Wallrock alteration at the Bulldog Mountain mine, Creede mining district, Colorado: Unpub. M.Sc. thesis, University of Illinois (Urbana-Champaign), 88p.

Vergo, N., 1987, Wallrock alteration at the Bulldog Mountain mine, Crede Colorado [abs]: Geol. Soc. America, Abstracts with Programs, v. 19, no. 5, p. 340.

Wason, D.J., 1983, The Bachelor Mountain silver deposit, Creede mining district, Colorado: Unpub. M.Sc. thesis, State University of New York (Stonybrook), 94p.

APPENDIX B. SAMPLING METHOD, AND ANALYTICAL DETAILS

Drillcore Data

Over 50,000 meters of drillcore from holes drilled throughout the mineralized area were available for examination. The drillcore was sampled during the Summers of 1986 and 1987, and the remains are archived in the U. S. Geological Survey Repository in Denver, Colorado. A working collection consisting of representative samples was prepared and stored in Reston for examination during the study. Samples from drillholes in the area around the North Amethyst mineralization were examined in more detail and description logs prepared.

Underground Workings

Exploratory mine workings developed at the site follow ore shoots and veins. Preliminary sampling of the workings was begun in the summer of 1987. More detailed sampling and photography of the mine working was continued in mid-August of 1987 and January of 1988. A final visit to the mine, to consult with mine geologists, was made in March of 1988.

Samples were collected with two main aims in mind: 1) to prepare a representative collection of samples from all levels and 2) to collect samples that highlight unique features of this deposit compared to other epithermal ore deposits. Well over 1500 pounds of samples were collected from over 100 localities to fulfill these aims.

Petrographic study

General paragenetic relationships and mineralogy were established by the author based on samples collected underground at the North Amethyst vein workings. Detailed paragenetic relationships and

mineralogy were set forth through study of hand samples, thin sections and polished mounts. Humdreds of hand samples, 105 polished thin sections and 85 polished mounts were examined. The samples used in this study include those collected by various researchers from the U.S. Geological Survey including Philip M. Bethke, and Geoffrey S. Plumlee, by Homestake Mining Company personnel including Craig Byington, Stan Caddey, and David M. Vardiman, and by the author as described above.

Electron Microprobe analysis

Minerals analyses were obtained for selected samples by electron microprobe analysis using a fully automated ARL-SEMQ nine-channel electron microprobe at the U.S.Geological Survey in Reston, Virginia. The operating voltage for silicates, and electrum was 15 kV and the beam current was held stable at 0.1 microamps using a beam current regulator. Sphalerite was analysed at 25kV. Carbonate minerals were analysed using an operating voltage of 12 kV and a beam current of 0.05 microamps. Correction procedures for silicates and carbonates are as given by Bence and Albee (1968) and Albee and Ray (1970), and for electrum and sulfides by Colby (1968), and adapted for the USGS microprobe by McGee (1983).

Carbonates

Elements analysed for include Ba, Ca, Mg, Fe, Mn, and Sr. Standards used include synthetic barium glass (BAGL), calcite (USNM 136321), Oberdorf, Austria dolomite (CDOS), Alma Park, New Mexico rhodocrosite (CRAP), Ivigtut, Greenland, siderite (CSIG), and strontianite (CSTR).

Electrums

Elements analysed for include gold and silver. Standards used include gold metal (MEAU) and silver metal (MEAG).

Feldspars

Elements analysed for include K, Ca, Na, Al, Si, Ba, Fe and Mg. Standards used include synthetic barium glass (BAGL), Kahanui, New Zealand hornblende (AMKH), Benson mines, New York orthoclase (FSBO), Lake County, Oregon plagioclase (FSBO), Tiburon Penn., California albite (FSTA), Brazil quartz (OXQZ), synthetic tephoite (OLST), synthetic periclase (OXPE), and synthetic vanadium oxide (OXVA).

Manganese silicates

Elements analysed for include Ca, Al, Fe, Mn, Zn, Mg, and Si. Standards used include Lake County, Oregon plagioclase (FSLC), Rockport, Massachusetts fayalite (OLRF), synthetic tephroite (OLST), Brazil gahnite (OXGH), M. olivine (OLMJ), synthetic silica glass (GLSI), synthetic bixbyite (OXPA), synthetic periclase (OXPE), and synthetic vanadium oxide (OXVA).

Sphalerite

Elements analysed for include Fe, Cd, Mn, Zn, and S. Standards used include synthetic sphalerites (ZnS, S22,S15,MN3) and synthetic vanadium oxide (OXVA).

X-ray diffraction analysis

X-ray diffraction patterns were obtained on selected samples of fine-grained material to aid in petrographic and microprobe study. Patterns were indexed using quartz as an internal standard and ASTM tables for values.

References

Albee, A.L., and Ray, L., 1970, Correction factors for electron probe microanalysis of silicates, oxides, carbonates, phosphates, and sulfates: Analytical Chemistry, v. 42, p. 1408-1414.

Bence, A.E., and Albee, A.L., 1968, Empirical correction factors for the electron microanalysis of silicates and oxides: Journal of Geology, v. 76, p. 382-403.

Colby, J.W., 1968, Quantitative microprobe analysis of thin insulating films: Advances in X-ray Analysis, v. 11, p. 287-305.

McGee, J.J., 1983, $ANBA - a rapid, combined data acquisition and correction program for the SEMQ electron microprobe: U.S. Geological Survey Open-file Report 83-817, 47p.

APPENDIX C

Electron microprobe analyses of carbonates, electrums, manganese-silicates, sphalerites and potassium feldspar. Analyses are listed by reference number (Ref. No.), sample location number (ID), and level of mine workings (Level). All named localities are plotted in Figure 6 of Foley (1990a).

APPENDIX C: CARBONATE ANALYSES

Ref.No.	2	273	247	100	275	249	246	248	103	104
ID	CDOS	AA1	AA1	AA3	AA1	AA1	A1	AA1	AA4	AA4
Level		10000	10000	10000	10000	10000	10000	10000	10000	10000
CaO	29.77	47.79	48.39	46.87	47.49	47.63	46.93	47.56	46.76	46.19
MgO	22.24	0.34	0.39	0.46	0.60	0.44	0.50	0.44	0.47	0.63
FeO	-	0.68	0.40	1.05	1.09	0.46	0.51	0.47	1.08	1.19
MnO	-	6.51	7.56	7.44	7.68	7.78	7.84	7.93	8.05	8.01
SrO	0.04	0.10	0.29	0.10	0.11	0.21	0.16	0.19	0.10	0.11
BaO	-	0.07	0.08	0.12	0.08	0.08	0.07	0.09	0.07	0.08
CO2*	47.66	42.39	43.48	42.62	43.43	43.08	42.64	43.12	42.93	42.70
TOTAL	99.71	97.88	100.59	98.6	100.48	99.68	98.65	99.80	99.46	98.91
#Ca	0.98	1.77	1.75	1.73	1.72	1.74	1.73	1.73	1.71	1.70
#Mg	1.02	0.02	0.02	0.02	0.03	0.02	0.03	0.02	0.02	0.03
#Fe	-	0.02	0.01	0.03	0.03	0.01	0.01	0.01	0.03	0.03
#Mn	-	0.19	0.22	0.22	0.22	0.22	0.23	0.23	0.23	0.23
#Sr	0.00	0.00	0.01	0.00	0.00	0.00	0.00	0.00	0.00	0.00
#Ba	-	0.00	0.00	0.00	0.00	0.00	0.00	0.00	0.00	0.00
#C	2.00	2.00	2.00	2.00	2.00	2.00	2.00	2.00	2.00	2.00

Ref. No.	115	291	251	116	293	292	101	255	254	113
ID	AA4	AA4	AA4	AA4	AA4	AA4	AA4	AA3	AA3	AA4
Level	10000	10000	10000	10000	10000	10000	10000	10000	10000	10000
CaO	47.52	47.65	46.19	44.63	46.96	47.28	44.95	46.81	46.11	46.11
MgO	0.16	0.17	0.13	1.40	0.19	0.21	0.94	0.09	0.13	0.23
FeO	0.64	0.52	0.91	1.90	0.65	0.78	1.43	0.70	0.85	0.73
MnO	8.08	8.13	8.12	8.34	8.29	8.44	8.54	9.08	9.03	9.15
SrO	0.09	0.12	0.13	0.05	0.12	0.12	0.12	0.07	0.10	0.08
BaO	0.12	0.05	0.10	0.06	0.06	0.07	0.07	0.05	0.08	0.03
CO2	42.94	43.01	42.07	42.93	42.67	43.12	42.55	42.94	42.52	42.60
TOTAL	99.55	99.65	97.65	99.31	98.94	100.02	98.60	99.74	98.82	98.93
#Ca	1.74	1.74	1.72	1.63	1.73	1.72	1.66	1.71	1.70	1.70
#Mg	0.01	0.01	0.01	0.07	0.01	0.01	0.05	0.00	0.01	0.01
#Fe	0.02	0.01	0.03	0.05	0.02	0.02	0.04	0.02	0.02	0.02
#Mn	0.23	0.23	0.24	0.24	0.24	0.24	0.25	0.26	0.26	0.27
#Sr	0.00	0.00	0.00	0.00	0.00	0.00	0.00	0.00	0.00	0.00
#Ba	0.00	0.00	0.00	0.00	0.00	0.00	0.00	0.00	0.00	0.00
#CO3	2.00	2.00	2.00	2.00	2.00	2.00	2.00	2.00	2.00	2.00

APPENDIX C: CARBONATE ANALYSES

Ref. No.	253	252	256	16	8	40	10	38	5	6
ID	AA3	AA3	AA3	BB	BB	BB	BB	BB	BB	BB
Level	10000	10000	10000	10250	10250	10250	10250	10250	10250	10250
CaO	46.76	46.39	46.25	45.25	41.73	41.53	40.76	40.95	37.39	38.84
MgO	0.10	0.15	0.09	0.08	0.07	0.04	0.11	0.06	0.32	0.04
FeO	0.77	0.86	0.60	0.22	0.16	0.08	0.20	0.09	2.00	0.18
MnO	9.33	9.63	10.07	10.65	15.04	15.65	15.64	16.17	17.55	17.84
SrO	0.07	0.08	0.07	0.12	0.06	0.03	0.05	0.04	0.06	0.06
BaO	0.09	0.04	0.07	0.01	-	-	0.01	0.03	-	-
CO2	43.12	43.12	43.06	42.39	42.28	42.41	41.96	42.31	41.83	41.73
TOTAL	100.24	100.27	100.21	98.72	99.34	99.74	98.73	99.65	99.15	98.69
#Ca	1.70	1.69	1.69	1.68	1.55	1.54	1.52	1.52	1.40	1.46
#Mg	0.01	0.01	0.00	0.00	0.00	0.00	0.01	0.00	0.02	0.00
#Fe	0.02	0.02	0.02	0.01	0.00	0.00	0.01	0.00	0.06	0.01
#Mn	0.27	0.28	0.29	0.31	0.44	0.46	0.46	0.47	0.52	0.53
#Sr	0.00	0.00	0.00	0.00	0.00	0.00	0.00	0.00	0.00	0.00
#Ba	0.00	0.00	0.00	0.00	-	-	0.00	0.00	-	-
#CO3	2.00	2.00	2.00	2.00	2.00	2.00	2.00	2.00	2.00	2.00

Ref. No.	7	4	12	45	47	46	34	36	35	129
ID	BB	BB	BB	EQ16	EQ10	EQ10	BB	BB	BB	EQ16
Level	10250	10250	10250	10000	10000	10000	10250	10250	10250	10000
CaO	38.09	36.15	37.45	37.74	37.54	37.62	25.10	25.21	21.94	12.35
MgO	0.08	0.43	0.03	0.06	-	0.07	-	-	-	0.03
FeO	0.18	1.66	1.17	0.04	0.08	0.06	0.55	0.55	0.67	0.73
MnO	18.10	18.40	18.87	19.21	19.54	19.56	32.52	32.67	35.70	46.20
SrO	0.08	0.05	0.10	0.15	0.14	0.18	0.01	0.01	0.01	-
BaO	-	0.01	-	-	0.03	-	-	-	0.01	0.13
CO2	41.35	41.30	40.49	40.51	40.52	40.28	39.51	39.69	39.39	38.87
TOTAL	97.88	98.00	98.11	97.71	97.85	97.77	97.69	98.13	97.72	98.31
#Ca	1.45	1.37	1.41	1.40	1.40	1.39	0.98	0.98	0.85	0.50
#Mg	0.00	0.02	0.00	0.00	-	0.00	-	-	-	0.00
#Fe	0.01	0.05	0.01	0.00	0.00	0.00	0.02	0.02	0.02	0.02
#Mn	0.54	0.55	0.58	0.59	0.60	0.60	1.01	1.01	1.12	1.47
#Sr	0.00	0.00	0.00	0.00	0.00	0.00	0.00	0.00	0.00	-
#Ba	-	0.00	-	-	0.00	-	-	-	0.00	0.00
#CO3	2.00	2.00	2.00	2.00	2.00	2.00	2.00	2.00	2.00	2.00

APPENDIX C: CARBONATE ANALYSES

Ref. No.	134	130	133	135	132	128	131	85	60	91
ID	EQ16	EQ16	EQ16	EQ16	EQ16	EQ16	EQ16	EQ16	EQ16	EQ16
Level	10000	10000	10000	10000	10000	10000	10000	10000	10000	10000
CaO	12.11	12.03	12.03	11.89	11.54	11.70	10.74	11.05	11.47	11.86
MgO	-	-	-	-	-	-	0.12	-	-	-
FeO	0.74	0.70	0.73	0.77	0.84	0.68	1.50	0.70	0.63	0.62
MnO	46.95	46.67	46.89	46.92	46.90	47.14	47.34	47.91	47.23	47.84
SrO	-	0.01	0.02	0.01	0.02	0.03	0.02	-	0.01	-
BaO	0.10	0.10	0.18	0.13	0.10	0.07	0.15	0.04	0.02	0.03
CO2	39.11	38.86	39.04	38.95	38.70	38.88	38.90	37.90	37.69	37.66
TOTAL	99.01	98.37	98.89	98.67	98.10	98.50	98.77	97.60	97.05	98.01
#Ca	0.49	0.49	0.48	0.48	0.47	0.47	0.43	0.46	0.46	0.45
#Mg	-	-	-	-	-	-	0.01	-	-	-
#Fe	0.02	0.02	0.02	0.02	0.03	0.02	0.05	0.02	0.02	0.02
#Mn	1.49	1.49	1.49	1.49	1.50	1.50	1.51	1.52	1.52	1.53
#Sr	-	0.00	0.00	0.00	0.00	0.00	0.00	-	0.00	-
#Ba	0.00	0.00	0.00	0.00	0.00	0.00	0.00	0.00	0.00	0.00
#CO3	2.00	2.00	2.00	2.00	2.00	2.00	2.00	2.00	2.00	2.00

Ref. No.	52	96	84	39	41	262	264	76	74	73
ID	EQ16	EQ16	EQ16	BB	BB	AA	AA	MN	MN	MN
Level	10000	10000	10000	10250	10250	10000	10000	10000	10000	10000
CaO	11.88	11.92	11.61	10.49	11.24	9.29	8.41	6.84	6.76	6.27
MgO	-	-	-	-	-	-	-	-	-	-
FeO	0.73	0.60	0.72	1.07	0.99	0.76	0.74	0.56	0.51	0.63
MnO	47.84	47.54	47.46	47.18	47.06	49.09	49.83	52.49	53.20	53.24
SrO	-	-	0.02	0.01	-	-	-	0.03	0.05	0.05
BaO	0.06	0.02	0.02	0.06	0.02	0.10	0.09	0.05	0.05	0.10
CO2	38.06	37.82	37.61	38.18	37.86	38.24	37.99	38.30	38.66	38.39
TOTAL	98.57	97.90	97.44	96.99	97.16	97.48	97.06	98.27	99.23	98.68
#Ca	0.45	0.45	0.44	0.43	0.42	0.38	0.35	0.28	0.27	0.26
#Mg	-	-	-	-	-	-	-	-	-	-
#Fe	0.02	0.02	0.02	0.03	0.03	0.02	0.02	0.02	0.02	0.02
#Mn	1.53	1.53	1.53	1.53	1.54	1.59	1.63	1.70	1.71	1.72
#Sr	-	-	0.00	0.00	-	-	-	0.00	0.00	0.00
#Ba	0.00	0.00	0.00	0.00	0.00	0.00	0.00	0.00	0.00	0.00
#CO3	2.00	2.00	2.00	2.00	2.00	2.00	2.00	2.00	2.00	2.00

APPENDIX C: CARBONATE ANALYSES

Ref. No.	125	127	126	17	1	56	59	66	70	77
ID	AA5	AA5	AA5	BB10	CRAP	MN	MN	MN	MN	MN
Level	10000	10000	10000	10250		10000	10000	10000	10000	10000
CaO	4.78	4.60	4.43	3.52	-	12.83	12.32	24.50	13.33	12.70
MgO	-	-	-	-	-	-	-	-	-	-
FeO	1.06	0.98	0.91	1.33	0.24	0.76	1.13	0.52	0.71	0.77
MnO	55.19	55.25	55.31	54.88	60.61	45.76	45.87	34.50	45.74	46.18
SrO	-	0.02	0.05	0.03	0.04	-	0.03	0.01	-	-
BaO	0.07	0.09	0.11	0.04	0.03	0.12	0.06	0.11	0.12	0.11
CO2	38.66	38.52	38.40	37.65	37.78	38.96	38.85	40.99	39.31	39.12
TOTAL	99.76	99.46	99.21	97.45	98.70	98.43	98.26	100.63	99.21	98.88
#Ca	0.19	0.19	0.18	0.15	-	0.52	0.50	0.94	0.53	0.51
#Mg	-	-	-	-	-	-	-	-	-	-
#Fe	0.03	0.03	0.03	0.04	0.01	0.02	0.04	0.02	0.02	0.02
#Mn	1.77	1.78	1.79	1.81	1.99	1.46	1.47	1.04	1.44	1.46
#Sr	-	0.00	0.00	0.00	0.00	-	0.00	0.00	-	-
#Ba	0.00	0.00	0.00	0.00	0.00	0.00	0.00	0.00	0.00	0.00
#CO3	2.00	2.00	2.00	2.00	2.00	2.00	2.00	2.00	2.00	2.00

Ref. No.	81	82	83	84	85	88	205	206	207	208
ID	MN	MN	MN	MN	MN	MN	A1	A1	A1	A1
Level	10000	10000	10000	10000	10000	10000	10250	10250	10250	10250
CaO	5.92	5.73	6.21	5.14	5.78	6.17	7.46	9.51	6.61	8.04
MgO	-	0.25	0.45	1.25	0.91	2.32	-	-	-	-
FeO	25.74	29.64	35.03	42.63	37.37	35.75	14.95	16.86	8.23	19.25
MnO	29.62	25.40	18.99	11.30	17.45	16.79	37.14	33.74	44.56	32.14
SrO	0.01	0.16	0.04	0.02	-	0.03	0.02	0.01	0.03	0.01
BaO	0.06	0.24	0.09	0.14	0.10	0.10	0.14	0.19	0.08	0.10
CO2	38.81	38.82	38.65	38.57	39.28	39.73	38.10	38.78	37.91	38.07
TOTAL	100.16	100.24	99.46	99.05	100.89	100.89	97.81	99.09	97.42	97.61
#Ca	0.24	0.23	0.25	0.21	0.23	0.24	0.31	0.38	0.27	0.33
#Mg	-	0.01	0.03	0.07	0.05	0.13	-	-	-	-
#Fe	0.81	0.94	1.11	1.35	1.17	1.10	0.48	0.53	0.27	0.62
#Mn	0.95	0.81	0.61	0.36	0.55	0.52	1.21	1.08	1.46	1.05
#Sr	0.00	0.00	0.00	0.00	-	0.00	0.00	0.00	0.00	0.00
#Ba	0.00	0.00	0.00	0.00	0.00	0.00	0.00	0.00	0.00	0.00
#CO3	2.00	2.00	2.00	2.00	2.00	2.00	2.00	2.00	2.00	2.00

APPENDIX C: CARBONATE ANALYSES

Ref. No.	209	210	211	212	213	214	215	216	217	218
ID	A1	A1	A1	A1	A1	A1	A1	A1	A1	A1
Level	10250	10250	10250	10250	10250	10250	10250	10250	10250	10250
CaO	7.95	8.05	7.76	9.33	8.34	7.83	9.44	8.51	7.99	8.98
MgO	-	-	-	-	-	0.01	-	-	-	-
FeO	19.69	21.60	21.63	10.25	12.83	19.59	5.32	5.16	13.14	6.02
MnO	31.54	30.40	30.19	39.71	39.00	31.69	44.68	45.39	38.72	44.17
SrO	-	0.01	0.04	-	-	-	-	-	-	-
BaO	0.08	0.15	0.10	0.09	0.09	0.13	0.10	0.08	0.07	0.05
CO2	37.89	38.46	38.12	38.26	38.63	37.85	38.42	38.02	38.36	38.15
TOTAL	97.15	98.67	97.84	97.64	98.89	97.10	97.96	97.16	98.28	97.37
#Ca	0.33	0.33	0.32	0.38	0.34	0.32	0.39	0.35	0.33	0.37
#Mg	-	-	-	-	-	0.00	-	-	-	-
#Fe	0.64	0.69	0.70	0.33	0.41	0.63	0.17	0.17	0.42	0.19
#Mn	1.03	0.98	0.98	1.29	1.25	1.04	1.44	1.48	1.25	1.44
#Sr	-	0.00	0.00	-	-	-	-	-	-	-
#Ba	0.00	0.00	0.00	0.00	0.00	0.00	0.00	0.00	0.00	0.00
#CO3	2.00	2.00	2.00	2.00	2.00	2.00	2.00	2.00	2.00	2.00

Ref. No.	219	220	221	222	223	224	226	231	233	234
ID	A1	A1	MO	MO	MO	MO	MO	MO	MO	MO
Level	10250	10250	10000	10000	10000	10000	10000	10000	10000	10000
CaO	8.83	9.78	45.78	48.65	44.61	44.84	6.51	44.21	4.35	4.67
MgO	-	-	-	-	-	-	-	-	-	-
FeO	7.32	14.08	0.28	1.11	0.42	0.27	13.85	0.30	33.63	30.12
MnO	43.91	35.91	12.36	7.14	11.49	11.27	39.03	11.98	22.00	25.17
SrO	-	-	0.05	0.01	0.08	0.02	0.05	0.03	0.03	-
BaO	0.11	0.08	0.05	0.05	0.09	0.12	0.06	0.07	0.10	0.13
CO2	38.69	38.60	43.80	43.31	42.45	42.39	37.85	42.34	37.70	37.77
TOTAL	98.86	98.45	102.32	100.27	99.14	98.91	97.35	98.93	97.81	97.86
#Ca	0.36	0.40	1.64	1.76	1.65	1.66	0.27	1.64	0.18	0.19
#Mg	-	-	-	-	-	-	-	-	-	-
#Fe	0.23	0.45	0.01	0.03	0.01	0.01	0.45	0.01	1.09	0.98
#Mn	1.41	1.15	0.35	0.20	0.34	0.33	1.28	0.35	0.72	0.83
#Sr	-	-	0.00	0.00	0.00	0.00	0.00	0.00	0.00	-
#Ba	0.00	0.00	0.00	0.00	0.00	0.00	0.00	0.00	0.00	0.00
#CO3	2.00	2.00	2.00	2.00	2.00	2.00	2.00	2.00	2.00	2.00

APPENDIX C: CARBONATE ANALYSES

Ref. No.	237	238	242
ID	MO	MO	BA
Level	10000	10000	10250
CaO	4.35	4.66	47.24
MgO	-	-	-
FeO	39.81	36.19	0.59
MnO	15.60	19.18	9.74
SrO	-	-	0.20
BaO	0.13	0.11	0.10
CO2	37.52	37.76	43.59
TOTAL	97.41	97.90	101.46
#Ca	0.18	0.19	1.70
#Mg	-	-	-
#Fe	1.30	1.17	0.02
#Mn	0.52	0.63	0.28
#Sr	-	-	0.00
#Ba	0.00	0.00	0.00
#CO3	2.00	2.00	2.00

APPENDIX C: ELECTRUM ANALYSES

Ref. No.	12	13	14	16	21	23	24	25	27	28
ID	AA	AA	AA	AA	AA	AA	AA	MM	MM	MM
Level	10000	10000	10000	10000	10000	10000	10000	10000	10000	10000
Ag	57.52	54.68	54.85	56.25	50.62	51.42	51.02	41.48	41.70	49.33
Au	40.74	43.56	43.40	42.49	48.12	46.70	47.41	57.11	56.55	49.31
TOTAL	98.26	98.24	98.25	98.74	98.74	98.12	98.43	98.59	98.25	98.64
						Atomic fraction				
#Ag+1	0.72	0.70	0.70	0.71	0.66	0.67	0.66	0.57	0.57	0.65
#Au+1	0.28	0.30	0.30	0.29	0.34	0.33	0.34	0.43	0.43	0.35

Ref. No.	29	30	31	34	37	38	39	42	44	45
ID	MM	MM	MM	MM	BM	BM	BM	BM	BM	BM
Level	10000	10000	10000	10000	10250	10250	10250	10250	10250	10250
Ag	42.77	44.30	43.93	42.53	51.08	36.80	38.84	43.98	38.74	38.42
Au	56.02	54.93	54.81	57.40	47.26	61.87	58.83	54.17	59.99	59.93
TOTAL	98.79	99.23	98.74	99.93	98.34	98.67	97.67	98.15	98.73	98.35
						Atomic fraction				
#Ag+1	0.58	0.60	0.59	0.58	0.66	0.52	0.55	0.60	0.54	0.54
#Au+1	0.42	0.40	0.41	0.42	0.34	0.48	0.45	0.40	0.46	0.46

Ref. No.	46	47	48	49	50	51	52	53	54	55
ID	BM	BM	BM	BM	BM	BM	BM	BM	R	R
Level	10250	10250	10250	10250	10250	10250	10250	10250	10000	10000
Ag	38.58	43.55	42.08	41.53	41.63	42.70	43.80	44.31	37.02	36.76
Au	59.96	56.15	59.20	59.34	57.77	56.84	56.97	55.58	62.47	61.31
TOTAL	98.54	99.70	101.28	100.87	99.40	99.54	100.77	99.89	99.49	98.07
						Atomic fraction				
#Ag+1	0.54	0.59	0.56	0.56	0.57	0.58	0.58	0.59	0.52	0.52
#Au+1	0.46	0.41	0.44	0.44	0.43	0.42	0.42	0.41	0.48	0.48

APPENDIX C: ELECTRUM ANALYSES

Ref. No.	56	57	58	59	60	61	62	63	64	65
ID	R	R	R	BN	BN	BN	BN	BN	BN	BN
Level	10000	10000	10000	10250	10250	10250	10250	10250	10250	10250
Ag	41.40	38.53	38.80	39.87	44.03	42.27	41.76	40.08	41.83	39.68
Au	56.65	59.73	59.65	58.28	54.10	56.39	56.38	58.68	56.96	58.62
TOTAL	98.05	98.26	98.45	98.15	98.13	98.66	98.14	98.76	98.79	98.30
					Atomic fraction					
#Ag+1	0.57	0.54	0.54	0.56	0.60	0.58	0.57	0.56	0.57	0.55
#Au+1	0.43	0.46	0.46	0.44	0.40	0.42	0.43	0.44	0.43	0.45

Ref. No.	66	67	69	70	72	73	74	76
ID	DMV3a	DMV3a	DMV3a	DMV3a	DMV3a	DMV3a	DMV3a	DMV3a
Level	10315	10315	10315	10315	10315	10315	10315	10315
Ag	39.15	39.74	38.65	38.11	44.04	33.40	32.90	35.41
Au	58.90	58.29	59.74	60.66	54.31	64.34	65.73	63.88
TOTAL	98.05	98.03	98.39	98.77	98.35	97.74	98.63	99.29
					Atomic fraction			
#Ag+1	0.55	0.55	0.54	0.53	0.60	0.49	0.48	0.50
#Au+1	0.45	0.45	0.46	0.47	0.40	0.51	0.52	0.50

APPENDIX C: FELDSPAR ANALYSES

Ref No.	1)	2)	3)	4)	5)	6)	7)	8)	9)	10)
ID	M13xl	M13xl	M13xl	M13xl	M13xl	M13xl	M13xl	M13xl	M13xl	M13xl
Level	10000	10000	10000	10000	10000	10000	10000	10000	10000	10000
K2O	16.10	16.00	16.10	16.10	16.06	15.37	15.96	15.50	15.58	15.59
Na2O	0.37	0.32	0.34	0.27	0.30	0.29	0.33	0.30	0.28	0.29
CaO	-	-	-	-	-	0.05	0.05	-	0.01	0.02
BaO	0.07	0.12	0.05	0.05	0.07	0.35	0.12	0.45	0.37	0.31
FeO	0.22	0.23	0.22	0.24	0.22	0.25	0.22	0.21	0.24	0.22
MgO	0.19	0.14	0.17	0.16	0.15	0.19	0.15	0.18	0.18	0.17
Al2O3	18.58	18.47	18.43	18.29	18.38	18.14	18.56	18.31	18.04	18.24
SiO2	64.90	65.33	65.06	65.15	65.17	63.33	65.16	64.12	64.11	64.17
Total	100.43	100.61	100.37	100.26	100.35	97.97	100.55	99.07	98.81	99.01
#K	0.95	0.94	0.95	0.95	0.94	0.93	0.94	0.92	0.93	0.93
#Na+1	0.03	0.03	0.03	0.02	0.03	0.03	0.03	0.03	0.03	0.03
#Ca+2	-	-	-	-	-	0.00	0.00	-	0.00	0.00
#Ba+2	0.00	0.00	0.00	0.00	0.00	0.01	0.00	0.01	0.01	0.01
#Fe+2	0.01	0.01	0.01	0.01	0.01	0.01	0.01	0.01	0.01	0.01
#Mg+2	0.01	0.01	0.01	0.01	0.01	0.01	0.01	0.01	0.01	0.01
#Al+3	1.01	1.00	1.00	0.99	1.00	1.01	1.00	1.01	0.99	1.00
#Si+4	2.99	3.00	3.00	3.00	3.00	2.99	2.99	2.99	3.00	3.00

Ref No.	11)	12)	13)	14)	16)	17)	18)	19)	20)	1)
ID	M13xl	M13xl	M13xl	M13xl	M13xl	M13xl	M13xl	M13xl	M13xl	M13mx
Level	10000	10000	10000	10000	10000	10000	10000	10000	10000	10000
K2O	15.79	15.87	16.01	15.81	16.11	16.00	16.18	15.98	16.07	15.74
Na2O	0.29	0.28	0.39	0.24	0.34	0.33	0.31	0.38	0.39	0.29
CaO	0.10	0.05	-	-	-	-	-	-	-	-
BaO	0.13	0.19	0.18	0.20	0.08	0.24	0.14	0.35	0.26	0.25
FeO	0.38	0.32	0.24	0.24	0.24	0.22	0.21	0.17	0.22	0.01
MgO	0.23	0.21	0.15	0.17	0.19	0.15	0.20	0.19	0.18	0.02
Al2O3	18.77	18.75	18.69	18.27	18.69	18.92	18.53	18.84	18.62	18.22
SiO2	65.76	65.56	65.50	65.95	65.91	65.78	65.69	65.42	65.57	64.62
Total	101.45	101.23	101.16	100.88	101.56	101.64	101.26	101.33	101.31	99.15
#K	0.92	0.92	0.93	0.92	0.93	0.93	0.94	0.93	0.94	0.93
#Na+1	0.03	0.02	0.03	0.02	0.03	0.03	0.03	0.03	0.03	0.03
#Ca+2	0.00	0.00	-	-	-	-	-	-	-	-
#Ba+2	0.00	0.00	0.00	0.00	0.00	0.00	0.00	0.01	0.00	0.00
#Fe+2	0.01	0.01	0.01	0.01	0.01	0.01	0.01	0.01	0.01	0.00
#Mg+2	0.02	0.01	0.01	0.01	0.01	0.01	0.01	0.01	0.01	0.00
#Al+3	1.01	1.01	1.01	0.98	1.00	1.01	1.00	1.01	1.00	1.00
#Si+4	2.99	2.99	2.99	3.01	3.00	2.99	3.00	2.99	2.99	3.01

APPENDIX C: FELDSPAR ANALYSES

Ref No.	2)	3)	4)	5)	6)	7)	8)	9)	10)	11)
ID	M13mx	M13mx	M13mx	M13mx	M13mx	M13mx	M13mx	M13mx	M13mx	M13mx
Level	10000	10000	10000	10000	10000	10000	10000	10000	10000	10000
K2O	15.45	15.39	15.32	15.39	15.77	15.56	15.29	15.44	15.83	15.52
Na2O	0.24	0.38	0.41	0.54	0.29	0.44	0.47	0.58	0.37	0.47
CaO	-	-	0.03	-	-	0.02	-	-	-	-
BaO	0.41	0.28	0.31	0.21	-	0.30	0.31	0.17	0.14	0.21
FeO	-	0.04	0.05	0.02	-	0.04	0.03	0.01	-	0.01
MgO	0.03	0.04	0.07	-	0.01	0.02	0.04	0.03	0.03	0.03
Al2O3	17.93	18.37	18.36	18.56	18.36	18.46	18.46	18.40	18.53	18.46
SiO2	63.99	64.25	64.01	64.64	64.82	64.57	63.74	64.80	64.66	64.40
Total	98.05	98.75	98.56	99.36	99.25	99.41	98.34	99.43	99.56	99.10
#K	0.93	0.92	0.91	0.91	0.93	0.92	0.92	0.91	0.94	0.92
#Na+1	0.02	0.03	0.04	0.05	0.03	0.04	0.04	0.05	0.03	0.04
#Ca+2	-	-	0.00	-	-	0.00	-	-	-	-
#Ba+2	0.01	0.01	0.01	0.00	-	0.01	0.01	0.00	0.00	0.00
#Fe+2	-	0.00	0.00	0.00	-	0.00	0.00	0.00	-	0.00
#Mg+2	0.00	0.00	0.00	-	0.00	0.00	0.00	0.00	0.00	0.00
#Al+3	0.99	1.01	1.01	1.01	1.00	1.01	1.02	1.00	1.01	1.01
#Si+4	3.01	3.00	3.00	3.00	3.01	3.00	2.99	3.00	3.00	3.00

Ref No.	12)	13)	14)	15)	16)	17)	18)	19)	20)	21)
ID	M13mx	M13mx	M13mx	M13mx	M13mx	M13mx	M13mx	M13mx	M13mx	M13mx
Level	10000	10000	10000	10000	10000	10000	10000	10000	10000	10000
K2O	15.65	15.58	15.67	15.44	15.71	15.47	15.76	15.32	14.05	15.28
Na2O	0.34	0.36	0.30	0.41	0.35	0.30	0.32	0.56	1.54	0.61
CaO	0.03	-	-	0.02	-	-	-	-	0.07	-
BaO	0.09	0.38	0.18	0.13	0.15	0.21	0.05	0.35	0.30	0.31
FeO	0.02	0.01	-	-	-	0.02	0.02	0.03	0.09	-
MgO	-	0.03	0.02	0.03	0.04	0.02	0.03	0.05	0.03	0.02
Al2O3	17.94	18.40	18.18	17.83	18.30	18.13	18.44	17.96	18.63	18.04
SiO2	64.15	64.78	64.51	64.61	64.45	64.44	64.56	64.13	64.89	64.23
Total	98.22	99.54	98.86	98.47	99.00	98.59	99.18	98.40	99.60	98.49
#K	0.94	0.92	0.93	0.92	0.93	0.92	0.93	0.92	0.83	0.91
#Na+1	0.03	0.03	0.03	0.04	0.03	0.03	0.03	0.05	0.14	0.06
#Ca+2	0.00	-	-	0.00	-	-	-	-	0.00	-
#Ba+2	0.00	0.01	0.00	0.00	0.00	0.00	0.00	0.01	0.01	0.01
#Fe+2	0.00	0.00	-	-	-	0.00	0.00	0.00	0.00	-
#Mg+2	-	0.00	0.00	0.00	0.00	0.00	0.00	0.00	0.00	0.00
#Al+3	0.99	1.01	1.00	0.98	1.00	1.00	1.01	0.99	1.01	1.00
#Si+4	3.01	3.00	3.01	3.02	3.00	3.01	3.00	3.01	2.99	3.01

APPENDIX C: FELDSPAR ANALYSES

Ref No.	22)	23)	24)	25)	26)	27)	28)	29)	30)	31)
ID	M13mx	M13ph	M13ph	M13ph	M13ph	M13ph	M13ph	M13ph	M13ph	M13ph
Level	10000	10000	10000	10000	10000	10000	10000	10000	10000	10000
K2O	15.42	15.63	15.32	15.52	15.64	15.77	15.64	15.74	15.65	15.50
Na2O	0.42	0.35	0.52	0.42	0.31	0.19	0.22	0.28	0.24	0.32
CaO	0.02	-	-	-	-	-	-	-	0.01	-
BaO	0.37	-	0.30	0.12	0.14	0.14	0.18	0.28	0.23	0.07
FeO	0.04	-	0.02	0.01	0.03	0.02	0.04	0.02	0.03	0.02
MgO	0.02	0.04	0.04	0.01	0.03	-	-	0.02	0.05	0.02
Al2O3	18.21	18.24	18.03	18.57	18.48	18.54	18.35	18.61	18.49	18.49
SiO2	63.99	64.70	64.38	64.96	64.87	65.29	64.67	64.38	65.14	64.81
Total	98.49	98.96	98.61	99.61	99.50	99.95	99.10	99.33	99.84	99.23
#K	0.92	0.93	0.91	0.91	0.92	0.93	0.93	0.93	0.92	0.92
#Na+1	0.04	0.03	0.05	0.04	0.03	0.02	0.02	0.03	0.02	0.03
#Ca+2	0.00	-	-	-	-	-	-	-	0.00	-
#Ba+2	0.01	-	0.01	0.00	0.00	0.00	0.00	0.01	0.00	0.00
#Fe+2	0.00	-	0.00	0.00	0.00	0.00	0.00	0.00	0.00	0.00
#Mg+2	0.00	0.00	0.00	0.00	0.00	-	-	0.00	0.00	0.00
#Al+3	1.01	1.00	0.99	1.01	1.01	1.01	1.01	1.02	1.01	1.01
#Si+4	3.00	3.01	3.01	3.00	3.00	3.01	3.01	2.99	3.01	3.00

Ref No.	32)	33)	34)	35)	36)	37)	38)	39)	40)	41)
ID	AA27	AA27	AA27	AA27	AA27	AA27	AA27	AA27	AA27	AA27
Level	10000	10000	10000	10000	10000	10000	10000	10000	10000	10000
K2O	15.52	15.75	15.83	15.57	15.70	15.19	15.61	15.79	15.82	15.58
Na2O	0.29	0.38	0.17	0.22	0.19	0.43	0.19	0.22	0.23	0.36
CaO	-	-	-	0.04	0.01	-	-	-	-	0.05
BaO	0.53	0.18	0.22	0.27	0.24	0.30	0.73	0.20	0.25	0.10
FeO	-	0.04	-	0.05	0.02	0.07	0.07	0.01	-	-
MgO	-	0.01	0.01	0.01	0.01	0.04	0.03	0.02	0.03	0.05
Al2O3	18.70	18.53	18.28	18.30	18.28	18.66	18.65	18.37	18.56	18.65
SiO2	64.56	64.96	64.69	64.50	64.60	64.50	63.89	65.48	64.56	64.48
Total	99.60	99.85	99.20	98.96	99.05	99.19	99.17	100.09	99.45	99.27
#K	0.92	0.93	0.94	0.93	0.93	0.90	0.93	0.93	0.94	0.92
#Na+1	0.03	0.03	0.02	0.02	0.02	0.04	0.02	0.02	0.02	0.03
#Ca+2	-	-	-	0.00	0.00	-	-	-	-	0.00
#Ba+2	0.01	0.00	0.00	0.00	0.00	0.01	0.01	0.00	0.00	0.00
#Fe+2	-	0.00	-	0.00	0.00	0.00	0.00	0.00	-	-
#Mg+2	-	0.00	0.00	0.00	0.00	0.00	0.00	0.00	0.00	0.00
#Al+3	1.02	1.01	1.00	1.00	1.00	1.02	1.03	1.00	1.02	1.02
#Si+4	2.99	3.00	3.01	3.01	3.01	2.99	2.98	3.01	3.00	2.99

APPENDIX C: FELDSPAR ANALYSES

Ref No.	42)	43)	30)	31)	32)	33)	34)	35)	1)	2)
ID	AA27	AA27	AA27	AA27	AA27	AA27	AA27	AA27	EQ16	EQ16
Level	10000	10000	10000	10000	10000	10000	10000	10000	10000	10000
K2O	15.77	15.67	15.16	15.61	15.72	15.54	15.67	15.64	15.71	15.82
Na2O	0.17	0.26	0.20	0.19	0.17	0.19	0.18	0.18	0.20	0.16
CaO	0.05	0.05	0.12	-	-	-	0.01	-	0.01	-
BaO	0.32	0.21	0.77	1.14	0.64	0.65	0.40	0.71	0.36	0.30
FeO	0.02	0.01	0.02	-	0.02	0.04	0.02	0.02	0.05	0.03
MgO	0.02	0.03	0.02	0.02	0.03	0.02	-	0.02	0.04	0.03
Al2O3	18.71	18.68	18.40	17.99	17.72	17.77	17.54	17.75	18.44	18.42
SiO2	64.38	64.43	63.98	64.08	64.61	65.07	64.84	64.65	63.97	64.57
Total	99.44	99.34	98.67	99.03	98.91	99.28	98.66	98.97	98.78	99.33
#K	0.93	0.93	0.91	0.93	0.94	0.92	0.94	0.93	0.94	0.94
#Na+1	0.02	0.02	0.02	0.02	0.02	0.02	0.02	0.02	0.02	0.01
#Ca+2	0.00	0.00	0.01	-	-	-	0.00	-	0.00	-
#Ba+2	0.01	0.00	0.01	0.02	0.01	0.01	0.01	0.01	0.01	0.01
#Fe+2	0.00	0.00	0.00	-	0.00	0.00	0.00	0.00	0.00	0.00
#Mg+2	0.00	0.00	0.00	0.00	0.00	0.00	-	0.00	0.00	0.00
#Al+3	1.02	1.02	1.02	0.99	0.98	0.97	0.97	0.98	1.02	1.01
#Si+4	2.99	2.99	3.00	3.01	3.02	3.03	3.03	3.02	2.99	3.00

Ref No.	3)	4)	5)	6)	7)	8)	9)	10)	11)	12)
ID	EQ16	EQ16	EQ16	EQ16	EQ16	EQ16	EQ16	EQ16	EQ16	EQ16
Level	10000	10000	10000	10000	10000	10000	10000	10000	10000	10000
K2O	15.76	15.84	15.84	15.84	15.70	15.74	15.64	15.69	15.63	15.45
Na2O	0.18	0.15	0.18	0.16	0.17	0.17	0.21	0.18	0.24	0.16
CaO	-	-	-	-	-	-	0.01	-	0.01	-
BaO	0.32	0.47	0.17	0.31	0.13	0.11	0.31	0.18	0.38	0.80
FeO	0.04	0.05	-	0.02	0.06	0.03	0.03	0.03	0.01	0.03
MgO	0.03	0.01	0.02	0.01	0.03	0.01	0.02	0.02	0.06	0.05
Al2O3	18.42	18.39	18.37	18.37	18.27	18.26	18.49	18.33	18.50	18.20
SiO2	64.26	64.87	64.85	64.86	64.98	65.04	64.39	64.80	64.53	64.27
Total	99.01	99.78	99.43	99.57	99.34	99.36	99.10	99.23	99.36	98.96
#K	0.94	0.94	0.94	0.94	0.93	0.93	0.93	0.93	0.93	0.92
#Na+1	0.02	0.01	0.02	0.01	0.02	0.02	0.02	0.02	0.02	0.01
#Ca+2	-	-	-	-	-	-	0.00	-	0.00	-
#Ba+2	0.01	0.01	0.00	0.01	0.00	0.00	0.01	0.00	0.01	0.01
#Fe+2	0.00	0.00	-	0.00	0.00	0.00	0.00	0.00	0.00	0.00
#Mg+2	0.00	0.00	0.00	0.00	0.00	0.00	0.00	0.00	0.00	0.00
#Al+3	1.01	1.00	1.00	1.00	1.00	1.00	1.01	1.00	1.01	1.00
#Si+4	3.00	3.00	3.01	3.01	3.01	3.01	3.00	3.01	3.00	3.00

APPENDIX C: FELDSPAR ANALYSES

Ref No.	13)	14)	15)	16)	17)	18)	19)	20)	21)	22)
ID	EQ16	EQ16	EQ16	EQ16	EQ16	EQ16	EQ16	EQ16	EQ16	EQ16
Level	10000	10000	10000	10000	10000	10000	10000	10000	10000	10000
K2O	15.66	15.85	15.27	15.72	15.63	15.58	15.55	15.59	15.31	15.52
Na2O	0.20	0.22	0.20	0.19	0.17	0.18	0.18	0.18	0.20	0.20
CaO	-	0.01	-	0.02	-	-	-	-	-	-
BaO	0.50	0.08	0.80	0.43	1.02	0.45	0.67	0.69	0.68	0.68
FeO	0.03	0.03	0.03	0.06	0.01	-	0.02	0.04	0.10	0.01
MgO	0.02	0.05	0.01	0.03	0.01	0.03	0.02	0.01	0.02	0.05
Al2O3	18.27	18.35	17.97	18.50	18.07	18.05	18.14	18.40	18.10	18.33
SiO2	64.72	65.23	64.97	64.64	63.80	64.14	64.39	64.03	63.12	63.77
Total	99.40	99.82	99.25	99.59	98.71	98.43	98.97	98.94	97.53	98.56
#K	0.93	0.93	0.91	0.93	0.94	0.93	0.93	0.93	0.93	0.93
#Na+1	0.02	0.02	0.02	0.02	0.02	0.02	0.02	0.02	0.02	0.02
#Ca+2	-	0.00	-	0.00	-	-	-	-	-	-
#Ba+2	0.01	0.00	0.01	0.01	0.02	0.01	0.01	0.01	0.01	0.01
#Fe+2	0.00	0.00	0.00	0.00	0.00	-	0.00	0.00	0.00	0.00
#Mg+2	0.00	0.00	0.00	0.00	0.00	0.00	0.00	0.00	0.00	0.00
#Al+3	1.00	1.00	0.99	1.01	1.00	1.00	1.00	1.01	1.01	1.01
#Si+4	3.01	3.01	3.02	3.00	3.00	3.01	3.01	3.00	3.00	2.99

Ref No.	23)	24)	25)	26)	27)	28)	29)	40)	41)	42)
ID	AA27	AA27	AA27	AA27	AA27	AA27	AA27	EQ-16	BK-63	BK-63
Level	10000	10000	10000	10000	10000	10000	10000	10000	10250	10250
K2O	15.55	15.53	15.53	15.66	15.63	15.16	15.48	15.60	15.61	15.61
Na2O	0.22	0.16	0.20	0.20	0.17	0.25	0.21	0.23	0.22	0.23
CaO	-	0.01	-	-	-	-	-	-	-	-
BaO	0.65	0.68	0.65	0.54	0.46	1.56	0.85	0.68	0.52	0.60
FeO	0.01	0.04	0.02	0.08	0.07	0.04	0.06	0.07	0.07	0.07
MgO	0.05	0.04	0.04	0.04	0.02	-	0.02	0.02	0.02	0.02
Al2O3	18.15	18.00	18.16	17.94	18.36	18.28	18.19	18.36	18.18	18.27
SiO2	64.25	63.65	64.04	63.96	63.92	62.37	63.41	64.26	65.14	64.70
Total	98.88	98.11	98.64	98.42	98.63	97.66	98.22	99.22	99.76	99.50
#K	0.93	0.93	0.93	0.94	0.93	0.92	0.93	0.93	0.92	0.93
#Na+1	0.02	0.01	0.02	0.02	0.02	0.02	0.02	0.02	0.02	0.02
#Ca+2	-	0.00	-	-	-	-	-	-	-	-
#Ba+2	0.01	0.01	0.01	0.01	0.01	0.03	0.02	0.01	0.01	0.01
#Fe+2	0.00	0.00	0.00	0.00	0.00	0.00	0.00	0.00	0.00	0.00
#Mg+2	0.00	0.00	0.00	0.00	0.00	-	0.00	0.00	0.00	0.00
#Al+3	1.00	1.00	1.00	0.99	1.01	1.03	1.01	1.01	0.99	1.00
#Si+4	3.00	3.00	3.00	3.01	3.00	2.98	2.99	3.00	3.01	3.01

APPENDIX C: FELDSPAR ANALYSES

Ref No.	43)	44)	45)	46)	47)	48)	49)	50)	51)	52)
ID	BK-63	BK-63	BK-63	BK-63	BK-63	BK-63	BK-63	BK-63	BK-63	BK-63
Level	10250	10250	10250	10250	10250	10250	10250	10250	10250	10250
K2O	15.60	15.35	15.40	15.45	15.49	14.98	15.48	14.84	15.07	15.57
Na2O	0.18	0.22	0.26	0.22	0.26	0.20	0.23	0.22	0.21	0.23
CaO	-	0.02	-	-	0.02	-	-	0.02	0.01	0.01
BaO	0.37	0.72	0.87	0.65	0.48	2.26	0.70	2.33	1.95	0.55
FeO	0.06	0.07	0.06	0.06	0.13	0.04	0.10	0.06	0.07	0.08
MgO	0.01	0.04	0.04	0.03	-	0.03	0.03	0.02	0.03	0.03
Al2O3	17.54	17.62	18.45	17.86	18.30	18.58	18.28	18.83	18.75	18.40
SiO2	64.95	64.78	64.54	64.75	64.58	63.04	64.53	62.90	63.33	64.54
Total	98.71	98.82	99.62	99.02	99.26	99.13	99.35	99.22	99.42	99.41
#K	0.93	0.92	0.91	0.92	0.92	0.90	0.92	0.89	0.90	0.92
#Na+1	0.02	0.02	0.02	0.02	0.02	0.02	0.02	0.02	0.02	0.02
#Ca+2	-	0.00	-	-	0.00	-	-	0.00	0.00	0.00
#Ba+2	0.01	0.01	0.02	0.01	0.01	0.04	0.01	0.04	0.04	0.01
#Fe+2	0.00	0.00	0.00	0.00	0.01	0.00	0.00	0.00	0.00	0.00
#Mg+2	0.00	0.00	0.00	0.00	-	0.00	0.00	0.00	0.00	0.00
#Al+3	0.97	0.97	1.01	0.98	1.00	1.03	1.00	1.05	1.04	1.01
#Si+4	3.03	3.03	3.00	3.02	3.00	2.97	3.00	2.96	2.97	3.00

Ref No.	53)	54)	55)	56)	57)	58)	59)	60)	61)	62)
ID	BK-63	BK-63	BK-63	BK-63	BK-63	EQ16f	EQ16f	EQ16f	EQ16f	EQ16f
Level	10250	10250	10250	10250	10250	10000	10000	10000	10000	10000
K2O	15.40	15.42	15.37	15.44	15.43	15.46	15.27	15.09	15.27	15.01
Na2O	0.23	0.28	0.23	0.22	0.20	0.30	0.34	0.30	0.31	0.33
CaO	0.02	0.06	0.03	0.02	0.01	0.03	0.12	0.09	0.08	0.09
BaO	1.19	0.82	0.81	0.76	0.63	0.24	0.18	0.13	0.18	0.20
FeO	0.05	0.31	0.37	0.30	0.19	0.04	0.15	0.09	0.09	0.14
MgO	0.01	0.02	0.05	0.03	0.02	0.01	0.03	0.03	0.02	-
Al2O3	18.55	18.57	18.28	18.45	18.09	18.39	18.06	18.68	18.37	17.57
SiO2	63.87	64.16	64.45	64.44	65.03	64.39	65.00	64.28	64.56	64.02
Total	99.32	99.64	99.59	99.66	99.60	98.86	99.15	98.69	98.88	97.36
#K	0.92	0.92	0.91	0.92	0.91	0.92	0.90	0.90	0.91	0.90
#Na+1	0.02	0.03	0.02	0.02	0.02	0.03	0.03	0.03	0.03	0.03
#Ca+2	0.00	0.00	0.00	0.00	0.00	0.00	0.01	0.00	0.00	0.00
#Ba+2	0.02	0.01	0.01	0.01	0.01	0.00	0.00	0.00	0.00	0.00
#Fe+2	0.00	0.01	0.01	0.01	0.01	0.00	0.01	0.00	0.00	0.01
#Mg+2	0.00	0.00	0.00	0.00	0.00	0.00	0.00	0.00	0.00	-
#Al+3	1.02	1.02	1.00	1.01	0.99	1.01	0.99	1.03	1.01	0.98
#Si+4	2.99	2.99	3.00	2.99	3.02	3.00	3.02	2.99	3.00	3.03

APPENDIX C: FELDSPAR ANALYSES

Ref No.	63)	64)	65)	66)	67)	68)	69)	70)	71)	72)
ID	EQ16f	EQ16f	EQ16f	EQ16f	EQ16f	EQ16f	EQ16f	EQ16f	EQ16f	EQ16f
Level	10000	10000	10000	10000	10000	10000	10000	10000	10000	10000
K2O	15.49	15.44	15.46	15.40	15.35	15.63	15.68	15.24	15.39	15.33
Na2O	0.26	0.24	0.25	0.39	0.55	0.27	0.40	0.50	0.41	0.45
CaO	0.01	0.05	0.03	-	-	-	-	-	-	-
BaO	0.26	0.28	0.27	0.03	0.03	0.14	0.08	0.04	0.09	0.01
FeO	0.05	0.03	0.04	-	0.02	-	0.04	0.03	0.06	0.04
MgO	0.03	0.04	0.03	0.02	0.05	0.06	-	0.03	0.05	0.04
Al2O3	18.40	17.99	18.19	17.79	18.06	17.55	17.89	17.72	17.56	18.22
SiO2	64.32	64.31	64.31	65.30	64.72	64.37	64.72	65.35	64.66	65.34
Total	98.82	98.38	98.58	98.93	98.78	98.02	98.81	98.91	98.22	99.43
#K	0.92	0.92	0.92	0.91	0.91	0.94	0.93	0.90	0.92	0.90
#Na+1	0.02	0.02	0.02	0.04	0.05	0.02	0.04	0.05	0.04	0.04
#Ca+2	0.00	0.00	0.00	-	-	-	-	-	-	-
#Ba+2	0.00	0.01	0.00	0.00	0.00	0.00	0.00	0.00	0.00	0.00
#Fe+2	0.00	0.00	0.00	-	0.00	-	0.00	0.00	0.00	0.00
#Mg+2	0.00	0.00	0.00	0.00	0.00	0.00	-	0.00	0.00	0.00
#Al+3	1.01	0.99	1.00	0.97	0.99	0.97	0.98	0.97	0.97	0.99
#Si+4	3.00	3.01	3.01	3.03	3.01	3.03	3.02	3.03	3.03	3.02

Ref No.	73)	74)	75)	76)	77)	78)	79)	80)	81)	82)
ID	EQ2p	EQ2p	EQ2p	EQ2p	EQ2p	EQ2p	EQ2p	EQ2p	EQ2p	EQ2p
Level	10000	10000	10000	10000	10000	10000	10000	10000	10000	10000
K2O	15.16	15.47	15.57	15.65	15.51	15.63	15.78	15.57	15.74	15.62
Na2O	0.63	0.27	0.22	0.35	0.33	0.27	0.26	0.37	0.29	0.34
CaO	0.02	0.02	0.01	-	0.02	-	-	-	-	-
BaO	-	0.32	0.26	0.14	0.09	0.09	0.14	0.10	0.08	0.10
FeO	0.02	0.06	0.09	0.03	0.04	0.01	0.03	0.02	0.04	0.01
MgO	0.04	0.04	0.02	0.05	0.02	0.01	-	0.02	0.03	0.01
Al2O3	18.21	17.86	18.23	18.23	18.18	18.23	18.45	18.34	18.34	18.37
SiO2	65.48	64.18	64.75	64.44	64.63	65.10	64.63	65.10	64.64	64.54
Total	99.56	98.22	99.15	98.89	98.82	99.34	99.29	99.52	99.16	98.99
#K	0.89	0.93	0.92	0.93	0.92	0.92	0.93	0.92	0.93	0.93
#Na+1	0.06	0.02	0.02	0.03	0.03	0.02	0.02	0.03	0.03	0.03
#Ca+2	0.00	0.00	0.00	-	0.00	-	-	-	-	-
#Ba+2	-	0.01	0.00	0.00	0.00	0.00	0.00	0.00	0.00	0.00
#Fe+2	0.00	0.00	0.00	0.00	0.00	0.00	0.00	0.00	0.00	0.00
#Mg+2	0.00	0.00	0.00	0.00	0.00	0.00	-	0.00	0.00	0.00
#Al+3	0.99	0.99	1.00	1.00	1.00	1.00	1.01	1.00	1.00	1.01
#Si+4	3.02	3.01	3.01	3.00	3.01	3.02	3.00	3.01	3.00	3.00

APPENDIX C: FELDSPAR ANALYSES

Ref No.	83)	84)	85)	86)	87)	88)	89)	90)	91)	92)
ID	M-13	M-13	M-13	M-13	M-13	M-13	M-13	M-13	M-13	M-13
Level	10090	10090	10090	10090	10090	10090	10090	10090	10090	10090
K2O	15.68	15.45	15.55	15.71	15.81	15.45	15.58	15.37	15.64	15.35
Na2O	0.30	0.28	0.34	0.29	0.28	0.30	0.45	0.50	0.45	0.42
CaO	-	0.02	-	-	-	-	0.01	-	-	-
BaO	0.18	0.17	0.11	0.15	0.13	0.14	0.29	0.35	0.22	0.54
FeO	0.02	0.01	-	0.02	0.05	0.10	0.07	0.04	0.04	0.01
MgO	0.02	0.01	0.01	0.02	-	0.03	0.02	0.04	0.01	0.01
Al2O3	18.37	17.82	18.01	18.52	18.48	18.19	18.30	18.31	18.28	18.42
SiO2	64.74	64.32	64.23	65.23	64.98	63.03	64.30	64.59	64.50	63.75
Total	99.31	98.08	98.25	99.94	99.73	97.24	99.02	99.20	99.14	98.50
#K	0.93	0.93	0.93	0.92	0.93	0.94	0.93	0.91	0.93	0.92
#Na+1	0.03	0.03	0.03	0.03	0.03	0.03	0.04	0.05	0.04	0.04
#Ca+2	-	0.00	-	-	-	-	0.00	-	-	-
#Ba+2	0.00	0.00	0.00	0.00	0.00	0.00	0.01	0.01	0.00	0.01
#Fe+2	0.00	0.00	-	0.00	0.00	0.00	0.00	0.00	0.00	0.00
#Mg+2	0.00	0.00	0.00	0.00	-	0.00	0.00	0.00	0.00	0.00
#Al+3	1.00	0.99	1.00	1.01	1.01	1.02	1.01	1.00	1.00	1.02
#Si+4	3.00	3.02	3.01	3.01	3.00	2.99	3.00	3.00	3.00	2.99

Ref No.	93)	94)	95)	96)	97)	98)	99)	100
ID	M-13	M-13	M-13	M-13	M-13	M-13	M-13	M-13
Level	10090	10090	10090	10090	10090	10090	10090	10090
K2O	15.60	15.64	15.72	15.85	15.85	15.66	15.53	15.70
Na2O	0.41	0.39	0.30	0.16	0.27	0.29	0.29	0.32
CaO	-	-	-	-	-	-	-	-
BaO	0.10	0.15	0.10	0.38	0.28	0.30	0.78	0.12
FeO	-	0.02	0.05	0.03	0.01	0.02	0.01	0.03
MgO	0.01	0.04	0.02	0.03	0.04	-	0.01	0.03
Al2O3	18.29	18.13	18.37	18.42	18.42	18.40	18.43	18.37
SiO2	64.51	64.44	64.73	64.28	64.64	64.14	63.69	64.73
Total	98.92	98.81	99.29	99.15	99.51	98.81	98.74	99.30
#K	0.93	0.93	0.93	0.94	0.94	0.93	0.93	0.93
#Na+1	0.04	0.04	0.03	0.01	0.02	0.03	0.03	0.03
#Ca+2	-	-	-	-	-	-	-	-
#Ba+2	0.00	0.00	0.00	0.01	0.01	0.01	0.01	0.00
#Fe+2	-	0.00	0.00	0.00	0.00	0.00	0.00	0.00
#Mg+2	0.00	0.00	0.00	0.00	0.00	-	0.00	0.00
#Al+3	1.00	1.00	1.00	1.01	1.01	1.01	1.02	1.00
#Si+4	3.00	3.01	3.00	3.00	3.00	3.00	2.99	3.00

APPENDIX C: SPHALERITE ANALYSES

Ref. No.	10	11	12	13	14	15	16	17	18	19
ID	1M13	1M13	1M13	1M13	1M13	1M13	1M13	1M13	1M13	1M13
Level	10090	10090	10090	10090	10090	10090	10090	10090	10090	10090
Fe+2	0.22	0.47	0.28	0.38	0.49	0.83	0.63	0.54	0.52	0.50
Cd+2	0.32	0.34	0.34	0.34	0.69	0.51	0.66	0.40	0.47	0.53
Mn+2	0.19	0.42	0.23	0.38	0.13	0.34	0.22	0.64	0.34	0.14
Zn+	66.86	66.03	66.65	66.34	66.69	66.12	66.33	66.10	66.32	66.65
S-2	32.69	32.39	32.54	32.73	32.61	32.43	32.61	32.55	32.55	32.71
TOTAL	100.28	99.65	100.04	100.17	100.61	100.23	100.45	100.23	100.20	100.53
#Fe+2	0.00	0.01	0.00	0.01	0.01	0.01	0.01	0.01	0.01	0.01
#Cd+2	0.00	0.00	0.00	0.00	0.01	0.00	0.01	0.00	0.00	0.00
#Mn+2	0.00	0.01	0.00	0.01	0.00	0.01	0.00	0.01	0.01	0.00
#Zn+2	0.99	0.98	0.99	0.98	0.98	0.98	0.98	0.98	0.98	0.98
#S	0.99	0.98	10.98	0.99	0.98	0.98	0.98	0.98	0.98	0.99

Ref. No.	20	21	22	23	24	25	26	27	28	29
ID	2M13	2M13	2M13	2M13	2M13	2M13	2M13	2M13	3M13	3M13
Level	10090	10090	10090	10090	10090	10090	10090	10090	10090	10090
Fe+2	0.58	0.47	0.52	0.82	0.67	0.57	0.66	0.54	0.65	0.55
Cd+2	0.57	0.79	0.63	0.38	0.36	0.34	0.34	0.39	0.36	0.40
Mn+2	0.26	0.10	0.17	0.35	0.43	0.60	0.38	0.60	0.47	0.28
Zn+	66.20	66.42	66.42	65.60	66.09	66.17	66.03	66.08	65.99	66.35
S-2	32.99	32.92	32.87	32.92	32.80	32.86	32.82	32.97	32.87	32.90
TOTAL	100.60	100.70	100.61	100.07	100.35	100.54	100.23	100.58	100.34	100.48
#Fe+2	0.01	0.01	0.01	0.01	0.01	0.01	0.01	0.01	0.01	0.01
#Cd+2	0.00	0.01	0.01	0.00	0.00	0.00	0.00	0.00	0.00	0.00
#Mn+2	0.00	0.00	0.00	0.01	0.01	0.01	0.01	0.01	0.01	0.00
#Zn+2	0.98	0.98	0.98	0.98	0.98	0.98	0.98	0.98	0.98	0.98
#S	1.00	0.99	0.99	1.00	0.99	0.99	0.99	0.99	0.99	0.99

APPENDIX C: SPHALERITE ANALYSES

Ref. No.	30	31	32	33	34	35	36	37	38	39
ID	3M13	3M13	3M13	3M13	3M13	3M13	AA-2	AA-2	AA-2	AA-2
Level	10090	10090	10090	10090	10090	10090	10090	10090	10090	10090
Fe+2	0.51	0.44	0.90	0.66	0.78	0.37	0.80	0.46	0.46	0.48
Cd+2	0.55	0.54	0.39	0.36	0.37	0.34	0.34	0.34	0.35	0.31
Mn+2	0.16	0.12	0.25	0.34	0.29	0.13	0.80	0.61	0.70	0.47
Zn+	66.27	66.51	65.80	66.30	66.05	67.09	64.99	65.93	66.28	66.55
S-2	32.65	32.71	32.91	32.85	32.88	32.86	33.11	32.96	32.89	32.81
TOTAL	100.14	100.32	100.25	100.51	100.37	100.79	100.04	100.30	100.68	100.62
#Fe+2	0.01	0.01	0.02	0.01	0.01	0.01	0.01	0.01	0.01	0.01
#Cd+2	0.00	0.00	0.00	0.00	0.00	0.00	0.00	0.00	0.00	0.00
#Mn+2	0.00	0.00	0.00	0.01	0.01	0.00	0.01	0.01	0.01	0.01
#Zn+2	0.98	0.99	0.98	0.98	0.98	0.99	0.97	0.98	0.98	0.98
#S	0.99	0.99	1.00	0.99	0.99	0.99	1.01	1.00	0.99	0.99

Ref. No.	40	41	42	43	44	45	46	47	48	49
ID	AA-2	AA-2	AA-2	AA-2	AA-2	AA-2	AA-2	AA-2	AA-2	AA-2
Level	10090	10090	10090	10090	10090	10090	10090	10090	10090	10090
Fe+2	0.47	0.55	0.60	0.24	0.27	0.35	0.29	0.17	0.16	0.17
Cd+2	0.33	0.33	0.34	0.34	0.34	0.34	0.34	0.29	0.34	0.31
Mn+2	0.58	0.71	0.50	0.17	0.41	0.67	0.42	0.11	0.09	0.10
Zn+	66.42	65.87	65.77	67.06	67.09	66.36	66.84	67.30	67.14	67.22
S-2	32.85	32.75	33.01	33.06	32.95	32.90	32.97	32.66	32.52	32.59
TOTAL	100.65	100.21	100.22	100.87	101.06	100.62	100.86	100.53	100.25	100.39
#Fe+2	0.01	0.01	0.01	0.00	0.00	0.01	0.01	0.00	0.00	0.00
#Cd+2	0.00	0.00	0.00	0.00	0.00	0.00	0.00	0.00	0.00	0.00
#Mn+2	0.01	0.01	0.01	0.00	0.01	0.01	0.01	0.00	0.00	0.00
#Zn+2	0.98	0.98	0.98	0.99	0.99	0.98	0.98	0.99	0.99	0.99
#S	0.99	0.99	1.00	1.00	0.99	0.99	0.99	0.98	0.98	0.98

APPENDIX C: SPHALERITE ANALYSES

Ref. No.	50	51	52	53	54	55	56	57	58	59
ID	AA-3	AA-3	AA-3	AA-3	AA-3	AA-3	AA-3	AA-3	AA-3	AA-3
Level	10090	10090	10090	10090	10090	10090	10090	10090	10090	10090
Fe+2	0.12	0.31	0.21	0.83	0.57	0.41	0.70	0.47	0.41	0.43
Cd+2	0.34	0.37	0.35	0.31	0.34	0.33	0.33	0.35	0.33	0.34
Mn+2	0.11	0.13	0.12	0.34	0.28	0.61	0.41	0.57	0.45	0.82
Zn+	66.82	66.76	66.79	65.43	66.06	66.28	64.99	65.80	66.47	66.04
S-2	32.73	32.51	32.62	32.91	32.79	32.82	32.96	33.10	33.09	33.25
TOTAL	100.12	100.08	100.09	99.82	100.04	100.45	99.39	100.29	100.75	100.88
#Fe+2	0.00	0.01	0.00	0.01	0.01	0.01	0.01	0.01	0.01	0.01
#Cd+2	0.00	0.00	0.00	0.00	0.00	0.00	0.00	0.00	0.00	0.00
#Mn+2	0.00	0.00	0.00	0.01	0.00	0.01	0.01	0.01	0.01	0.01
#Zn+2	0.99	0.99	0.99	0.98	0.98	0.98	0.98	0.98	0.98	0.98
#S	0.99	0.98	0.99	1.00	0.99	0.99	1.01	1.00	1.00	1.00

Ref. No.	60	61	62	63	64	65	66	67	68	69
ID	BM	BM	BM	BM	BM	BM	BM	BM	BM	BM
Level	10250	10250	10250	10250	10250	10250	10250	10250	10250	10250
Fe+2	0.42	0.46	0.43	0.42	0.68	0.60	0.77	1.58	1.30	1.16
Cd+2	0.32	0.30	0.31	0.32	0.32	0.31	0.34	0.28	0.31	0.31
Mn+2	0.34	0.65	0.45	0.36	0.45	0.63	0.62	0.69	0.64	0.66
Zn+	66.79	66.23	66.58	66.68	65.06	65.98	64.93	64.08	64.04	64.53
S-2	32.78	32.94	32.76	32.54	32.87	32.88	32.97	33.03	32.85	32.87
Total	100.65	100.58	100.53	100.32	99.38	100.40	99.63	99.66	99.14	99.53
#Fe+2	0.01	0.01	0.01	0.01	0.01	0.01	0.01	0.03	0.02	0.02
#Cd+2	0.00	0.00	0.00	0.00	0.00	0.00	0.00	0.00	0.00	0.00
#Mn+2	0.01	0.01	0.01	0.01	0.01	0.01	0.01	0.01	0.01	0.01
#Zn+2	0.98	0.98	0.98	0.98	0.98	0.98	0.97	0.96	0.96	0.97
#S	0.98	0.99	0.99	0.98	1.01	0.99	1.01	1.01	1.01	1.00

APPENDIX C: SPHALERITE ANALYSES

Ref. No.	70	71	72	73	74	75	76	77	78	79
ID	BM	BM	BM	BM	BM	BM	BM	BM	BM	BS
Level	10250	10250	10250	10250	10250	10250	10250	10250	10250	10250
Fe+2	0.79	0.56	0.37	0.38	0.39	0.38	0.40	0.38	0.39	0.46
Cd+2	0.30	0.31	0.29	0.31	0.30	0.30	0.33	0.31	0.29	0.31
Mn+2	0.52	0.41	0.34	0.34	0.34	0.34	0.34	0.35	0.35	0.44
Zn+	65.96	66.45	66.89	66.64	66.91	66.81	66.94	66.85	66.96	66.42
S-2	32.91	32.80	33.05	32.79	33.01	32.95	33.22	33.36	33.21	32.82
TOTAL	100.48	100.53	100.94	100.46	100.95	100.78	101.23	101.25	101.20	100.45
#Fe+2	0.01	0.01	0.01	0.01	0.01	0.01	0.01	0.01	0.01	0.01
#Cd+2	0.00	0.00	0.00	0.00	0.00	0.00	0.00	0.00	0.00	0.00
#Mn+2	0.01	0.01	0.01	0.01	0.01	0.01	0.01	0.01	0.01	0.01
#Zn+2	0.97	0.98	0.99	0.98	0.98	0.98	0.98	0.98	0.98	0.98
#S	0.99	0.99	0.99	0.99	0.99	0.99	1.00	1.00	1.00	0.99

Ref. No.	80	81	82	83	84	85	86	87	88	89
ID	BS	BS	BS	BS	BS	BS	BS	BS	BS	BS
Level	10250	10250	10250	10250	10250	10250	10250	10250	10250	10250
Fe+2	0.33	0.40	0.45	0.46	0.46	0.45	0.48	0.47	0.99	0.43
Cd+2	0.32	0.31	0.32	0.30	0.27	0.32	0.33	0.33	0.31	0.35
Mn+2	1.72	0.98	0.39	0.66	0.46	0.39	0.47	0.51	0.42	0.50
Zn+	65.22	66.02	66.53	66.37	66.59	66.58	65.70	66.24	64.48	66.32
S-2	32.86	32.92	32.50	32.44	32.14	32.72	32.95	32.76	32.75	32.77
TOTAL	100.45	100.63	100.19	100.23	99.92	100.46	99.93	100.31	98.95	100.37
#Fe+2	0.01	0.01	0.01	0.01	0.01	0.01	0.01	0.01	0.02	0.01
#Cd+2	0.00	0.00	0.00	0.00	0.00	0.00	0.00	0.00	0.00	0.00
#Mn+2	0.03	0.02	0.01	0.01	0.01	0.01	0.01	0.01	0.01	0.01
#Zn+2	0.96	0.97	0.98	0.98	0.98	0.98	0.98	0.98	0.97	0.98
#S	0.99	0.99	0.98	0.97	0.97	0.98	1.00	0.99	1.01	0.99

APPENDIX C: SPHALERITE ANALYSES

Ref. No.	90	91	92	93	94	95	96	97	98	99
ID *	BS	BS	BS	BS	BS	BS	BS	BS	BS	BS
Level	10250	10250	10250	10250	10250	10250	10250	10250	10250	10250
Fe+2	0.43	0.56	0.51	0.46	0.44	0.46	0.54	0.48	0.47	0.69
Cd+2	0.30	0.32	0.31	0.32	0.31	0.30	0.31	0.30	0.32	0.33
Mn+2	0.58	0.48	0.42	0.50	0.56	0.49	0.54	0.53	0.51	0.50
Zn+	66.36	66.01	65.31	66.20	66.14	66.46	66.04	65.99	66.03	65.83
S-2	32.21	32.60	32.39	32.49	32.67	32.54	32.57	32.86	32.71	32.63
TOTAL	99.88	99.97	98.94	99.97	100.12	100.25	100.00	100.16	100.04	99.98
#Fe+2	0.01	0.01	0.01	0.01	0.01	0.01	0.01	0.01	0.01	0.01
#Cd+2	0.00	0.00	0.00	0.00	0.00	0.00	0.00	0.00	0.00	0.00
#Mn+2	0.01	0.01	0.01	0.01	0.01	0.01	0.01	0.01	0.01	0.01
#Zn+2	0.98	0.98	0.98	0.98	0.98	0.98	0.98	0.98	0.98	0.98
#S	0.97	0.99	0.99	0.98	0.99	0.98	0.98	0.99	0.99	0.99

Ref.No.	100	101	102	103	104	105	106	107	108	109
ID	BS	X24	X24	X24	X24	X24	X24	X24	X24	X24
Level	10000	10000	10000	10000	10000	10000	10000	10000	10000	10000
Fe+2	0.38	0.90	1.13	0.91	1.05	0.74	0.89	0.67	0.71	0.54
Cd+2	0.33	0.38	0.37	0.37	0.34	0.37	0.37	0.53	0.50	0.41
Mn+2	0.46	0.24	0.26	0.24	0.25	0.18	0.20	0.24	0.23	0.24
Zn+	65.88	66.06	65.95	65.80	65.97	66.69	66.35	66.56	66.63	66.92
S-2	32.05	32.44	32.39	32.22	32.70	32.90	32.66	32.77	32.76	32.55
TOTAL	99.10	100.02	100.10	99.54	100.31	100.88	100.47	100.77	100.83	100.66
#Fe+2	0.01	0.02	0.02	0.02	0.02	0.01	0.02	0.01	0.01	0.01
#Cd+2	0.00	0.00	0.00	0.00	0.00	0.00	0.00	0.00	0.00	0.00
#Mn+2	0.01	0.00	0.00	0.00	0.00	0.00	0.00	0.00	0.00	0.00
#Zn+2	0.98	0.98	0.97	0.98	0.97	0.98	0.98	0.98	0.98	0.98
#S	0.97	0.98	0.97	0.98	0.99	0.99	0.98	0.98	0.98	0.98

APPENDIX C: SPHALERITE ANALYSES

Ref. No.	110	111	112	113	114	115	116	117	118	119
ID	X24	BM	BM	BM	BM	X24	X24	X24	X24	X24
Level	10000	10000	10000	10000	10000	10000	10000	10000	10000	10000
Fe+2	0.64	0.94	0.70	0.77	0.81	0.77	0.66	0.73	0.54	0.75
Cd+2	0.48	0.35	0.38	0.48	0.40	0.35	0.52	0.67	0.41	0.38
Mn+2	0.24	0.22	0.20	0.21	0.21	0.22	0.24	0.27	0.24	0.16
Zn+	66.70	66.22	66.85	66.38	66.48	66.44	66.46	66.21	66.48	66.32
S-2	32.69	32.62	32.56	32.54	32.57	33.02	32.78	32.87	32.76	32.81
TOTAL	100.75	100.35	100.69	100.38	100.47	100.80	100.66	100.75	100.43	100.42
#Fe+2	0.01	0.02	0.01	0.01	0.01	0.01	0.01	0.01	0.01	0.01
#Cd+2	0.00	0.00	0.00	0.00	0.00	0.00	0.00	0.01	0.00	0.00
#Mn+2	0.00	0.00	0.00	0.00	0.00	0.00	0.00	0.00	0.00	0.00
#Zn+2	0.98	0.98	0.98	0.98	0.98	0.98	0.98	0.98	0.98	0.98
#S	0.98	0.98	0.97	0.98	0.98	0.99	0.99	0.99	0.99	0.99

Ref. No.	120	121	122	123	124	125	126	127	128	129
ID	R-18	R-18	R-18	R-18	R-18	R-18	R-18	R-18	R-18	R-18
Level	10000	10000	10000	10000	10000	10000	10000	10000	10000	10000
Fe+2	0.69	1.69	1.33	0.59	1.83	1.62	1.63	1.44	1.45	1.41
Cd+2	0.47	0.39	0.40	0.34	0.39	0.39	0.43	0.35	0.38	0.39
Mn+2	0.22	0.03	0.10	0.06	0.06	0.05	0.03	0.03	0.05	0.15
Zn+	66.38	65.32	65.96	66.90	64.85	65.67	65.40	65.90	65.71	65.29
S-2	32.85	32.51	33.07	33.10	33.05	33.20	32.82	33.17	32.99	32.84
TOTAL	100.61	99.94	100.86	100.99	100.18	100.93	100.31	100.89	100.58	100.08
#Fe+2	0.01	0.03	0.02	0.01	0.03	0.03	0.03	0.02	0.03	0.02
#Cd+2	0.00	0.00	0.00	0.00	0.00	0.00	0.00	0.00	0.00	0.00
#Mn+2	0.00	0.00	0.00	0.00	0.00	0.00	0.00	0.00	0.00	0.00
#Zn+2	0.98	0.97	0.97	0.99	0.96	0.97	0.97	0.97	0.97	0.97
#S	0.99	0.98	0.99	0.99	1.00	1.00	0.99	1.00	0.99	0.99

APPENDIX C: SPHALERITE ANALYSES

Ref. No.	130	131	132	133	134	135	136	138	139	140
ID	R-18	R-18	R-18	R-18	R-18	R-18	R-18	R-18	R-18	R-18
Level	10000	10000	10000	10000	10000	10000	10000	10000	10000	10000
Fe+2	1.63	1.62	0.69	1.54	1.55	1.67	1.72	1.12	0.90	0.67
Cd+2	0.40	0.37	0.35	0.35	0.36	0.43	0.44	0.42	0.42	0.41
Mn+2	0.03	0.04	0.07	0.04	0.03	0.03	0.04	0.21	0.17	0.08
Zn+	65.63	65.38	66.50	65.59	65.64	65.68	65.51	65.84	66.30	66.69
S-2	33.13	32.91	33.19	32.96	33.30	33.28	33.41	33.23	32.95	32.92
TOTAL	100.82	100.32	100.80	100.48	100.88	101.09	101.12	100.82	100.74	100.77
#Fe+2	0.03	0.03	0.01	0.03	0.03	0.03	0.03	0.02	0.02	0.01
#Cd+2	0.00	0.00	0.00	0.00	0.00	0.00	0.00	0.00	0.00	0.00
#Mn+2	0.00	0.00	0.00	0.00	0.00	0.00	0.00	0.00	0.00	0.00
#Zn+2	0.97	0.97	0.98	0.97	0.97	0.97	0.97	0.97	0.98	0.98
#S	1.00	0.99	1.00	0.99	1.00	1.00	1.00	1.00	0.99	0.99

Ref. No.	141	142	143	144	145	146	147	148	149	150
ID	R-18	R-18	R-18	R-18	R-18	R-18	R-18	R-18	MN	MN
Level	10000	10000	10000	10000	10000	10000	10000	10000	10000	10000
Fe+2	0.90	0.39	0.40	4.18	4.78	3.84	4.08	4.22	2.47	2.36
Cd+2	0.41	0.45	0.46	0.40	0.43	0.36	0.36	0.39	0.35	0.34
Mn+2	0.15	0.11	0.12	0.75	0.57	0.49	0.45	0.57	0.10	0.09
Zn+	66.27	67.03	67.02	61.81	61.27	62.59	62.30	61.99	64.77	65.01
S-2	33.03	32.72	32.67	32.97	32.96	33.04	32.93	32.97	32.98	33.08
Total	100.76	100.70	100.67	100.11	100.01	100.32	100.12	100.14	100.67	100.88
#Fe+2	0.02	0.01	0.01	0.07	0.08	0.07	0.07	0.07	0.04	0.04
#Cd+2	0.00	0.00	0.00	0.00	0.00	0.00	0.00	0.00	0.00	0.00
#Mn+2	0.00	0.00	0.00	0.01	0.01	0.01	0.01	0.01	0.00	0.00
#Zn+2	0.98	0.99	0.99	0.91	0.90	0.92	0.92	0.91	0.95	0.95
#S	0.99	0.98	0.98	0.99	0.99	0.99	0.99	0.99	0.99	0.99

APPENDIX C: RHODONITE AND PYROXMANGITE ANALYSES

Ref No.	3	4	5	6	7	8	9	10	11	13
ID	AA271	AA271	AA271	AA271	AA271	AA271	AA271	AA271	AA271	AA271
Level	10000	10000	10000	10000	10000	10000	10000	10000	10000	10000
SiO2	45.99	45.87	45.94	45.18	46.00	46.54	45.41	45.82	45.38	46.26
TiO2	-	-	-	-	-	-	-	-	-	-
Al2O3	0.23	0.22	0.19	0.19	0.28	0.26	0.51	0.25	0.41	0.26
Cr2O3	-	-	-	-	-	-	-	-	-	-
Fe2O3	-	0.00	0.00	0.00	-	-	0.00	0.00	-	0.00
FeO	1.68	1.52	1.49	1.78	1.42	1.88	1.76	1.15	1.59	1.47
MnO	44.00	43.02	43.64	47.87	44.46	41.90	44.37	46.01	45.66	42.34
NiO	-	-	-	-	-	-	-	-	-	-
MgO	0.70	0.65	0.64	0.53	0.62	0.60	0.56	0.41	0.49	0.60
CaO	6.93	7.62	7.63	3.68	6.77	8.70	6.31	5.84	4.51	7.82
Na2O	-	-	-	-	-	-	-	-	-	-
K2O	-	-	-	-	-	-	-	-	-	-
Total	99.53	98.90	99.53	99.23	99.55	99.88	98.92	99.48	98.04	98.75
#Si IV	1.98	1.98	1.98	1.97	1.98	1.98	1.97	1.98	1.99	1.99
#Al IV	0.01	0.01	0.01	0.01	0.01	0.01	0.03	0.01	0.01	0.01
T site	1.99	1.99	1.98	1.98	1.99	2.00	2.00	1.99	2.00	2.00
#Al VI	-	-	-	-	-	-	-	-	0.01	0.01
#Ti	-	-	-	-	-	-	-	-	-	-
#Cr	-	-	-	-	-	-	-	-	-	-
#Fe +3	-	0.00	0.00	0.00	-	-	0.00	0.00	-	0.00
#Fe +2	0.06	0.05	0.05	0.06	0.05	0.07	0.06	0.04	0.06	0.05
#Mn +2	1.60	1.57	1.59	1.77	1.62	1.51	1.63	1.68	1.69	1.54
#Ni	-	-	-	-	-	-	-	-	-	-
#Mg	0.04	0.04	0.04	0.03	0.04	0.04	0.04	0.03	0.03	0.04
#Ca	0.32	0.35	0.35	0.17	0.31	0.40	0.29	0.27	0.21	0.36
#Na	-	-	-	-	-	-	-	-	-	-
#K	-	-	-	-	-	-	-	-	-	-
M1,M2	2.03	2.02	2.04	2.04	2.02	2.01	2.02	2.02	2.00	2.00
#O	6.00	6.00	6.00	6.00	6.00	6.00	6.00	6.00	6.00	6.00

APPENDIX C: RHODONITE AND PYROXMANGITE ANALYSES

Ref No.	14	15	16	17	18	19	20	21	22	23
ID	AA271	AA271	AA271	AA271	AA271	AA271	AA271	AA271	AA271	AA271
Level	10000	10000	10000	10000	10000	10000	10000	10000	10000	10000
SiO2	46.23	46.53	46.35	46.13	46.49	45.43	46.51	46.67	46.88	46.29
TiO2	-	-	-	-	-	-	-	-	-	-
Al2O3	0.25	0.21	0.16	0.17	0.19	0.18	0.20	0.20	0.18	0.31
Cr2O3	-	-	-	-	-	-	-	-	-	-
Fe2O3	-	0.00	0.00	0.00	0.00	0.00	-	-	-	-
FeO	1.52	1.72	1.69	1.49	2.01	1.89	1.48	0.94	1.88	1.42
MnO	43.22	43.47	43.54	45.21	41.38	47.93	41.01	42.71	42.74	43.46
NiO	-	-	-	-	-	-	-	-	-	-
MgO	0.66	0.73	0.66	0.53	0.71	0.50	0.63	0.31	0.59	0.53
CaO	7.37	6.67	7.02	6.11	8.08	3.48	9.19	9.00	7.55	7.31
Na2O	-	-	-	-	-	-	-	-	-	-
K2O	-	-	-	-	-	-	-	-	-	-
Total	99.25	99.33	99.42	99.64	98.86	99.41	99.02	99.83	99.82	99.32
#Si IV	1.99	2.00	1.99	1.98	2.00	1.98	1.99	1.99	2.00	1.99
#Al IV	0.01	0.00	0.01	0.01	0.00	0.01	0.01	0.01	0.00	0.01
T site	2.00	2.00	2.00	1.99	2.00	1.99	2.00	2.00	2.00	2.00
#Al VI	-	0.01	-	-	0.01	-	0.00	-	0.01	0.00
#Ti	-	-	-	-	-	-	-	-	-	-
#Cr	-	-	-	-	-	-	-	-	-	-
#Fe +3	-	0.00	0.00	0.00	0.00	0.00	-	-	-	-
#Fe +2	0.05	0.06	0.06	0.05	0.07	0.07	0.05	0.03	0.07	0.05
#Mn +2	1.57	1.58	1.58	1.65	1.50	1.77	1.49	1.54	1.54	1.58
#Ni	-	-	-	-	-	-	-	-	-	-
#Mg	0.04	0.05	0.04	0.03	0.05	0.03	0.04	0.02	0.04	0.03
#Ca	0.34	0.31	0.32	0.28	0.37	0.16	0.42	0.41	0.34	0.34
#Na	-	-	-	-	-	-	-	-	-	-
#K	-	-	-	-	-	-	-	-	-	-
M1,M2	2.01	2.00	2.01	2.02	2.00	2.03	2.00	2.01	2.00	2.00
#O	6.00	6.00	6.00	6.00	6.00	6.00	6.00	6.00	6.00	6.00

APPENDIX C: RHODONITE AND PYROXMANGITE ANALYSES

Ref No.	24	25	26	27	28	29	30	31	32	33
ID	AA271	AA271	AA271	AA271	AA271	AA271	AA271	AA271	AA271	AA271
Level	10000	10000	10000	10000	10000	10000	10000	10000	10000	10000
SiO2	46.05	46.25	45.41	45.94	45.83	45.89	46.18	45.82	46.62	46.18
TiO2	-	-	-	-	-	-	-	-	-	-
Al2O3	0.19	0.18	0.13	0.23	0.18	0.21	0.22	0.24	0.22	0.10
Cr2O3	-	-	-	-	-	-	-	-	-	-
Fe2O3	0.00	-	0.00	0.00	0.00	0.00	-	0.00	0.00	-
FeO	1.74	1.98	1.91	1.54	1.35	1.45	0.99	1.35	1.50	0.66
MnO	45.37	46.13	47.95	44.41	44.47	44.45	43.75	46.20	44.20	45.30
NiO	-	-	-	-	-	-	-	-	-	-
MgO	0.50	0.52	0.42	0.69	0.58	0.64	0.48	0.40	0.57	0.40
CaO	5.46	5.13	3.65	6.84	7.36	7.10	8.05	5.40	6.95	6.91
Na2O	-	-	-	-	-	-	-	-	-	-
K2O	-	-	-	-	-	-	-	-	-	-
Total	99.31	100.19	99.47	99.65	99.77	99.74	99.67	99.41	100.06	99.55
#Si IV	1.99	1.98	1.98	1.98	1.97	1.97	1.98	1.98	1.99	1.99
#Al IV	0.01	0.01	0.01	0.01	0.01	0.01	0.01	0.01	0.01	0.01
T site	2.00	1.99	1.98	1.99	1.98	1.98	1.99	1.99	2.00	1.99
#Al VI	-	-	-	-	-	-	-	-	0.00	-
#Ti	-	-	-	-	-	-	-	-	-	-
#Cr	-	-	-	-	-	-	-	-	-	-
#Fe +3	0.00	-	0.00	0.00	0.00	0.00	-	0.00	0.00	-
#Fe +2	0.06	0.07	0.07	0.06	0.05	0.05	0.04	0.05	0.05	0.02
#Mn +2	1.66	1.68	1.77	1.62	1.62	1.62	1.59	1.69	1.60	1.65
#Ni	-	-	-	-	-	-	-	-	-	-
#Mg	0.03	0.03	0.03	0.04	0.04	0.04	0.03	0.03	0.04	0.03
#Ca	0.25	0.24	0.17	0.32	0.34	0.33	0.37	0.25	0.32	0.32
#Na	-	-	-	-	-	-	-	-	-	-
#K	-	-	-	-	-	-	-	-	-	-
M1,M2	2.01	2.02	2.04	2.03	2.04	2.04	2.02	2.02	2.01	2.02
#O	6.00	6.00	6.00	6.00	6.00	6.00	6.00	6.00	6.00	6.00

APPENDIX C: RHODONITE AND PYROXMANGITE ANALYSES

Ref No.	34	35	36	37	38	39	40	41	42	43
ID	AA271	AA272	AA272	AA272	AA272	AA272	AA272	AA272	AA272	AA272
Level	10000	10000	10000	10000	10000	10000	10000	10000	10000	10000
SiO2	45.95	46.46	46.37	45.62	45.86	45.89	45.82	46.40	45.46	44.55
TiO2	-	-	-	-	-	-	-	-	-	-
Al2O3	0.30	0.16	0.25	0.19	0.22	0.32	0.16	0.18	0.09	0.18
Cr2O3	-	-	-	-	-	-	-	-	-	-
Fe2O3	0.00	0.00	-	0.00	0.00	0.00	0.00	0.00	0.00	-
FeO	1.36	1.98	1.50	1.64	1.48	1.59	1.92	1.49	1.34	2.05
MnO	47.65	40.02	42.75	43.33	44.09	44.68	44.61	45.16	46.02	47.14
NiO	-	-	-	-	-	-	-	-	-	-
MgO	0.29	0.69	0.67	0.58	0.61	0.56	0.68	0.55	0.38	0.52
CaO	3.90	10.21	7.70	7.49	6.50	5.98	6.20	6.47	5.21	4.12
Na2O	-	-	-	-	-	-	-	-	-	-
K2O	-	-	-	-	-	-	-	-	-	-
Total	99.45	99.52	99.24	98.85	98.76	99.02	99.39	100.25	98.50	98.56
#Si IV	1.99	1.98	1.99	1.98	1.99	1.98	1.98	1.98	1.99	1.96
#Al IV	0.01	0.01	0.01	0.01	0.01	0.02	0.01	0.01	0.00	0.01
T site	2.00	1.99	2.00	1.99	2.00	2.00	1.99	1.99	1.99	1.97
#Al VI	0.01	-	0.00	-	-	0.00	-	-	-	-
#Ti	-	-	-	-	-	-	-	-	-	-
#Cr	-	-	-	-	-	-	-	-	-	-
#Fe +3	0.00	0.00	-	0.00	0.00	0.00	0.00	0.00	0.00	-
#Fe +2	0.05	0.07	0.05	0.06	0.05	0.06	0.07	0.05	0.05	0.08
#Mn +2	1.75	1.45	1.55	1.59	1.62	1.64	1.63	1.64	1.70	1.76
#Ni	-	-	-	-	-	-	-	-	-	-
#Mg	0.02	0.04	0.04	0.04	0.04	0.04	0.04	0.04	0.02	0.03
#Ca	0.18	0.47	0.35	0.35	0.30	0.28	0.29	0.30	0.24	0.19
#Na	-	-	-	-	-	-	-	-	-	-
#K	-	-	-	-	-	-	-	-	-	-
M1,M2	2.00	2.03	2.00	2.03	2.01	2.01	2.03	2.02	2.02	2.06
#O	6.00	6.00	6.00	6.00	6.00	6.00	6.00	6.00	6.00	6.00

APPENDIX C: RHODONITE AND PYROXMANGITE ANALYSES

Ref No.	44	45	47	48	49	50	51	52	53	54
ID	AA272	AA272	AA272	AA272	AA272	AA272	MM	MM	MM	MM
Level	10000	10000	10000	10000	10000	10000	10000	10000	10000	10000
SiO2	45.87	45.59	46.28	45.66	46.77	46.23	46.02	46.00	46.08	46.24
TiO2	-	-	-	-	-	-	-	-	-	-
Al2O3	0.30	0.25	0.40	0.20	0.16	0.18	0.30	0.21	0.20	0.12
Cr2O3	-	-	-	-	-	-	-	-	-	-
Fe2O3	0.00	0.00	0.00	0.00	-	-	0.00	-	-	0.00
FeO	1.49	1.51	0.68	2.26	1.53	1.71	1.16	1.17	1.42	1.83
MnO	46.90	47.84	41.93	44.29	40.75	43.20	45.15	46.08	41.86	40.29
NiO	-	-	-	-	-	-	-	-	-	-
MgO	0.38	0.37	0.51	0.67	0.78	0.52	0.42	0.32	0.66	0.56
CaO	4.36	4.48	9.64	6.10	9.90	7.72	5.71	5.44	9.14	9.45
Na2O	-	-	-	-	-	-	-	-	-	-
K2O	-	-	-	-	-	-	-	-	-	-
Total	99.30	100.04	99.44	99.18	99.89	99.56	98.76	99.22	99.36	98.49
#Si IV	1.99	1.97	1.98	1.98	1.98	1.98	1.99	1.99	1.98	1.99
#Al IV	0.01	0.01	0.02	0.01	0.01	0.01	0.01	0.01	0.01	0.01
T site	2.00	1.98	2.00	1.99	1.99	1.99	2.00	2.00	1.99	2.00
#Al VI	0.00	-	-	-	-	-	0.01	0.00	-	-
#Ti	-	-	-	-	-	-	-	-	-	-
#Cr	-	-	-	-	-	-	-	-	-	-
#Fe +3	0.00	0.00	0.00	0.00	-	-	0.00	-	-	0.00
#Fe +2	0.05	0.05	0.02	0.08	0.05	0.06	0.04	0.04	0.05	0.07
#Mn +2	1.72	1.75	1.52	1.62	1.46	1.57	1.66	1.69	1.52	1.47
#Ni	-	-	-	-	-	-	-	-	-	-
#Mg	0.02	0.02	0.03	0.04	0.05	0.03	0.03	0.02	0.04	0.04
#Ca	0.20	0.21	0.44	0.28	0.45	0.35	0.26	0.25	0.42	0.44
#Na	-	-	-	-	-	-	-	-	-	-
#K	-	-	-	-	-	-	-	-	-	-
M1,M2	2.00	2.04	2.02	2.03	2.02	2.02	2.00	2.00	2.03	2.01
#O	6.00	6.00	6.00	6.00	6.00	6.00	6.00	6.00	6.00	6.00

APPENDIX C: RHODONITE AND PYROXMANGITE ANALYSES

Ref No.	55	56	58	59	60	61	62	63	64	65
ID	MM	MM	MM	MM	MM	MM	MM	MM	MM	MM
Level	10000	10000	10000	10000	10000	10000	10000	10000	10000	10000
SiO2	46.39	46.30	46.36	46.21	47.10	46.73	45.26	46.57	46.44	45.73
TiO2	-	-	-	-	-	-	-	-	-	-
Al2O3	0.32	0.12	0.08	0.12	0.17	0.20	0.90	0.41	0.23	0.22
Cr2O3	-	-	-	-	-	-	-	-	-	-
Fe2O3	0.00	-	-	0.00	0.00	0.00	0.00	-	0.00	0.00
FeO	1.55	3.66	2.03	1.56	3.59	2.09	1.84	1.59	0.54	0.34
MnO	43.06	44.50	45.27	44.24	42.19	42.81	45.25	46.13	46.63	44.94
NiO	-	-	-	-	-	-	-	-	-	-
MgO	0.57	0.47	0.43	0.56	0.53	0.69	0.31	0.54	0.40	0.41
CaO	7.53	3.88	4.87	5.98	5.39	6.87	5.80	5.77	5.64	7.61
Na2O	-	-	-	-	-	-	-	-	-	-
K2O	-	-	-	-	-	-	-	-	-	-
Total	99.42	98.93	99.04	98.67	98.97	99.39	99.36	101.01	99.88	99.25
#Si IV	1.99	2.01	2.00	2.00	2.02	2.00	1.96	1.98	1.99	1.97
#Al IV	0.01	-	-	0.00	-	0.00	0.04	0.02	0.01	0.01
T site	2.00	2.01	2.00	2.00	2.02	2.00	2.00	2.00	2.00	1.99
#Al VI	0.00	0.01	0.00	0.01	0.01	0.01	0.00	-	0.00	-
#Ti	-	-	-	-	-	-	-	-	-	-
#Cr	-	-	-	-	-	-	-	-	-	-
#Fe +3	0.00	-	-	0.00	0.00	0.00	0.00	-	0.00	0.00
#Fe +2	0.06	0.13	0.07	0.06	0.13	0.07	0.07	0.06	0.02	0.01
#Mn +2	1.56	1.63	1.66	1.62	1.53	1.55	1.66	1.66	1.69	1.64
#Ni	-	-	-	-	-	-	-	-	-	-
#Mg	0.04	0.03	0.03	0.04	0.03	0.04	0.02	0.03	0.03	0.03
#Ca	0.35	0.18	0.23	0.28	0.25	0.31	0.27	0.26	0.26	0.35
#Na	-	-	-	-	-	-	-	-	-	-
#K	-	-	-	-	-	-	-	-	-	-
M1,M2	2.00	1.98	1.99	2.00	1.95	2.00	2.02	2.01	2.00	2.03
#O	6.00	6.00	6.00	6.00	6.00	6.00	6.00	6.00	6.00	6.00

APPENDIX C: RHODONITE AND PYROXMANGITE ANALYSES

Ref No.	66	67	68	69	70	72	73	74	78	79
ID	MM	MM	MM	MM	MM	MM	MM	MM	MM	MM
Level	10000	10000	10000	10000	10000	10000	10000	10000	10000	10000
SiO2	45.35	45.64	46.68	46.11	46.17	46.71	45.85	46.20	46.25	46.61
TiO2	-	-	-	-	-	-	-	-	-	-
Al2O3	0.13	0.27	0.22	0.23	0.10	0.27	0.22	0.21	0.20	0.10
Cr2O3	-	-	-	-	-	-	-	-	-	-
Fe2O3	0.00	0.00	0.00	-	0.00	0.00	0.00	0.00	0.00	0.00
FeO	2.70	5.87	1.70	1.41	4.26	4.82	1.94	2.02	1.82	1.65
MnO	47.79	47.01	40.45	43.26	46.12	44.65	43.50	44.23	44.20	44.02
NiO	-	-	-	-	-	-	-	-	-	-
MgO	0.56	0.31	0.69	0.59	0.52	0.46	0.77	0.75	0.69	0.60
CaO	1.73	1.51	9.31	7.24	1.66	2.47	5.83	5.85	5.88	6.37
Na2O	-	-	-	-	-	-	-	-	-	-
K2O	-	-	-	-	-	-	-	-	-	-
Total	98.26	100.61	99.05	98.84	98.83	99.38	98.11	99.26	99.04	99.35
#Si IV	2.00	1.98	1.99	1.99	2.01	2.02	1.99	1.99	1.99	2.00
#Al IV	0.00	0.01	0.01	0.01	0.01	-	0.01	0.01	0.01	-
T site	2.00	1.99	2.00	2.00	2.01	2.02	2.00	2.00	2.00	2.00
#Al VI	0.00	-	0.01	0.00	0.01	0.01	0.01	0.00	0.00	0.01
#Ti	-	-	-	-	-	-	-	-	-	-
#Cr	-	-	-	-	-	-	-	-	-	-
#Fe +3	0.00	0.00	0.00	-	0.00	0.00	0.00	0.00	0.00	0.00
#Fe +2	0.10	0.21	0.06	0.05	0.16	0.17	0.07	0.07	0.07	0.06
#Mn +2	1.78	1.72	1.46	1.58	1.70	1.63	1.60	1.61	1.61	1.60
#Ni	-	-	-	-	-	-	-	-	-	-
#Mg	0.04	0.02	0.04	0.04	0.03	0.03	0.05	0.05	0.04	0.04
#Ca	0.08	0.07	0.43	0.33	0.08	0.11	0.27	0.27	0.27	0.29
#Na	-	-	-	-	-	-	-	-	-	-
#K	-	-	-	-	-	-	-	-	-	-
M1,M2	2.00	2.03	2.00	2.00	1.97	1.96	2.00	2.00	2.00	2.00
#O	6.00	6.00	6.00	6.00	6.00	6.00	6.00	6.00	6.00	6.00

APPENDIX C: RHODONITE AND PYROXMANGITE ANALYSES

Ref No.	80	81	82	83	84	85	86	88	89	90
ID	BK16	BK16	BK16	BK16	BK16	BK16	BK16	BK16	BK16	BK16
Level	10250	10250	10250	10250	10250	10250	10250	10250	10250	10250
SiO2	46.32	46.21	46.63	46.61	46.50	45.80	45.96	45.51	45.73	45.28
TiO2	-	-	-	-	-	-	-	-	-	-
Al2O3	0.10	0.12	0.16	0.18	0.26	0.17	0.18	0.14	0.20	0.19
Cr2O3	-	-	-	-	-	-	-	-	-	-
Fe2O3	0.00	0.00	0.00	0.00	0.00	-	-	-	0.00	-
FeO	1.74	2.07	1.43	1.96	1.35	1.85	1.65	1.63	1.63	2.13
MnO	44.49	40.92	43.94	39.10	41.33	45.81	43.32	46.27	45.53	45.02
NiO	-	-	-	-	-	-	-	-	-	-
MgO	0.68	0.77	0.65	0.73	0.71	0.51	0.57	0.43	0.44	0.66
CaO	6.16	8.69	7.00	10.86	9.04	5.12	7.54	4.93	5.72	4.84
Na2O	-	-	-	-	-	-	-	-	-	-
K2O	-	-	-	-	-	-	-	-	-	-
Total	99.49	98.78	99.81	99.44	99.19	99.26	99.22	98.91	99.25	98.12
#Si IV	1.99	1.99	1.99	1.98	1.99	1.98	1.98	1.98	1.98	1.98
#Al IV	0.01	0.01	0.01	0.01	0.01	0.01	0.01	0.01	0.01	0.01
T site	2.00	1.99	2.00	1.99	2.00	1.99	1.99	1.99	1.99	1.99
#Al VI	-	-	0.00	-	0.00	-	-	-	-	-
#Ti	-	-	-	-	-	-	-	-	-	-
#Cr	-	-	-	-	-	-	-	-	-	-
#Fe +3	0.00	0.00	0.00	0.00	0.00	-	-	-	0.00	-
#Fe +2	0.06	0.07	0.05	0.07	0.05	0.07	0.06	0.06	0.06	0.08
#Mn +2	1.62	1.49	1.59	1.41	1.50	1.68	1.58	1.71	1.67	1.67
#Ni	-	-	-	-	-	-	-	-	-	-
#Mg	0.04	0.05	0.04	0.05	0.05	0.03	0.04	0.03	0.03	0.04
#Ca	0.28	0.40	0.32	0.50	0.41	0.24	0.35	0.23	0.27	0.23
#Na	-	-	-	-	-	-	-	-	-	-
#K	-	-	-	-	-	-	-	-	-	-
M1,M2	2.01	2.02	2.00	2.02	2.01	2.02	2.03	2.02	2.02	2.02
#O	6.00	6.00	6.00	6.00	6.00	6.00	6.00	6.00	6.00	6.00

APPENDIX C: RHODONITE AND PYROXMANGITE ANALYSES

Ref No.	92	93	94	95	96	97	98	99	100	101
ID	BK16	BK16	BK16	BK16	BK16	BK16	BK16	BK16	BK16	BK16
Level	10250	10250	10250	10250	10250	10250	10250	10250	10250	10250
SiO2	45.62	46.02	45.72	45.47	46.34	45.64	46.35	45.87	46.12	46.14
TiO2	-	-	-	-	-	-	-	-	-	-
Al2O3	0.16	0.32	0.42	0.34	0.11	0.66	0.19	0.09	0.15	0.08
Cr2O3	-	-	-	-	-	-	-	-	-	-
Fe2O3	0.00	0.00	-	0.00	-	0.00	0.00	-	0.00	-
FeO	1.51	1.61	1.29	1.40	1.74	1.54	2.13	1.53	1.84	3.61
MnO	45.14	45.72	44.94	47.08	43.94	45.28	40.92	45.47	43.21	45.94
NiO	-	-	-	-	-	-	-	-	-	-
MgO	0.52	0.50	0.46	0.29	0.77	0.52	0.70	0.69	0.71	0.29
CaO	5.34	5.18	5.50	4.03	5.87	5.11	8.68	5.29	6.98	3.03
Na2O	-	-	-	-	-	-	-	-	-	-
K2O	-	-	-	-	-	-	-	-	-	-
Total	98.29	99.35	98.33	98.61	98.77	98.75	98.97	98.94	99.01	99.09
#Si IV	1.99	1.99	1.99	1.99	2.00	1.98	1.99	1.99	1.99	2.01
#Al IV	0.01	0.01	0.01	0.01	-	0.02	0.01	0.00	0.01	-
T site	2.00	2.00	2.00	2.00	2.00	2.00	2.00	1.99	2.00	2.01
#Al VI	-	0.00	0.01	0.00	0.01	0.01	-	-	-	0.00
#Ti	-	-	-	-	-	-	-	-	-	-
#Cr	-	-	-	-	-	-	-	-	-	-
#Fe +3	0.00	0.00	-	0.00	-	0.00	0.00	-	0.00	-
#Fe +2	0.06	0.06	0.05	0.05	0.06	0.06	0.08	0.06	0.07	0.13
#Mn +2	1.67	1.67	1.66	1.74	1.61	1.66	1.49	1.67	1.58	1.69
#Ni	-	-	-	-	-	-	-	-	-	-
#Mg	0.03	0.03	0.03	0.02	0.05	0.03	0.04	0.04	0.05	0.02
#Ca	0.25	0.24	0.26	0.19	0.27	0.24	0.40	0.25	0.32	0.14
#Na	-	-	-	-	-	-	-	-	-	-
#K	-	-	-	-	-	-	-	-	-	-
M1,M2	2.01	2.00	2.00	2.00	2.00	2.00	2.01	2.02	2.01	1.99
#O	6.00	6.00	6.00	6.00	6.00	6.00	6.00	6.00	6.00	6.00

APPENDIX C: RHODONITE AND PYROXMANGITE ANALYSES

Ref. No.	102	103	104	105	106	107	108	144	147	148
ID	BK16	BK16	BJ16	BJ16	BJ16	BJ16	BJ16	BJ16	BJ16	BJ16
Level	10250	10250	10250	10250	10250	10250	10250	10250	10250	10250
SiO2	45.38	46.48	45.61	45.83	46.36	46.01	45.56	46.99	44.92	45.07
TiO2	-	-	-	-	-	-	-	-	-	-
Al2O3	0.22	0.07	0.20	0.17	0.17	0.25	0.13	0.16	0.41	0.37
Cr2O3	-	-	-	-	-	-	-	-	-	-
Fe2O3	-	-	-	0.00	-	0.00	0.00	0.00	0.00	-
FeO	1.71	1.80	1.76	1.76	1.61	1.56	1.45	1.27	0.52	0.52
MnO	46.56	45.13	45.88	45.86	41.05	44.99	45.51	40.69	48.28	47.67
NiO	-	-	-	-	-	-	-	-	-	-
MgO	0.55	0.42	0.57	0.53	0.73	0.54	0.58	0.96	0.52	0.57
CaO	4.07	5.09	4.45	4.54	8.98	5.47	5.47	9.44	3.89	4.51
Na2O	-	-	-	-	-	-	-	-	-	-
K2O	-	-	-	-	-	-	-	-	-	-
Total	98.49	98.99	98.47	98.69	98.90	98.82	98.70	99.51	98.54	98.71
#Si IV	1.98	2.01	1.99	1.99	1.99	1.99	1.98	1.99	1.97	1.97
#Al IV	0.01	-	0.01	0.01	0.01	0.01	0.01	0.01	0.02	0.02
T site	2.00	2.01	2.00	2.00	2.00	2.00	1.99	2.00	1.99	1.99
#Al VI	-	0.00	0.00	0.00	-	0.01	-	0.00	-	-
#Ti	-	-	-	-	-	-	-	-	-	-
#Cr	-	-	-	-	-	-	-	-	-	-
#Fe +3	-	-	-	0.00	-	0.00	0.00	0.00	0.00	-
#Fe +2	0.06	0.07	0.06	0.06	0.06	0.06	0.05	0.05	0.02	0.02
#Mn +2	1.72	1.65	1.70	1.69	1.49	1.65	1.68	1.46	1.79	1.76
#Ni	-	-	-	-	-	-	-	-	-	-
#Mg	0.04	0.03	0.04	0.03	0.05	0.03	0.04	0.06	0.03	0.04
#Ca	0.19	0.24	0.21	0.21	0.41	0.25	0.26	0.43	0.18	0.21
#Na	-	-	-	-	-	-	-	-	-	-
#K	-	-	-	-	-	-	-	-	-	-
M1,M2	2.01	1.98	2.00	2.00	2.01	2.00	2.02	2.00	2.03	2.03
#O	6.00	6.00	6.00	6.00	6.00	6.00	6.00	6.00	6.00	6.00

APPENDIX C: RHODONITE AND PYROXMANGITE ANALYSES

Ref No.	150	152	153	154	155	156	162	163	164	165
ID	BJ16	BJ16	BJ16	BJ16	BJ16	BJ16	BJ16	BJ16	BJ16	BJ16
Level	10250	10250	10250	10250	10250	10250	10250	10250	10250	10250
SiO2	44.45	44.13	45.44	44.64	45.79	46.01	45.79	46.29	46.26	45.17
TiO2	-	-	-	-	-	-	-	-	-	-
Al2O3	0.37	0.31	0.44	0.53	0.24	0.36	0.23	0.24	0.20	0.28
Cr2O3	-	-	-	-	-	-	-	-	-	-
Fe2O3	-	0.00	0.00	-	-	0.00	-	0.00	-	0.00
FeO	0.57	0.38	0.60	0.54	1.28	1.90	1.54	1.15	1.46	1.81
MnO	47.31	48.58	46.02	47.44	42.70	38.02	46.57	46.88	41.88	45.94
NiO	-	-	-	-	-	-	-	-	-	-
MgO	0.13	0.15	0.65	0.32	0.75	0.93	0.54	0.86	0.85	0.62
CaO	5.59	4.83	5.63	5.02	7.73	10.96	5.10	4.92	9.22	5.01
Na2O	-	-	-	-	-	-	-	-	-	-
K2O	-	-	-	-	-	-	-	-	-	-
Total	98.42	98.38	98.78	98.49	98.49	98.18	99.77	100.34	99.87	98.83
#Si IV	1.96	1.95	1.97	1.96	1.98	1.98	1.98	1.98	1.97	1.97
#Al IV	0.02	0.02	0.02	0.03	0.01	0.02	0.01	0.01	0.01	0.01
T site	1.98	1.97	2.00	1.99	1.99	2.00	1.99	1.99	1.98	1.98
#Al VI	-	-	-	-	-	-	-	-	-	-
#Ti	-	-	-	-	-	-	-	-	-	-
#Cr	-	-	-	-	-	-	-	-	-	-
#Fe +3	-	0.00	0.00	-	-	0.00	-	0.00	-	0.00
#Fe +2	0.02	0.01	0.02	0.02	0.05	0.07	0.06	0.04	0.05	0.07
#Mn +2	1.76	1.82	1.69	1.76	1.57	1.38	1.70	1.70	1.51	1.70
#Ni	-	-	-	-	-	-	-	-	-	-
#Mg	0.01	0.01	0.04	0.02	0.05	0.06	0.03	0.05	0.05	0.04
#Ca	0.26	0.23	0.26	0.24	0.36	0.50	0.24	0.23	0.42	0.23
#Na	-	-	-	-	-	-	-	-	-	-
#K	-	-	-	-	-	-	-	-	-	-
M1,M2	2.06	2.07	2.02	2.04	2.02	2.02	2.03	2.02	2.04	2.04
#O	6.00	6.00	6.00	6.00	6.00	6.00	6.00	6.00	6.00	6.00

APPENDIX C: RHODONITE AND PYROXMANGITE ANALYSES

Ref No.	166	168	169	170	171	172	173	174	175	176
ID	BJ16	BJ16	BJ16	BJ16	BJ16	BJ16	BJ16	BJ16	BJ16	BJ16
Level	10250	10250	10250	10250	10250	10250	10250	10250	10250	10250
SiO2	46.13	44.93	45.38	46.63	45.99	46.08	45.81	46.11	46.45	45.87
TiO2	-	-	-	-	-	-	-	-	-	-
Al2O3	0.29	0.38	0.36	0.32	0.41	0.47	0.25	0.24	0.66	0.30
Cr2O3	-	-	-	-	-	-	-	-	-	-
Fe2O3	-	0.00	0.00	0.00	0.00	0.00	0.00	-	-	0.00
FeO	2.36	2.05	1.81	2.78	1.73	1.30	1.86	2.22	0.72	2.50
MnO	39.85	43.81	43.42	41.88	44.03	43.60	44.42	44.97	40.79	44.07
NiO	-	-	-	-	-	-	-	-	-	-
MgO	0.72	0.63	0.74	0.80	0.62	0.53	0.70	0.79	0.84	0.81
CaO	9.65	6.42	6.84	7.81	6.89	7.98	6.69	5.60	10.23	5.50
Na2O	-	-	-	-	-	-	-	-	-	-
K2O	-	-	-	-	-	-	-	-	-	-
Total	99.00	98.22	98.55	100.22	99.67	99.96	99.73	99.93	99.69	99.05
#Si IV	1.98	1.97	1.97	1.98	1.97	1.97	1.97	1.98	1.97	1.98
#Al IV	0.01	0.02	0.02	0.02	0.02	0.02	0.01	0.01	0.03	0.02
T site	1.99	1.98	1.99	2.00	2.00	1.99	1.98	1.99	2.00	2.00
#Al VI	-	-	-	-	-	-	-	-	0.00	-
#Ti	-	-	-	-	-	-	-	-	-	-
#Cr	-	-	-	-	-	-	-	-	-	-
#Fe +3	-	0.00	0.00	0.00	0.00	0.00	0.00	-	-	0.00
#Fe +2	0.08	0.07	0.07	0.10	0.06	0.05	0.07	0.08	0.03	0.09
#Mn +2	1.45	1.62	1.60	1.51	1.60	1.58	1.62	1.64	1.47	1.61
#Ni	-	-	-	-	-	-	-	-	-	-
#Mg	0.05	0.04	0.05	0.05	0.04	0.03	0.04	0.05	0.05	0.05
#Ca	0.44	0.30	0.32	0.36	0.32	0.37	0.31	0.26	0.46	0.25
#Na	-	-	-	-	-	-	-	-	-	-
#K	-	-	-	-	-	-	-	-	-	-
M1,M2	2.02	2.04	2.03	2.01	2.02	2.02	2.04	2.02	2.01	2.01
#O	6.00	6.00	6.00	6.00	6.00	6.00	6.00	6.00	6.00	6.00

APPENDIX C: RHODONITE AND PYROXMANGITE ANALYSES

Ref No.	177	178	179	180	181	182	183	184	185	186
ID	BJ16	BJ16	BJ16	BJ16	BJ16	BJ16	BJ16	BJ16	BJ16	BJ16
Level	10250	10250	10250	10250	10250	10250	10250	10250	10250	10250
SiO2	45.41	46.05	45.98	45.51	46.13	44.31	45.57	45.98	45.74	46.08
TiO2	-	-	-	-	-	-	-	-	-	-
Al2O3	0.30	0.33	0.50	0.32	0.32	0.33	0.26	0.34	0.34	0.29
Cr2O3	-	-	-	-	-	-	-	-	-	-
Fe2O3	-	0.00	0.00	-	-	0.00	-	0.00	-	0.00
FeO	1.08	1.56	1.15	2.37	1.55	2.52	1.81	2.03	1.78	1.62
MnO	45.56	44.63	44.15	45.36	41.96	45.33	46.96	45.44	44.69	45.85
NiO	-	-	-	-	-	-	-	-	-	-
MgO	0.52	0.52	0.50	0.79	0.95	0.67	0.72	0.70	0.70	0.65
CaO	6.95	6.70	7.39	4.90	8.88	5.01	4.73	5.59	6.48	6.11
Na2O	-	-	-	-	-	-	-	-	-	-
K2O	-	-	-	-	-	-	-	-	-	-
Total	99.82	99.79	99.67	99.25	99.79	98.17	100.05	100.08	99.73	100.60
#Si IV	1.96	1.98	1.97	1.97	1.97	1.95	1.97	1.97	1.97	1.97
#Al IV	0.02	0.02	0.03	0.02	0.02	0.02	0.01	0.02	0.02	0.01
T site	1.97	1.99	2.00	1.99	1.98	1.97	1.98	1.99	1.99	1.98
#Al VI	-	-	-	-	-	-	-	-	-	-
#Ti	-	-	-	-	-	-	-	-	-	-
#Cr	-	-	-	-	-	-	-	-	-	-
#Fe +3	-	0.00	0.00	-	-	0.00	-	0.00	-	0.00
#Fe +2	0.04	0.06	0.04	0.09	0.06	0.09	0.07	0.07	0.06	0.06
#Mn +2	1.66	1.62	1.60	1.67	1.52	1.69	1.72	1.65	1.63	1.66
#Ni	-	-	-	-	-	-	-	-	-	-
#Mg	0.03	0.03	0.03	0.05	0.06	0.04	0.05	0.04	0.04	0.04
#Ca	0.32	0.31	0.34	0.23	0.41	0.24	0.22	0.26	0.30	0.28
#Na	-	-	-	-	-	-	-	-	-	-
#K	-	-	-	-	-	-	-	-	-	-
M1,M2	2.06	2.02	2.02	2.03	2.04	2.07	2.05	2.03	2.04	2.04
#O	6.00	6.00	6.00	6.00	6.00	6.00	6.00	6.00	6.00	6.00

APPENDIX C: RHODONITE AND PYROXMANGITE ANALYSES

Ref No.	188	189	190	191	192	193	194	195	196	207
ID	3EQ16	3EQ16	3EQ16	3EQ16	3EQ16	3EQ16	3EQ16	3EQ16	3EQ16	3EQ16
Level	10000	10000	10000	10000	10000	10000	10000	10000	10000	10000
SiO2	45.30	46.03	45.90	45.70	45.56	45.64	45.07	45.73	45.56	45.37
TiO2	-	-	-	-	-	-	-	-	-	-
Al2O3	0.55	0.43	0.43	0.33	0.39	0.42	0.42	0.35	0.38	0.24
Cr2O3	-	-	-	-	-	-	-	-	-	-
Fe2O3	-	0.00	0.00	0.00	-	0.00	-	-	0.00	0.00
FeO	1.45	1.89	2.38	1.89	1.18	1.51	0.92	0.87	0.74	2.33
MnO	45.62	43.14	44.33	45.46	47.27	47.36	47.66	44.40	44.65	45.44
NiO	-	-	-	-	-	-	-	-	-	-
MgO	0.44	0.71	0.55	0.54	0.60	0.51	0.57	0.54	0.45	0.53
CaO	6.47	7.36	6.35	6.34	5.05	4.48	4.50	7.43	8.00	5.45
Na2O	-	-	-	-	-	-	-	-	-	-
K2O	-	-	-	-	-	-	-	-	-	-
Total	99.83	99.56	99.94	100.26	100.05	99.92	99.14	99.32	99.78	99.36
#Si IV	1.96	1.97	1.97	1.96	1.96	1.97	1.96	1.97	1.96	1.97
#Al IV	0.03	0.02	0.02	0.02	0.02	0.02	0.02	0.02	0.02	0.01
T site	1.98	2.00	1.99	1.98	1.98	1.99	1.99	1.99	1.98	1.98
#Al VI	-	-	-	-	-	-	-	-	-	-
#Ti	-	-	-	-	-	-	-	-	-	-
#Cr	-	-	-	-	-	-	-	-	-	-
#Fe +3	-	0.00	0.00	0.00	-	0.00	-	-	0.00	0.00
#Fe +2	0.05	0.07	0.09	0.07	0.04	0.05	0.03	0.03	0.03	0.08
#Mn +2	1.67	1.57	1.61	1.65	1.73	1.73	1.76	1.62	1.63	1.67
#Ni	-	-	-	-	-	-	-	-	-	-
#Mg	0.03	0.05	0.04	0.03	0.04	0.03	0.04	0.03	0.03	0.03
#Ca	0.30	0.34	0.29	0.29	0.23	0.21	0.21	0.34	0.37	0.25
#Na	-	-	-	-	-	-	-	-	-	-
#K	-	-	-	-	-	-	-	-	-	-
M1,M2	2.05	2.02	2.03	2.05	2.04	2.03	2.04	2.03	2.05	2.04
#O	6.00	6.00	6.00	6.00	6.00	6.00	6.00	6.00	6.00	6.00

APPENDIX C: RHODONITE AND PYROXMANGITE ANALYSES

Ref No.	319	332	333	334	335	336	337	338	339	341
ID	1EQ16	1EQ16	1EQ16	1EQ16	1EQ16	1EQ16	1EQ16	1EQ16	1EQ16	1EQ16
Level	10000	10000	10000	10000	10000	10000	10000	10000	10000	10000
SiO2	46.36	46.28	45.81	46.46	46.37	45.72	46.18	46.32	45.53	45.92
TiO2	-	-	-	-	-	-	-	-	-	-
Al2O3	0.26	0.47	0.29	0.57	0.30	0.20	0.33	0.34	0.31	0.23
Cr2O3	-	-	-	-	-	-	-	-	-	-
Fe2O3	0.00	0.00	-	-	0.00	0.00	-	0.00	0.00	-
FeO	2.90	2.05	3.05	0.99	1.77	1.30	1.61	1.83	3.31	1.50
MnO	41.52	44.55	43.48	44.90	38.51	47.39	44.03	45.61	46.09	48.37
NiO	-	-	-	-	-	-	-	-	-	-
MgO	0.73	0.46	0.78	0.41	0.51	0.47	0.77	0.69	0.74	0.52
CaO	7.50	6.74	6.42	7.20	11.93	5.32	7.33	6.13	4.53	4.14
Na2O	-	-	-	-	-	-	-	-	-	-
K2O	-	-	-	-	-	-	-	-	-	-
Total	99.27	100.55	99.83	100.53	99.39	100.40	100.25	100.92	100.51	100.68
#Si IV	1.99	1.97	1.97	1.98	1.97	1.97	1.97	1.97	1.96	1.97
#Al IV	0.01	0.02	0.01	0.02	0.02	0.01	0.02	0.02	0.02	0.01
T site	2.00	2.00	1.98	2.00	1.99	1.98	1.99	1.99	1.98	1.98
#Al VI	0.00	-	-	0.00	-	-	-	-	-	-
#Ti	-	-	-	-	-	-	-	-	-	-
#Cr	-	-	-	-	-	-	-	-	-	-
#Fe +3	0.00	0.00	-	-	0.00	0.00	-	0.00	0.00	-
#Fe +2	0.10	0.07	0.11	0.04	0.06	0.05	0.06	0.07	0.12	0.05
#Mn +2	1.51	1.61	1.58	1.62	1.39	1.73	1.59	1.64	1.68	1.76
#Ni	-	-	-	-	-	-	-	-	-	-
#Mg	0.05	0.03	0.05	0.03	0.03	0.03	0.05	0.04	0.05	0.03
#Ca	0.34	0.31	0.30	0.33	0.54	0.25	0.34	0.28	0.21	0.19
#Na	-	-	-	-	-	-	-	-	-	-
#K	-	-	-	-	-	-	-	-	-	-
M1,M2	2.01	2.02	2.04	2.01	2.03	2.05	2.03	2.03	2.06	2.04
#O	6.00	6.00	6.00	6.00	6.00	6.00	6.00	6.00	6.00	6.00

APPENDIX C: RHODONITE AND PYROXMANGITE ANALYSES

Ref No.	348	349	350	351	352	353	354	355	356	357
ID	1EQ16	1EQ16	1EQ16	1EQ16	1EQ16	1EQ16	1EQ16	1EQ16	1EQ16	1EQ16
Level	10000	10000	10000	10000	10000	10000	10000	10000	10000	10000
SiO2	46.53	46.01	46.77	46.90	45.98	46.25	47.11	46.31	46.98	46.66
TiO2	-	-	-	-	-	-	-	-	-	-
Al2O3	0.33	0.43	0.22	0.58	0.60	0.31	0.22	0.48	0.29	0.31
Cr2O3	-	-	-	-	-	-	-	-	-	-
Fe2O3	0.00	0.00	0.00	0.00	-	-	0.00	0.00	-	-
FeO	2.32	2.71	2.34	1.13	0.68	1.96	2.67	2.00	2.67	2.43
MnO	45.55	42.52	41.41	44.16	43.43	44.29	41.23	44.45	40.13	44.14
NiO	-	-	-	-	-	-	-	-	-	-
MgO	0.51	0.80	0.58	0.42	0.52	0.49	0.64	0.46	0.79	0.51
CaO	5.79	6.62	9.05	7.20	8.72	7.25	8.99	6.58	9.65	6.91
Na2O	-	-	-	-	-	-	-	-	-	-
K2O	-	-	-	-	-	-	-	-	-	-
Total	101.03	99.09	100.37	100.39	99.93	100.55	100.86	100.28	100.51	100.96
#Si IV	1.98	1.98	1.98	1.99	1.96	1.97	1.99	1.98	1.98	1.98
#Al IV	0.02	0.02	0.01	0.01	0.03	0.02	0.01	0.02	0.01	0.02
T site	1.99	2.00	1.99	2.00	1.99	1.99	2.00	2.00	2.00	1.99
#Al VI	-	0.00	-	0.02	-	-	-	0.00	-	-
#Ti	-	-	-	-	-	-	-	-	-	-
#Cr	-	-	-	-	-	-	-	-	-	-
#Fe +3	0.00	0.00	0.00	0.00	-	-	0.00	0.00	-	-
#Fe +2	0.08	0.10	0.08	0.04	0.02	0.07	0.09	0.07	0.09	0.09
#Mn +2	1.64	1.55	1.49	1.59	1.57	1.60	1.47	1.61	1.43	1.59
#Ni	-	-	-	-	-	-	-	-	-	-
#Mg	0.03	0.05	0.04	0.03	0.03	0.03	0.04	0.03	0.05	0.03
#Ca	0.26	0.31	0.41	0.33	0.40	0.33	0.41	0.30	0.44	0.31
#Na	-	-	-	-	-	-	-	-	-	-
#K	-	-	-	-	-	-	-	-	-	-
M1,M2	2.02	2.01	2.02	2.00	2.03	2.03	2.01	2.01	2.01	2.02
#O	6.00	6.00	6.00	6.00	6.00	6.00	6.00	6.00	6.00	6.00

APPENDIX C: RHODONITE AND PYROXMANGITE ANALYSES

Ref No.	358	359	361	362	363	364	365	366	367	368
ID	1EQ16	1EQ16	1EQ16	1EQ16	1EQ16	1EQ16	1EQ16	1EQ16	1EQ16	1EQ16
Level	10000	10000	10000	10000	10000	10000	10000	10000	10000	10000
SiO2	46.31	46.93	45.69	46.13	46.58	46.95	46.20	46.31	46.37	45.86
TiO2	-	-	-	-	-	-	-	-	-	-
Al2O3	0.30	0.39	0.30	0.25	0.19	0.18	0.22	0.20	0.47	0.37
Cr2O3	-	-	-	-	-	-	-	-	-	-
Fe2O3	-	0.00	0.00	0.00	0.00	0.00	0.00	0.00	0.00	0.00
FeO	2.07	1.49	2.12	0.70	2.33	1.61	2.00	1.80	2.04	2.15
MnO	46.09	44.65	46.92	45.41	43.87	41.54	45.85	44.38	45.13	45.62
NiO	-	-	-	-	-	-	-	-	-	-
MgO	0.46	0.50	0.48	0.61	0.50	0.73	0.60	0.44	0.43	0.45
CaO	5.56	7.38	4.60	7.40	7.08	9.95	5.69	7.18	5.19	6.16
Na2O	-	-	-	-	-	-	-	-	-	-
K2O	-	-	-	-	-	-	-	-	-	-
Total	100.79	101.34	100.11	100.50	100.55	100.96	100.56	100.31	99.63	100.61
#Si IV	1.98	1.98	1.97	1.97	1.98	1.98	1.98	1.98	1.99	1.96
#Al IV	0.02	0.02	0.02	0.01	0.01	0.01	0.01	0.01	0.01	0.02
T site	1.99	2.00	1.99	1.98	1.99	1.99	1.99	1.99	2.00	1.98
#Al VI	-	-	-	-	-	-	-	-	0.02	-
#Ti	-	-	-	-	-	-	-	-	-	-
#Cr	-	-	-	-	-	-	-	-	-	-
#Fe +3	-	0.00	0.00	0.00	0.00	0.00	0.00	0.00	0.00	0.00
#Fe +2	0.07	0.05	0.08	0.02	0.08	0.06	0.07	0.06	0.07	0.08
#Mn +2	1.67	1.59	1.71	1.64	1.58	1.48	1.66	1.61	1.64	1.66
#Ni	-	-	-	-	-	-	-	-	-	-
#Mg	0.03	0.03	0.03	0.04	0.03	0.05	0.04	0.03	0.03	0.03
#Ca	0.25	0.33	0.21	0.34	0.32	0.45	0.26	0.33	0.24	0.28
#Na	-	-	-	-	-	-	-	-	-	-
#K	-	-	-	-	-	-	-	-	-	-
M1,M2	2.02	2.01	2.03	2.04	2.02	2.03	2.03	2.03	2.00	2.04
#O	6.00	6.00	6.00	6.00	6.00	6.00	6.00	6.00	6.00	6.00

APPENDIX C: RHODONITE AND PYROXMANGITE ANALYSES

Ref. No.	369	370	371	372	373	374	409	410	411	412
ID	1EQ16	1EQ16	1EQ16	1EQ16	1EQ16	1EQ16	Q17	Q17	Q17	Q17
Level	10000	10000	10000	10000	10000	10000	10000	10000	10000	10000
SiO2	46.15	46.03	46.00	46.30	46.34	44.76	45.86	46.04	46.03	45.98
TiO2	-	-	-	-	-	-	-	-	-	-
Al2O3	0.40	0.50	0.40	0.34	0.23	0.25	0.25	0.21	0.22	0.22
Cr2O3	-	-	-	-	-	-	-	-	-	-
Fe2O3	-	0.00	-	-	0.00	0.00	0.00	0.00	-	0.00
FeO	2.28	2.02	2.11	1.87	3.10	1.34	2.77	1.98	2.02	2.26
MnO	45.51	45.05	45.76	42.31	41.88	46.95	44.16	45.30	45.20	44.89
NiO	-	-	-	-	-	-	-	-	-	-
MgO	0.58	0.46	0.43	0.47	0.68	0.45	0.48	0.46	0.38	0.44
CaO	5.55	6.61	6.01	9.21	7.92	5.28	6.49	5.98	5.75	6.08
Na2O	-	-	-	-	-	-	-	-	-	-
K2O	-	-	-	-	-	-	-	-	-	-
Total	100.47	100.67	100.71	100.50	100.15	99.03	100.01	99.97	99.60	99.87
#Si IV	1.97	1.96	1.97	1.97	1.98	1.96	1.97	1.98	1.98	1.98
#Al IV	0.02	0.03	0.02	0.02	0.01	0.01	0.01	0.01	0.01	0.01
T site	1.99	1.99	1.99	1.98	1.99	1.97	1.98	1.99	2.00	1.99
#Al VI	-	-	-	-	-	-	-	-	-	-
#Ti	-	-	-	-	-	-	-	-	-	-
#Cr	-	-	-	-	-	-	-	-	-	-
#Fe +3	-	0.00	-	-	0.00	0.00	0.00	0.00	-	0.00
#Fe +2	0.08	0.07	0.08	0.07	0.11	0.05	0.10	0.07	0.07	0.08
#Mn +2	1.65	1.63	1.66	1.52	1.51	1.74	1.61	1.65	1.65	1.64
#Ni	-	-	-	-	-	-	-	-	-	-
#Mg	0.04	0.03	0.03	0.03	0.04	0.03	0.03	0.03	0.02	0.03
#Ca	0.25	0.30	0.28	0.42	0.36	0.25	0.30	0.28	0.27	0.28
#Na	-	-	-	-	-	-	-	-	-	-
#K	-	-	-	-	-	-	-	-	-	-
M1,M2	2.02	2.03	2.04	2.04	2.03	2.07	2.04	2.03	2.01	2.03
#O	6.00	6.00	6.00	6.00	6.00	6.00	6.00	6.00	6.00	6.00

APPENDIX C: RHODONITE AND PYROXMANGITE ANALYSES

Ref. No.	413	414	415	416	417	418	419	420	421	422
ID	Q17	Q17	Q17	Q17	Q17	Q17	Q17	Q17	Q17	Q17
Level	10000	10000	10000	10000	10000	10000	10000	10000	10000	10000
SiO2	46.78	46.84	46.48	45.52	46.59	46.44	46.66	46.52	46.05	46.41
TiO2	-	-	-	-	-	-	-	-	-	-
Al2O3	0.51	0.48	0.49	0.31	0.29	0.42	0.20	0.26	0.20	0.22
Cr2O3	-	-	-	-	-	-	-	-	-	-
Fe2O3	-	0.00	0.00	-	0.00	0.00	0.00	0.00	0.00	0.00
FeO	2.36	2.30	2.60	3.38	2.17	2.56	1.86	1.36	2.62	1.95
MnO	44.26	44.71	44.66	44.75	46.24	44.93	46.05	45.23	44.79	45.36
NiO	-	-	-	-	-	-	-	-	-	-
MgO	0.41	0.41	0.36	0.49	0.38	0.41	0.44	0.45	0.46	0.45
CaO	7.18	6.83	6.34	5.81	5.02	6.24	5.33	6.37	5.85	5.85
Na2O	-	-	-	-	-	-	-	-	-	-
K2O	-	-	-	-	-	-	-	-	-	-
Total	101.50	101.57	100.93	100.26	100.69	101.00	100.54	100.19	99.97	100.24
#Si IV	1.97	1.98	1.98	1.96	1.99	1.97	1.99	1.99	1.98	1.99
#Al IV	0.03	0.02	0.02	0.02	0.01	0.02	0.01	0.01	0.01	0.01
T site	2.00	2.00	2.00	1.98	2.00	2.00	2.00	2.00	1.99	2.00
#Al VI	-	-	0.00	-	0.00	-	0.00	0.00	-	-
#Ti	-	-	-	-	-	-	-	-	-	-
#Cr	-	-	-	-	-	-	-	-	-	-
#Fe +3	-	0.00	0.00	-	0.00	0.00	0.00	0.00	0.00	0.00
#Fe +2	0.08	0.08	0.09	0.12	0.08	0.09	0.07	0.05	0.09	0.07
#Mn +2	1.58	1.60	1.61	1.63	1.67	1.62	1.66	1.64	1.63	1.64
#Ni	-	-	-	-	-	-	-	-	-	-
#Mg	0.03	0.03	0.02	0.03	0.02	0.03	0.03	0.03	0.03	0.03
#Ca	0.32	0.31	0.29	0.27	0.23	0.28	0.24	0.29	0.27	0.27
#Na	-	-	-	-	-	-	-	-	-	-
#K	-	-	-	-	-	-	-	-	-	-
M1,M2	2.02	2.01	2.01	2.05	2.00	2.02	2.00	2.01	2.02	2.01
#O	6.00	6.00	6.00	6.00	6.00	6.00	6.00	6.00	6.00	6.00

APPENDIX C: RHODONITE AND PYROXMANGITE ANALYSES

Ref. No.	423	424	424	425	426	427	428	429	430	431
ID	Q17	Q17	Q17	Q17	Q17	Q17	Q17	Q17	Q17	Q17
Level	10000	10000	10000	10000	10000	10000	10000	10000	10000	10000
SiO2	47.08	47.10	45.60	47.08	46.59	47.30	46.84	47.21	46.98	46.64
TiO2	-	-	-	-	-	-	-	-	-	-
Al2O3	0.30	0.55	0.20	0.43	0.37	0.59	0.14	0.16	0.32	0.32
Cr2O3	-	-	-	-	-	-	-	-	-	-
Fe2O3	0.00	0.00	0.00	0.00	0.00	0.00	0.00	0.00	0.00	0.00
FeO	2.21	2.21	0.61	2.21	2.62	1.93	2.23	2.56	2.34	2.96
MnO	46.36	45.22	49.00	45.79	44.81	43.20	46.01	44.79	44.70	43.25
NiO	-	-	-	-	-	-	-	-	-	-
MgO	0.45	0.39	0.40	0.42	0.42	0.41	0.44	0.37	0.41	0.44
CaO	5.34	6.02	3.18	5.68	6.27	8.22	5.50	6.63	6.65	6.80
Na2O	-	-	-	-	-	-	-	-	-	-
K2O	-	-	-	-	-	-	-	-	-	-
Total	101.74	101.49	98.99	101.61	101.08	101.65	101.16	101.72	101.40	100.41
#Si IV	1.99	1.99	1.99	1.99	1.98	1.98	1.99	1.99	1.98	1.99
#Al IV	0.01	0.01	0.01	0.01	0.02	0.02	0.01	0.01	0.02	0.01
T site	2.00	2.00	2.00	2.00	2.00	2.00	2.00	2.00	2.00	2.00
#Al VI	0.00	0.01	-	0.01	-	0.01	-	-	-	0.00
#Ti	-	-	-	-	-	-	-	-	-	-
#Cr	-	-	-	-	-	-	-	-	-	-
#Fe +3	0.00	0.00	0.00	0.00	0.00	0.00	0.00	0.00	0.00	0.00
#Fe +2	0.08	0.08	0.02	0.08	0.09	0.07	0.08	0.09	0.08	0.11
#Mn +2	1.66	1.61	1.81	1.64	1.61	1.53	1.65	1.60	1.60	1.56
#Ni	-	-	-	-	-	-	-	-	-	-
#Mg	0.03	0.02	0.03	0.03	0.03	0.03	0.03	0.02	0.03	0.03
#Ca	0.24	0.27	0.15	0.26	0.29	0.37	0.25	0.30	0.30	0.31
#Na	-	-	-	-	-	-	-	-	-	-
#K	-	-	-	-	-	-	-	-	-	-
M1,M2	2.01	2.00	2.01	2.00	2.02	2.00	2.01	2.01	2.01	2.01
#O	6.00	6.00	6.00	6.00	6.00	6.00	6.00	6.00	6.00	6.00

APPENDIX C: RHODONITE AND PYROXMANGITE ANALYSES

Ref. No.	432	433	434	435	436	437	438	439	440	441
ID	Q17	Q17	Q17	Q17	Q17	Q17	Q17	Q17	Q17	Q17
Level	10000	10000	10000	10000	10000	10000	10000	10000	10000	10000
SiO2	46.43	47.06	46.72	46.72	46.95	47.18	47.11	47.08	47.16	47.42
TiO2	-	-	-	-	-	-	-	-	-	-
Al2O3	0.21	0.20	0.34	0.27	0.25	0.16	0.20	0.20	0.27	0.47
Cr2O3	-	-	-	-	-	-	-	-	-	-
Fe2O3	0.00	0.00	0.00	0.00	-	-	0.00	0.00	0.00	-
FeO	1.58	2.98	1.28	2.20	2.16	2.77	1.49	2.14	2.75	1.58
MnO	41.74	43.23	45.43	43.41	47.05	43.52	41.66	44.08	44.07	43.02
NiO	-	-	-	-	-	-	-	-	-	-
MgO	0.53	0.71	0.39	0.52	0.56	0.49	0.40	0.48	0.51	0.50
CaO	8.45	6.32	6.21	6.94	4.54	7.04	9.47	7.01	6.50	8.71
Na2O	-	-	-	-	-	-	-	-	-	-
K2O	-	-	-	-	-	-	-	-	-	-
Total	98.94	100.50	100.37	100.06	101.51	101.16	100.33	100.99	101.26	101.70
#Si IV	1.99	2.00	1.99	1.99	1.99	1.99	1.99	1.99	1.99	1.98
#Al IV	0.01	0.00	0.01	0.01	0.01	0.01	0.01	0.01	0.01	0.02
T site	2.00	2.00	2.00	2.00	2.00	2.00	2.00	2.00	2.00	2.00
#Al VI	0.00	0.01	0.01	0.01	0.00	0.00	0.00	0.00	0.00	0.01
#Ti	-	-	-	-	-	-	-	-	-	-
#Cr	-	-	-	-	-	-	-	-	-	-
#Fe +3	0.00	0.00	0.00	0.00	-	-	0.00	0.00	0.00	-
#Fe +2	0.06	0.11	0.05	0.08	0.08	0.10	0.05	0.08	0.10	0.06
#Mn +2	1.52	1.55	1.64	1.57	1.69	1.56	1.49	1.58	1.58	1.52
#Ni	-	-	-	-	-	-	-	-	-	-
#Mg	0.03	0.04	0.02	0.03	0.04	0.03	0.03	0.03	0.03	0.03
#Ca	0.39	0.29	0.28	0.32	0.21	0.32	0.43	0.32	0.29	0.39
#Na	-	-	-	-	-	-	-	-	-	-
#K	-	-	-	-	-	-	-	-	-	-
M1,M2	2.00	2.00	2.00	2.00	2.01	2.00	2.00	2.00	2.00	2.01
#O	6.00	6.00	6.00	6.00	6.00	6.00	6.00	6.00	6.00	6.00

APPENDIX C: RHODONITE AND PYROXMANGITE ANALYSES

Ref No.	442	538	539	541	542	543	544	545	546	549
ID	Q17	M13	M13	M13	M13	M13	M13	M13	M13	M13
Level	10000	10090	10090	10090	10090	10090	10090	10090	10090	10090
SiO2	47.29	46.49	46.42	47.12	46.65	46.15	45.15	45.80	45.68	45.95
TiO2	-	-	-	-	-	-	-	-	-	-
Al2O3	0.37	0.25	0.28	0.23	0.24	0.74	0.88	0.39	0.66	0.32
Cr2O3	-	-	-	-	-	-	-	-	-	-
Fe2O3	-	-	0.00	0.00	0.00	-	-	0.00	0.00	0.00
FeO	2.16	1.03	0.94	1.20	1.04	1.24	1.39	1.43	1.34	1.55
MnO	43.54	41.79	43.49	43.44	42.90	42.62	45.77	44.33	44.24	46.13
NiO	-	-	-	-	-	-	-	-	-	-
MgO	0.50	0.03	0.10	0.18	0.08	0.05	0.09	0.18	0.09	0.27
CaO	7.60	10.59	8.57	8.51	9.22	9.04	5.50	7.32	7.28	5.62
Na2O	-	-	-	-	-	-	-	-	-	-
K2O	-	-	-	-	-	-	-	-	-	-
Total	101.46	100.18	99.80	100.68	100.13	99.84	98.78	99.45	99.29	99.84
#Si IV	1.99	1.98	1.99	1.99	1.99	1.97	1.97	1.97	1.97	1.98
#Al IV	0.01	0.01	0.01	0.01	0.01	0.03	0.03	0.02	0.03	0.02
T site	2.00	1.99	2.00	2.00	2.00	2.00	2.00	1.99	2.00	2.00
#Al VI	0.01	-	-	0.00	-	0.01	0.01	-	0.00	-
#Ti	-	-	-	-	-	-	-	-	-	-
#Cr	-	-	-	-	-	-	-	-	-	-
#Fe +3	-	-	0.00	0.00	0.00	-	-	0.00	0.00	0.00
#Fe +2	0.08	0.04	0.03	0.04	0.04	0.04	0.05	0.05	0.05	0.06
#Mn +2	1.55	1.51	1.58	1.56	1.55	1.54	1.69	1.62	1.62	1.68
#Ni	-	-	-	-	-	-	-	-	-	-
#Mg	0.03	0.00	0.01	0.01	0.01	0.00	0.01	0.01	0.01	0.02
#Ca	0.34	0.48	0.39	0.39	0.42	0.41	0.26	0.34	0.34	0.26
#Na	-	-	-	-	-	-	-	-	-	-
#K	-	-	-	-	-	-	-	-	-	-
M1,M2	2.00	2.03	2.01	2.00	2.01	2.01	2.01	2.02	2.01	2.02
#O	6.00	6.00	6.00	6.00	6.00	6.00	6.00	6.00	6.00	6.00

APPENDIX C: RHODONITE AND PYROXMANGITE ANALYSES

Ref. No.	550	551	555	556	557	570	579	580	581	582
ID	M13	M13	M13	M13	M13	M13	BB54	BB54	BB54	BB54
Level	10090	10090	10090	10090	10090	10090	10250	10250	10250	10250
SiO2	45.82	45.86	45.61	45.85	45.71	45.45	45.80	45.88	45.86	45.83
TiO2	-	-	-	-	-	-	-	-	-	-
Al2O3	0.34	0.49	0.83	0.62	0.72	0.70	0.33	0.29	0.33	0.31
Cr2O3	-	-	-	-	-	-	-	-	-	-
Fe2O3	-	0.00	-	-	0.00	0.00	0.00	-	-	-
FeO	1.60	0.93	0.85	0.96	0.89	0.89	1.47	1.33	1.35	1.37
MnO	41.16	43.03	43.60	43.89	43.74	43.72	43.36	44.46	43.05	43.62
NiO	-	-	-	-	-	-	-	-	-	-
MgO	0.37	0.08	0.10	0.11	0.08	0.08	0.16	0.22	0.19	0.17
CaO	9.65	9.31	8.44	8.14	8.28	8.19	8.04	6.93	8.23	7.73
Na2O	-	-	-	-	-	-	-	-	-	-
K2O	-	-	-	-	-	-	-	-	-	-
Total	98.94	99.70	99.43	99.57	99.42	99.03	99.16	99.11	99.01	99.03
#Si IV	1.97	1.97	1.96	1.97	1.97	1.96	1.98	1.98	1.98	1.98
#Al IV	0.02	0.02	0.04	0.03	0.03	0.04	0.02	0.01	0.02	0.02
T site	1.99	1.99	2.00	2.00	2.00	2.00	1.99	2.00	2.00	2.00
#Al VI	-	-	0.00	0.00	0.00	0.00	-	-	-	-
#Ti	-	-	-	-	-	-	-	-	-	-
#Cr	-	-	-	-	-	-	-	-	-	-
#Fe +3	-	0.00	-	-	0.00	0.00	0.00	-	-	-
#Fe +2	0.06	0.03	0.03	0.03	0.03	0.03	0.05	0.05	0.05	0.05
#Mn +2	1.50	1.56	1.59	1.60	1.59	1.60	1.59	1.63	1.57	1.60
#Ni	-	-	-	-	-	-	-	-	-	-
#Mg	0.02	0.01	0.01	0.01	0.01	0.01	0.01	0.01	0.01	0.01
#Ca	0.45	0.43	0.39	0.37	0.38	0.38	0.37	0.32	0.38	0.36
#Na	-	-	-	-	-	-	-	-	-	-
#K	-	-	-	-	-	-	-	-	-	-
M1,M2	2.03	2.03	2.02	2.01	2.02	2.02	2.02	2.01	2.02	2.02
#O	6.00	6.00	6.00	6.00	6.00	6.00	6.00	6.00	6.00	6.00

APPENDIX C: RHODONITE AND PYROXMANGITE ANALYSES

Ref. No.	602	603	604	621	622	623	624	625	627
ID	BB54	BB54	BB54	BB54	BB54	BB54	BB54	BB54	BB54
Level	10250	10250	10250	10250	10250	10250	10250	10250	10250
SiO2	45.56	46.02	45.68	44.88	44.71	44.75	44.53	44.59	45.00
TiO2	-	-	-	-	-	-	-	-	-
Al2O3	0.34	0.30	0.26	0.06	0.26	0.07	0.06	0.07	0.07
Cr2O3	-	-	-	-	-	-	-	-	-
Fe2O3	0.00	0.00	0.00	0.00	0.00	0.00	0.00	0.00	0.00
FeO	1.26	6.73	7.59	2.77	2.80	2.54	2.75	1.32	2.81
MnO	44.60	45.68	45.05	49.83	49.14	49.68	49.26	51.49	49.56
NiO	-	-	-	-	-	-	-	-	-
MgO	0.26	0.82	0.65	0.48	0.50	0.87	0.54	0.34	0.51
CaO	6.58	1.37	1.34	1.30	1.47	1.32	1.35	1.06	1.68
Na2O	-	-	-	-	-	-	-	-	-
K2O	-	-	-	-	-	-	-	-	-
Total	98.60	100.92	100.57	99.29	98.99	99.26	98.51	98.84	99.62
#Si IV	1.98	1.98	1.98	1.97	1.98	1.97	1.97	1.97	1.97
#Al IV	0.02	0.02	0.01	0.00	0.00	0.00	0.00	0.00	0.00
T site	2.00	1.99	1.99	1.97	1.98	1.98	1.98	1.98	1.98
#Al VI	-	-	-	-	-	-	-	-	-
#Ti	-	-	-	-	-	-	-	-	-
#Cr	-	-	-	-	-	-	-	-	-
#Fe +3	0.00	0.00	0.00	0.00	-	0.00	-	-	0.00
#Fe +2	0.05	0.24	0.27	0.10	0.10	0.09	0.10	0.05	0.10
#Mn +2	1.64	1.66	1.65	1.86	1.84	1.86	1.85	1.93	1.84
#Ni	-	-	-	-	-	-	-	-	-
#Mg	0.02	0.05	0.04	0.03	0.03	0.03	0.04	0.02	0.03
#Ca	0.31	0.06	0.06	0.06	0.07	0.06	0.06	0.05	0.08
#Na	-	-	-	-	-	-	-	-	-
#K	-	-	-	-	-	-	-	-	-
M1,M2	2.01	2.02	2.03	2.05	2.04	2.05	2.05	2.05	2.05
#O	6.00	6.00	6.00	6.00	6.00	6.00	6.00	6.00	6.00

VITA

Nora Katherine Foley received a Bachelor of Science degree in geology from The University of Michigan at Ann Arbor in 1978, and a Master of Science degree in geology from Virginia Polytechnic Institute and State University in 1980. After working at the United States Geological Survey for a number of years, she resumed studies at Virginia Polytechnic Institute and State University and completed requirements for a Doctor of Philosophy degree in geology in 1990. She is presently employed at the United States Geological Survey in Reston, Virginia.